

An Investigation of the Biological Effects of Non-Thermal Energy Technologies on Prokaryotic and Eukaryotic Cells

Rebecca Lucy O'Brien

A thesis submitted in partial fulfilment of the requirements of the University of the West of England, Bristol for the degree of Doctor of Philosophy

This research was carried out in association with Creo Medical Ltd

School of Applied Sciences, University of the West of England

September 2024

Abstract

With the increasing use of antimicrobial products, particularly in the healthcare sector and agri-food industry, there has been a concomitant rise in the prevalence of antimicrobial-resistant (AMR) and multi-drug resistant (MDR) microorganisms. The involvement of pathogenic MDR strains in healthcare-associated infections (HAI) poses serious challenges in terms of treatment options, increasing pressure on the drive to discover effective alternative antimicrobial strategies. To this end, non-thermal plasma (NTP) technologies and electrochemically-activated solutions (ECAS) may provide viable means of helping to control the spread of drug-resistant pathogens.

The effects of a novel Radio Frequency – Microwave (RF-MW) NTP system against planktonic microbes and single-species bacterial biofilms were investigated, using short-contact treatments of 30 – 180 seconds on non-porous surfaces, using *Staphylococcus aureus* and *Pseudomonas aeruginosa* as target organisms. Against dried surface-associated microbial loads, significant reductions in viable bioburden were achieved in both species, reaching a maximal 3.1 Log₁₀ reduction in *S. aureus*, and 4.6 Log₁₀ reduction in *P. aeruginosa* following treatments of 180s. Treatments with an ECAS solution of 200ppm FAC produced superior antimicrobial effects in parallel surface-decontamination tests, surpassing a reduction of 6 Log₁₀ at contact times of 30 - 300 seconds. Direct NTP treatments applied against single-species *S. aureus* and *P. aeruginosa* biofilms for either 60 or 120 seconds showed a much lower efficacy, achieving a maximal reduction of <1.0 Log₁₀ in *S. aureus* and up to approximately 1.4 Log₁₀ in *P. aeruginosa*.

Plasma-activated solutions (PAS) were produced using the MW-RF NTP system, and two Surface Barrier Discharge (SBD) plasma systems, and were applied to planktonic microbial loads, and to *S. aureus* and *P. aeruginosa* biofilms, to determine the efficacy of indirect NTP treatment. Although moderate inhibition was noted using SBD-plasma-activated water (PAW) against surface-associated *S. aureus*, these effects were not reproducible with repeat testing, indicating a decline in the concentration of key reactive species responsible for the antimicrobial activity of PAW during the storage period. Similarly, despite showing a significant effect initially, SBD-PAW showed a decline in antimicrobial activity against *P. aeruginosa* in suspension tests when repeated after a period of refrigerated storage of the PAW. No effects were seen with PAW treatment of biofilms

for up to 300 seconds. In contrast, ECAS achieved significant and reproducible reductions of up to 2.5 Log₁₀ in *P. aeruginosa* biofilms.

Cytotoxicity testing performed on immortalised human epithelial cell lines H103 and A375 demonstrated sensitivity to all antimicrobial treatments investigated, including direct and indirect NTP application. Aqueous antimicrobial solutions were investigated in dose-response studies, from which IC₅₀ values were derived for both cell lines. The 50% inhibitory dose thresholds for ECAS, and the topical antiseptic povidone-iodine (PVP-I) appeared at concentrations 10 – 100-fold below those seen to exert effective antimicrobial activity against planktonic microbial loads.

The effects of RF-MW NTP plasma-activated culture medium (PAM) and PBS (pPBS) on H103 and A375 cell cultures were explored by monitoring cellular proliferation over 72 hours, using live-cell imaging and analysis of confluence. Both plasma-activated solutions appeared to reduce the viable population, but did not produce complete growth inhibition in either cell line. PAM produced a significant growth deficit reaching up to 13.64% in A375 when applied in complete medium, whilst pPBS treatment appeared to suppress proliferation more markedly in serum-free medium, eliciting a maximal effect of up to 13.32% confluence deficit at 72h, which was not significant. In H103, the effects of both PAM and pPBS were greater in serum-free medium, with maximal growth deficits of 21.34% and 18.52% seen, respectively (both $p > 0.05$), at 72h. PAM treatment significantly limited H103 growth in complete medium, by up to 11.59% at 72h ($p < 0.05$).

This research has explored the biological effects of two relatively novel non-thermal energy technologies upon prokaryotic and eukaryotic cells, using various treatment methods. Although some promising antimicrobial efficacy was seen, significant cytotoxic effects were exerted upon both eukaryotic cell lines, indicating limitations in terms of the biocompatibility of these treatments.

Acknowledgements:

I would like to thank everyone who has helped and supported me throughout the whole course of my PhD, which has been challenging in many ways, but has brought many positive experiences and allowed me to meet and work with some really inspiring, and wonderful people. It would really not have been possible without any one of you, so you have my heartfelt gratitude!

Professor Darren Reynolds, Associate Prof. Dr Robin Thorn, Dr Liz Anderson, Dr Gareth Robinson and Dr Dann Turner, I have relied on your supervision, skill and expertise, as well as your encouragement, kindness, and patience, at various times along this journey. Many thanks for keeping things moving and helping enlighten me on the many occasions I needed it. Also, to the many other academics and researchers in Applied Sciences, and the School of Engineering, and the brilliant CRIB and Micro Technical Team, Paul, Jasper, and everyone in Technical Services who so often work 'invisibly' to ensure we have a functioning and well-equipped lab. Thanks, too, to Dr Keith Hewitt who has helped with numerous technical issues, Drs Lynne Lawrance and Carrie Brady, our lovely PGR Tutors, and the Directorial team for SoAS PG research, for all you do to support the PGR community.

Special thanks to everyone in the PGR group who I've had the pleasure and privilege to work alongside in the lab during my time at UWE. Dr Gill Clayton, Dr Lizzy Slade, and Dr Beth Fox, Josh, Eva, Savannah, and the current team, Alex, Harsh, Chitra, Chika, and Rachel, as well as the many other PGRs who have come and gone.

Huge thanks to Creo Medical, my industrial partner, and in particular Professor Chris Hancock, George Hodgkins, and the engineering team at Bath. You made this happen quite literally, and your enthusiasm, determination and resourcefulness have been inspiring from the start. Professor James Walsh and both his teams from Liverpool and York, thank you for all your help and advice, and the PAW!

And finally, but most importantly, thank you to my family and friends, for your love and support at every stage, I absolutely could not have kept going without you. Thanks for the many acts of kindness, for helping me laugh and take time out, and for the constant moral support and words of wisdom. This is dedicated to you.

Contents

List of Figures 13

Abbreviations and acronyms 23

1. Introduction 26

- 1.1. Non-thermal plasma: sources and applications 26
 - 1.1.1. Plasma applications in biomedicine 26
- 1.2. Antimicrobial resistance the development of new interventions 27
- 1.3. Healthcare-associated infections and chronic wounds: the scale of the problem 30
- 1.4. Pathophysiological events in wound repair: skewing of healthy healing processes and the impacts of chronic wound biofilms 32
 - 1.4.1. Resolution of wounding healthy tissues 32
 - 1.4.2. Failure to heal: a self-perpetuating state of dysregulation 35
 - 1.4.3. The wound infection continuum and the pathogenesis of chronic wounds 37
- 1.5. The epidemiology of non-healing wounds and principle aetiologies 38
 - 1.5.1. Major types of chronic wounds 39
- 1.6. Microbial biofilms: a persistent problem 40
- 1.7. Clinical interventions to promote wound healing 42
 - 1.7.1. Wound cleansing 43
 - 1.7.2. Application of antiseptics of antimicrobial disinfectant agents 44
 - 1.7.3. Common antimicrobial agents used for wound antisepsis in healthcare 47
 - 1.7.3.1. PHMB 47
 - 1.7.3.2. Povidone iodine 47
 - 1.7.3.3. Silver sulfadiazine 48
 - 1.7.3.4. Chlorhexidine 49
 - 1.7.3.5. Hydrogen peroxide 50
 - 1.7.3.6. Electrochemically-activated solutions (ECAS) 51
- 1.8. Developing the evidence-base for novel antiseptics and wound-cleansers: towards a better understanding of the wound microenvironment 52
 - 1.8.1. Mimicking the biochemical and structural profile of the wound environment *in vitro* 53
- 1.9. Project aims and objectives 54

2. Methods and materials 55

- 2.1. Microorganisms used in experimental procedures 55
- 2.2. Plasma system design and standard testing procedures 55

2.3.	Measurement of NTP-induced Zone in Inhibition (ZOI)	58
2.4.	Assessment of the antimicrobial effects of NTP on planktonic microbial loads on solid, non-porous surfaces	58
2.4.1.	Surface inoculation, disinfection and recovery procedures	58
2.4.2.	Initial validation of microbial loading of test surfaces	59
2.4.2.1.	Preparation of microbial suspension for antimicrobial efficacy testing	59
2.4.2.2.	Optimisation of inoculation parameters	60
2.4.3.	Confirmation of microbial viability with extended drying	60
2.4.4.	Application of NTP and biocidal treatments to test coupons, and determination of antimicrobial efficacy	61
2.4.5.	Validation of the non-toxicity and efficacy of neutralisation in non-porous surface-disinfection methodology	61
2.5.	Assessment of the antimicrobial effects of indirect plasma treatments and alternative antimicrobials on planktonic microbials in suspension	63
2.5.1.	Validation of antimicrobial suspension testing method, and non-toxicity of the neutraliser	64
2.6.	Biofilm culture models and treatments	66
2.6.1.	CDC Biofilm Reactor system (CBR)	66
2.6.1.1.	Formation of biofilms within the reactor	66
2.6.1.2.	Application of antimicrobial treatment to mature CBR biofilms	68
2.7.	Biofilm culture within the Drip-Flow Reactor (DFR) – collagen matrix wound model	68
2.7.1.	Biofilm culture under standard operating parameters	68
2.7.2.	Biofilm recovery from microscope slides within the DFR-collagen matrix model	70
2.7.3.	Adapted operation of the DFR-collagen matrix model for miniaturised biofilm replicates	70
2.8.	Generation of plasma-activated solutions: PAW, PAM, and pPBS	71
2.8.1.	Activation via RF-MW plasma	71
2.8.2.	Small-batch SBD-PAW	72
2.8.3.	Large-batch PAW generated by falling film exposure	72
2.9.	Generation of Electrochemically-Activated Saline Solution (ECAS)	73
2.10.	Mammalian cell culture and treatments	74
2.10.1.	Subculture routine	75
2.10.2.	Cryopreservation of cells and revival from frozen storage	75
2.11.	Delivery of plasma and aqueous antimicrobial treatments to cell cultures	75
2.11.1.	Direct NTP treatment protocol	75
2.11.2.	Aqueous treatment protocol	76

- 2.12. Assessment of cytotoxicity **77**
 - 2.12.1. Trypan Blue Dye Exclusion (TBDE) **77**
 - 2.12.2. CellTiter Glo 2.0 **77**
 - 2.12.3. MTS-PMS assay **78**
- 2.13. Incucyte Live-Cell Imaging Analysis **79**
 - 2.13.1. Direct NTP treatments **79**
 - 2.13.2. Indirect NTP treatments **79**
- 2.14. Statistical Analysis **79**

3. Investigation of the antimicrobial effects of non-thermal energy technologies on prokaryotes 81

- 3.1. Antimicrobial applications in the healthcare setting **81**
- 3.2. Antimicrobial efficacy testing **82**
 - 3.2.1. Methodology for the investigation of antimicrobial efficacy of selected agents on carrier surfaces **82**
- 3.3. Determination of the NTP-induced Zone of Inhibition **84**
- 3.4. Evaluation of antimicrobial efficacy using a quantitative non-porous surface test for bactericidal/ fungicidal activity **88**
 - 3.4.1. Optimisation of test methodology: the investigation of microbial viability on inoculated carrier surfaces **89**
 - 3.4.2. The effects of extended drying on surface-associated microbial viability **91**
- 3.5. Direct NTP treatment of surface-associated planktonic microbial loads **94**
 - 3.5.1. Preliminary test findings against a Gram-positive microorganism **94**
 - 3.5.2. Preliminary test findings against a Gram-negative microorganism **95**
- 3.6. Comparison of effects on an alternative test surface material **97**
 - 3.6.1. Direct NTP treatment of microbial loads applied to silicone carriers **97**
- 3.7. Comparative antimicrobial efficacy of alternative antimicrobial products on surface-associated planktonic microbial viability **99**
 - 3.7.1. Efficacy of hydrogen peroxide against *S. aureus* on stainless steel **99**
 - 3.7.2. Efficacy of PVP-I against *S. aureus* on stainless steel **100**
 - 3.7.3. Efficacy of Electrochemically-activated saline solutions (ECAS) against *S. aureus* on stainless steel **101**
- 3.8. Efficacy of indirect NTP against planktonic microorganisms **103**
 - 3.8.1. Preliminary testing against *S. aureus* on stainless steel, using Plasma-Activated Solutions (PAS) **103**
- 3.9. Comparative effects of small-batch PAW generated by SBD-NTP treatment **105**

3.9.1.	Effects against surface-associated <i>S. aureus</i> on stainless steel	105
3.9.2.	Assessment of the antimicrobial efficacy of small-batch SBD-NTP-generated PAW in suspension	106
3.9.3.	The effects of small-batch SBD-PAW against <i>P. aeruginosa</i> in suspension	107
3.10.	Antimicrobial suspension testing using PAW generated via large-batch Surface Barrier Discharge (SBD)-NTP and falling-film flow	108
3.10.1.	The effects of SBD-falling film PAW against <i>P. aeruginosa</i> and <i>S. aureus</i> in suspension	108
3.11.	Antimicrobial suspension testing: dose-response of <i>S. aureus</i> and <i>P. aeruginosa</i> to ECAS	110
3.12.	Discussion	112
3.12.1.	Key Conclusions	114
4.	The effects of NTP and alternative antimicrobials on bacterial biofilms	116
4.1.	Background and introduction	116
4.2.	Surface-associated biofilms cultured within the CDC Biofilm Reactor (CBR)	117
4.2.1.	Comparison on biofilm density formed on different coupon materials	117
4.3.	Investigation of the effects of direct NTP on <i>P. aeruginosa</i> and <i>S. aureus</i> mono-species biofilms grown within the CBR	119
4.3.1.	Comparative efficacy of direct NTP and 10% PVP-I	119
4.3.1.1.	Effects on <i>P. aeruginosa</i> biofilms	119
4.3.1.2.	Effects on <i>S. aureus</i> biofilms	120
4.4.	The comparative anti-biofilm activities of ECAS, hydrogen peroxide and PAW	122
4.4.1.	Effects on <i>P. aeruginosa</i> biofilms	122
4.5.	Investigation of the effects of aqueous antimicrobial agents against collagen matrix-associated biofilms	123
4.5.1.	Culture of <i>P. aeruginosa</i> biofilms within the DFR-collagen matrix model: steady state densities obtained under control conditions	123
4.5.2.	Antimicrobial treatment of DFR-collagen matrix biofilms: methods of delivery	125
4.5.3.	Initial adaptation of the DFR-collagen matrix model	125
4.5.4.	Application of antimicrobial treatments to collagen matrix-associated <i>P. aeruginosa</i> biofilms	126
4.5.5.	Application of antimicrobial treatments to collagen matrix-associated <i>P. aeruginosa</i> biofilms: periods irrigation of biofilms within the DFR	127

4.5.6. Investigation of the effects of single versus repeated exposures to antimicrobial irrigation of collagen matrix-associated <i>P. aeruginosa</i> biofilms	130
4.5.6.1. Consideration of technical approach in repeated irrigation treatments in the DFR model	132
4.6. Discussion	133
4.6.1. Key Conclusions	135
5. Investigation of the eukaryotic response to NTP	138
5.1. Selection of alternative antimicrobial products for comparison of cytotoxic effect	138
5.1.1. Povidone-iodine	138
5.1.2. Hydrogen peroxide	139
5.2. Cell line selection for <i>in vitro</i> cytotoxicity assay of antimicrobial agents	139
5.2.1. Determination of cell growth rate under control conditions	140
5.3. Assessment of cytotoxic response to known antimicrobial compounds	140
5.3.1. Selection and optimisation of viability assay for accurate evaluation of treatment toxicity	140
5.3.2. Preliminary studies of antiseptic treatment in short-term exposures	141
5.3.2.1. Assessment of hydrogen peroxide treatment of H103 by CTG2.0	141
5.3.2.2. Assessment of ECAS treatment of H103 by TBDE	143
5.3.2.3. Appraisal of cytotoxicity assessment methods	144
5.4. Investigation of the effect of direct NTP on cellular viability	144
5.4.1. Comparative assessment of NTP-mediated cytotoxicity via CellTiter Glo 2.0 and MTS-PMS assay	144
5.4.1.1. Determination of post-treatment viability by CellTiter Glo 2.0	145
5.4.1.2. Alternative assessment of post-treatment viability by MTS-PMS	146
5.4.1.2.1. MTS-PMS assay calibration	147
5.4.1.3. Determination of post-treatment viability by MTS-PMS	148
5.5. Extended measurement of the effects of NTP on cell proliferation via live-cell imaging	149
5.5.1. Extended monitoring of H103: post-treatment growth response to NTP	150
5.5.1.1. Interpretation of the NTP-response in H103 during extended cell-monitoring	150
5.5.2. Extended monitoring of A375: post-treatment growth response to NTP	155
5.5.2.1. Interpretation of the NTP-response in A375 during extended cell-monitoring	156
5.6. Investigation of the cytotoxic response to topical antimicrobial agents	159

5.6.1. Dose-response studies of PVP-I and ECAS in H103 and A375 cells via CTG2.0 and MTS-PMS assay	159
5.6.1.1. Determination of the IC ₅₀ of PVP-I in H103 cells	160
5.6.1.2. Determination of the IC ₅₀ of ECAS in H103 cells	161
5.6.1.3. Determination of the IC ₅₀ of PVP-I in A375 cells	162
5.6.1.4. Determination of the IC ₅₀ of ECAS in A375 cells	163
5.6.2. Potential sources of error and variability in cytotoxic dose-response determination	165
5.7. Cellular response to plasma-activated solutions (PAS)	165
5.7.1. Plasma-activated PBS	166
5.7.2. Extended monitoring of the H103 growth response to pPBS	167
5.7.3. Extended monitoring of the H103 growth response to PAM	168
5.7.4. Extended monitoring of the A375 growth response to pPBS	169
5.7.5. Extended monitoring of the A375 growth response to PAM	170
5.8. Discussion	172
5.8.1. Key Conclusions	174
6. Summary of conclusions and final discussion	177
6.1. Alternative antimicrobial technologies: addressing the need for innovation	177
6.2. Relevance to the development of potential applications of NTP in healthcare	177
6.2.1. Outcomes of microbiological investigations into the effects of NTP	178
6.2.2. Outcomes of investigations into the effects of NTP on eukaryotic cells	179
6.2.2.1. Direct versus indirect NTP treatment of mammalian epithelial cells	179
6.3. Relevance of this work to the field of electrochemical-activation technologies for application in healthcare	180
6.3.1. Outcomes of microbiological investigation into the effect of ECAS	181
6.3.2. Outcomes of investigations of the effects of alternative antimicrobial products in eukaryotic cells: results obtained with ECAS and PVP-I	182
6.4. Challenges in the design and realisation of a physiologically representative wound-biofilm model	182
6.4.1. Co-culture models	184
6.5. Areas for investigation in future work	185
6.6. Translatability of <i>in vitro</i> research findings to clinical applications	186
6.6.1. Considerations in evaluating the suitability of novel antimicrobial treatments	186
6.6.1.1. NTP technologies	186

6.6.1.2. Electrochemically-activated solutions **187**

6.7. Concluding remarks **189**

References 191

List of Figures

Chapter 1

Figure 1.1: Typical wound repair events within a healthy (healing) wound (reproduced from (Eming, Martin and Tomic-Canic, 2014). **33**

Figure 1.2: Pathological changes occurring within a chronic wound, reproduced from (Eming, Martin and Tomic-Canic, 2014). **36**

Figure 1.3: The wound infection continuum (reproduced from (Brown, 2018) portraying the sequence of events in the progression from wound contamination to infection and sepsis, or widespread systemic infection. **38**

Figure 1.4: Hierarchy of susceptibility of microorganisms to biocides, reproduced from (Maillard and Pascoe, 2023) **46**

Figure 1.5: Microbial cell target sites disrupted by biocides, reproduced from (Maillard and Pascoe, 2024) **47**

Chapter 2

Table 2.1: Reference strains of microbial species used in antimicrobial efficacy testing protocols. **55**

Figure 2.1: Schematic illustration of the combined source RF-MW plasma system, produced by Creo Medical. **57**

Figure 2.2: Atmospheric Pressure Plasma Jet (APPJ) device: (Left) The applied electric voltage passes through a pulse generator/alternator to the first electrode, which is proximal to the second, a grounded tube electrode. An inert gas feed carries the plasma constituents to the APPJ terminal aperture, creating a plasma plume. The biological target was placed directly below the aperture, being separated by a discharge gap of approximately 10mm. (Right) The brass housing and quartz tube of the torch-style applicator used in the RF-MW system. **58**

Figure 2.3: Validation of surface disinfection neutralisation step, performed on stainless steel carriers, in duplicate; n=3 (except for 6% hydrogen peroxide, where n=1). The Log [total viable load] recovered from each coupon following addition of the test product was compared to a water control by 2-way ANOVA with Dunnett's correction for multiple comparisons. **62**

Figure 2.4: Validation of the neutralisation method used in antimicrobial suspension testing. Viable loads were recovered from suspensions after 5 minutes neutralisation of each test product,

followed by 30 minutes incubation with a validation suspension of each test organism. Validation was performed in duplicate; n=3. **65**

Figure 2.5: CDC Biofilm Reactor (CBR) apparatus used for continuously stirred chamber biofilm growth. **67**

Figure 2.6: Assembled CBR reactor chamber (left) and a single coupon-holding rod (left) with coupons and securing screws (reproduced from (BioSurface Technologies Corp, 2016)) **67**

Figure 2.7: Illustration of the collagen wound biofilm model, reproduced from (Slade et al., 2019), incorporating collagen-coated slides into the 6-channel drip flow reactor. **70**

Figure 2.8: Schematic of small-batch SBD PAW generation system, using high-powered 14kVpp input electrode, quartz layer dielectric, and aluminium mesh counter-electrode on the opposing face, to generate the plasma discharge layer. **72**

Figure 2.9: Schematic of SBD-plasma falling film system, including coaxial aligned cylindrical quartz tubing to channel water circulation, and to facilitate SBD-discharge at the inner surface of the larger of the two cylinders, forming across the mesh of the grounded electrode, thereby allowing plasma species to diffuse across the void between inner and outer quartz tubes to activate the falling film of water streaming down the outer surface of the inner quartz tube. **73**

Figure 2.10: Schematic of the Enviolyte generator used to generate ECAS, consisting of an electrochemical cell containing two chambers – one for the cathode (left), the other housing the anode (right), separated by an ion-permeable exchange membrane. Saline is pumped continuously from a supply tank into both chambers, and undergoes electrochemical activation when unipolar direct current is applied, resulting in the generation of catholyte and anolyte solutions, exiting the generator by separate conduits. **74**

Figure 2.11: Illustration of 24-well treatment plate and shielding Perspex template, enabling delivery of single-well NTP treatments of cell monolayers. **76**

Figure 2.12: Application of direct NTP treatments to cell cultures in 24-well plates prior to analysis of viability/ proliferation. **76**

Figure 2.13: CellTiter Glo assay: generation of the luminescent signal correlating to viable cell population catalysed by UltraGlo™ rLuciferin, supplied with cellular ATP released upon reagent-mediated cell lysis. **78**

Chapter 3:

Figure 3.1: Optical density to CFU/mL calibration for each of the ESKAPE species used. Mean total viable count was obtained at each adjusted optical density with OD600 by sampling each suspension and plating out, via spiral plating in triplicate or Miles and Misra plating in sextuplicate. The line of regression for each organism was plotted in GraphPad Prism, taking the corresponding mean viable count \pm SD for each optical density; n=3. **83**

Figure 3.2: Determination of the diameter of ZOI induced by increasing duration of NTP treatment. Exposures performed at approximately 10mm torch-target distance, in triplicate; n=3. Significance was determined by 2-way ANOVA with Tukey's correction for multiple comparisons, comparing ZOI diameter at sequential treatment times with that seen at 30s. Thresholds for significance were determined as: * p<0.05, ** p< 0.01, *** p<0.001, ****p<0.0001. **85**

Figure 3.3: Illustration of ZOIs resulting from NTP treatment of *S. aureus* ATCC 6538 lawns following increasing exposure times. Plates are shown in ascending order of duration of treatment: 30s (a), 60s (b), 120s (c), and 180s (d). **86**

Figure 3.4: Illustration of ZOIs resulting from NTP treatment of *A. baumannii* and *C. albicans* lawns following increasing exposure times. The inhibition of growth was observed to be more complete in some species, such as *A. baumannii* - images a) (30s) and b) (60s) - than in others, e.g. *C. albicans* - images c) (120s) and d) (180s) - where breakthrough colonies were visible, and/or the ZOI was less sharply demarcated. **87**

Figure 3.5: Viability of recovered 50 μ L inoculum after drying only (untreated), and after visible drying followed by sham treatment with H₂O (water treated), in comparison to the initial microbial load applied ('actual inoculum'), in *S. aureus* (left) and *P. aeruginosa* (right); n=3. Thresholds for significance were determined as: * p<0.05, ** p< 0.01, *** p<0.001. ****p<0.0001. **90**

Figure 3.6: Comparison of the applied versus recovered viable load on stainless steel surfaces, following inoculation and drying, using a standardised microbial load (10 μ L of a 50% 0.5OD600: 50% 0.6g/L BSA suspension, or for *C. albicans*, 50% 0.7OD600: 50% 0.6g/L BSA suspension). *E. coli* NCTC 13919 (carbapenem-resistant) was included in addition to non-resistant strain ATCC 10536, to allow within-species comparison with a more clinically-relevant strain. **91**

Figure 3.7: Time-course of extended drying of applied microbial inoculum on stainless steel, recovering the remaining viable load at time-points beyond 'visibly dry'. Stainless steel coupons were inoculated, allowed to visibly dry, and were subjected to extended drying for up to 30 minutes. n=3. **93**

Table 3.1: Energy delivered via the RF-NTP plasma system over a range of increasing exposure times, at 40W and 80W MW power settings, using 25% duty cycle (40ms ON: 160ms ON+OFF). **94**

Figure 3.8: Log reduction in *S. aureus* recovered load from stainless steel coupons following treatment with RF-MW NTP generated at either 40W MW or 80W MW power, or an argon-only control, comparing the two treatment power settings against a single control group. Treatments were performed in triplicate; n=3. Thresholds for significance were determined as: * p<0.05, **p< 0.01, *** p<0.001, **** p<0.0001. **94**

Figure 3.9: Log reduction in *S. aureus* viable recovered load from stainless steel surfaces following treatment with RF-MW NTP using 80W MW power, versus an argon-only control; test and control treatments performed in triplicate; n=3. Thresholds for significance were determined as: * p<0.05, ** p< 0.01, *** p<0.001, ****p<0.0001. **94**

Figure 3.10: Treatment time-course of NTP against *P. aeruginosa* on stainless steel carriers, showing corresponding mean Log reduction per coupon. Treatments were performed in triplicate and results presented as mean Log reduction (n=3). Multiple paired t-tests were performed, one per time-point, to determine significance. Thresholds for significance were determined as: * p<0.05, ** p< 0.01, *** p<0.001, ****p<0.0001. **96**

Figure 3.11: Treatment time-course of *S. aureus* on silicone rubber coupons, showing corresponding mean Log reductions per disc, with respect to untreated dried-only inoculum. Treatments were performed in triplicate, n=3. Multiple paired t-tests were performed, one per time-point, to test for significance. Thresholds for significance were determined as: * p<0.05, ** p< 0.01, *** p<0.001, ****p<0.0001. **98**

Figure 3.12: Treatment time-course of *S. aureus* treated with 3% or 6% H₂O₂ on stainless steel coupons, for contact times of 0-300s, showing corresponding Log reductions relative to the initial dried microbial load at T₀. Treatments were performed in triplicate; n=3. Significance was determined by two-way ANOVA with Tukey's multiple comparisons test. Thresholds for significance were determined as: * p<0.05, ** p< 0.01, *** p<0.001, **** p<0.0001. **100**

Figure 3.13: Treatment time-course of *S. aureus* treated with either 5% or 10% PVP-I on stainless steel surfaces, showing corresponding Log reductions relative to the initial dried microbial load at T₀. Treatments were performed in triplicate, n=3. Significance was determined by 2-way ANOVA with Tukey's correction for multiple comparisons, comparing Log reduction achieved with PVP-I to that seen with H₂O controls. Thresholds for significance were determined as: * p<0.05, ** p<0.01, *** p<0.001, ****p<0.0001. **101**

Figure 3.14: Treatment time-course with ECAS against *S. aureus* on stainless steel, showing corresponding Log reductions relative to the initial dried microbial load at T₀. Treatments

performed in triplicate, n=3. Significance was determined by multiple t-tests (one per time-point), with comparison to the Log change occurring in water controls. Thresholds for significance: *p<0.05, **p<0.01, ***p<0.001, ****p<0.0001. **102**

Figure 3.15: Log reduction in viable surface-associated *S. aureus* on stainless steel following treatment with plasma-activated solutions generated via RF-MW NTP exposure. Treatments were performed in triplicate; n=3. Significance was determined by 2-way ANOVA with Sidak's correction for multiple comparisons. Threshold for significance: p<0.05. **104**

Figure 3.16: Treatment time-course of surface-associated *S. aureus* on stainless steel, treated with PAW generated in small batches by an alternative SDB-NTP system. PAW was tested on the day of generation (d0) in triplicate; n=1. Significance was determined by 2-way ANOVA, with Sidak's test for multiple comparisons. Thresholds for significance were determined as: * p<0.05, ** p< 0.01, *** p<0.001, ****p<0.0001. **106**

Figure 3.17: Treatment of surface-associated *S. aureus* on stainless steel with PAW generated in small batches by an alternative, SDB-NTP system, tested 2 days post-generation, in triplicate; n=1. Significance was determined by 2-way ANOVA, with Sidak's multiple comparisons test. Thresholds for significance were determined as: * p<0.05, ** p< 0.01, *** p<0.001, ****p<0.0001. **106**

Figure 3.18: Log reduction in viable *P. aeruginosa* following suspension testing with PAW generated via small-batch SDB plasma system. Suspension treatments were carried out at 48h and 15 days after PAW generation, for a contact time of 300s, performed in triplicate; n=1. Significance was determined by 2-way ANOVA with Sidak's multiple comparisons test. Thresholds for significance were determined as: * p<0.05, ** p< 0.01, *** p<0.001, ****p<0.0001. **107**

Figure 3.19: Log viable *P. aeruginosa* and *S. aureus* recovered following suspension testing with large-batch SDB-PAW, applied to test surfaces for a contact time of 300s, performed in triplicate; n=3. Significance was determined by paired t-test. Threshold for significance: p<0.05. **109**

Figure 3.20: Log *P. aeruginosa* and *S. aureus* viable load recovered following extended exposure-time suspension testing with large-batch SDB-PAW. Treatments were applied for contact times of 300s – 30 minutes, and were performed in triplicate, n=1. Threshold for significance: p<0.05. **109**

Figure 3.21: Antimicrobial suspension testing performed against *P. aeruginosa* (a) and *S. aureus* (b) using a fixed contact time of 300s, applying treatments with 0.1% - 100% ECAS (200ppm FAC) and 5% PVP-I as a positive control; treatments performed in triplicate, n=3. Analysis was performed using 2-way ANOVA with Dunnett's test for multiple comparisons. Thresholds for significance were determined as: * p<0.05, ** p< 0.01, *** p<0.001. ****p<0.0001. **111**

Chapter 4:

Figure 4.1: Total biofilm density of single species *P. aeruginosa* NCIMB 10548 biofilms grown within the CBR on three different surface materials for 48 hours (Polycarbonate and silicone coupons, $n=9\pm SD$; steel coupons, $n=6\pm SD$). Mean recovered load per coupon was compared between materials by 2-way ANOVA with Tukey's test for multiple comparisons. Thresholds for significance: * $p<0.05$, ** $p<0.01$, *** $p<0.001$, **** $p<0.0001$. **118**

Figure 4.2: *P. aeruginosa* NCIMB 10548 biofilms grown for 48h within the CBR, whereby coupons were subsequently removed and subjected to either a 60s or 120s NTP treatment or a 30s PVP-I treatment, each performed in triplicate ($n=3$). Mean Log recovered load per coupon was compared between treatments by 2-way ANOVA with multiple comparisons. Thresholds for significance were determined as * $p<0.05$, ** $p<0.01$, *** $p<0.001$, **** $p<0.0001$. **120**

Figure 4.3: *S. aureus* ATCC 6538 biofilms grown for 48h within the CBR, whereby coupons were subsequently removed and subjected to either a 60s or 120s NTP treatment or a 30s PVP-I treatment, each performed in triplicate ($n=3$). Mean Log recovered load per coupon was compared between treatments by 2-way ANOVA with multiple comparisons. Thresholds for significance were determined as * $p<0.05$, ** $p<0.01$, *** $p<0.001$, **** $p<0.0001$. **121**

Figure 4.4: *P. aeruginosa* biofilms were grown to 48h within the CBR whereby coupons were removed and subjected to 300s treatment with either ECAS (200ppm FAC), 6% H_2O_2 , or PAW (each performed in triplicate, $n=3$). The mean Log recovered load per coupon was compared between treatments by 2-way ANOVA with Dunnett's multiple comparisons test. Thresholds for significance were determined as * $p<0.05$, ** $p<0.01$, *** $p<0.001$, **** $p<0.0001$. **122**

Figure 4.5: Mean biofilm density of *P. aeruginosa* biofilms cultured within the DFR – collagen matrix model, comparing growth at 48h and 72h in two strains, with reference to previously published ('standardised') data (Slade et al., 2019) obtained using the clinically-associated strain, NCIMB 10548. Mean CFU/ slide per time-point was compared, for within-strain and inter-strain differences, using Mixed Effects analysis, with Sidak's test for multiple comparisons; $n=3$. Significance thresholds were determined as * $p<0.05$; ** $p<0.01$; *** $p<0.001$, **** $p<0.0001$. **124**

Figure 4.6: *P. aeruginosa* NCIMB viable load recovered from full slide biofilms and coverslip-adherent biofilms cultured to 48h within the DFR-collagen matrix model, subjected to single immersion treatments. Log CFU/coverslip was compared between treatments using one-way ANOVA with Dunnett's multiple comparison test. Log CFU/full slide were compared by unpaired t-test. Biofilms were sampled in triplicate; $n=3$ coverslip biofilms; $n=2$ full slide control; $n=1$ full-slide

PAW treatment. Significance thresholds were determined as * $p < 0.05$; ** $p < 0.01$, *** $p < 0.001$, **** $p < 0.0001$. **127**

Figure 4.7: Viable load recovered from *P. aeruginosa* NCIMB 10548 biofilms adherent to 13mm diameter coverslips, cultured for 48h within the DFR-collagen matrix model, subjected to three repeat ECAS treatments via continuous instillation, with intervening re-feed periods of 1hr; $n=4$ per treatment group, sampled in triplicate. a) Recovered load per coverslip, shown; i-iv denote the descending order down the length of the slide; b) Mean recovered load per treatment group, shown. Comparisons by ordinary one-way ANOVA, with thresholds for significance: * $p > 0.05$, ** $p < 0.01$, *** $p < 0.001$, **** $p < 0.0001$. Significant differences stated within the text. **130**

Figure 4.8: Viable load recovered from coverslip-adherent *P. aeruginosa* biofilms grown to 48h within the DFR-collagen matrix model, subjected to up to three repeat ECAS treatments via continuous instillation, with intervening re-feed periods of 1hr. Treatments were performed in quadruplicate, $n=1$. Significant differences were determined by two-tailed unpaired t-test (treatment versus control), and one-way ANOVA with multiple comparisons (single versus repeat treatment, within-group). Significance thresholds were determined as: * $p < 0.05$, ** $p < 0.01$, *** $p < 0.001$, **** $p < 0.0001$. **131**

Chapter 5:

Figure 5.1: 96h growth curves of H103 (left panel) and A375 (right panel) epithelial cell lines, assessed by TBDE, to determine PD rate. Cells were cultured in triplicate wells to determine mean cell count per time-point \pm SD; $n=3$. Simple linear regression performed on GraphPad Prism. **140**

Figure 5.2: ECAS (200ppm) dose-response in H103 cells, over treatment periods of 24h (left) ($n=3$) and 48h (right) ($n=2$), determined by viable cell count using TBDE. Treatments were applied to 70% confluent cultures, 1:1 with complete culture medium in 24-well plates, to give the final 'in-well' concentrations shown. Viability was determined by dissociation and resuspension of cells for TBDE enumeration, expressing viability at % of untreated control viability (values represent mean \pm SD). **142**

Figure 5.3: Non-linear regression of Log[inhibitor] versus response (variable slope, four parameters), obtained following 24h and 48h treatment of H103 with ECAS (200ppm), determining residual viability via TBDE count, results plotted using GraphPad Prism. Treatments were performed in triplicate; $n=3$ for 24h treatments, $n=2$ for 48h treatments. **143**

Figure 5.4: Hydrogen peroxide dose-response curve performed on H103, using Cell TiterGlo assay to evaluate viability relative to PBS-treated controls. Treatments performed in triplicate, plotting mean % viability \pm SD; $n=3$. **144**

Figure 5.5: Treatment time-course of direct NTP application to H103 (left) and A375 (right) cells, assessed via CellTiter Glo 2.0 luminescent assay at 24h post-treatment; treatments were performed in triplicate; n=2 for H103, n=3 for A375. **145**

Figure 5.6: Calibration of cell density versus absorbance at 492nm using MTS-PMS metabolic activity assay, for quantification of viable cell population of H103 (left) and A375 (right). Standard cell suspensions were prepared by dilution from a concentrated starting suspension in phenol-red- and FBS-free medium, incubated with MTS-PMS reagent and the coloured product formed was measured by absorbance, in triplicate wells; n=3 for H103, n=4 for A375. **147**

Figure 5.7: Treatment time-course of direct NTP application to H103 cells at 24h post-treatment, assessed via MTS-PMS colorimetric assay; treatments were performed in triplicate, and the effects on viability assessed by 2-way ANOVA n=4. **148**

Figure 5.8: Post-treatment growth course of H103 cells from 0 -72h, following 0-90s direct NTP treatments, versus time-matched argon control. Percentage confluence was determined through Incucyte Live Cell analysis, performed in triplicate. Graphed values represent mean % confluence \pm SD; n=3. Two-way ANOVA with multiple comparisons was applied to determine significance relative to untreated controls, and multiple paired t-tests applied between NTP- and argon-control groups. **150**

Figure 5.9: Image snapshots of H103 cells following no treatment (top), 30s argon control (middle), and 60s direct NTP (bottom), acquired at 10x magnification using Incucyte® Live Cell imaging analysis. **154**

Figure 5.10: 72h post-treatment growth course of A375 cells following 0-90s direct NTP treatments, versus time-matched argon controls. Percentage confluence was determined through Incucyte® Live Cell analysis, performed in triplicate. Graphed values represent mean % confluence \pm SD; n=3. Two-way ANOVA with multiple comparisons was applied to determine significance relative to untreated controls, and multiple paired t-tests used to compare cultures treated in complete-medium versus serum-free. **156**

Figure 5.11: Image snapshots of A375 cells following no treatment (top), 30s argon control (middle), and 60s direct NTP (bottom), acquired at 10x magnification using Incucyte® Live Cell imaging analysis. **158**

Figure 5.12: Dose-response curve for PVP-I treatment of H103 cells over a 24-h treatment period, assessed via CTG2.0 (left), and by MTS-PMS (right). Doses shown represent the final PVP-I concentration after adding in a 1:1 ratio to standard culture medium. **161**

Figure 5.13: Dose-response curve for ECAS treatment of H103 cells over a 24h period, assessed via CTG2.0 assay (left), and MTS-PMS (right). Doses shown represent Log₁₀ of the final ECAS concentration, after adding in 1:1 ratio with standard cell culture medium. **162**

Figure 5.14: Dose response curve for PVP-I treatment of A375 cells over a 24h period, assessed via CTG2.0 (left) and by MTS-PMS assay (right). Doses shown represent Log₁₀ of the final PVP-I concentration, after adding in 1:1 ratio with standard cell culture medium. **163**

Figure 5.15: Dose response curve for ECAS treatment of A375 cells over 24h, assessed by CTG 2.0 assay (left) and MTS-PMS (right). Doses indicate Log₁₀ of the final ECAS concentration, after adding in 1:1 ratio with standard cell culture medium. **164**

Table 5.1: Summary of the IC₅₀ of ECAS and PVP-I in H103 and A375 cell lines, as determined by CellTiter Glo2.0 and MTS-PMS assay; values were derived from non-linear regression (Log₁₀[inhibitor] vs response – variable slope, four-parameter). IC₅₀ doses are quoted with 95% confidence intervals, following n=3 dose-response assays, performed in triplicate for each cell line. **164**

Figure 5.16: 48h treatment time-course of H103 treatments with either plasma-activated medium (PAM) or plasma-activated PBS (pPBS). Treatments were added to cells at T₀ and replaced at respective time-points with control media during the remaining culture period, to 48h. Treatments were performed in triplicate, n=1. **166**

Figure 5.17: 72h growth course of H103 cells treated with 120s or 300s plasma-activated PBS (pPBS). Cell cultures were seeded in either complete (comp) or serum- and phenol red-free (SF) culture medium, to which pPBS or non-activated PBS (control) was added in an equal volume. Incucyte[®] Live Cell Analysis was used for quantification of mean % confluence, using 9 FOV per well, from treatments applied in triplicate. Percentage confluence between group was compared at 6-hourly intervals by 2-way ANOVA with multiple comparisons, using Dunnett's correction; n=3. **167**

Figure 5.18: 72h growth course of H103 cells treated with 120s or 300s plasma-activated medium (PAM). Cell cultures were seeded in either complete (comp) or serum- and phenol red-free (SF) medium, to which PAM or non-activated SF medium (control) was added in 1:1 ratio. Mean % confluence was calculated from triplicate wells, each imaged using Incucyte[®] Live Cell Analysis using 9 FOV, analysed by 2-way ANOVA with Dunnett's correction for multiple comparisons, at 6-hourly intervals. **169**

Figure 5.19: 72h growth course of A375 cells treated with 120s or 300s plasma-activated PBS (pPBS). Cell cultures were seeded in either complete (comp) or serum- and phenol red-free (SF) culture medium, to which pPBS or non-activated PBS (control) was added in an equal volume, **21**

treating in triplicate. Incucyte® Live Cell Analysis was used for quantification of mean % confluence, using 9 FOV per well, analysed by 2-way ANOVA with Dunnett's correction for multiple comparisons, at 6-hourly intervals; n=3. **170**

Figure 5.20: 72h growth course of A375 cells treated with 120s or 300s plasma-activated medium (PAM). Cell cultures were seeded in either complete (comp) or serum- and phenol red-free (SF) culture medium, to which pPBS or non-activated PBS (control) was added in an equal volume, to triplicate wells. Incucyte® Live Cell Analysis was used for quantification of mean % confluence, using 9 FOV per well. Analysis of measurements at 6-hourly intervals was performed by 2-way ANOVA with Dunnett's correction for multiple comparisons; n=3. **171**

Abbreviations and acronyms

AGE	Advanced glycation end-products
ANOVA	Analysis of variance
ATCC	American type culture collection
ATP	Adenosine triphosphate
BMI	Body mass index
BSA	Bovine serum albumin
BS EN	British standard – European standard
BSI	British standards institute
CBR	Center for Disease Control Biofilm Reactor®
CFU	Colony-forming units
CSLM	Confocal laser scanning microscopy
CTG2.0	CellTiter Glo 2.0
DBD	Dielectric barrier discharge
DFU	Diabetic foot ulcer
DMEM	Dulbecco's modified Eagles medium
ECCAC	European collection of authenticated cell cultures
ECAS	Electrochemically-activated solution
ECM	Extracellular matrix
EDTA	Ethylenediamine tetra-acetic acid
EPS	Extracellular polymeric substances
EN	European standard
ESKAPE	<i>Escherichia coli</i> , <i>Staphylococcus aureus</i> , <i>Klebsiella pneumoniae</i> , <i>Acinetobacter baumannii</i> , <i>Pseudomonas aeruginosa</i> , and <i>Enterobacter spp.</i> pathogens
FAC	Free available chlorine
FBS	Foetal bovine serum
HAI	Healthcare-associated infection/ hospital-acquired infection
H ₂ O ₂	Hydrogen peroxide
HOCl	Hypochlorous acid
ID	Inner diameter
IPC	Infection prevention and control
LPS	Lipopolysaccharide

MDR	Multi-drug resistant
MMP	Matrix metalloproteinase
MOPS	3-(N-Morpholino)propanesulfonic acid, C ₇ H ₁₅ NO ₄ S
MW	Microwave
MTS	3-(4,5-dimethylthiazol-2-yl)-5-(3-carboxymethoxyphenyl)-2-(4-sulfophenyl)-2H-tetrazolium
NCIMB	National Collection of Industrial, Food, and Marine Bacteria
NCTC	National Collection of Type Cultures
NSAID	Non-steroidal anti-inflammatory
NTP	Non-thermal plasma
OD	Optical density
ORP	Oxidation – reduction potential
PAA	Peracetic acid
PAL	Plasma-activated liquid
PAM	Plasma-activated medium
PAS	Plasma-activated solution
PAW	Plasma-activated water
PBS	Phosphate-buffered saline
PDT	Population doubling time
PET	polyethylene terephthalate
PHMB	polyhexamethylene biguanide
PMS	phenazine methosulfate
PVP-I	Polyvinylpyrrolidone-iodine
QAC	Quaternary ammonium compound
RAGE	Receptor for advanced glycation end-products
RF	Radiofrequency
RO(N)S	Reactive oxygen (and nitrogen) species
SBD	Surface barrier discharge
SDA	Sabouraud's dextrose agar
SEM	Scanning Electron Microscopy
SF	Serum-free
Slm ⁻¹	Standard litres per minute
TBDE	Trypan Blue Dye Exclusion

TGF	Transforming growth factor
TNF	Tumour necrosis factor
TSA	Tryptone soya agar
TSB	Tryptone soya broth
UV	Ultra-violet
WHO	World Health Organisation
ZOI	Zone of inhibition

Chapter 1: Introduction

1.1 Non-thermal plasma: sources and applications

Plasma is the fully or partially ionised state produced by excitation of a gas, creating a profusion of reactive species in ground, excited and metastable states, as well as charged particles, photons in both UV and visible ranges, and electromagnetic fields. Plasma occurs in nature, for example, in the aurora borealis, lightning during electrical storms, and in the sun and stars (Dobrynin *et al.*, 2009; Von Woedtke *et al.*, 2019; Busco *et al.*, 2020). Artificially generated plasmas can be produced by exposing an inert gas to an applied energy source, such as electrical, radiofrequency, or microwave, with the precise profile of plasma species formed being dependent on both the gas, and the system parameters used for generation (Dobrynin *et al.*, 2009; Scholtz *et al.*, 2015; Katsigiannis, Bayliss and Walsh, 2021).

Plasma may be termed thermal or non-thermal, depending on its temperature at generation. In the production of thermal or 'hot' plasma, thermal energy is transferred equally between electrons and heavy particles, thus raising the plasma temperature to thousands of Kelvins (Dobrynin *et al.*, 2009; Scholtz *et al.*, 2015; Gupta and Ayan, 2019; Busco *et al.*, 2020). Thermal plasma often requires high pressure generation systems, and is used in industrial processes such as cutting hard materials, breaking down toxic waste, and other applications (Gupta and Ayan, 2019; Busco *et al.*, 2020). By contrast, non-thermal plasma (NTP) demonstrates a state of thermodynamic disequilibrium, since thermal energy transfer occurs much more rapidly to the electrons than to the ions and neutrons of the plasma, resulting in a far smaller temperature increase overall, which does not typically exceed the range of 300 – 400K (40°C at most) (Babaeva and Naidis, 2018; Privat-Maldonado *et al.*, 2019; Šimončicová *et al.*, 2019). NTP thus comprises a highly reactive mixture of charged and neutral species, energised electrons, photons, and generated space-charge electric fields, which, despite their low temporal stability (typically up to 10ns), can initiate a complex chain of chemical reactions, leading to a plethora of physicochemical effects on target materials within the direct path of the plasma (Dobrynin *et al.*, 2009; Chen *et al.*, 2014; Šimončicová *et al.*, 2019; Feibel *et al.*, 2023).

1.1.1 Plasma applications in biomedicine

In recent decades, the potential for developing NTP technologies for application within the biomedical field has gained significant interest, and research into the biological responses elicited by NTP interactions is continuing to gain momentum. Not only has NTP been demonstrated to exert powerful antimicrobial activity, it has also been reported to induce apoptosis in cancer cells, and to enhance healing mechanisms in wound models, both *in vitro* and *in vivo* (Mai-Prochnow *et al.*, 2014; Kaushik *et al.*, 2018; Metelmann, von Woedtke and Weltmann, 2018; Von Woedtke *et al.*, 2019; Busco *et al.*, 2020; Poramapijitwat, P, *et al.*, 2020). However published findings in these

areas exhibit considerable variability, and NTP generation systems are equally diverse in their design and conformation, which limits the comparability of studies issuing from different groups (Haertel *et al.*, 2014; Gilmore *et al.*, 2018; Šimončicová *et al.*, 2019).

Research harnessing the biological effects of NTP for biomedical applications has tended towards generation systems taking the form of plasma jets, plasma ‘needles’ (which enable more precise application of the plasma, with very fine resolution), or Dielectric Barrier Discharge (DBD) systems, in which the plasma discharge forms upon the dielectric surface, the size of which can be adapted to suit the requirements of the application. Although hybridised systems, and specialised micro-plasma generation configurations are emerging ever more frequently, through plasma engineering innovation, plasma discharges used in healthcare applications are largely generated via atmospheric pressure plasma jet (APPJ) or DBD, since the typical system geometry and characteristics are easily applicable for surface treatments (Weltmann *et al.*, 2009; Bourke, *et al.*, 2017). Surface Barrier Discharge (SBD) plasmas constitute a specialised sub-group of DBDs in which both the high voltage and ground electrode are placed in contact with the same dielectric, allowing efficient plasma-gas activation along the dielectric surface (Bednar, Matovic, and Stojanovic, 2013; Brandenburg, 2017).

The use of plasma-based technologies as clinical tools, particularly within the context of antimicrobial therapy, and also in cancer treatment, has opened up new avenues for the application of both direct and indirect non-thermal plasma. Termed ‘plasma medicine’ (Von Woedtke *et al.*, 2019; Plattfaud, Besser, Severing, *et al.*, 2021), this novel discipline offers potential benefits for manipulating biological pathways to achieve positive clinical outcomes, using NTP as an adjuvant or primary therapy in cases where alternative options have proven inadequate or ineffective.

1.2 Antimicrobial resistance and the development of new interventions:

The targeting of microbial biofilms represents one particularly attractive application for NTP in biomedicine, since the mechanisms by which NTP disrupts biofilms and damages the resident microorganisms are thought to act via alternative pathways to those exploited by currently available antibiotics and biocidal products. Due to the alarming increase in the emergence of antimicrobial resistance (AMR) and the loss of efficacy of antibiotics of last resort (Mohapatra, Dwibedy and Padhy, 2021), the development of new and highly effective antimicrobial technologies for both cleaning and disinfection practices, but also for therapeutic applications, is of paramount importance. Innovative solutions are needed now, more than ever before, to combat microbial contamination within the clinical environment, and to limit the spread of infection from reservoirs such as invasive medical devices and re-useable medical instruments

which fail to undergo adequate decontamination during reprocessing (Alkawareek *et al.*, 2012; Ofstead *et al.*, 2015; Percival, Suleman, *et al.*, 2015; Gupta and Ayan, 2019).

Microbial resistance was first reported in the mid-20th century, within only a few decades of the advent of clinical antibiotic use, and the “antibiotic golden age” (Lebeaux, Ghigo and Beloin, 2014; Ventola, 2015). Increasing antibiotic usage within primary and secondary healthcare settings, but also within veterinary and the agri-food sectors, leads to the frequent exposure of a range of pathogenic organisms to antimicrobial therapies, and as such, favours the development of AMR by selective pressure. Repeated contact with sub-inhibitory concentrations of antibiotics, and the presence of multiple pathogenic species and strains within a fixed environment permits microbial adaptation, and the development of resistance genes which can rapidly be exchanged between organisms (Boucher *et al.*, 2009; Holmes *et al.*, 2016).

Besides the rapid adaptation of microbes to antibiotics and biocides, and the acquisition of resistance genes via horizontal transfer, numerous societal factors have accelerated the spread of AMR, including:

- inappropriate prescribing and consumption of antibiotics, often reflecting inadequate diagnostic procedures, suboptimal dosing (including via low-quality medicines) and poor patient compliance with prescribed regimens;
- prophylactic use in animals, particularly via mass administration;
- transmission within food products;
- transmission via wastewater processing and pharmaceutical industrial plants;
- international travel and trade;

(Holmes *et al.*, 2016; O’Neill, 2016; Shrestha *et al.*, 2018)

Therefore, rising rates of AMR may be attributed to inconsistencies in clinical usage of antimicrobial agents and medications, but also due to the prevalence of antibiotic supplementation in farm animal feeds, and contamination of the food chain and watercourses stemming from pharmaceutical and healthcare waste and agricultural applications, from which both antibiotic residues and resistance genes may be disseminated (Fletcher, 2015; Holmes *et al.*, 2016). Challenges also lie in controlling the sale and procurement of antibiotics and products containing bactericidal compounds, which may be more readily accessible through unregulated trade pathways, internationally, thus risking inappropriate and potentially dangerous use (Sifri, *et al.*, 2019; Tang, Miller and Moore, 2023).

AMR has, in recent years, generated rising concern across the scientific and clinical sectors, and also from governing authorities, as it poses an increasing global health risk whereby the decline in the breadth of efficacy of existing antibiotics leaves prescribing clinicians with only a limited range

of therapeutics for the treatment of patients suffering with infections involving AMR pathogens (Holmes *et al.*, 2016; Meade, Slattery and Garvey, 2021; Mohapatra, Dwibedy and Padhy, 2021; WHO, 2021). Microbial resistance against antiseptics and biocides is now also being reported, meaning that decontamination practices must be monitored and adjusted accordingly to prevent current agents from becoming redundant due to loss of microbial susceptibility (Maillard, 2005; Meade, Slattery and Garvey, 2021; Pereira, Wang, and Tagkopoulos, 2021; Maillard and Pascoe, 2024)

Various mechanisms of microbial resistance have been identified, with the four main strategies being: modification of the microbial cellular target (for instance alteration of a key enzyme), increased drug efflux (thus lowering the effective concentration), inactivation of the drug by the microorganism (via enzymatic action), or the activation of protective responses (such as the expression of DNA-binding proteins) (Blair *et al.*, 2015; Holmes *et al.*, 2016). Resistance may occur naturally within a microbial species, i.e. intrinsic resistance, even if it has never been exposed to the microbicidal agent in question; or alternatively it may arise through selective pressure as a novel characteristic, through mutation or uptake of exogenous DNA conferring a survival advantage, i.e. acquired resistance (Holmes *et al.*, 2016; Handorf *et al.*, 2018; Maillard and Pascoe, 2024).

Inappropriate choice of antimicrobial agent, or incorrect application - for example, administration at ineffective concentrations, or for insufficient contact times - may provoke the development of resistance by activating stress responses in the pathogen without inducing absolute elimination of the infection (Holmes *et al.*, 2016; Maillard and Pascoe, 2024). Resistance genes may be rapidly transferred within and between species, potentially leading to uncontrolled outbreaks of infection, and dissemination to other environments/ hosts, as well as increasing the risk of cross-resistance developing to other, unrelated compounds, and the emergence of multi-drug resistance (MDR) (Holmes *et al.*, 2016; Maillard, Kampf and Cooper, 2021; Maillard and Pascoe, 2024). Cases of microbial resistance have been noted with commonly applied compounds including chlorhexidine, quaternary ammonium compounds (QACs), triclosan and other phenolics (Maillard, Kampf and Cooper, 2021; Maillard and Pascoe, 2024), demonstrating the phenotypic adaptation of which microorganisms are capable when placed under selective pressure.

A surveillance programme was introduced by the WHO in 2015, to gain a more accurate understanding of the rate of AMR spread and the scale of the problem, globally, whilst also importantly underlining the severity and implications of this issue on the global stage (WHO, 2020). The need for improved surveillance, reporting and responsiveness regarding the rates of AMR infections has subsequently been acknowledged in many countries with the instigation of formalised processes and standards for the monitoring of antibiotic use and AMR detection,

education and training in the disciplines of infection control and antimicrobial stewardship, and measurement of the effectiveness of interventions (O'Neill, 2016; Tacconelli *et al.*, 2018). The extra healthcare costs associated with AMR worldwide have been estimated as being in the region of \$1 billion, whilst GDP losses attributable to AMR amount to as much as \$3 trillion (Naylor *et al.*, 2018; Shrestha *et al.*, 2018), underlining the catastrophic consequences wrought by AMR infections, in economic as well as humanitarian terms. Such exorbitant costs are clearly even more devastating to developing countries whose healthcare infrastructure and economic status are less able to absorb the impacts of widespread uncontrolled transmissible disease (Allegranzi *et al.*, 2011; World Health Organisation, 2011).

The declining rates of novel antibiotic development, and the need to preserve the efficacy of existing treatments further add to the urgency with which alternative solutions for the management of infections must be sought. A combined therapy approach, exploiting the complementary modes of action of NTP together with other antimicrobial treatments, could improve patient outcomes by more effectively targeting recalcitrant infection via synergistic pathways, reducing net microbial bioburden. In the case of chronic wounds, this could facilitate progression through the normal phases of healing (Von Woedtke *et al.*, 2019; Lou *et al.*, 2020; Choi, Uhm and Kaushik, 2021; Khosravi, S, Jafari, A, Zamani, H, Nilkar, 2022), and help to limit wound microbial load to a level at which pharmacological interventions, and standard wound management measures were sufficient to restore the wound microenvironment to a state at which the normal healing process could resume.

1.3 Healthcare-associated infections and chronic wounds: the scale of the problem

Healthcare associated infections (HAIs) are a significant concern within the health service sector, occurring as a direct result of service-users receiving a healthcare intervention, including medical care or surgical procedures, or subsequent to contact with a healthcare setting. Also described as nosocomial infections, HAIs are defined as transmissible illnesses appearing within 2 days of hospital admission, within 3 days of discharge, or during the 30 days after having received a healthcare intervention (Boev and Kiss, 2017; Alamer *et al.*, 2022). For patients already experiencing an underlying health condition, the development of HAI may rapidly lead to further medical deterioration, complications, and delayed recovery, whilst secondary transmission to carers or family members presents further risks, spreading the infection to new hosts. Worryingly, the involvement of MDR strains in HAIs is high, with an estimated 15.5% of hospital-acquired infections attributed to these pathogens, globally (Mulani *et al.*, 2019).

HAIs originating from care given within the NHS are estimated to affect 300 000 patients annually, with a prevalence of 6.4% in English hospitals cited in 2011 (Public Health England, 2012). Point-prevalence survey results from a UK Government survey at this time identified the most prevalent

HAIs as including respiratory infections (22.8%), urinary tract infections (17.2%), and surgical site infections (15.7%). HAIs can negatively impact the quality of life and health status of both the healthy population and those suffering comorbidities, compromising patient safety and placing additional demand on NHS resources. Methicillin-resistant *Staphylococcus aureus* (MRSA) bloodstream infections and *Clostridium difficile* infections account for a large proportion of HAIs, but improvements in infection prevention and control practices (IPC) have brought about reductions in these infections (Maillard and Pascoe, 2024)

Despite increases in awareness of the risks associated with HAI, and in the stringency of IPC measures, rates of HAIs remain alarmingly high, with 2011 estimates issued by the WHO of 4.5 million cases and 37000 deaths annually attributable to HAI in Europe, and respective figures for the USA of 1.7 million cases, and 99000 deaths. These statistics likely underestimate the current severity of the situation, and in developing countries where rates of reporting and access to appropriate medicines are more variable, the prevalence of HAI is likely to be higher still (WHO, 2016; Shrestha *et al.*, 2018). Further quality improvements are called for, however, to further address the continuing issue of HAIs and chronic wounds relating to in-patient hospital care, the costs of which are substantial, and likely to increase in the imminent future, due to the increasing older population in whom chronic wounds are more prevalent (Järbrink *et al.*, 2016; Olsson *et al.*, 2019; Manoukian *et al.*, 2021).

Amongst the microbial species of highest concern are the ESKAPE pathogens, which are recognised as most commonly responsible for HAIs, and amongst which rising rates of MDR and increased virulence have been reported (Boucher *et al.*, 2009; Mulani *et al.*, 2019). The ESKAPE pathogens comprise *Enterococcus faecium*, *Staphylococcus aureus*, *Klebsiella pneumoniae*, *Acinetobacter baumannii*, *Pseudomonas aeruginosa*, and *Enterobacter* species, and have been cited as the most costly causes of infection in terms of both treatment and care expenditure, and also in rates of mortality (Founou, Founou and Essack, 2017). The mechanisms of AMR development in the ESKAPE pathogens align with the principal resistance mechanisms previously mentioned, occurring either via drug inactivation (typically via enzymatic cleavage), modification of the target binding-site, or reduced drug concentration at the target due to either enhanced efflux of the agent, or reduced permeability within the target organism (Santajit and Indrawattana, 2016).

Although the ESKAPE species are acknowledged major pathogenic determinants of HAIs, and also frequently demonstrating resistance to biocides as well as antibiotics (Shrestha *et al.*, 2018; Mulani *et al.*, 2019; Meade, Slattery and Garvey, 2021), more recent assessment of the predominant antibiotic resistant bacterial species has led to the publication of the WHO Bacterial Priority Pathogens List (BPPL) 2024, a synthesis of global data on the AMR bacterial phenotypes

posing the greatest threat to public health based on a multi-criteria decision analysis (MCDA) assessment method (WHO, 2024). This comprehensive analysis considered not only the incidence, mortality and non-fatal health-burden associated with each AMR pathogen, but additional indicators including trend of resistance, transmissibility, preventability in healthcare and community settings, treatability and the number of potential therapies in the development pipeline. The report stratifies 15 families of antibiotic-resistant pathogens into critical, high, or medium priority categories, depending on their burden of infection and the public health risk posed by each. Amongst the pathogens of greatest concern were carbapenem-resistant *Acinetobacter baumannii*, *Enterobacteriales* species (such as *E.coli* and *K. pneumoniae*) demonstrating resistance to third generation cephalosporins or to carbapenem, and rifampicin-resistant *Mycobacterium tuberculosis*, whilst other organisms within the ESKAPE group, such as *E. faecium* (vancomycin-resistant), MRSA, and *P. aeruginosa* (carbapenem-resistant) were classified as high priority. Therefore, as the 2024 BPPL report articulates, it is vital that ongoing surveillance, recording and data-sharing are maintained and regularly updated, in order to gauge changes in the trends of AMR incidence, distribution and specific antibiotic-pathogen resistance phenotypes. Regional epidemiological differences, as well as variability in the burden of bacterial infectious diseases and the availability of standard and alternative treatments, also must be taken into account as important determinants of human and economic cost, and therefore risk priority level, incurred with AMR pathogens.

1.4 Pathophysiological events in wound repair: skewing of healthy healing processes and the impacts of chronic wound biofilms:

1.4.1 Resolution of wounding in healthy tissues:

Wound healing involves a series of complex physiological processes, occurring in co-ordinated and progressive sequence to restore structural and functional integrity to the damaged tissue or organ. Typically, these stages will entail haemostasis with the formation of a fibrin clot, closely followed by an inflammatory response, and subsequent cellular migration and proliferation, with the deposition of extracellular matrix (ECM) and tissue remodelling taking place to enable scar formation, and ultimately, wound closure (Atiyeh, Dibo and Hayek, 2009; Eming, Martin and Tomic-Canic, 2014). These stages will be briefly outlined here.

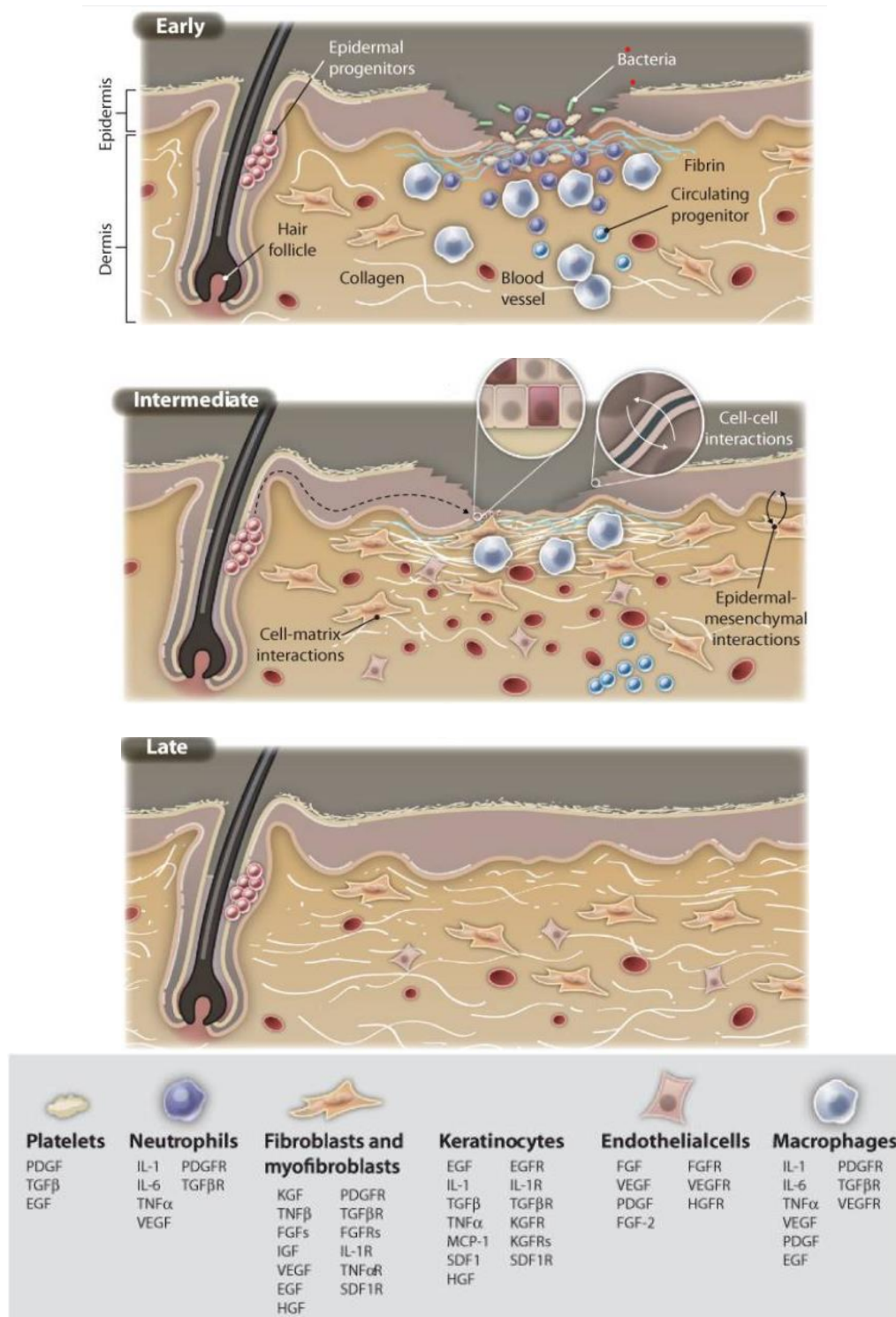


Figure 1.1: Typical wound repair events within a healthy (healing) wound (reproduced from (Eming, Martin and Tomic-Canic, 2014)). Initial breach of the epidermal/ dermal barrier prompts activation of the clotting cascade and haemostasis. The fibrin clot formed creates a protective seal and a scaffold via which infiltrating inflammatory cells are drawn to the wound (top). Inflammatory phase entails the activation of local and systemic effector mechanisms, serving to clear nonviable tissue and pathogens from the wound, and stimulating ECM synthesis and angiogenesis via the release of growth factors (centre). Proliferative phase follows, with the migration and proliferation of epidermal and dermal progenitor cells (centre), the induction of angiogenesis and vascularisation, and the formation of granulation tissue by fibroblasts, replacing the original fibrin clot. In late healing, remodelling of the ECM is completed, scar tissue is formed and carrier function is restored (bottom). Box: cell types and their secreted factors.

A breach in the epidermis, due to wounding, exposes the underlying dermis to microbial contamination, from resident skin flora and microorganisms from the external environment (Figure 1.1, top). The initial inflammatory phase occurs soon after injury, establishing haemostasis to prevent excessive bleeding, whilst also removing devitalised tissue and clearing invading pathogenic microorganisms from the site (Han *et al.*, 2011; Eming, Martin and Tomic-Canic, 2014). Clotting occurs via platelet adhesion, activation and aggregation to form a thrombus, and also via the activation of fibrinogen to fibrin, causing polymerisation into a matrix which maintains haemostasis and serves as a scaffold for inflammatory cells attracted to the wound site (Figure 1.1, top). Neutrophils are drawn to the wound site by chemical signals, including tumour necrosis factor- α (TNF- α), interleukin-1 (IL-1), platelet-derived growth factors, and microbial endotoxins such as lipopolysaccharide (LPS). Early wound-healing involves cross-talk between the different cell types within the skin tissue compartment, with the activation of keratinocytes and inflammatory cells, particularly neutrophils, and the release of important growth factors from the platelets trapped within the thrombus (Demidova-Rice, Hamblin and Herman, 2012; Eming, Martin and Tomic-Canic, 2014). Cell debris and invading microorganisms are eliminated from the injury site via phagocytosis, performed by macrophages and neutrophils, which also release an array of growth factors, pro-inflammatory chemokines and cytokines to promote successful progression towards the next stage of healing, and ECM synthesis (Eming, Martin and Tomic-Canic, 2014; Boothby, Cohen and Rosenblum, 2020; Knoedler, *et al.*, 2023). The release of antimicrobial peptides, reactive oxygen species (ROS), and proteases by activated neutrophils supports these processes by efficiently destroying any remaining pathogens and degrading necrotic material, optimising conditions for the initiation of connective tissue repair. Regulatory T-cells are also critical during inflammatory phase, playing a key role in both the immediate post-injury response, and the termination of inflammation, regulating the immediate immune response, and also mediating tissue reparative processes (Boothby, Cohen, and Rosenblum, 2020; Knoedler, *et al.*, 2023).

The intermediate healing phase sees the formation of granulation tissue, recruitment and proliferation of connective tissue cells and commencement of re-epithelialisation, in which keratinocytes at the wound edges begin migration across the wound site, restoring epidermal integrity (Figure 1.1, centre). There is proliferation and migration of epidermal progenitor cells to the injury site, with keratinocytes and fibroblasts interacting with the preliminary fibrin-based matrix, and depositing new ECM to create granulation tissue, principally composed of type III collagen, fibrin, fibronectin and hyaluronic acid, in place of the former provisional fibrin matrix (Eming, Martin and Tomic-Canic, 2014; Boothby, Cohen and Rosenblum, 2020; Knoedler, *et al.*, 2023). Granulation tissue serves as a network by which progenitor cells can navigate the wound-bed, undergoing differentiation and gradually restoring the full array of functional cell types.

Angiogenesis and vasculogenesis ensure adequate perfusion of newly regenerated tissue, supplying the expanding population of cells at the wound repair site with nutrients and oxygen. Abundant myofibroblasts also migrate to the wound bed, in preparation for wound contraction.

The late stage of wound-healing entails remodelling of the ECM where the granulation tissue matrix is replaced with a type I collagen network forming mature scar tissue, via the action of the proliferating fibroblast population (Figure 1.1, bottom). Specialised myofibroblasts expressing α -smooth muscle actin initiate wound closure in response to a number of signals, including tissue tension and the presence of certain matrix component proteins, as well as TGF- α , deploying contractile mechanisms via interactions with cytoskeletal- and matrix-associated receptors (Demidova-Rice, Hamblin and Herman, 2012; Wilkinson and Hardman, 2023). Reorganisation of the ECM is achieved through carefully orchestrated cycles of synthesis and degradation, regulated by stromal cell- and fibroblast-dependent mechanisms, and the activity of matrix metalloproteinases (MMPs). Once scar formation is complete, apoptosis of fibroblasts is initiated, granulation tissue blood vessels regress, and immune cell numbers are depleted, and remodelling therefore ceases (Figure 1.1, bottom).

1.4.2 Failure to heal: a self-perpetuating state of dysregulation

Chronic wounds exhibit a number of functional aberrations, including elevated levels of proinflammatory cellular infiltrate, predominantly comprising neutrophils and macrophages, and in turn, disproportionate expression of major proinflammatory cytokines, including TNF- α and IL-1 β (Demidova-Rice, Hamblin and Herman, 2012; Karaman, *et al.*, 2016; Li, *et al.*, 2021; Wilkinson and Hardman, 2023). Downstream effectors such as matrix metalloproteases are overexpressed as a result, and disrupt the repair processes by preventing successful ECM re-modelling and cell migration, and angiogenesis (Eming, Martin and Tomic-Canic, 2014; Powell, Pujji and Jeffery, 2021). Within the wound-bed, there may be a reduction in the density of growth factor receptors, alongside diminished mitogenic potential and motility amongst fibroblasts, both contributing to impaired granulation tissue formation and ECM deposition (Demidova-Rice, Hamblin and Herman, 2012; Scalise *et al.*, 2015; Swanson *et al.*, 2016). Chronic wound-derived keratinocytes also exhibit an altered phenotype, with elevated expression of markers of proliferative activity, but simultaneously suppressed migratory potential and differentiation markers, resulting in a hyperproliferative state in which fails to translate into effective re-epithelialisation (Demidova-Rice, Hamblin and Herman, 2012) (Figure 1.2).

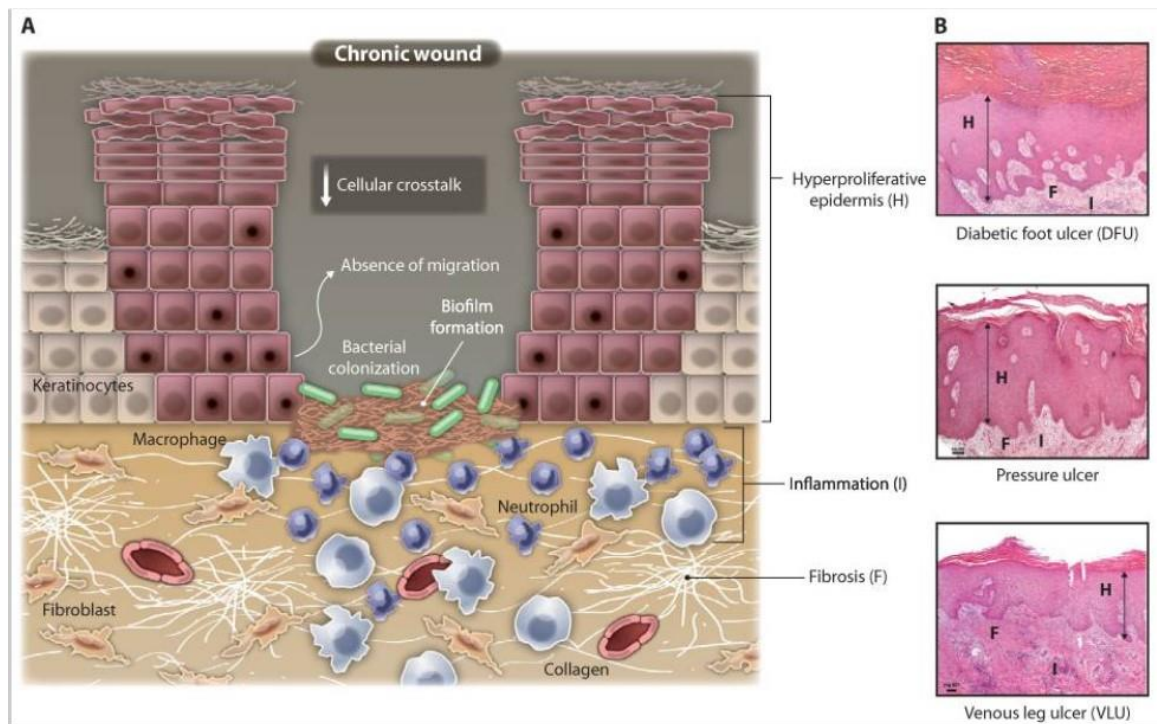


Figure 1.2: Pathological changes occurring within a chronic wound, reproduced from Eming, Martin and Tomic-Canic, 2014. Despite showing ongoing proliferative activity, epidermal keratinocytes fail to demonstrate normal migratory potential, and do not initiate re-epithelialisation. Persistent inflammatory cell infiltration of the wound site leads to excessive levels of ROS and pro-inflammatory cytokine release, with subsequent induction of degradative enzymes, which interfere with the processes of ECM deposition and growth factor signalling. Despite the prolonged inflammatory response, microbial contamination is ineffectually controlled, and host-tissue damage is inflicted by the continued presence of inflammatory mediators, including Langerhans cells, neutrophils, pro-inflammatory macrophages and proteases. Chronic wound infection may further reinforce these degradative effects, perpetuating the failure to heal.

Histopathological analysis of chronic wound tissue from non-healing skin lesions, including diabetic foot ulcers (DFUs), pressure ulcers and vascular leg ulcers, demonstrates the pathologic hallmarks of this abnormal phenotype, notably the hyperproliferative epidermal wound edge, together with fibrotic lesions and prolonged activity of inflammatory cell within the wound bed (Figure 1.2, right) (Eming, Martin and Tomic-Canic, 2014; Raziyeveva *et al.*, 2021). This dysfunctional state of upregulated inflammation illustrates the failure to progress through a well-ordered proliferative and granulation phase, preventing effective tissue repair, and in contrast, causing self-perpetuating degradative effects.

In diabetic individuals, poor control of blood glucose has also been shown to interfere with wound-healing at the molecular level, via improper leukocyte function, cell senescence, and the glycation of ECM components (Demidova-Rice, Hamblin and Herman, 2012; Wilkinson and Hardman, 2023). Furthermore, the synthesis of advanced glycation end-products (AGEs) introduce a number of negative effects, not only modifying the dermal structural arrangement, but also activating downstream inflammation and release of ROS via the receptor for AGEs (RAGE) (Khalid,

Petroianu and Adem, 2022; Schilrreff, P, Alexiev, 2022; Wilkinson and Hardman, 2023). The complexity of chronic wound pathology is clear, and must be considered on an individual case-by-case basis, since effective and appropriate intervention will be aided by a detailed understanding of both the cellular and molecular pathways involved.

1.4.3 The wound infection continuum and the pathogenesis of chronic wounds:

Microbial presence is normal within wounds, since the human skin microbiome comprises a number of bacterial species which do not pose an infection risk when present at lower densities, and when regulated by normal immune system function (Misic, Gardner and Grice, 2014; Scalise *et al.*, 2015; Kim, JH, Ahamed, A, Chen, K, Lebig, EG, *et al.*, 2022). Resident skin microflora and exogenous microbes may contaminate and colonise the wound-bed initially, but in healthy individuals the host immune defence limits the levels of invading microbes, preventing their excessive proliferation. This scenario represents the earlier stages of the wound infection continuum, where the risk of clinical infection is low, and therefore no antimicrobial therapy strictly required (Figure 1.3).

However, when healing is delayed, and the wound remains open for a longer period of time, microbial colonisation may increase, allowing penetration deeper into the wound-bed, and an elevation in pathogenic load, resulting in localised and/or spreading infection (Swanson *et al.*, 2016). Continuing microbial proliferation, in concert with additional physiological features associated with chronicity, including sub-optimal blood supply, impaired oxygenation of the wound-bed, and the presence of metabolic disorders or other co-morbidities, can cause further critical interruption to the healing process (Li, *et al.*, 2021). This expansion of the infectious reservoir may be accompanied by increased microbial virulence and ongoing deterioration of the wound-bed, whilst also risking dissemination of pathogens into the surrounding tissues, biofilm formation, and the development of systemic infection (Swanson *et al.*, 2016). Without appropriate intervention and management, the clinical consequences of progression to this most advanced stage of the wound infection continuum can be debilitating, and ultimately fatal.

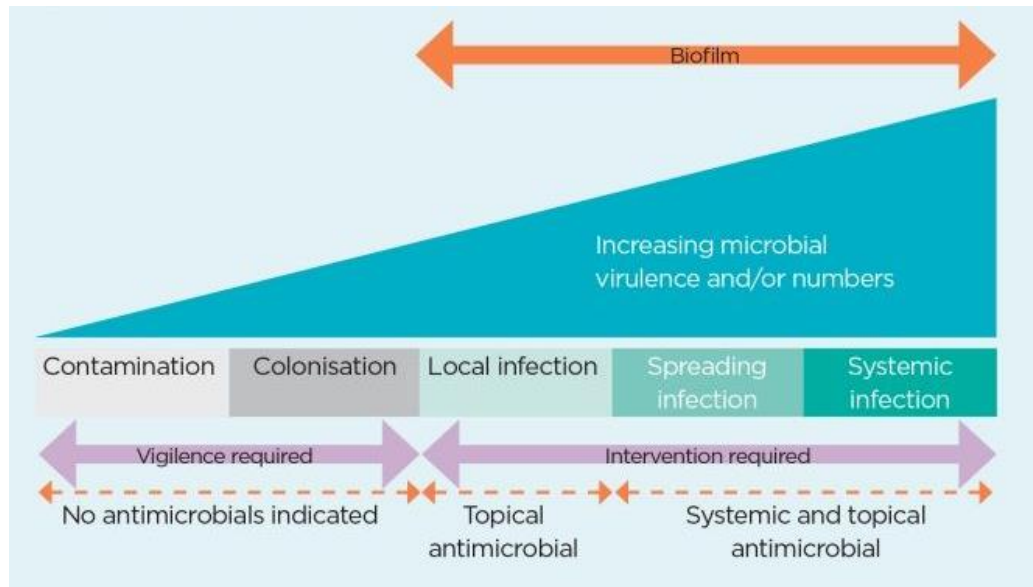


Figure 1.3: The wound infection continuum (reproduced from (Brown, 2018) portraying the sequence of events in the progression from wound contamination to infection and sepsis, or widespread systemic infection.

An unchecked elevation in the wound microbial bioburden can thus pre-empt effective wound repair, and initiate an exaggerated inflammatory response which, rather than efficiently reducing microbial contamination of the wound site, delays healing and generates substantial damage to the affected tissues, owing to the neutrophilic release of cytotoxic enzymes, free radicals, and inflammatory factors (Han *et al.*, 2011; Eming, Martin and Tomic-Canic, 2014; Schilrreff and Alexiev, 2022).

1.5 The epidemiology of non-healing wounds and principle aetiologies

Chronic wounds affect a significant portion of the patient population in the UK, and globally, leading not only to substantial increased in morbidity and mortality, and impaired quality of life for the patients themselves and their families, but also substantial healthcare costs due to the need for longer term clinical input and treatment. In the UK alone, healthcare systems provide care for over 2 million wounds each year (note that some patients present with multiple wounds), and in the period 2017-18, approximately 3.8 million acute or chronic wound patients were treated, with a 70% healing rate reported (Guest, Fuller and Vowden, 2020; Powell, Pujji and Jeffery, 2021). Annually, NHS expenditure on the management of wounds and related health complications amounts to an estimated £5.3 billion, covering the clinical input provided by nursing, podiatry, and surgical specialties, as well as General Practitioners, and also incorporating operating theatre costs, the supply of dressings and equipment, and in-patient care (Lindholm and Searle, 2016; Powell, Pujji and Jeffery, 2021).

For the patient, the cost in terms of physical pain and discomfort, psychosocial burden, time spent receiving treatment, and overall impact on daily living, is great, particularly for those suffering

non-healing, or chronic wounds (Green *et al.*, 2014). Chronic wounds are those failing to progress through the normal stages of healing over a period of 4 - 6 weeks, or, by some definitions, longer than 3 months (Leaper and Durani, 2008; Siddiqui and Bernstein, 2010; Järbrink *et al.*, 2016). Instead of proceeding through the typical sequence of healing phases, a persistent inflammatory state is maintained, and the successful barrier function of the affected tissue is not restored (Eming, Martin and Tomic-Canic, 2014). The wound healing process is complex and dependent on a number of factors, particularly physiological parameters such as patient age, BMI, vascularisation (and hence oxygenation) of the injured tissue, comorbidities (particularly those negatively impacting immune function), and also concurrent treatment regimens, including chemotherapy, radiotherapy, and extended use of corticosteroids, and non-steroidal anti-inflammatories (NSAIDs) (Scalise *et al.*, 2015). Rises in the ageing population, as well as the increasing prevalence of diabetes, in both developed and developing nations, will likely impact the rates of chronic wound incidence on a global scale (Sen *et al.*, 2009; Järbrink *et al.*, 2016; Sen, 2019), underlining the need to develop more effective and sustainable strategies for the management of chronic wounds.

1.5.1 Major types of chronic wounds

Chronic wounds mainly fall within three principal categories, namely vascular leg ulcers – both venous and arterial, diabetic foot ulcers (DFUs), and pressure or decubitus ulcers.

Vascular leg ulcers:

Pathological changes in the vasculature result in altered tissue perfusion, and the development of ulcers which present characteristically as either venous or arterial ulcers. Venous ulcers arise from when the function of valves in both deep and superficial veins is defective, i.e. in cases of venous insufficiency, leading to backflow of blood, and an elevation in venous pressure (Lloyd *et al.*, 2010; Demidova-Rice, Hamblin and Herman, 2012). This in turn causes increased permeability in the blood vessel walls, allowing components of blood plasma, critically including fibrin, to leak into the peri-vascular space. Accumulation of fibrin around the blood vessels subsequently impairs vascular function, via mechanisms which are as yet incompletely understood, leading to reduced oxygen tension in the surrounding tissue, and ultimately, ulceration. Thromboses and varicoses can also precipitate the development of venous ulcers, via the impairment of venous function (Lloyd *et al.*, 2010; Stacey, 2011; Hofman, *et al.*, 2024).

Arterial ulcers occur more infrequently, and are the result of arterial insufficiency, which may arise due to atherosclerosis, vascular embolism, or any other pathology restricting arterial blood-flow, causing ischaemia and tissue deterioration (Lloyd *et al.*, 2010; Demidova-Rice, Hamblin and Herman, 2012). In contrast to venous ulcers, which typically develop between the knee and ankle,

arterial ulcers may occur over a wider anatomical distribution, distal to arterial perfusion, including the toes and plantar regions (Hofman, *et al.*, 2024).

Pressure ulcers:

Pressure ulcers develop when the skin and underlying muscle tissue are subjected to prolonged, unrelieved pressure and shearing forces, such as may arise in patients whose mobility is markedly reduced, and in those suffering neuropathies or vascular insufficiencies. Anatomical areas featuring bony prominences are particularly vulnerable to pressure ulceration, such as the heel and ankle. Impaired circulatory perfusion leads to decreased tissue oxygen tension, ischaemia-reperfusion injury, and ultimately tissue necrosis (Demidova-Rice, Hamblin and Herman, 2012; Eming, Martin and Tomic-Canic, 2014). The severity of the ulcer is described via a clinical grading system, with more chronic wounds demonstrating fibrosis and coagulation necrosis, and loss of epidermis (Lloyd *et al.*, 2010; Hofmann *et al.*, 2023).

Diabetic foot ulcers:

DFUs affect 15-25% of diabetic patients during their lives, caused by a combination of disease-related factors, including peripheral arterial disease, peripheral neuropathy, autonomic dysfunction, and altered immune function, leading to chronically infected ulcers in 10-15% of cases (Price *et al.*, 2016). Poorly-controlled diabetes has been shown to exacerbate vascular impairment, inducing microvascular angiopathies with associated tissue hypoxia, which together with arterial vasculopathy and lower-limb neuropathy, significantly raises the risk for developing chronic wounds (Noor, A, Zubair, M, 2015).

Post-operative/ surgical site wounds:

Although not defined as one of the classic chronic wound presentations, the healing of surgical incision sites can be significantly delayed by adverse factors such as infection, cellulitis, the development of seroma or haematoma, separation of the wound edges (dehiscence), or tissue necrosis (Kawakita and Landy, 2017). Surgical site infections represent almost one fifth of nosocomial (hospital or healthcare-associated) infections, and are responsible for prolonging the length of hospitalised care, and increasing the likelihood of re-admission and further surgical intervention (Posnett *et al.*, 2009; Powell, Pujji and Jeffery, 2021).

1.6 Microbial biofilms: a persistent problem

Pathological microbial involvement in the development of chronic wounds, specifically the prevalence of recalcitrant biofilms, is significant and cannot be overlooked: if improperly managed, a contaminated wound may progress from contamination through critical colonisation and localised infection to a systemic infection, which may ultimately become life-threatening (Gilliver, 2009; Gray *et al.*, 2010; King and Barrett, 2016; Brown, 2018) (Figure 1.3). In order to improve detection rates and implement more effective wound-management strategies, improving

our understanding of the role of biofilms in wound pathogenesis, and the mechanisms involved in their development and persistence must be made a priority.

Biofilms are complex consortia of microorganisms embedded within a self-produced, hydrated protective matrix of extra-cellular polymeric substances (EPS), which affords the resident microorganisms a greatly enhanced ability to persist in the face of biochemical and physical challenge (Flemming *et al.*, 2016; Malone *et al.*, 2017). Indeed, biofilm-dwelling microorganisms may tolerate antimicrobial concentrations at elevated concentrations, ranging from tenfold to as much as 1000-fold that seen to inhibit growth of the same organisms in planktonic state (Donlan and Costerton, 2002; Olsen, 2015), effectively arming the biofilm with phenotypic antimicrobial resistance. Biofilms represent the dominant growth mode of bacteria in nature, existing typically as multispecies entities attached to abiotic or biotic surfaces, and exhibiting remarkable phenotypic heterogeneity and architectural organisation, enabling efficient adaptation to the surrounding environmental conditions (Flemming *et al.*, 2016; Schroeder, Brooks and Brooks, 2017). The process of biofilm formation has previously been modelled as a five-stage process beginning with reversible attachment, then irreversible attachment to a surface, followed by two-stage maturation, and finally dispersion (*et al.*, 2002), however, a revised conceptual model of biofilm growth in both surface-adherent and non-adherent forms has more recently been proposed, to encompass the breadth of biofilm growth presentations occurring in real-world settings, from environmental to clinical to industrial, comprising aggregation, growth and disaggregation phases (Sauer, *et al.*, 2022). Microbial survival within the biofilm is supported by a number of features, such as the presence of biochemical gradients, e.g. localised variations in nutrient availability and oxygenation, allowing resident microorganisms to adopt differing phenotypes, adapting their metabolic activity according to their local microenvironment within the biofilm (Lebeaux, Ghigo and Beloin, 2014; Flemming *et al.*, 2016). In deeper regions of the biofilm, microbes can enter a dormant state in which their metabolic and proliferative activity are vastly reduced, but viability is retained. This adaptation allows the survival of this subpopulation, known as 'persisters', during extremely hostile environmental conditions which may eliminate biofilm cells located nearer the surface (Lebeaux, Ghigo and Beloin, 2014; Mishra *et al.*, 2020). Persister cells are believed to play a key role in the seeding of new microbial colonies, capable of re-forming a biofilm following effective removal of extensive portions of the rest of the original biofilm community.

The development of microbial biofilm is estimated to represent the principal cause of around 80% of all human infections, and is suspected to be present in the majority of device-related infections (Khatoon, Z, *et al.*, 2018; Alves *et al.*, 2021), however, accurate and timely identification of biofilm is challenging, due to a number of factors. Biofilm colonisation of wounds can be difficult to discern and diagnose clinically, and may require tissue biopsy for definitive identification,

necessitating an invasive and painful procedure for the patient, and often requiring specialist expertise, clinical costs, and additional time for analysis (Alves *et al.*, 2021). Rates of biofilm involvement in chronic wounds have been variously cited as being between 60 – 80% (Malone *et al.*, 2017; Khatoon, *et al.* 2018). Recently, efforts have been made within and between clinical and scientific communities and governing bodies to generate a systematic algorithm for the recognition and management of chronic wound biofilms, to support and improve current standards and practices (Percival, Vuotto, *et al.*, 2015; Schultz *et al.*, 2017; Swanson and Angel, 2017). The principal of ‘biofilm-based wound care’ could assist the delivery of more appropriate and efficacious treatments (Goswami, *et al.*, 2023), by promoting an individualised approach to wound management, centred on the particular presentation, microbial biofilm composition and distribution, and patient-specific criteria, with the objective of achieving the best possible outcome for each unique case.

Detection of biofilm formation in a chronic wound is not clear-cut, since the physical appearance within the wound bed may be difficult to distinguish from sloughy tissue which occurs naturally in chronic or infected wounds, and which is normally removed or reduced during debridement (Percival, Vuotto, *et al.*, 2015; Swanson and Angel, 2017). Microbial biofilm may present as a thick, slimy film in the wound, which resists removal via cleansing and debridement, or may be temporarily reduced but reappears within 2-4 days of debridement. Other typical indicators of biofilm colonisation of the wound may include:

- Failure to show clinical improvement despite implementation of appropriate wound care and treatment.
- Alteration in the level of exudate, deposition of excessive granulation tissue within the wound, tendency to bleed easily, or increased sensitivity.
- Signs of localised infection at the wound site, seen in the absence of systemic infection indicators. (Percival, Vuotto, *et al.*, 2015; Schultz *et al.*, 2017; Goswami, *et al.*, 2023)

1.7 Clinical interventions to promote wound healing

To promote wound healing and improvement in clinical condition, prompt and effective wound management is imperative. Regular and careful assessment of the wound should be performed, taking into consideration the patient’s overall health and nutritional status, the nature of the wound, including aetiology, duration, size, position, circulatory perfusion, and the presence of any exudate and bioburden (Swanson and Angel, 2017). Effective wound management requires regular assessment of the wound, appropriate cleansing, debridement and treatment, and dressing application, in order to support the healing process, eliminate any existing infection,

regulate moisture levels, and prevent localised or systemic infection (Dowsett, C, Newton, 2005; Harries, Bosquanet, and Harding, 2016; Swanson *et al.*, 2016).

As outlined earlier, the wound healing process involves a series of co-ordinated phases from initial haemostasis, thrombosis and inflammation, through to cellular proliferation and migration, tissue remodelling and fibrosis. Successful healing relies upon the maintenance of a sterile environment, in which microbial burden is controlled and maintained below the 'critical colonisation' level which can lead to development of a clinical infection. A bioburden exceeding 10^5 CFU per gram of tissue is considered above this critical colonisation threshold, and thus more likely to become infected (White and Cutting, 2008), however microbial load is only one of the determinants of infection, and does not necessarily lead to chronic infection without the influence of additional factors, such as species profile and virulence, which affect biofilm formation (Han, *et al.*, 2011; Scalise *et al.*, 2015; Goswami, *et al.*, 2023). Biofilm growth within wounds represents one of the major determinants of chronicity and delayed healing, with an estimated 60% of chronic wounds positively infected with bacterial biofilm (James, *et al.*, 2008; Høiby, *et al.*, 2015). Therefore, it is vitally important that microbial presence within the wound is carefully monitored and controlled in order to facilitate successful healing.

1.7.1 Wound cleansing:

Wound cleansing may be recommended at every dressing change (Harries, Bosquanet, and Harding, 2016; Swanson *et al.*, 2016; Eriksson, *et al.*, 2022), although careful clinical judgement, technique and selection of cleansing agent must be applied, since physical interference with the granulating wound bed may damage newly forming capillaries and tissue (Wolcott and Fletcher, 2014; Brown, 2018). This could trigger subsequent inflammation within the wound, and lead to delayed healing, therefore nursing practice guidelines recommend that cleansing procedures should only be performed if there are indicators of wound infection, sloughing, or visible contamination with faecal material or debris (Brown, 2018).

Since optimal cellular activity within a wound is achieved at 37°C, (Lock, 1979), as it promotes the ideal level of wound-bed oxygenation and leukocyte infiltration (Feinstein and Maskiewicz, 2009), avoidance of frequent exposure and rinsing of the wound with cool solutions is recommended (Brown, 2019). Normal sterile saline (0.9%) has been historically used to cleanse wounds, being isotonic to the body's interstitial fluid, although some studies have suggested ordinary potable tap-water as a suitable alternative (Fernandez and Griffith, 2012; Weir and Swanson, 2019). This has not been adopted in universal clinical practice, however, and the risk of microbial contamination from bacteria in the surrounding environment advocates against this mode of wound irrigation. The use of sterile solutions for wound cleansing is especially recommended for patients whose immune function is impaired, or who are suffering diabetic wounds, foot ulcers, or

deeper wounds with exposed bone or tendon (Peate and Glencross, 2015; Cutting *et al* 2010), due to the elevated risk factors for wound infection and failure to heal. NICE guidance advises sterile saline cleansing for surgical wounds during the 48 hour post-surgical period, but no further cleansing should be required once wound closure has occurred (NICE, 2013).

1.7.2 Application of antiseptics or antimicrobial disinfectant agents:

Selection of the appropriate antimicrobial agent is vital to ensure optimal efficacy of biocidal action, duration of effect, and compatibility with the target surface, material, or tissue, and must demonstrate specificity and potency against the microbial contaminants in question, whilst producing minimal residual or collateral toxicity. The increased application of biocidal products in recent years, particularly since the Covid-19 pandemic, has heightened public awareness and institutional agency regarding environmental disinfection and hygiene, but has also expanded the generalised usage of disinfecting agents, in healthcare, food, transport, business, and domiciliary industries, and thus elevated the risk of the development of resistance and cross-resistance (Maillard and Pascoe, 2024).

A single antimicrobial compound may be used across a number of different settings, within a range of different formulations, and across a range of appropriate concentrations, depending on the precise context and application, whether that be for surface disinfection, antiseptics, or as a preservative (Maillard, 2005). Therefore, careful selection of the product of choice, its concentration, preparation and storage, and adherence to the correct mode of application, and disposal procedures, are all critical to maintaining antimicrobial efficacy and limiting the development of resistance.

Skin and wound antiseptics, prior to surgery and as part of routine wound-care, is an important means of localised infection control and prevention (Cambiaso-Daniel *et al.*, 2018; Alves *et al.*, 2021; Parvin, *et al.*, 2022). Rapidly-acting antimicrobial agents which are well-tolerated, non-irritant/ non-allergenic, and which exhibit low or negligible cytotoxicity are useful in the cleansing of potential sites of opportunistic infection at the skin surface, and at entry sites of invasive medical devices, through which commensal microorganisms normally resident on the skin surface may access and colonise tissues from which they are normally absent (Maillard, 2005; Percival, Suleman, *et al.*, 2015; Percival, Vuotto, *et al.*, 2015; Swanson *et al.*, 2016; Maillard, Kampf and Cooper, 2021).

The biocidal action of chemical antiseptics and disinfectants is mediated through interaction of the active components with multiple targets on the microbial cells, causing either irreversible damage and death (i.e. a bactericidal effect), or reversible inhibition of the organism (a bacteriostatic effect). The majority of antiseptic agents act via interference with the cytoplasmic membrane and bacterial enzymes, but the precise mode of microbial inactivation varies with the

particular chemistry of the biocide used. The mechanisms by which biocides induce their antimicrobial effects are not as clearly elucidated as those of antibiotics, and their mode of action is less specific than that of antibiotics, therefore there is limited understanding of the potential for resistance to develop with their use, however a growing awareness of the risks of cross-resistance occurring in pathogens exposed to commonly used biocides has sparked an increase in research in this area (Meade, Slattery and Garvey, 2021; Sethi, *et al.*, 2024).

Several biocidal agents are used in antiseptics applications and also in products designed for environmental and medical device decontamination purposes, each within concentration ranges adjusted appropriately for the intended use, considering parameters including surface area, contact time, therapeutic index, patient demographic and clinical context, amongst others (Sethi, *et al.*, 2021; Maillard and Pascoe, 2024). Biocides formulated for environmental disinfection may be applied in hospital areas requiring high-, medium- or low-level treatment, with selection of the particular product and applied concentration dictated by the setting, the risks and potential consequences of transmission of infection to patients, and/or healthcare practitioners.

Pathogenic microorganisms exhibit diversity in their tolerance of, or resistance to, different microbicidal products (Figure 1.4), therefore the IPC measures used in every clinical setting must correspond appropriately to the level of risk, and the standards of disinfection or asepsis required. Widespread and frequent usage of high-level disinfectant/ microbicidal agents in non-critical areas may be inadvisable in the light of the risk of acquired resistance, and other potential adverse effects such as deleterious effects on the target site or surface, or toxicity (Maillard, 2005; Vickery *et al.*, 2012; Ledwoch *et al.*, 2019).

Biocidal efficacy *in situ* is critically influenced by a number of factors relating to the target surface and organisms to be inactivated, including surface properties (porosity, roughness, hydrophobicity), microbial identity and characteristics (fungal, bacterial, protozoal, presence of spores, formation of biofilm), the intended contact time, the humidity, temperature and pH of the treatment milieu, and the presence and extent of organic and inorganic soiling, which can impair biocidal activity and limit its bioavailability (Maillard, 2005a; Maillard, 2005b).

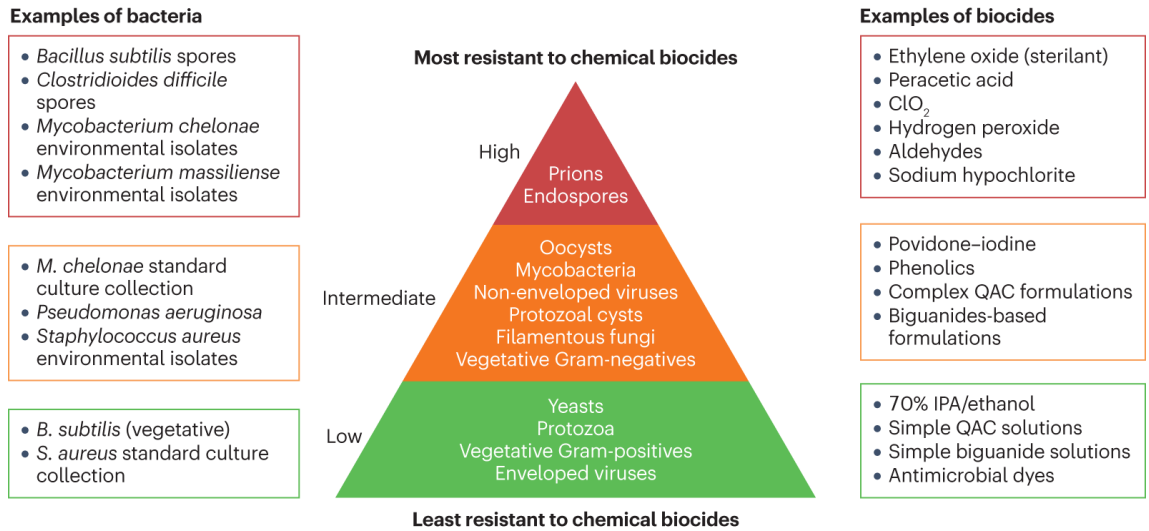


Figure 1.4. Hierarchy of susceptibility of microorganisms to biocides, reproduced from (Maillard and Pascoe, 2024)

The target sites acted upon by biocidal or antiseptic agents are numerous, and are differentially affected according to the particular compound used (Jones and Joshi, 2021; Meade, Slattery and Garvey, 2021), and the cell morphology/ structure of the microorganism targeted (Figure 1.5). Initial biocide-microbe interactions are typically reversible processes, encompassing interference with the cytoplasmic membrane, which in turn may disrupt membrane potential, via depletion of intracellular potassium ions, causing a reduction in cellular proton-motive force, upon which the organism is dependent for the production of ATP. Subsequent failure of active transport processes and metabolic dysregulation may then follow, and cell replication ceases as a result. Prolonged exposure to the biocidal agent can inflict greater damage upon the target cell, extensively impairing the integrity of the cytoplasmic membrane, progressive deterioration in cellular homeostasis, loss of enzyme function and, ultimately, loss of intracellular components including proteins, nucleotides, and ions (Maillard and Pascoe, 2024).

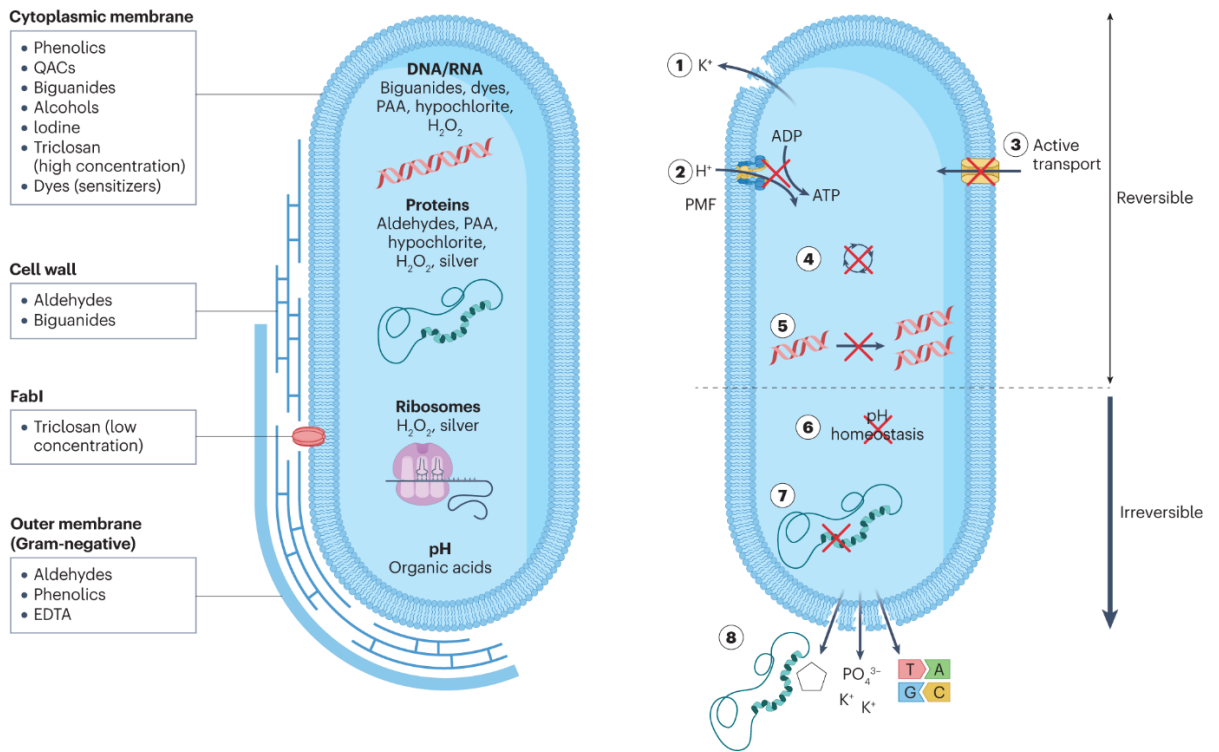


Figure 1.5: Microbial cell target sites disrupted by biocides, reproduced from (Maillard and Pascoe, 2024)

1.7.3 Common antimicrobial agents used for wound antiseptics in healthcare:

1.7.3.1 PHMB:

The compound polyhexamethylene biguanide (also referred to as PHMB or polyhexanide), is a broad-spectrum antiseptic product, which is effective against Gram-negative and Gram-positive bacteria, fungi, and microbial biofilms, and has previously been used as a preservative in personal hygiene products, a multi-purpose disinfectant, and a deodoriser (Gilliver, 2009). It has been used as the treatment of choice in locally infected and critically colonised wounds, as well as for second-degree burns, refractory wounds (incompletely healing), and as a lavage or wound-cleansing product. Its mechanism of action, as a cationic biocide, is primarily by interference with the negatively-charged bacterial cytoplasmic membrane, and disruption of inter-molecular bonds within the phospholipid bilayer, causing phase separation, and allowing its penetration into the cell.

1.7.3.2 Povidone iodine

This compound has been demonstrated to exert broad-spectrum antimicrobial activity against Gram-positive and Gram-negative bacteria, fungi, protozoa, viruses, bacterial spores and amoeba (Woo, 2014; Alves *et al.*, 2021). Polyvinylpyrrolidone-iodine (PVP-I) is an iodine-releasing agent, which contains polyvinylpyrrolidone - a neutral, water-soluble polymer base, in complex with iodine. Its microbicidal effects are exerted via the release of free iodine in aqueous media, initiating deleterious oxidation reactions with microbial membrane proteins, causing denaturation

and allowing entry of iodine into the intracellular environment, where it can form complexes with amino acids and unsaturated fatty acids, inactivating cytosolic enzymes and impeding protein synthesis (Dopcea and Matei, 2018; Grzybowski, Kanclerz and Myers, 2018). Thus vital microbial metabolic processes are disrupted, including nucleic acid synthesis, which together with irreparable membrane damage, leads to microbial cell death (Maillard and Pascoe, 2024).

Iodophors such as PVP-I have long been employed as disinfectants and antiseptic agents, being well-tolerated, showing broad-spectrum efficacy, and producing swift antimicrobial effects (Metcalf, Bowler and Parsons, 2016; Tan and Johari, 2021). The rapid onset of activity of PVP-I has been demonstrated after as little as 60 seconds contact time, and within shorter timeframes for certain viral pathogens (Bigliardi *et al.*, 2017; Greenhalgh, Dempsey-Hibbert and Whitehead, 2019; Alves *et al.*, 2021; Tan and Johari, 2021). Potent anti-biofilm activity has also been reported *in vitro*, inactivating biofilms involving bacterial and fungal species, including MDR strains (Capriotti, *et al.*, 2018). Dilute preparations of iodophors have been reported to exhibit more immediate antimicrobial activity than undiluted applications, possibly due to a weakening of the iodine-carrier association when in solution, and a subsequent increase in available free iodine (Bigliardi *et al.*, 2017; Hoekstra, Westgate and Mueller, 2017).

Despite demonstrating cytotoxic effects against keratinocytes and fibroblasts *in vitro*, with reductions in cell proliferation and migration reported at sub-therapeutic concentrations (Ortega-Llamas *et al.*, 2022; Steins *et al.*, 2023), PVP-I has shown favourable biocompatibility in comparison to other common topical antiseptic agents (Müller and Kramer, 2008; Bigliardi *et al.*, 2017). In combination with its purported effects on cellular redox potential, povidone iodine appears to promote angiogenesis and re-epithelialisation (Leaper and Durani, 2008; Wang *et al.*, 2017), thus it is effective both as an anti-biofilm agent and as an aid to the healing of wounds, although in certain groups there are preclusions to its use, as in patients suffering disorders of thyroid or renal function, or iodine sensitivity (Bigliardi *et al.*, 2017).

1.7.3.3 Silver sulfadiazine:

The antimicrobial properties of silver are well established and documented, and products containing silver compounds are recognised as effective treatments against wound infection and in the management of biofilm (Swanson and Angel, 2017). Topical silver sulfadiazine is used commonly as a prophylactic treatment in burn wounds, and also as a short-term adjunctive therapeutic in other skin conditions, such as leg ulcers, pressure sores, infected skin graft donor sites, and larger abrasion injuries (Oaks and Cindass, 2021). Silver sulfadiazine impregnated dressings present a low-cost option for antiseptic treatment of burn wounds, with a low level of systemic absorption incurred, making this a well-tolerated wound management strategy. Silver sulfadiazine is effective against Gram-positive and Gram-negative microorganisms, and certain

strains of yeast infection. Although it incorporates a sulphonamide component, its bactericidal properties are attributed to the action of the release of silver ions, rather than the inhibition of folic acid synthesis, and it is understood to interfere with DNA replication, and to induce an increase in bacterial cell wall permeability via interactions with the lipid cell membrane, potentially involving free radical formation. Ionic silver is also believed to disrupt electron-transport systems and ion-exchange systems within the bacterial cell wall, thereby impeding microbial energy production, and reducing viability (Muller, 2018; Alves *et al.*, 2021).

Clinically employed products typically contain 1% silver sulfadiazine. Although regarded as a clinically safe compound, its use has been noted to reduce re-epithelialisation rates in wounds, and can result in the formation of pseudo-eschar in burn wounds, which, without debridement, can impair evaluation of the healing stage/ state of the wound. Haematologic side effects may arise with treatment, such as agranulocytosis, aplastic anaemia, haemolytic anaemia, or leukopenia, whilst dermatological effects, including pruritis, erythema multiforme, photosensitivity and discolouration may also occur (Oaks and Cindass, 2021). Cases of a Stevens-Johnson Syndrome, a rare and life-threatening hypersensitivity reaction occurring as a serious adverse effect of certain classes of medications, have been recorded with particular prevalence with the use of silver sulfadiazine, underlining the need for thorough appraisal of risk factors and scrupulous prescribing practices when selecting antibiotic therapies (Oaks and Cindass, 2021; Foster, 2023; Lee, Knox, and Phillips, 2023). Systemic absorption of silver is understood to be a risk with more liberal use of the drug, and concerns have been articulated regarding its cytotoxic effects observed *in vitro* and potential impairment of healing, therefore silver-containing formulations must be prescribed only at appropriate doses, and applied with particular caution to avoid mucosal or ocular areas (Khansa, *et al.*, 2019; Oaks and Cindass, 2021).

1.7.3.4 Chlorhexidine:

The biguanide chlorhexidine is included in numerous products for its antiseptic properties, including washes and lotions for cleansing of the skin, and for wound and burn antisepsis, and an aid to debridement (Atiyeh, Dibo and Hayek, 2009; Harries, Bosquanet and Harding, 2016). Further uses include the treatment of oral plaque, gingivitis and oral candidiasis, and it is commonly a component of antimicrobial mouthwashes. Typical formulations include chlorhexidine at concentrations between 0.05% and 4%, although it has additionally been administered during catheterisation, and as a bladder irrigant in cases of UTI, at 0.02% (Maillard, 2005). Chlorhexidine has been incorporated as a coating component of indwelling medical devices, commonly in combination with silver sulfadiazine, to reduce the risk of device-associated infections, via prevention of microbial adhesion and biofilm formation (Greenhalgh, Dempsey-Hibbert and Whitehead, 2019)

Chlorhexidine damages bacterial outer and inner cell membranes, interfering with anionic phosphate groups in the bacterial lipid layer and also perturbing membrane potentials, causing leakage of intracellular contents, and at higher antiseptic concentrations, coagulation of the cytoplasm (Mcdonnell and Russell, 1999; Atiyeh, Dibo and Hayek, 2009; Greenhalgh, Dempsey-Hibbert and Whitehead, 2019). Histological studies suggest significant cytotoxicity upon prolonged or repeated contact with fibroblasts and keratinocytes, and delayed healing in wounds treated with chlorhexidine has been reported (Mcdonnell and Russell, 1999; WHM Node Group, 2016; Ortega-Llamas *et al.*, 2022), although in clinical usage, chlorhexidine absorption through the skin is low, and irritation is generally mild, when used within recommended dose ranges (Atiyeh, Dibo and Hayek, 2009; WHM Node Group, 2016). The antimicrobial efficacy of is greater against Gram-positive organisms than Gram-negative bacteria, fungi and tuberculous bacteria (Atiyeh, Dibo and Hayek, 2009), and although rapidly-acting, its activity is pH-dependent and may be dampened by the presence of organic contamination (Russell and Day, 1993; Sahiner, Halat, and Algin Yapar, 2019; Ortega-Llamas *et al.*, 2022).

1.7.3.5 Hydrogen peroxide:

Hydrogen peroxide (H_2O_2) is a reactive oxygen species which has traditionally been used as a topical antiseptic in wound care (Mcdonnell and Russell, 1999; Linley *et al.*, 2012). Its antimicrobial properties derive from its oxidising effects, via similar mechanisms to those exerted during the 'oxidative burst' generated endogenously within damaged tissue and executed by activated phagocytes, where the activity of NADPH oxidase induces the liberation of ROS, providing a strong bactericidal effect (Wittmann, *et al.*, 2012; Van Der Vliet and Janssen-Heininger, 2014) The subsequent generation of secondary ROS, such as hydroxyl radicals, and oxidising species hypothiocyanite and hypochlorous acid mediated via peroxidase and myeloperoxidase, exerts destabilising and deleterious effects on microbial cell constituents, including amino acids, lipids and proteins (Wittmann, *et al.*, 2012; Curieses Andres *et al.* 2022). H_2O_2 is an important biochemical signalling molecule which acts as a messenger molecule attracting effector cells to the site of a wound, eliciting inflammatory cell responses and triggering further redox signalling cascades (Wittmann, *et al.*, 2012; Van Der Vliet and Janssen-Heininger, 2014; Zhu *et al.*, 2017; Murphy and Friedman, 2019). Due to its comparatively low reactivity relative to other reactive oxygen species (ROS), H_2O_2 persists sufficiently within the wound environment to enable its diffusion into the surrounding tissue following injury, and within specific concentration ranges it can induce a plethora of response mechanisms, including the regulation of transcription factors and their DNA affinity, promotion of cytokine secretions which assist in tissue regeneration, and activation of haemostasis (Wittmann, *et al.*, 2012; Van Der Vliet and Janssen-Heininger, 2014; Lisse, King, and Rieger, 2016; Zhu *et al.*, 2017; Curieses Andres, *et al.*, 2022). Furthermore, this compound has the advantageous effect of loosening particulate

debris from the wound bed, thus assisting in wound cleansing and debridement (Murphy and Friedman, 2019; Rai *et al.*, 2021).

Historically, H₂O₂ has been applied in both low and high level disinfection of clinical surfaces and inanimate materials, in contact lens disinfection, as well as in the cleansing and deodorisation of wounds and ulcers, typically within a concentration range of 3-7% (Maillard, 2005; Babalska, Korbecka-Paczkowska and Karpiński, 2021; Rai *et al.*, 2021), although its use on wounds has declined in recent years due to concerns over its tolerability and potential for provoking irritation/ adverse reaction at the site of contact (Murphy and Friedman, 2019), with *in vitro* studies substantiating its cytotoxicity against various cell types including fibroblasts (Loo and Halliwell, 2012; Rueda-Fernández *et al.*, 2022) and endothelial cells (Park, 2013).

The antimicrobial efficacy of H₂O₂ against simple monospecies biofilms and more complex multispecies biofilms in a wound model has been demonstrated *in vitro* (Presterl, *et al.*, 2007; Brown *et al.*, 2022), however, the presence of contaminant organic compounds, and the expression of peroxidase or catalase at low concentrations antagonises its microbicidal activity (Sahiner, Halat, and Algin Yapar, 2019), therefore against catalase-positive organisms species exhibiting greater tolerance, extended contact times and elevated concentrations of H₂O₂ are required (Ríos-Castillo, González-Rivas and Rodríguez-Jerez, 2017).

1.7.3.6 Electrochemically-Activated Solutions (ECAS)

Electrochemically Activated Solutions (ECAS) have been recognised for a number of decades as effective disinfection agents, however their application in the clinical setting, particularly for topical antimicrobial therapy, has emerged only relatively recently (Rasmussen, 2020; Yan, Daliri and Oh, 2021). Hypochlorous acid (HOCl)-based solutions have gained selective approval across the globe for use in disinfection and sterilisation of medical instrumentation, and for topical cleansing and antisepsis (Gold *et al.*, 2020), however, despite acknowledgment of the substantial breadth of supportive research and clinical trial outcomes, it has been denied inclusion on the WHO Model List of Essential Medicines, on the grounds of insufficient availability of evidence (WHO Expert Committee, 2021).

The low toxicity, ease and low cost of production, rapid onset and wide spectrum of activity underline the suitability of ECAS for use in healthcare institutions (Thorn *et al.*, 2012; Ding *et al.*, 2016; Chen and Wang, 2022). The electrolysis of a weak saline solution within a generation unit incorporating a semi-permeable membrane facilitates the production of ECAS, comprising an alkaline catholyte solution, with potent reductive properties (ORP <-800mV, pH>8), and a weakly acidic, highly oxidative anolyte solution (ORP between +800mV and 1200mV, pH<3.5), which can be effectively harnessed as a biocompatible antimicrobial (Cai, 2005; Robinson *et al.*, 2010; Thorn *et al.*, 2012).

The antimicrobial activity of ECAS is attributed to its physicochemical properties: the anolyte product solution is characterised by low pH, high ORP and freely available chloride ion levels which favour the formation of hypochlorous acid (HOCl), when at slightly acidic pH (5.0 - 6.5) (Ding *et al.*, 2016). The microbicidal potency of HOCl is well-recognised, occurring endogenously in the innate immune response to infection, produced by myeloid-derived effector cells, such as neutrophils, eosinophils, mononuclear phagocytes, and B-lymphocytes (Block and Rowan, 2020; Dissemond, 2020). HOCl is generated by the myeloperoxidase system in neutrophils during the oxidative burst, inflicting powerful oxidative damage on nucleotides, proteins and microbial membranes, leading to cell lysis (Kettle and Winterbourn, 1997; Dissemond, 2020; Curiesnes Andres, *et al.*, 2022). In recent years, electrochemically-activated solutions have been adopted for biocidal applications, owing to their microbicidal efficacy in the decontamination of food products, industrial surfaces and infections (Dissemond, 2020; Rasmussen, 2020; Yan, Daliri and Oh, 2021), and compatibility with different surface materials, biotic and abiotic, without evidence of deleterious collateral effects (Veasey and Muriana, 2016; Wilsmann *et al.*, 2023).

1.8 Developing the evidence-base for novel antiseptics and wound-cleansers: towards a better understanding of the wound microenvironment

The development of relevant laboratory models which closely replicate the conditions of the wound microenvironment *in vitro* is highly important, in order to extract relevant and translatable results which can inform scientific understanding of wound pathophysiology, microbial colonisation and biofilm formation, and constitute a comparable model platform for the testing of antimicrobial and antibiofilm interventions. A number of well-characterised model systems have been conceived, which facilitate the growth of microbial biofilms in wound-like settings, varying in the level of complexity and mode of culture involved (Alves *et al.*, 2018; Kadam *et al.*, 2019; Chen *et al.*, 2021; Dhekane, Mhade and Kaushik, 2022). Investigations determining the efficacy of antimicrobial dressings and topical treatments have effectively utilised more advanced biofilm growth substrates, such as hydrogels (Werthén *et al.*, 2010; Townsend *et al.*, 2016; Slade *et al.*, 2019), porous polymeric or composite matrix (Oates, and McBain, 2016; Oates, *et al.*, 2018), and enriched multi-layered agar models (Chen *et al.*, 2021), incorporating mixed species consortia, and in certain models using fluidics to enable growth under flow conditions (Lipp *et al.*, 2010; Woods *et al.*, 2012; Duckworth *et al.*, 2018), to establish a more clinically relevant wound-like milieu and thus provide a more appropriate testing platform for topical antimicrobial testing.

1.8.1 Mimicking the biochemical and structural profile of the wound environment *in vitro*

Key factors in the modelling and investigation of wound biofilms *in vitro*

It has been shown that the composition of the selected growth medium has a significant effect not only on the growth dynamics of the *in vitro* biofilm, but also on the response to applied microbicidal test substances, and therefore may influence the interpretation of the efficacy and selectivity of these compounds (Paleczny *et al.*, 2021). Standard testing protocols have been established to define the minimal required efficacies of antiseptic/ antimicrobial substances under specified conditions, however the far greater complexity of the wound milieu *in vivo*, where interactions with immune system factors, components of wound exudate, paracrine factors, wound location, tissue oxygenation (reflecting circulatory efficiency), and patient comorbidities may all impact upon the processes of healing and rate of progress along the infection continuum (Brown, 2018; Wilkinson and Hardman, 2023).

The wound microenvironment has been described as an extracellular compartment containing cells, growth factors, inflammatory mediators, and host-derived biochemical elements (Junker, Caterson and Eriksson, 2013; Kim, JH, Ahamed, A, Chen, K, Lebig, *et al.*, 2022). The wound bed biochemical profile will undergo dynamic changes depending on the stage of healing, as will the volume and composition of wound fluid present, and in terms of other variables such as pH, metalloproteinase activity, and levels of reactive oxygen species. Incorporation of host cellular elements of the wound environment together with a growth medium which better simulates the biochemical profile of wound exudate, to form a more accurate model platform for culture of wound-like biofilms *in vitro*, is technically challenging to undertake, although has been successfully demonstrated in more recent studies (Grassi *et al.*, 2019; Brown *et al.*, 2022; Dhekane, Mhade and Kaushik, 2022; Tsoukou, Bourke and Boehm, 2022). However, inherent limitations exist as to the maintenance of eukaryotic host cell viability in co-culture with microbial species, since the innate immune response cannot be replicated fully in *in vitro* laboratory models. Nonetheless, the development of more physiologically relevant model systems, integrating both mammalian cells, or surrogate wound-bed components and microbial pathogens, has the potential to provide further insight into the interactions occurring during biofilm formation in wounds, and to facilitate preliminary antimicrobial efficacy testing under controlled conditions, without the ethical concerns associated with *in vivo* models.

1.9 Project aims and objectives:

The principle aim of this project is to explore possible applications of novel non-thermal energy technologies, such as non-thermal plasma (NTP) generation and electrochemical-activation systems, with respect to microbial contamination and biofilm infection in the healthcare setting. It aims to investigate the effects of non-thermal energy technologies on prokaryotic and eukaryotic cells, and to determine the efficacy of different modes of treatment using these technologies, measuring the resultant biological effects, including antimicrobial and anti-biofilm activity, and cytotoxicity assay. Comparison will be made to currently-available, in-use antimicrobial agents, to provide a relevant reference by which the effects of NTP and electrochemically-activated solutions may be evaluated. The outcomes of this study may therefore further elucidate the potential efficacy and biocompatibility of products generated by these novel technologies in the context of microbial decontamination and antisepsis in healthcare environments. It is hoped that the findings obtained from the work undertaken herein will contribute to the evaluation of innovative alternative approaches to the control of pathogenic infection and transmission in the era of increasing rates of healthcare-associated infections and spread of AMR.

Chapter 2: Methods and materials

2.1 Microorganisms used in experimental procedures:

Organism	Accession number	Source and storage
<i>Escherichia coli</i>	ATCC 10536/ NCTC 10418	Reference strain; obtained from UWE repository. Cryopreserved at -80°C.
<i>Escherichia coli (carbapenem-resistant)</i>	NCTC 13919	Reference strain – clinical isolate (human rectum); obtained from UWE repository. Cryopreserved at -80°C.
<i>Staphylococcus aureus</i>	ATCC 6538/ NCTC 10788	Reference strain; obtained from UWE repository. Cryopreserved at -80°C.
<i>Klebsiella pneumoniae</i>	NCIMB 13281/ ATCC 13883	Reference strain; associated with urinary tract and respiratory tract infections; obtained from UWE repository. Cryopreserved at -80°C.
<i>Acinetobacter baumannii</i>	ATCC 17978	Reference strain derived from clinical isolate (bacterial meningitis); obtained from UWE repository. Cryopreserved at -80°C.
<i>Pseudomonas aeruginosa</i>	ATCC 15442/ NCTC 13359	Reference strain; obtained from UWE repository. Cryopreserved at -80°C.
<i>Pseudomonas aeruginosa</i>	NCIMB 10548	Reference strain, associated with wound, burn, and urinary tract infection; obtained from UWE repository. Cryopreserved at -80°C.
<i>Enterococcus faecalis</i>	NCTCC 12697/ ATCC 29212	Reference strain; obtained from UWE repository. Cryopreserved at -80°C.
<i>Candida albicans</i>	NCTC 10231/ NCPF 3179	Reference strain; obtained from UWE repository. Cryopreserved at -80°C.

Table 2.1. Reference strains of microbial species used in antimicrobial efficacy testing protocols.

2.2 Plasma system design and standard testing procedures:

The effects of NTP were investigated using a combined source RF-MW plasma system (Figure 2.1) and torch-style applicator (engineered by Creo Medical, Bath, UK), operated with pure (99.999%) argon as the carrier gas. Argon gas is suitable for plasma generation, due to its chemically inert character, thus reducing the risk of production of toxic gaseous species, whilst being easily ionised during plasma generation, moreso than ambient air (Baeva *et al.*, 2012). The noble gases also demonstrate characteristically low breakdown voltages, enabling the formation of ionized plasma components at lower input voltages (Das, Dalei, and Barik, 2018; Mestre, *et al.*, 2024).

Using this combined source RF-MW system, the generator 'strikes' the NTP by applying a transient burst of high voltage 100 kHz RF energy, at 100 W, to the neutral carrier gas, argon, subjecting it to an electromagnetic field, then to a pulsed train of 2.45 GHz low-voltage MW energy, of up to 100W, to sustain a regular pulsed discharge of NTP, produced at the terminal aperture of the torch applicator. A trigger unit between the RF strike unit and MW source facilitates the burst of MW strike pulses to ignite the plasma, via a 20dB microwave coupler, diode detector, and a smoothing capacitor (Hancock *et al.*, 2017) (Figure 2.1). The trigger unit is linked via a micro-controller to a user-controlled interface, to allow certain system parameters to be varied by the operator, such as the amplitude and duration of the RF burst, the MW duty cycle (the ratio of 'on time': 'on + off time') and MW power setting. A low pass filter within a power combiner unit connecting the two energy sources is included, to allow 100kHz RF energy through, whilst filtering out 2.45GHz MW energy which would damage the RF source. The combined RF-MW energy is transmitted via a co-axial cable assembly to the NTP 'torch'-style applicator, which takes the form of a co-axial transmission line, comprising a quartz (dielectric) tube, inner tungsten rod (waveguide) with proximal end PTFE insulation, and gas inlet, housed within a brass block. The quartz tubing acts to separate inner and outer electrodes, and prevents voltage breakdown between these two conductors (Hancock, *et al.*, 2017).

The effects of adjusting plasma generator parameters may thus be studied, to determine the influence of each on resultant plasma characteristics and performance, such as antimicrobial efficacy, and reactive species profile. Increasing the duty cycle increases the power delivery into the plasma, and similarly, increasing the amplitude of the microwave power (the predominant energy source), and/or lengthening the total treatment time enables user-adjustable increases in plasma intensity and overall energy delivered to the target to be applied (Hancock, *et al.*, 2017). Altering the frequency of the energy source and/ or power level can affect the power, and therefore energy, transferred to the plasma effluent, leading to changes in the physicochemical properties, performance, and under some conditions, appearance of the plasma produced (Gerling, *et al.*, 2017).

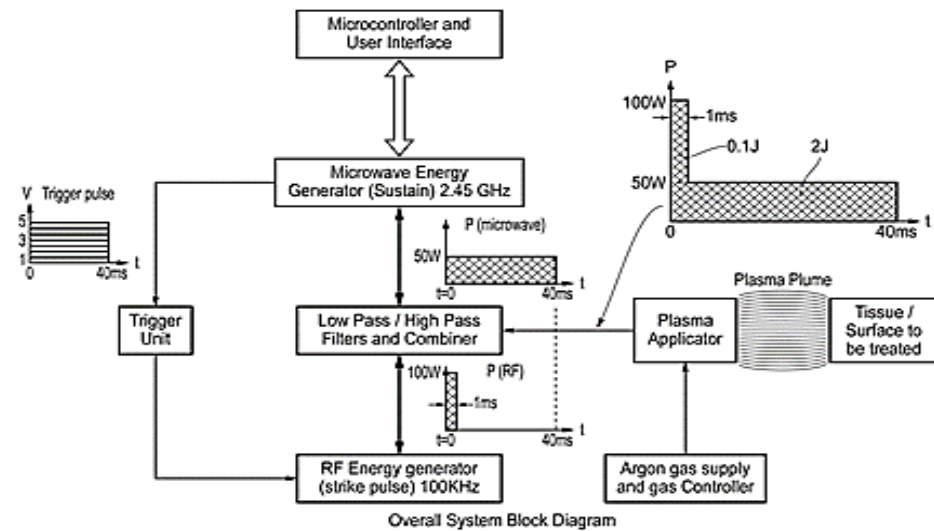


Figure 2.6 Schematic illustration of the combined source RF-MW plasma system, produced by Creo Medical (Hancock, *et al.*, 2017).

The Creo Medical combined RF-MW NTP generator was placed adjacent to a class II microbiological safety cabinet during experiments, connected to mains AC power supply, with argon supplied via a pressurised 300 bar cylinder, passed through a regulator and dual-meter flowmeter, set manually to a 4L min^{-1} flow rate, and connected to the NTP torch-style applicator (Figure 2.2) via flexible PVC tubing. The applicator itself was housed within a class II microbiological safety cabinet and positioned over the target using a clamp stand, so that the distance from the quartz effluent port to the target surface was approximately 10mm. Between treatments, the NTP applicator was cleaned using 70% ethanol in order to prevent potential cross-contamination by aerosolised microorganisms or cell suspension.

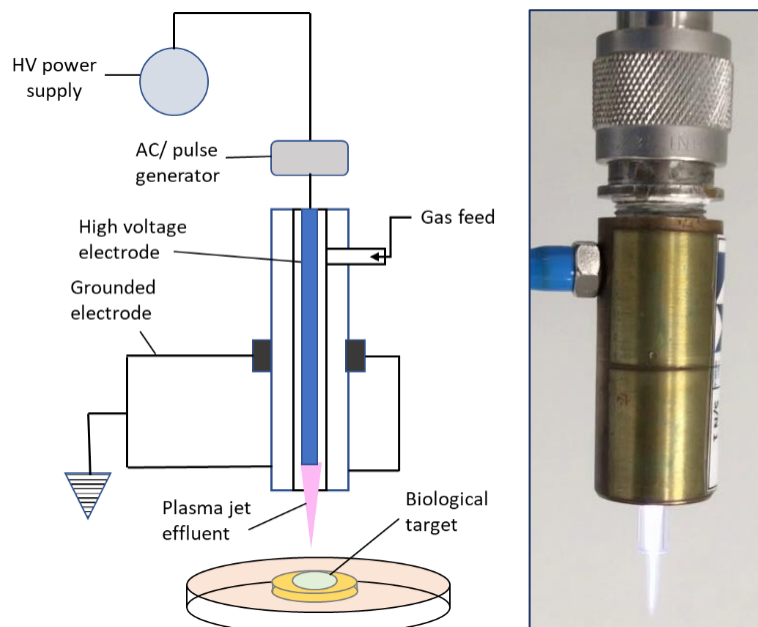


Figure 7.2. Atmospheric Pressure Plasma Jet (APPJ) device: (Left) The applied electric voltage passes through a pulse generator/alternator to the first electrode, which is proximal to the second, a grounded tube electrode. An inert gas feed carries the plasma constituents to the APPJ terminal aperture, creating a plasma plume. The biological target was placed directly below the aperture, being separated by a discharge gap of approximately 10mm. (Right) The brass housing and quartz tube of the torch-style applicator used in the RF-MW system.

2.3 Measurement of NTP-induced Zone of Inhibition (ZOI):

To determine the size of the area targeted by the NTP torch-style applicator, simple zone of inhibition studies were undertaken against the microbial species of interest. Briefly, microbial lawns of each test species were inoculated on TSA plates (excepting *C. albicans*, for which Sabouraud's Dextrose Agar (SDA) was used) as follows: 100 μ L of 0.2OD₆₂₀ suspension (equivalent to 7 Log₁₀ – 9 Log₁₀ CFU/mL) was spread across the agar surface using a sterile L-shaped spreader, or alternatively by soaking a sterile cotton swab in the test suspension and swabbing across each plate three directions successively, and allowing to dry, before exposure to either NTP or argon gas alone (negative control) for up to 180s. For *C. albicans*, the test suspension used was adjusted to 0.4 OD₆₂₀, (equivalent to 7 Log₁₀ CFU/mL), due to its higher optical density: CFU ratio. Plates were incubated for 16-20h at 37°C, and the diameter of the cleared zone was measured using dialled-gauge callipers. Treatments were performed in triplicate and reported as mean ZOI diameter \pm SD.

2.4 Assessment of the antimicrobial effects of NTP on planktonic microbial loads on solid, non-porous surfaces

2.4.1 Surface inoculation, disinfection and recovery protocol

The efficacy of treatments against microbially contaminated surfaces was investigated using a modification of the British Standard BS EN 13697 Quantitative non-porous surface test for the

evaluation of bactericidal and/or fungicidal activity of chemical disinfectants (BSI, 2020). BS EN 13697 defines the standards required of chemical disinfectants for approved use in food processing, distribution and retailing areas, domestic, industrial, and institutional settings. To attain the British Standard's criteria for bactericidal, fungicidal and/or yeasticidal activity, the test product or agent must achieve a minimum 4 Log reduction in viability of the bacterial test species, and/or a minimum 3 Log₁₀ reduction in viability of fungal test species when applied to surfaces loaded with a specific concentration of a representative microbial contaminant under specified controlled test conditions (BSI, 2020).

Although further regulatory criteria exist for biocidal products intended for use in healthcare, such as disinfecting agents to be used on medical equipment or devices, or those designed for use on human tissue as a skin cleansing agent prior to surgical procedures, the modified BS EN 13697 Standard was used as a robust testing paradigm to assess the antimicrobial efficacy of NTP treatment. Comparison was made with the antimicrobial efficacy of commercially available antiseptic or biocidal products used commonly in clinical settings for cleansing of wounds and disinfection of fomites: polyvinylpyrrolidone iodine (PVP-I), hydrogen peroxide (H₂O₂), and ECAS (Electrochemically-Activated Saline solution), used as a representative hypochlorous acid-based solution similar to those currently marketed products for application in wound irrigation and skin antisepsis in clinical settings.

2.4.2 Initial validation of microbial loading of test surfaces:

Prior to the commencement of antimicrobial treatment testing, the duration of microbial viability following inoculation and drying onto surface carriers was determined over an extended drying period. This was performed to ascertain whether evaporation of the test suspension during surface drying caused a significant reduction in the recoverable viable load, since the stability of the microbial survival upon test surfaces within the experimental timeframe is critical to accurate evaluation of antimicrobial efficacy of applied treatments.

Prior to testing, the surface carriers (sterile 304 grade 2b stainless steel discs, 10mm diameter) (F.C. Hammonds, Bristol/ Fisher Scientific, Loughborough UK) were prepared by immersion in a ≥20mL solution of 5% (v/v) De-Con90 (Decon Laboratories, Sussex) for 1 hour, before rinsing with sterile deionised water for 10 seconds, and immersion for 10 minutes in 70% ethanol, followed by drying in a laminar flow cabinet in sterile Petri dishes. These measures were performed to ensure the removal of any particulate contaminants, and/or any residual surfactant prior to inoculation, treatment and recovery of microbial loads during subsequent test procedures.

2.4.2.1 Preparation of microbial suspensions for antimicrobial efficacy testing:

The test suspension for surface inoculation was prepared from a reference stock of the selected microbial strain maintained in -80°C storage, plated onto tryptone soy agar (TSA) (Thermo

Scientific/ Oxoid, UK) and incubated in aerobic conditions at 37°C for 16-24h, to obtain pure colonies. Microbial test suspensions were prepared by transferring colonies into 10mL of 0.85% (w/v) NaCl, 1% (w/v) tryptone diluent (prepared in distilled water) and 5g sterile glass beads. Suspensions were homogenised by brief vortexing, and then adjusted to an OD_{600nm} of between 0.1 – 0.3 (Jenway 6715 UV/Vis), equivalent to a microbial density of 1.5 – 5.0 x 10⁸ CFU/mL. From this test suspension, a working suspension was made by mixing 1:1 with 1mL of a 0.06% (w/v) suspension of Bovine Serum Albumin (Acros Organics, NJ USA) (BSA), prepared in pure water and passed through a 0.45µm sterile filter, therefore giving a final 0.3g/L concentration of BSA. BSA was included as a soiling substance, to simulate low level proteinaceous contamination in the industrial or clinical environment, referred to as ‘clean conditions’ within the BS EN 13697 protocol. A 50µL volume of the final working suspensions was then pipetted onto each test surface and placed in a class II biosafety cabinet until visibly dry.

2.4.2.2 Optimisation of inoculation parameters

During initial experiments, it was noted that a 50µL inoculation volume required a drying period of >30 minutes, and resulted in variability in the viability of the recovered microbial load equivalent to ≥1 Log₁₀ reduction. To achieve more consistent drying times between replicate inoculated discs, a smaller inoculation volume (10µL) was chosen, using microbial suspension at an increased density, i.e. 0.5 OD₆₀₀ instead of 0.3 OD₆₀₀, (mixed 1:1 with 0.6g/L BSA). This adjustment ensured that the applied microbial load remained within the order of 6 Log₁₀ CFU/mL but was visibly dry and ready for treatments within approximately half the time required when a 50µL inoculum volume was used (i.e. 20 - 30 minutes, versus 50 - 60 minutes).

2.4.3 Confirmation of microbial load viability within extended drying

The nature of the NTP test system necessitated performing multiple treatments in sequence on simultaneously inoculated individual carriers. It was therefore investigated whether inter-replicate time delay in treating and recovering the dried inocula from the test surfaces led to significant variation in baseline viability, thereby introducing a source of error in the calculation of the (untreated) control microbial load. This was determined by performing an extended drying time-course, in which test surfaces were subjected to further drying, beyond the initial ‘visibly dry’ test point cited within the BS EN 13697 test methodology.

Recovery from stainless steel coupons was performed at 5, 10, 15, 20 and 30 minutes additional drying time under laminar flow, after reaching the ‘visibly dry’ state. Microbial viability was then evaluated by dissociation of the treated inoculum from the coupon surface, neutralisation of antimicrobial agent activity, and serial dilution of the resultant suspension, plating out samples for total viable count (TVC), as described in the following test protocol.

2.4.4 Application of NTP and biocidal treatments to test coupons, and determination of antimicrobial efficacy

Once visibly dry, inoculated coupons were subjected to treatment with either NTP or a 100µL volume of the relevant biocidal agent, for up to 3 minutes (NTP exposures), or 5 minutes (aqueous biocides). Coupons were then placed separately into sterile 50mL centrifuge tubes, containing 10mL Lethen broth neutralising solution (28.5g/ L, in sterile dH₂O) (Thermo Scientific Ltd, UK) and 5g sterile glass beads (3-4mm diameter), and vortex mixed for 60 seconds to detach microbial cells. For treatments with electrochemically-activated saline solution (ECAS), Lethen broth was constituted with the addition of 5g/L sodium thiosulphate (Na₂S₂O₃) to neutralise any residual chlorine species. Recovery suspensions were serially diluted with 0.1% (w/v) tryptone, 0.85% (w/v) NaCl diluent (prepared in distilled water, as used in preparation of the test suspension), and plated onto TSA by spread-plate, Miles and Misra, or automated spiral-plating (Whitley WASP TOUCH spiral plater, Don Whitley Scientific, UK), before overnight incubation at 37°C. Calculation of surviving microbial load per carrier was made by total viable count, and compared to untreated (dried only) inoculated controls.

The effects of NTP and of the alternative test biocidal products were evaluated by comparing Log₁₀ reduction in viable bioburden (with respect to the initial dried untreated load at T₀) following each treatment, and analysed using a two-way ANOVA with multiple comparisons (using Šidák's correction) (GraphPad Prism version 9.5.1 (733)). Time-matched control treatments in the form of argon gas only (for NTP treatments), or sterile deionised water (for liquid biocidal products) were carried out in parallel. Baseline microbial viability was determined by recovering the dried inoculum from surface carriers to which no treatments had been applied, quantifying the initial dried load per coupon at T=0. The procedure was performed in triplicate, in entirety at least three times unless otherwise stated, to obtain results from independent biological repeats.

2.4.5 Validation of the non-toxicity and efficacy of neutralisation in non-porous surface-disinfection methodology:

To verify that the Lethen broth neutraliser (1% meat peptone, 0.5% beef extract, 0.5% polysorbate 80, 0.5% sodium hydrochloride, 0.07% lecithin, prepared in 1L dH₂O) used in the porous surface disinfection protocol effectively terminated the antimicrobial activity of the test treatments, and also was compatible with the test organisms, exerting no effects on microbial viability itself, validation procedures was performed, as indicated in the BS EN 13697 Standard (British Standards Institution, 2020).

To confirm absence of toxicity of the neutraliser, stainless steel test coupons were prepared and inoculated with microbial working suspension as described in Section 2.4.2.2, and, when dry, were added to 50mL centrifuge tubes containing 10mL Lethen neutraliser and 5g sterile glass beads.

100µL water was added, and left in contact for a period of 5 minutes at room temperature, before vigorous agitation of each tube using a vortex for 60s, to detach the microbial load from each coupon. Each recovery suspension was sampled in duplicate and plated onto TSA before incubation overnight at 37°C under aerobic conditions, for colony enumeration. Validation was carried out for both *S. aureus* ATCC 6538 and *P. aeruginosa* NCIMB 10548.

To validate test product neutralisation (i.e. cessation of antimicrobial activity by the addition of Lethen), this procedure was repeated, but, in place of water, adding 100µL of the maximum tested concentration of each aqueous antimicrobial product to the neutraliser: 220ppm ECAS, 6% hydrogen peroxide, and 10% (w/v) PVP-I (5% PVP-I was also tested, to ensure equal efficacy of neutralisation). The BS EN 13697 test protocol states that for method validation, the recovered viable load obtained following test product neutralisation, and from the water control, should differ by no more than ± 0.3 Log, thus demonstrating only negligible effects of the neutralisation step on microbial viability.

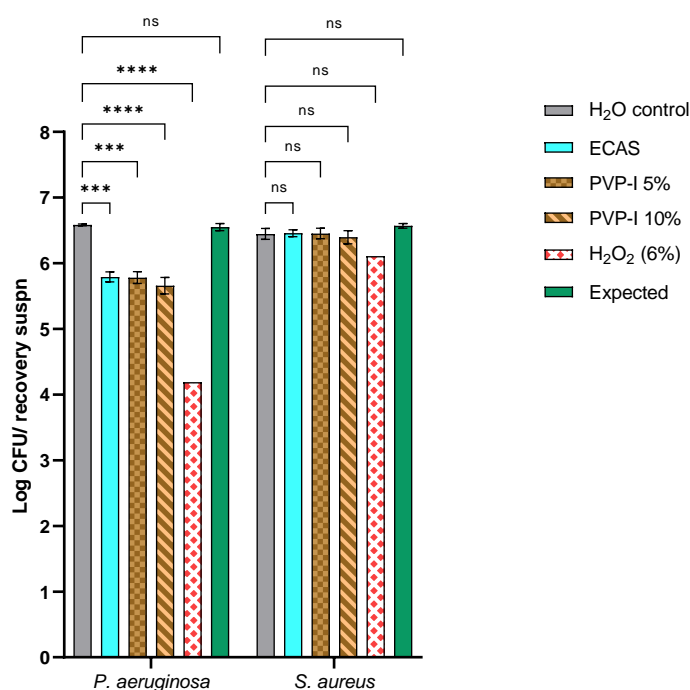


Figure 2.3. Validation of surface disinfection neutralisation step, performed on stainless steel carriers, in duplicate; n=3 (except for 6% hydrogen peroxide, where n=1). The Log [total viable load] recovered from each coupon following addition of the test product was compared to a water control by 2-way ANOVA with Dunnett's correction for multiple comparisons.

The total viable load obtained after neutralisation of each test product revealed no significant difference in recovery with respect to the water control in coupons inoculated with *S. aureus*, where mean CFU/disc was within 0.18 Log₁₀ of control, with the exception of 6% H₂O₂ which showed a 0.34 Log difference (p>0.05) (Figure 2.3). In contrast, *P. aeruginosa* recovered loads were significantly lower following product neutralisation, with a reduction relative to water controls of 0.79 Log for ECAS (p<0.001), 0.80 Log for 5% PVP-I (p<0.001), 0.93 Log for 10% PVP-I

($p < 0.0001$) and 2.4 Log for 6% H_2O_2 ($p < 0.0001$) (Figure 8). These findings indicated that residual antimicrobial activity was present following the 5-minute neutralisation process, to a degree which exerted negative effects on the viability of the *P. aeruginosa* inoculum. Given the increased susceptibility of *P. aeruginosa* to post-inoculation drying, these results indicate that the further physiological stress introduced by incomplete neutralisation of antimicrobial activity when aqueous test products were added to Lethen neutraliser was poorly tolerated by the remaining viable microbial load. Therefore, the established neutralisation procedure was deemed appropriate for *S. aureus* only, in efficacy testing of PVP-I, ECAS, and hydrogen peroxide for surface disinfection.

2.5 Assessment of the antimicrobial effects of indirect plasma treatments and alternative antimicrobials on planktonic microbes in suspension

The efficacy of aqueous plasma-activated solutions (PAS) against test microbial suspensions was investigated using a modified method based on British Standard BS EN 1040: 2005 Chemical disinfectants and antiseptics - Quantitative suspension test for the evaluation of basic bactericidal activity of chemical disinfectants and antiseptics (Phase 2, step 1) (BSI, 2005), which is a testing procedure used to assess basic bactericidal activity in chemical disinfectants and antiseptic products to be applied in aqueous solution within similar settings to those designated in the BS EN 13697 (non-porous surface disinfection) test. Therefore, it serves as a product efficacy testing protocol suitable for ascertaining the biocidal performance of products intended for use in situations where disinfection is medically indicated, but not for the certification of high-level disinfectants or those to be applied to living tissue other than hand hygiene.

The BS EN 1040 Standard protocol is designed to ascertain the inhibitory effects of the test products when applied at a maximum concentration equivalent to 80% (diluted in water) of that of the initial preparation, for a contact period of 5 minutes \pm 10s, at room temperature ($20 \pm 1^\circ\text{C}$), without the addition of interfering substances. Similarly to quantitative non-porous surface disinfection testing procedures (Section 2.4.1), the microbicidal activity of the test products is halted by neutralisation, and the surviving microbial load is then quantified by total viable count. The test organisms specified within the test methods are *S. aureus* ATCC 6538 and *P. aeruginosa* ATCC 15442, providing evidence of the comparative efficacy on both a Gram-positive and a Gram-negative species, and treatment under test conditions should produce a minimum 5 Log reduction to qualify as a biocide, according to the Standard requirements (BSI, 2005). In the suspension tests performed here, the more clinically-relevant *P. aeruginosa* NCIMB 10548 strain was used to

assess the microbicidal activity of applied treatments, as a more appropriate test organism than ATCC 15442 in the context of clinical antiseptics and disinfection.

Briefly, test suspensions of each organism, *S. aureus* ATCC 6538 and *P. aeruginosa* NCIMB 10548 (clinical isolate associated with burn wounds), were separately prepared as described in Section 2.4.2.1, but adjusting the optical density of each to 0.2 ± 0.05 OD₆₂₀, equivalent to $1.5 - 5 \times 10^8$ CFU/mL in 0.1% tryptone/ 0.85% NaCl diluent, and omitting the addition of BSA as an interfering substance. The density of each test suspension was confirmed as before, by serial dilution and plating onto TSA to obtain total viable counts.

A 1mL volume of each test suspension was then added to a sterile universal tube containing 1.0mL sterile dH₂O, mixed by vortexing, and allowed to rest at room temperature ($20 \pm 1^\circ\text{C}$) for 2 minutes \pm 10s. Then, 8.0mL of the antimicrobial test solution was added to the diluted microbial suspension, mixed well and incubated at room temperature for a contact period of 5 minutes. At the end of the treatment period, the suspension was once again mixed, before transferring a 1.0mL sample to a separate tube containing 8.0mL Letheen broth neutraliser (Thermo Scientific Ltd, UK) and 1.0mL sterile dH₂O. This neutralisation mixture was briefly vortexed and incubated at room temperature for a further 5 minutes \pm 10s. Immediately following this step, a 1.0mL sample of the neutralised suspension was taken, serially diluted and plated onto TSA. After overnight incubation at 37°C, colonies were enumerated to enable evaluation of biocidal effect. Plates were re-incubated for another 16-20h if colonies were absent or poorly visible after the first overnight incubation.

2.5.1 Validation of antimicrobial suspension testing method, and non-toxicity of the neutraliser

To ascertain effective neutralisation of the antimicrobial test products following the addition of the selected neutraliser - Letheen broth – under test conditions (method validation), and to demonstrate the absence of toxic effects of the neutraliser itself (verification of neutraliser non-lethality), the experimental procedure was validated for both test species. To demonstrate adequate inactivation of antimicrobial activity of each test product during neutralisation, an 8mL volume of each antimicrobial solution at the maximum tested concentration was added to separate sterile 30mL vials, each containing 1mL dH₂O and 1mL 0.1% tryptone/ 0.85% NaCl diluent, mixed well by vortexing, and left to equilibrate for 5 minutes. This mixture was the briefly vortexed again, 1mL was transferred to a second 30mL tube containing 8mL Letheen broth, and mixed well to commence neutralisation. A validation suspension of the test microbial species was prepared in the diluent, using a similar method to that used in the suspension test (see Section 2.5), but adjusted to a density of $1 \times 10^3 - 3 \times 10^3$ CFU/mL. After 5 minutes neutralisation time, 1mL of the validation suspension was added to the neutralisation mixture, vortexed once more,

and left at room temperature for 30 minutes. At the end of this time, the neutralised test mixture was sampled in duplicate and plated onto TSA, incubated at 37°C overnight, for quantification of viable colonies.

The non-lethality of the neutraliser was tested by vortex-mixing 1mL dH₂O and 8mL Lethen broth in a sterile vial, then adding 1mL of the validation suspension, and mixing a second time. This test mixture was incubated at room temperature for 5 minutes, then sampled in duplicate, plated onto TSA and incubated at 37°C overnight, for subsequent viable colony-counting.

The BS EN 1040 protocol specifies that the number of viable colonies recovered from 1mL of each of the neutralised test product suspension should yield no fewer than half the viable count obtained from 1mL of the 10⁻¹ diluted validation suspension. In the same way, the neutraliser control suspension should contain a total viable load no less than half that within a 10⁻¹ dilution of the validation suspension, indicating no significant reduction as a result of exposure to the neutraliser during the test neutralisation period.

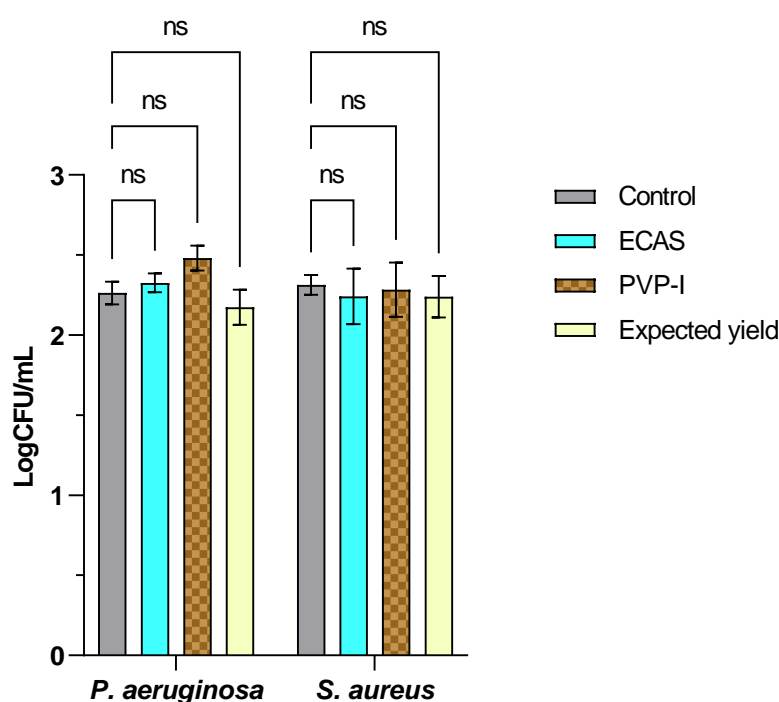


Figure 2.4. Validation of the neutralisation method used in antimicrobial suspension testing. Viable loads were recovered from suspensions after 5 minutes neutralisation of each test product, followed by 30 minutes incubation with a validation suspension of each test organism. Validation was performed in duplicate; n=3.

The results of the validation test demonstrated that the yield of all neutralised test suspensions and the neutraliser validation suspension satisfied the requirements specified, with a difference of <50% between the viable yield from each recovery suspension and that of a tenfold dilution of the validation suspension. No significant difference was seen between viable Log₁₀[recovered load] following neutralisation of any of the test products, within either microbial species (Figure 2.4).

2.6 Biofilm culture models and treatments

2.6.1 CDC Biofilm Reactor system

2.6.1.1 Formation of biofilms within the reactor

Single species biofilms were cultured within a Center for Disease Control (CDC) Biofilm Reactor® (CBR) (BioSurface Technologies Corporation, Bozeman, Montana) (Figures 2.5 and 2.6) comprising a 1L borosilicate glass reactor housing eight removable reactor rods (Figure 2.6), each supporting three 12.7mm diameter, 3.8mm thick discs or coupons which form the substrate for biofilm growth. Coupons are subjected to high fluid shearing force via continuous rotation of a magnetically propelled baffle within the reactor chamber, stirring the medium within at a constant rate. The reactor was connected via size 18 silicone tubing to a 20L polypropylene carboy filled with input medium (100mg/L tryptone soya broth) (TSB) (Thermo Scientific/ Oxoid, UK), and a length of size 16 silicone tubing passed through a peristaltic pump, calibrated to a flow rate equivalent to approximately 11.6 mL/min, ensuring a dwell-time within the reactor of 30 minutes. This continuous flow and stirring of medium enables biofilm formation to occur on the coupons colonised by the test organism under constant high shear force, whilst the residence time of input medium and suspended planktonic organisms within the reactor is controlled, to prevent waste material accumulation and to regulate bacterial biofilm growth. Waste medium from the reactor drained freely into a second 20L carboy placed below the reactor, and connected to its effluent port by a section of size 18 silicone tubing.

Biofilm formation involved two culture phases, batch and continuous. Initial inoculation of the reactor at batch phase was performed with the reactor fully assembled and all components sterile. Batch phase culture medium (300mg/L TSB) was added aseptically to the reactor chamber to the fill line (approximately 420mL) with all rods and baffle in place, and the effluent port tubing clamped shut. For inoculation of the reactor, a broth culture of the test organism was prepared, by adding a single isolated colony from a pure culture to 100mL sterile batch phase culture medium, and incubating overnight (16-22h) at $36 \pm 2^\circ\text{C}$ with shaking (125rpm). A 10mL aliquot of this culture was taken and adjusted to a density of 0.05 OD_{620nm} to obtain a suspension equivalent to $3 \times 10^7 - 2 \times 10^8$ CFU/mL, from which a 1mL volume was then used to inoculate the CBR. A serial dilution of the inoculum suspension was prepared and plated onto TSA for incubation overnight for quantitative confirmation of viable microbial density, and its purity. Batch phase growth was timed from the point of inoculation and proceeded for a period of 24 h at 22°C with continuous stirring at 120 rpm.

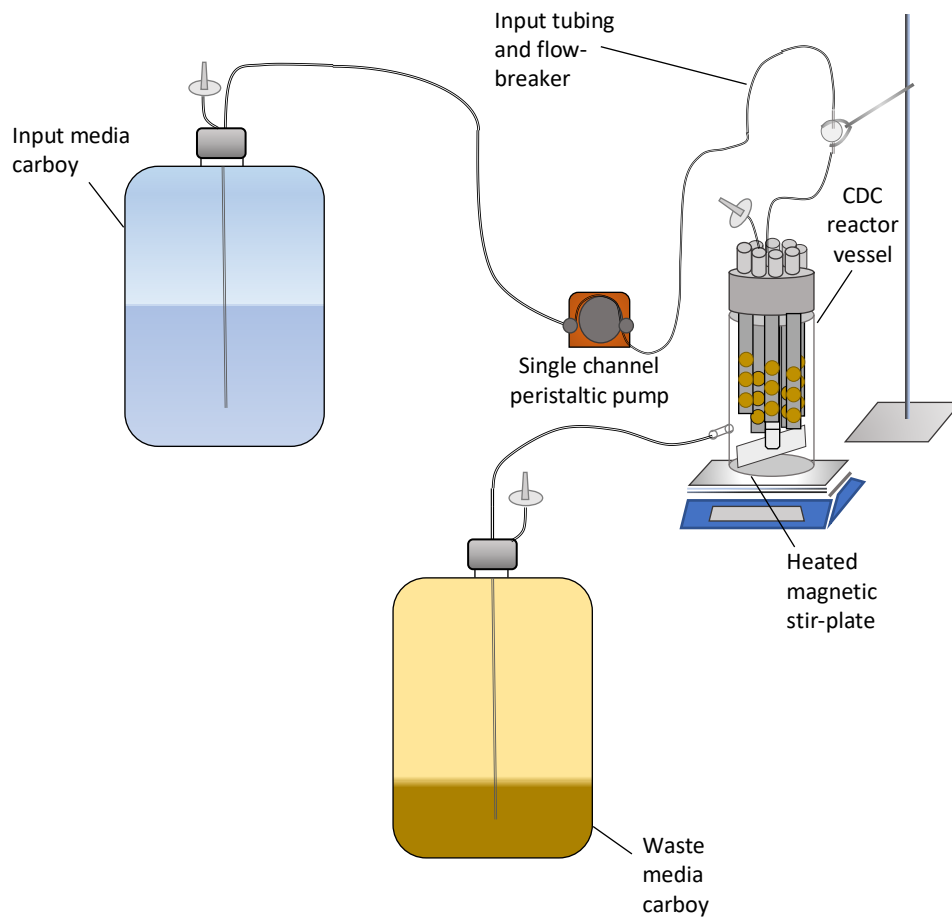


Figure 2.5: CDC Biofilm Reactor (CBR) apparatus used for continuously stirred chamber biofilm growth.



Figure 2.6: Assembled CBR reactor chamber (left) and a single coupon-holding rod (left) with coupons and securing screws (reproduced from BioSurface Technologies Corp, 2016)

Continuous phase was initiated after 24 hours by opening the reactor effluent tubing port and initiating the flow of input medium (100mg/L TSB) via the peristaltic pump, allowing passage of media through the entire system at a constant rate of 11.6 mL/min, maintained at 22°C, with stirring at 120 rpm. Following 24h of continuous phase culture, the reactor rods were removed aseptically for treatment and sampling of the coupon-associated biofilms.

These operating parameters were used for culturing single species *P. aeruginosa* NCIMB 10548 biofilms, but were modified for *S. aureus* ATCC 6538 due to inferior biofilm formation under the standard conditions described earlier. To promote *S. aureus* biofilm growth, the batch phase medium concentration was increased ten-fold to 3g/L TSB, and for continuous phase medium 1g/L TSB was used. Stir rate remained at 120 ± 2 rpm, but the reactor operating temperature was raised to $28 \pm 2^\circ\text{C}$.

2.6.1.2 Application of antimicrobial treatment to mature CBR biofilms

At the end of the continuous growth phase, the reactor was stopped, and each of the rods containing biofilm-coated coupons were removed in turn, and rinsed with 3 x 1mL sterile PBS on each side, to remove any non-adherent cells. For NTP treatments and argon controls, each reactor rod was transferred to a class II microbiological safety cabinet and firmly fixed in a clamp stand. Positioning each coupon in turn directly below the NTP applicator aperture at approximately 10mm applicator-target distance, direct plasma treatments were delivered to the adherent biofilm. Coupons were subjected to pulsed NTP treatment for either 60s or 120s, with generator operating parameters at standard settings (80W MW power, 25% duty cycle, using 4slm^{-1} argon) on one side before rotating the rod 180° to treat the opposite side in the same way. Aqueous treatments were applied by flooding the coupon surface with the test product for the chosen exposure time, and rinsing with sterile PBS before repeating the procedure on the opposite side. Treated coupons were released from the reactor rods and placed aseptically into separate 50mL centrifuge tubes containing 10mL Lethen broth neutraliser. To dissociate and disaggregate the attached biofilms, each coupon was subjected to 30s agitation by vortexing, followed by 60s sonication at 35kHz in a sonicating water bath, and a further 30s of vortexing. Serial dilutions of the resulting recovery suspension were made in 0.1% tryptone/ 0.85% NaCl diluent and plated onto TSA for overnight (16-22h) incubation at 37°C, and enumeration of colony-forming units.

2.7 Biofilm culture within the Drip-Flow Reactor (DFR) - collagen matrix wound model

2.7.1 Biofilm culture under standard operating parameters

Collagen-matrix associated biofilms were grown within a BioSurface Technologies Drip Flow Reactor (BioSurface Technologies Corporation, Bozeman, MA, USA) using the approach described

previously by Slade *et al* (2019), with minor modifications. A simulated wound fluid (SWF) was first prepared, composed of a complex mixture of electrolytes and solutes found in physiological wound exudate (Oates, A, McBain, 2016). The following constituents were dissolved in 1L deionised water and sterilised by autoclaving: 20.9g MOPS (3-(N-Morpholino)propanesulfonic acid, $C_7H_{15}NO_4S$) (Thermo Fisher), 6.025g NaCl, 0.372g KCl, 0.54g Urea, 0.0132g creatinine, 0.324g D-glucose, 1.0g yeast extract, 3.0g peptone, 0.109g potassium phosphate (K_3PO_4), 2.0g NaOH, and 2mL haemin stock solution (250 μ g/mL in 50mM NaOH). Sterile glass slides (Corning, Fisher Scientific UK) measuring 76 x 26 mm were coated upon one surface using a 2mg/mL collagen suspension in SWF, prepared using a concentrated type I collagen stock of approximately 10mg/mL, supplied in 0.2M acetic acid (Corning, Fisher Scientific). For a 10mL volume of 2mg/mL collagen suspension (sufficient to coat 6 slides), the appropriate volume of concentrated stock was calculated, and also the required volume of 1M NaOH for neutralisation to pH7, using 0.023mL 1M NaOH per 1 mL collagen stock. The residual volume for 10mL final suspension volume was constituted with SWF, to which the sodium hydroxide was added, followed by the collagen concentrate, mixing gently, with all constituents pre-chilled on ice to prevent rapid polymerisation of the collagen. From this final collagen suspension, 1.5mL volumes were pipetted gently onto individual slides to ensure an even coating, before carefully transferring the slides to a 37°C incubator for 1hr, to allow the polymerisation and solidification of the collagen matrix.

After incubation, each collagen-coated slide was inoculated using 1mL of a 2×10^8 CFU/mL microbial suspension of the test organism, prepared in SWF, using single colonies in Log phase growth taken from a pure culture on TSA incubated overnight at 37°C. All experiments reported here used single species biofilms of *P. aeruginosa* NCIMB 10548, being a microbial strain associated with infected wounds, and which has been demonstrated in publications to form mature, three-dimensional biofilms within the collagen-DFR model (Slade *et al.*, 2019). Inoculated slides were incubated at 33°C (mimicking wound surface temperature (Dini, *et al.* 2015; Gethin *et al.*, 2021)) for 2 hours, to allow initial bacterial adherence and permeation of the collagen matrix. Following this second incubation, slides were gently rinsed thrice with 1mL PBS, to remove any non-adherent microorganisms, and were then individually placed within the channels of a previously sterilised polyethylene terephthalate (PET) drip-flow reactor, and the lids secured. The assembled reactor (Figure 2.7) was then transferred to a 33°C incubator, positioned at a 10° angle on its base support, and each channel was connected via a 23 gauge 1.25" sterile syringe needle to a length of silicone media input tubing (3mm ID) connected to Marprene peristaltic pump manifold tubing (1.29mm ID) (Watson Marlow, UK). The peristaltic pump was then started, supplying each channel with sterile SWF fed via drip-flow at a rate of 2mL/hr for a culture period of 48-72h, to enable mature biofilm formation upon and within the collagen matrices.

2.7.2 Biofilm recovery from microscopes slides within the DFR-collagen matrix model

Recovery of biofilms was achieved by scraping each biofilm using a sterile L-shaped scraper and rinsing the carrier surface thrice with 1mL PBS, to collect the residual biofilm into a separate sterile 50mL centrifuge tube, containing 2mL collagenase Type I (Gibco, Fisher Scientific ,UK) solution (500µg/mL in sterile PBS). After briefly vortexing to mix the obtained biofilm suspension, each tube was incubated at 37°C for 20 minutes, then vortexed a second time, and returned to 37°C incubation for a further 20 minutes, to complete collagenase digestion of the hydrogel. The resulting suspension was transferred to a sonicating water-bath, and sonicated for 5 minutes at 35kHz, to disaggregate the biofilm, then pelleted by centrifugation at 4000 x g, for 10 minutes at 4°C. The supernatant was then aspirated, and the pelleted cells were re-suspended in 10mL PBS, and centrifuged a second time, at 4000 x g for 10 minutes. The supernatant was then removed and the bacterial cells re-suspended in 10mL PBS, before serially diluting, and plating out onto TSA for overnight culture and enumeration of colonies.

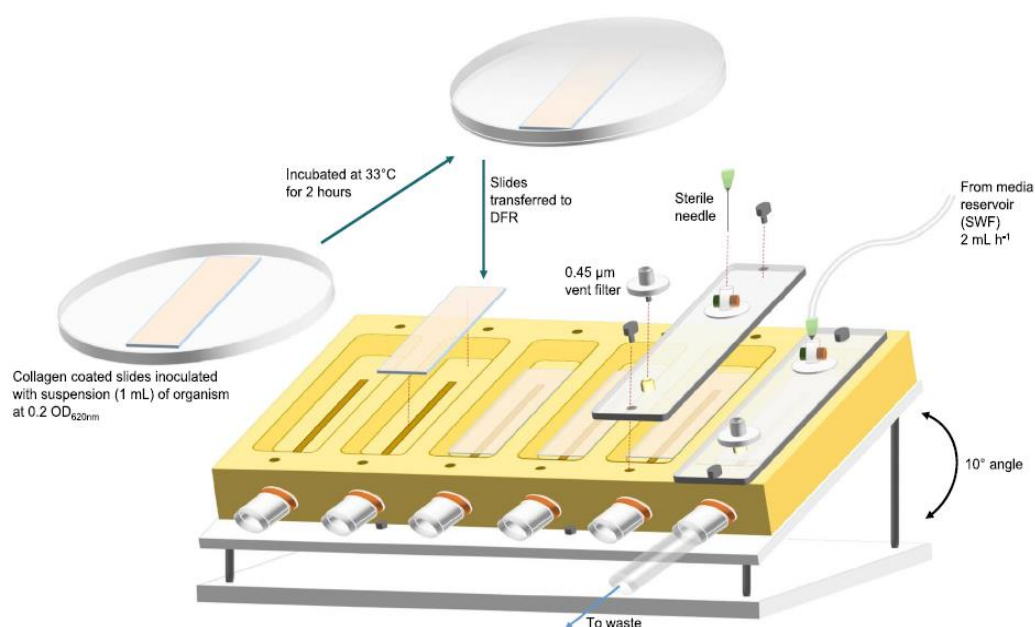


Figure 2.7: Illustration of the collagen wound biofilm model, reproduced from (Slade et al., 2019), incorporating collagen-coated slides into the 6-channel drip flow reactor.

2.7.3 Adapted operation of the DFR-collagen matrix model for miniaturised biofilm replicates

To obtain collagen-associated biofilms of smaller surface area to facilitate antimicrobial treatments of samples grown in parallel, 13mm diameter circular coverslips were incorporated prior to sterilisation of the reactor and collagen-coating of the slides, positioning up to 5 individual coverslips along the length of the surface of each slide. Following operation of the reactor, biofilm-coated coverslips were aseptically extracted from the slides using a sterilised circular steel cutter (15mm diameter).

Treatments were performed either upon coverslip biofilms extracted from the reactor at 48h maturity (method 1), or by continued drip-flow instillation of coverslip biofilms, within the reactor (method 2). Using the former approach, biofilms were placed into separate well of a 12-well microtitre plate, hydrated by the addition of 0.5mL PBS, and immersed in 1mL aqueous antimicrobial agent, or PBS (control) for a treatment duration of 5 minutes, before neutralisation and recovery. For the second method, antimicrobial treatments were introduced after 48h growth under control conditions, at which point the SWF feed was stopped, and lines were primed with either PBS (control) or ECAS (treatment), supplying each of the three test channels of the reactor with a different concentration of ECAS: either 200ppm, 300ppm, or 500ppm FAC. The peristaltic pump rate was temporarily raised to a flow rate of approximately 50mL/h in order to purge the DFR input tubing of SWF, and was then adjusted to approximately 11mL/h for a 30-minute treatment period, irrigating each biofilm with PBS or ECAS. Treatments were then stopped, and the SWF feed to each channel was restarted, purging ECAS from the lines, continuing for 1hr at a flow rate of 11mL/hr, before switching again to ECAS-only infusion for another 30-minute period. This second treatment period was again followed by a 1-hour SWF re-feeding period, before repeating ECAS treatment a third and final time. Biofilm-coated coverslips were subsequently extracted aseptically from each of the slides, placed into separate wells of a 12-well microtiter plate. To terminate any residual antimicrobial activity, 1mL Lethen neutraliser with 5g/L sodium thiosulphate was added to each well, prior to recovery of each biofilm.

Coverslip-associated biofilms were recovered by a similar but slightly amended procedure to that used for full-slide biofilms, namely by placing biofilm-coated carriers into separate wells of a 12-well microtiter plate, to which were added 1mL Lethen broth neutraliser and 0.5mL PBS. Treated and untreated samples were dissociated from the respective coverslips by scraping with a sterile 1000 μ L pipette tip. The obtained suspension was then transferred from each well to separate 50mL centrifuge tubes containing 3mL collagenase solution, and mixed briefly by vortexing. Recovery then proceeded as previously described for collagenase digestion, sonication and centrifugation.

2.8 Generation of plasma-activated solutions: PAW, PAM and pPBS

2.8.1 Activation via RF-MW plasma:

Indirect NTP treatments were performed using plasma-activation of aqueous solutions, namely deionised or distilled water, cell culture medium, or PBS. As an initial methodological approach, plasma-activated solutions were generated using the same combined RF-MW NTP system used in direct plasma treatments, and were produced by exposing a 6mL volume of the selected solution contained within a 6-well micro-titre plate to the NTP jet, gently moving the plate by slow rotation, to ensure exposure of the entire liquid volume. After the specified activation time (up to

300s), the plasma-activated solution - plasma activated PBS (pPBS), plasma-activated-medium (PAM) or plasma-activated water (PAW) - was transferred to a sterile 7mL bijou, before application to either microbial or mammalian cell cultures. Physicochemical parameters (pH, ORP and conductivity) for each plasma-activated solution were measured from a sample at ambient temperature, following application to cell cultures.

2.8.2 Small-batch SBD-PAW:

A Surface Barrier Discharge (SBD) plasma system was employed for the production of plasma-activated water (PAW) of small batch size (activation of individual 15mL aliquots) (Figure 2.8). Using this alternative NTP system, SBD plasma was generated using a 14kV peak-to-peak AC power source at 25.5kHz, 1.285A, passed through an oscilloscope, and applied to 15mL of non-stirred ultra-pure water contained within a sterile Petri dish for 5 minutes per aliquot. Batches of PAW were stored in sterile 15mL centrifuge tubes at 4°C until the point of use.

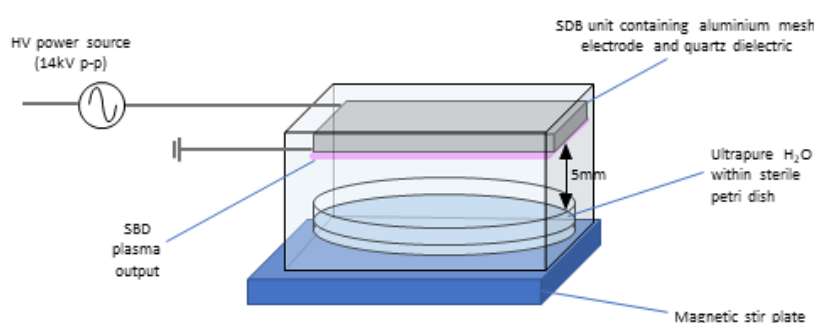


Figure 2.8: Schematic of small-batch SBD PAW generation system, using high-powered 14kV_{pp} input electrode, quartz layer dielectric, and aluminium mesh counter-electrode on the opposing face, to generate the plasma discharge layer.

2.8.3 Large-batch SBD-PAW generated by falling-film exposure:

A third plasma-generation configuration was used for the production of PAW in larger volumes, using a coaxial falling film reactor in which SBD-plasma was generated and exposed to a continuous flowing film of water (Figure 2.9), allowing its activation by the mass-transport of SBD-plasma reactive species (as described by Jabbariesgandani and Walsh, 2023). SBD-plasma was produced using two cylindrical electrodes aligned with two quartz tubes, one separating the high voltage (HV) copper electrode from the grounded stainless-steel mesh electrode, the other providing a surface for falling film exposure. A high voltage generator with variable amplitude between 1 – 20kV, supplied an input of 29-30V DC to the HV electrode, at 12kHz constant frequency, passing through an oscilloscope, maintained at 8.21kWpp. The high voltage outer electrode was separated from a mesh inner electrode, by the larger of the two quartz tubes (30mm diameter), which was coaxially aligned to the inner quartz tube (14mm diameter) through which water was pumped from a 500mL storage reservoir, circulating over the top of the inner quartz tube and flowing down its outer face, allowing exposure to the SBD-plasma emitted from the inner (mesh) electrode. The system was operated using a pump rate of 5.30mL/s, treating

ultrapure dH₂O for periods of 15 minutes, allowing multiple-pass exposure to SBD-plasma across the discharge gap of approximately 16mm. As an indicator of consistency between batches, it was ensured that a pH of ≤ 3.3 was attained in each batch of PAW, measured directly post-activation.

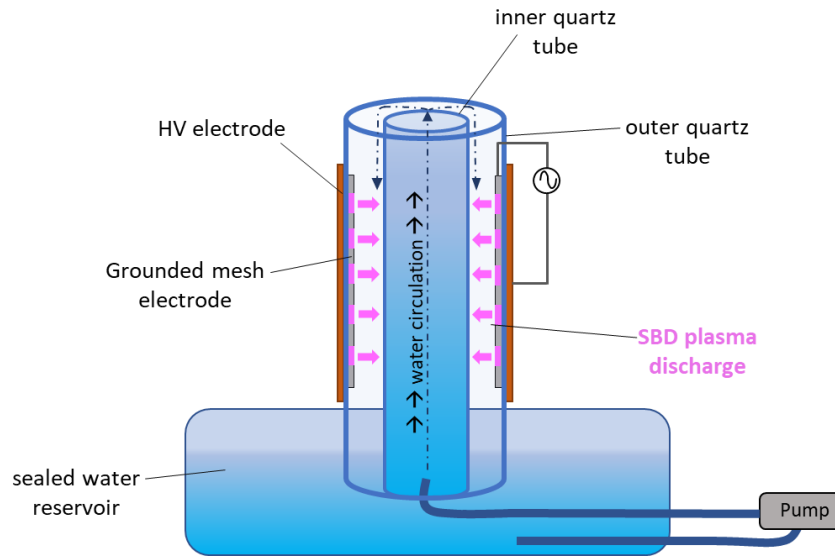


Figure 2.9: Schematic of SBD-plasma falling film system, including coaxial aligned cylindrical quartz tubing to channel water circulation, and to facilitate SBD-discharge at the inner surface of the larger of the two cylinders, forming across the mesh of the grounded electrode, thereby allowing plasma species to diffuse across the void between inner and outer quartz tubes to activate the falling film of water streaming down the outer surface of the inner quartz tube.

2.9 Generation of Electrochemically Activated Saline Solution (ECAS):

Electrochemical activation has emerged relatively recently as an effective, low-cost and sustainable means of producing solutions possessing potent antimicrobial properties. The system used to generate ECAS for application in experiments described here was the Envirolyte Cla900 unit (Envirolyte ECA Ltd, UK), consisting of a saline solution holding tank, pump, and electrochemical activation unit. Using mains water and saline solution as substrates, the system applies electrochemical unipolar (anodic or cathodic) activation to produce two metastable product solutions, separated by an ion-permeable exchange diaphragm, or membrane: the catholyte, which is highly reducing, and the anolyte, which has a high oxidising potential (Figure 2.10). In the anodic chamber, reactions between the anodic electrode surface and the continuously infused saline solution lead to the generation of chlorine, oxygen and other reactive oxidant species which are released into the anolyte bulk solution. In the cathodic chamber, electrolytic activation leads to generation of hydrogen, sodium hydroxide, and other reactive components, the majority being antioxidants, causing a decrease in the redox potential and a rise in pH of the catholyte bulk solution. The anolyte solution was the product collected and used in microbial and mammalian cell treatments described here (and referred to hereafter as 'ECAS'). ECAS was generated at 200ppm freely available chlorine (FAC) concentration, unless otherwise

specified, and stored at 4°C, protected from light, until the point of use, for a maximum of 3 days, to preserve reactive constituent levels.

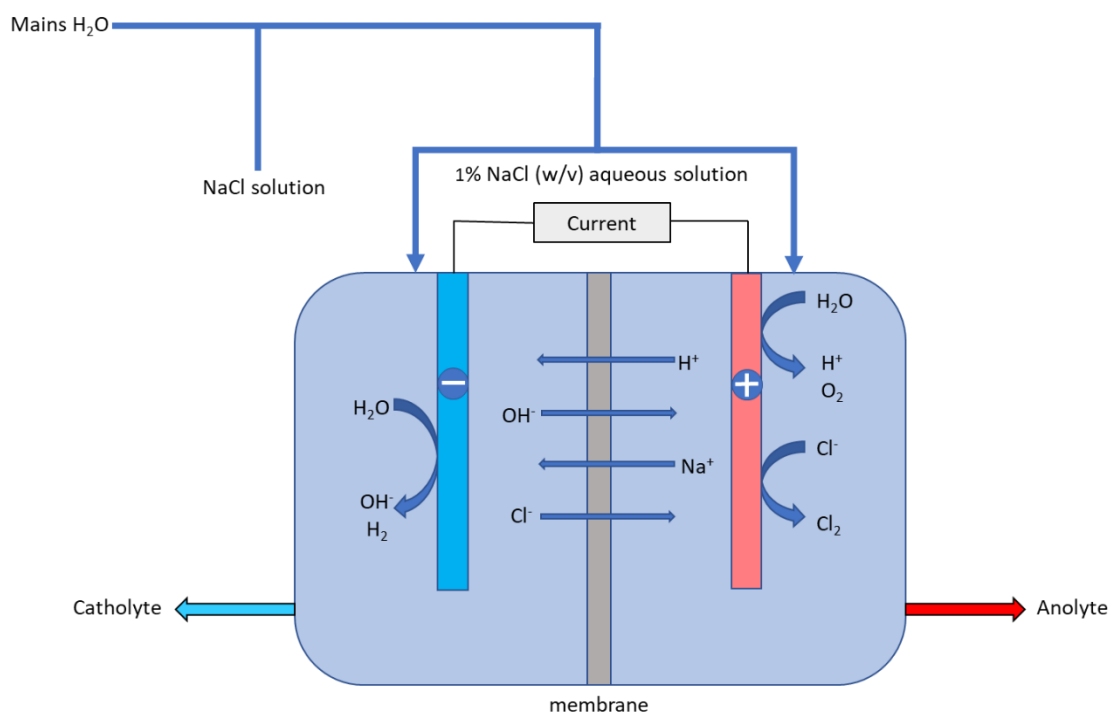


Figure 2.10: Schematic of the Envirolyte generator used to generate ECAS, consisting of an electrochemical cell containing two chambers – one for the cathode (left), the other housing the anode (right), separated by an ion-permeable exchange membrane. Saline is pumped continuously from a supply tank into both chambers, and undergoes electrochemical activation when unipolar direct current is applied, resulting in the generation of catholyte and anolyte solutions, exiting the generator by separate conduits.

The antimicrobial properties of ECAS are attributed to its distinct chemical composition and reactivity profile: being high in hypochlorous acid, having a high oxidation-reduction potential (ORP) typically between +800mV and +1200mV, and a mildly acidic pH (5.5 – 6.5). Therefore, basic physicochemical parameters (FAC, ORP and conductivity, and pH) were measured each time a fresh batch of ECAS was generated, to confirm batch-to-batch consistency. Freely available chlorine was adjusted, where necessary, by dilution with sterile dH₂O.

2.10 Mammalian cell culture and treatments

Immortalised human epithelial cell lines H103 (of oral squamous cell carcinoma origin; ECACC 06092001) and A375 (derived from a malignant melanoma; ECACC 88113005) were used in mammalian cell studies, and were maintained in Dulbecco's Modified Eagle Medium/Nutrient Mixture F-12 (DMEM F12/HAMS) (Gibco, Fisher Scientific UK) supplemented with 10% foetal bovine serum (FBS), L- glutamine (2 mM) and 5 µg/mL sodium hydrocortisone succinate, at 37°C with 5% CO₂.

2.10.1 Subculture routine:

Cells were passaged once confluence reached 70 – 80%, using 0.05% trypsin/EDTA for dissociation, requiring ≥ 10 minutes incubation at 37°C. Seeding densities for subculture were $5 \times 10^3/\text{cm}^2$ for H103, and $1 \times 10^4/\text{cm}^2$ for A375. For treatments, the standard seeding density recommended for each respective cell line was doubled, to achieve a higher degree of confluence prior to treatment initiation, at 24h post-seeding. Both cell lines were confirmed to be free of mycoplasma by out-sourced ISO17025-accredited mycoplasma qPCR-based methods (Eurofins Applied Genomics GmbH, Ebersberg, Germany), and were used in experiments at passage numbers between (5 and 25).

2.10.2 Cryopreservation of cells and revival from frozen storage

To maintain cryopreserved stocks of H103 and A375 within appropriate passage numbers, cells were frozen down periodically. Cells were dissociated from culture flasks by routine trypsinisation and resuspended in freeze-medium, consisting of 80% standard DMEM F12/HAMS culture medium supplemented with 10% dimethyl sulfoxide (DMSO) and 10% additional FBS, at a density of $1 - 3 \times 10^6$ cells/mL. This suspension was then aliquoted into 2mL cryovials and placed within a passive cooling container at -80°C before transferring to long-term storage in liquid nitrogen.

For the resuscitation of cells from deep-freeze, aliquots of 1-2mL frozen cells were rapidly thawed within a 37°C heat-bath, and diluted to 10mL with pre-warmed culture media, added drop-wise to the thawed suspension. The cell suspension was gently mixed, centrifuged for 5 minutes at 1300rpm, and the pelleted cells then resuspended in DMEM F12/HAMS supplemented with 10% additional FBS and transferred to a culture flask for incubation at 37°C to promote adhesion and proliferation.

2.11 Delivery of plasma and aqueous antimicrobial treatments to cell cultures

2.11.1 Direct NTP treatment protocol

Cells were seeded in 500 μL standard culture medium in 24-multiwell plates, initially using standard seeding densities (Section 2.10.1) and culturing for 72h, in order to attain 70% confluence prior to treatments. To enable clearer detection of treatment-mediated effects by exposing a less mature/ dense cell monolayer, subsequent studies used a slightly modified protocol, seeding H103 at an elevated density of $1 \times 10^4/\text{cm}^2$, and A375 at $2 \times 10^4/\text{cm}^2$, and culturing for 24h before applying treatments in triplicate.

For the application of direct NTP and argon control treatments, a 25cm x 16cm Perspex shield with a central 1.8cm diameter aperture was used to expose individual wells, and to shield neighbouring wells during application of NTP, preventing contamination (Figure 2.11). The treatment distance from NTP applicator to adherent cell monolayer was fixed at 10mm, with the

matched widths of torch applicator and well aperture ensuring consistent positioning at each treatment delivery. Immediately before treatment, the culture medium was aspirated from each well and replaced with 200 μ L/well PBS to maintain hydration, during the delivery of pulsed NTP or argon alone. Following treatment of all replicates, unless otherwise stated, PBS was removed from each well and replaced with fresh culture medium, after which the plate were re-lidded and returned to incubation at 37°C for a minimum of 24h, prior to assay (Figure 2.12).

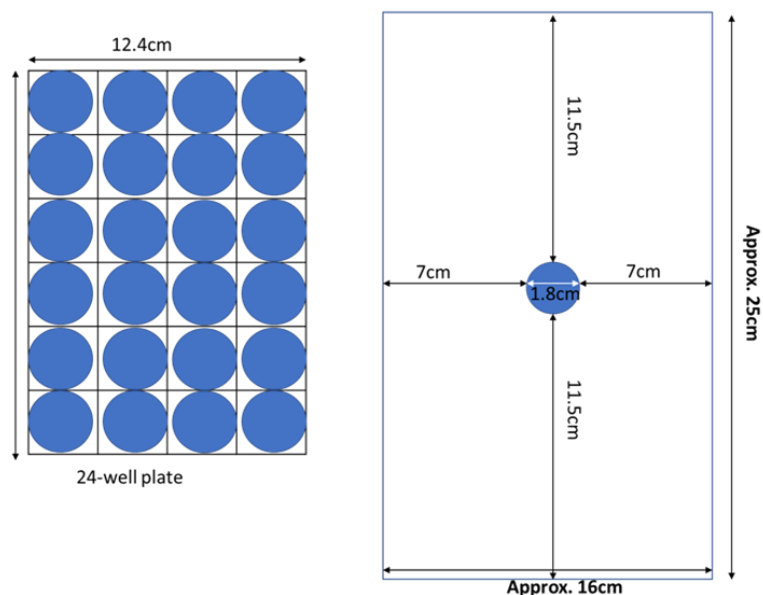


Figure 2.11: Illustration of 24-well treatment plate and shielding Perspex template, enabling delivery of single-well NTP treatments of cell monolayers.

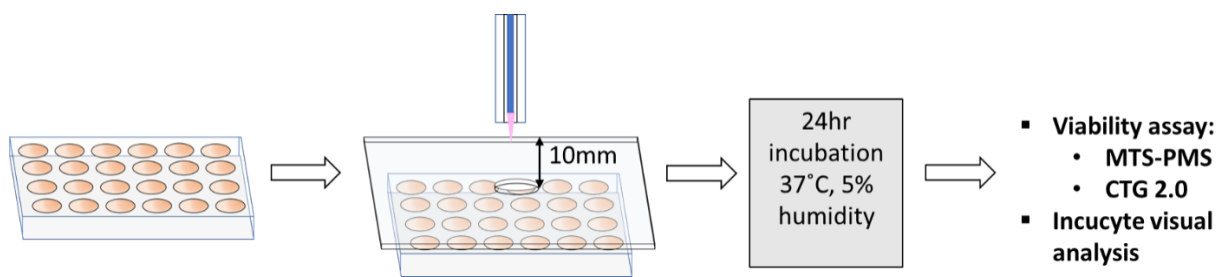


Figure 2.12: Application of direct NTP treatments to cell cultures in 24-well plates prior to analysis of viability/proliferation.

2.11.2 Aqueous treatment protocol:

Treatments with ECAS (0 - 50%, v/v), PVP-I (0 - 1%, w/v), and H₂O₂ (0 – 10%, v/v) were applied to sub- confluent cell monolayers, seeded at standard density in 24-well (for MTS-PMS) or 96-well (for TBDE or CTG2.0) plates and cultured for 72h, or double standard density and cultured for 24h, as specified. Directly before treatments, the culture medium was removed and replaced with a 50% volume of fresh medium, (250 μ L for 24-well plates, 50 μ L for 96-wells) to which the respective test product was added in 1:1 ratio, mixing gently by triturating, and incubating for the cited exposure period.

For single end-point viability assays, plasma-activated liquids (pPBS, PAM and PAW) were applied in triplicate to cells at 24h post-seeding, by adding to culture medium in a 50:50 ratio, swirling gently to mix, and returning cell cultures to 37°C incubation until the point of assay (Figure 2.12). For extended live-cell analysis, freshly-seeded cells in with complete or serum-free medium were allowed to adhere in 24-well plates for approximately 4h prior to the addition of respective treatments in a 1:1 (v/v) ratio, in triplicate. Plates were transferred promptly to the Incucyte, and incubated at 37°C for 72h. A positive cytotoxic control was included to verify detection of the absence of proliferation during Incucyte scans.

2.12 Assessment of cytotoxicity

Cellular responses to treatments were assessed either by trypan blue dye exclusion assay (TBDE), CellTiter Glo 2.0 (CTG2.0) luminescence assay for the determination of cellular ATP, or MTS-PMS assay which provides a measure of metabolically active cells via enzyme-mediated generation of a coloured product, and thus a quantitative indicator of viability.

2.12.1 Trypan Blue Dye Exclusion (TBDE)

Enumeration of viable and non-viable cell populations was performed by standard trypan blue dye exclusion (TBDE). Briefly, a 20µL sample of trypsinised cell suspension from the test culture was mixed with 20µL 0.4% trypan blue solution (Fisher Scientific, UK), which selectively permeates cells whose membranes have been compromised, differentiating viable from non-viable cells when viewed under magnification in a Neubauer ruled haemocytometer. Viable and non-viable cell counts per mL were obtained from average count obtained from a minimum of three 1.0mm² squares, corrected for dilution.

2.12.2 CellTiter Glo 2.0

The ATP content of metabolically active cells is used as a quantitative indicator of viable cell population in this assay. The catalytic mono-oxygenation of luciferin to oxyluciferin by the UltraGlo recombinant Luciferase present in the Cell TiterGlo (Promega, UK) reagent, in the presence of Mg²⁺, molecular oxygen, and ATP generates a luminescent signal which is detected on a plate-reader (Figure 2.13).

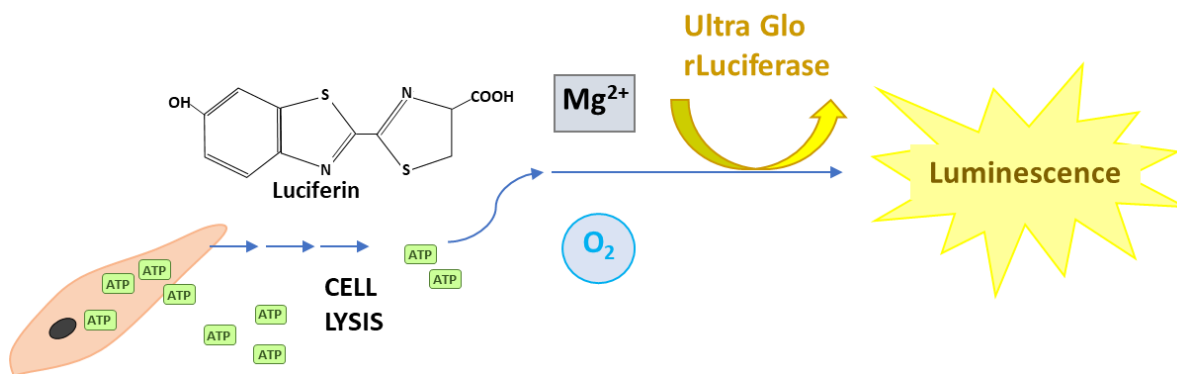


Figure 2.13. CellTiter Glo assay: generation of the luminescent signal correlating to viable cell population catalysed by UltraGlo™ rLuciferin, supplied with cellular ATP released upon reagent-mediated cell lysis.

CellTiter Glo reagent was added to cell cultures in a 96-well plate, using equal volumes of reagent to cell culture medium (100 µL:100 µL), gently mixed via orbital shaking for 2 minutes to allow cell lysis, and a luminescence reading was taken via micro-plate reader (Tecan Infinite 200 Pro) after 10 minutes reaction time, using 100ms integration time. ATP levels were reported as the normalised mean percentage relative to untreated controls.

2.12.3 MTS-PMS assay

A modified version of the MTT (3-[4,5-dimethylthiazol-2-yl]-2,5 diphenyltetrazolium bromide) colorimetric assay for quantification of viable cells, was used as a simple one-step approach for the determination of metabolically active cells via spectrophotometric measurement of the water-soluble formazan product. Introduction of the tetrazolium compound MTS [3-(4,5-dimethylthiazol-2-yl)-5-(3-carboxymethoxyphenyl)-2-(4-sulfophenyl)-2H-tetrazolium, inner salt] (Merck, UK) to cell cultures, together with the electron-acceptor reagent phenazine methosulfate (PMS) (Promega UK Ltd, UK), results in generation of a coloured product via the action of NADPH-dependent dehydrogenase enzymes, with peak absorption at 492nm. Due to the non-toxic and soluble nature of the reagents, cells remain viable throughout the assay and can be cultured further after, if required.

Cells were seeded in 24-well plates and grown to 70% confluence before the application of specified treatments (Section 2.11.2). At the end of the treatment period, cell culture medium in each well was replaced with 500µL F12: HAMS DMEM without phenol red (PR) and FBS (Gibco), in order to eliminate interference with the absorbance readings of the formazan product. MTS-PMS reagent was freshly prepared before performing the assay, and was constituted by adding PMS (1mg/mL, prepared in pre-warmed PR-free FBS-free medium) to MTS (2mg/mL, also prepared in warmed PR- and FBS-free DMEM) in a 1:19 ratio, i.e. for a 6mL final volume of MTS-PMS, 0.3mL PMS was mixed gently with 5.7mL MTS. A 100uL volume of MTS-PMS reagent was added to each well, and gently mixed. The plate was then returned to 37°C incubation for 50 minutes to allow the chromogenic reaction to occur. The culture medium from each well was then sampled in

triplicate into a 96-well micro-titre plate for measurement of the amber-brown product on a plate-reader (Omega), recording the absorbance at 490nm. Cell viabilities were reported relative to the untreated controls. Standard reference curves of cell number versus absorbance were generated using cell suspensions of known density on three separate occasions.

2.13 Incucyte® Live-Cell Imaging Analysis

2.13.1 Direct NTP treatments:

Cells were seeded in 24-well plates, grown to 70% confluence, and direct NTP or argon-only control treatments applied as previously described. Fresh medium was added and plates transferred to the Incucyte® S3 Live-Cell Analysis incubator (Sartorius, Goettingen, Germany) within 1-2 hours, and maintained at $37\pm 2^{\circ}\text{C}$, 5% CO_2 , for monitoring of cell proliferation. Imaging of each well was programmed at 2 hourly intervals, initially using 3, but thereafter 9 fields of view across the well surface area, with filters set at $150\mu\text{m}^2$, for a period of 72h. Post-acquisition analysis was performed using cell line-specific masks to determine the percentage confluence within each well at each scan, using Incucyte® 2021C Basic Analysis software. Treatments were performed in triplicate on three separate occasions, to obtain independent biological repeats.

2.13.2 Indirect NTP treatments:

Cell cultures were seeded at twice the standard seeding density in 24-well plates, using 500 μL of either complete culture medium, or serum- and phenol red- free medium, then returned to incubation before the addition of treatments. To each freshly seeded well, 500 μL freshly-generated serum-free or complete plasma-activated medium (PAM), or PBS (pPBS) (produced as described in section 2.8.1), was taken from a 7mL aliquot and added to each well, diluting the seeded cell suspension 1:1, giving a final 1mL volume per well. Cell culture plates were then incubated within the Incucyte system and monitored for up to 72h via live-cell imaging (as outlined in 2.13.1). Post-imaging basic analysis was performed by Incucyte software, reporting the percentage confluence per well at each 2-hourly time-point. Results were reported as % confluence \pm SD, taking the mean of three independent biological repeats.

2.14 Statistical Analysis:

For determination of cytotoxic effects, the percentage of viable cells post-treatment was compared to controls to which received PBS addition to culture medium in place of antimicrobial product. Baseline viability of the control group was normalised to 100% and treated groups were compared via two-way ANOVA with either Sidak's test or Tukey's test for multiple comparisons, as indicated, or one-way ANOVA with Dunnett's multiple comparisons test, with significance set at $p < 0.05$.

For the determination of IC_{50} , each dataset was analysed by Log transformation of treatment dose, subsequently plotting the non-linear regression (Log(inhibitor) vs. response – variable slope (four parameters)) in GraphPad Prism (version 9.5.1 (733)), using the mean of three separate experimental means to calculate the dose at which 50% inhibitory response was elicited.

Chapter 3: Investigation of the antimicrobial effects of non-thermal energy technologies on prokaryotes

3.1 Antimicrobial applications in the healthcare setting

The preliminary assessment of antimicrobial activity of any novel technology or pharmacological treatment on planktonic microorganisms serves as an important initial measure of efficacy, allowing treatment parameters such as contact time, concentration or dose, mode of delivery, and frequency of application to be investigated. In clinical environments, the control of microbial contamination on contact surfaces, instrumentation, and human skin (of both professional practitioners and service-users), is critical to the provision of safe care, prevention of infection, and maintenance of health and functionality (Percival *et al.*, 2015; Storr *et al.*, 2017; Suleyman, Alangaden, and Bardossy, 2018; Masia and Dettori, 2022). The implementation of robust and appropriate infection prevention and control (IPC) measures ensures that potential sources of pathogen transmission are correctly managed, reducing the risk of nosocomial infection through environmental contamination, medical equipment, and person-to-person contact (Suleyman, Alangaden, and Bardossy, 2018; ARHAI, NHS National Services Scotland, 2021,; NHS England, 2022). In response to surges in the rates of HAIs and AMR reported in the healthcare setting, and unequivocally the recent Covid-19 pandemic, the scrutiny and implementation of infection prevention and control measures have intensified, leading to higher standards of cleaning and disinfection practices, public health visibility, and institutional accountability (NICE, 2011, 2012, 2014; Assadian *et al.*, 2021; NHS England, 2022; Tomczyk *et al.*, 2022; Scottish Government, 2023).

Biocides must comply with rigorous standards of efficacy, which have historically been determined on the basis of testing against specified microbial species, in planktonic suspension or inoculation, such as broth microdilution methods, quantitative suspension testing, and quantitative surface disinfection testing (Sattar, 2004; BSI, 2005; European Committee for Standardization, 2013, 2015; International Standards Organization (ISO), 2019, 2021) There has been increasing recognition of the need for standardised anti-biofilm testing protocols, to provide a more accurate and appropriate measure of efficacy of commonly-used antimicrobial agents in the context of recalcitrant infection or biofilm contamination, with one standardised anti-biofilm testing protocol issued recently for plastic and non-porous surfaces (BSI, 2023). The designation of agreed biofilm-inhibitory testing parameters and standards remains challenging, in part due to the more time-consuming and complex nature of configuring relevant biofilm culture conditions, and modes of treatment application, as well as establishing acceptable standards for efficacy levels, which must be considered in the context of specific applications. Therefore, planktonic

testing protocols remain the first-choice for microbicide certification, with recognition of the need to simulate 'in-use' conditions in test procedures, to provide greater clinical relevance, in terms of safety and efficacy standards. Products intended for environmental disinfection applications are controlled by Biocidal Products Regulations (GB BPR in the UK, EU BPR in the UK) (UK Health and Safety Executive (HSE); UK Government, 2022) whilst agents developed for medicinal use must comply with medicines/ medicinal devices legislation and are subject to both regulatory frameworks, if they are designed for use under both categories (MHRA, UK Government 2020; HSE, UK Government, 2022).

Although it is widely acknowledged that microbial biofilms demonstrate a far greater resistance to antibiotics and biocidal agents (Olsen, 2015; Flemming *et al.*, 2016), and therefore typically respond only to more aggressive antimicrobial therapy than their planktonic counterparts, the application of treatments to microbial bioburden occurring in a simpler growth mode provides an informative basis from which more advanced treatment regimens can be developed. Moreover, early intervention and application of antimicrobial treatments for disinfection and antisepsis can prevent the formation of pathogenic biofilms, ensuring that any viable microbial organisms are inactivated whilst in their relatively susceptible planktonic form.

To assess the efficacy and spectrum of activity of antimicrobial agents or biocides, certified testing procedures must be undertaken to verify quality standards are met, using planktonic microbial susceptibility as an initial indicator of product efficacy (Gajic *et al.*, 2022). Therefore, initial antimicrobial efficacy testing was undertaken against planktonic microbial loads, to quantify the reduction elicited in contaminant bioburden.

3.2 Antimicrobial efficacy testing

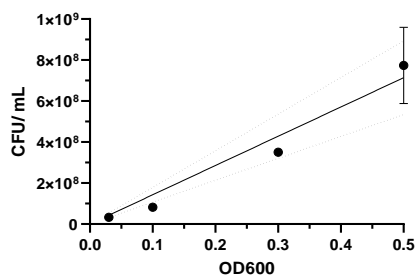
3.2.1 Methodology for the investigation of antimicrobial efficacy of selected agents on carrier surfaces:

The test organisms initially selected for study were members of the ESKAPE group of pathogens, which are commonly involved in nosocomial infections, and frequent carriers of AMR genes. The species and strains chosen comprised: *Escherichia coli* NCTC 13919 (carbapenem resistant) *Staphylococcus aureus* ATCC6538, *Acinetobacter baumannii* ATCC 17978, *Pseudomonas aeruginosa* ATCC 15442, *Klebsiella pneumoniae* NCIMB 13281, *Enterococcus faecalis* NCTCC 12697, and the opportunistic fungal pathogen *Candida albicans* NCTC 10231.

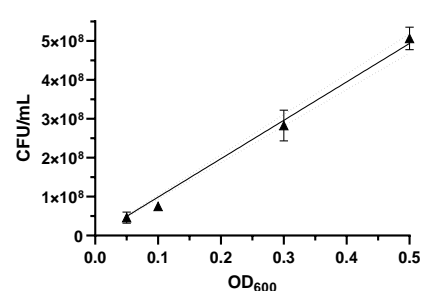
A basic initial calibration of optical density (OD) and equivalent CFU/mL was performed for test species, to determine the approximate viable microbial load present in a standardised test suspension prepared and adjusted using spectrophotometric measurement of absorbance at

600nm. Suspensions were constituted in saline-tryptone diluent (0.85% NaCl (w/v), 0.1% tryptone, in sterile dH₂O) for a minimum of three ODs and plotted against mean resultant CFU/mL (Figure 3.1), to provide a proxy for quantitation of cell concentration (Myers, Curtis and Curtis, 2013).

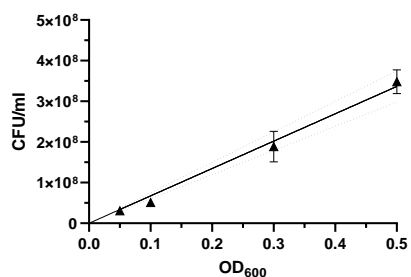
***S. aureus* ATCC 6538: OD versus CFU/mL calibration**



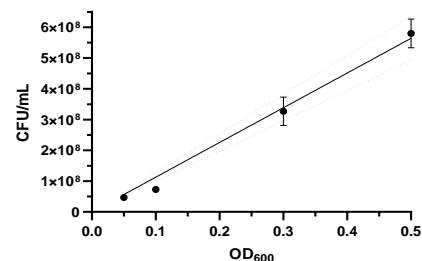
***E faecalis* NCTC 12697: OD versus CFU/mL calibration**



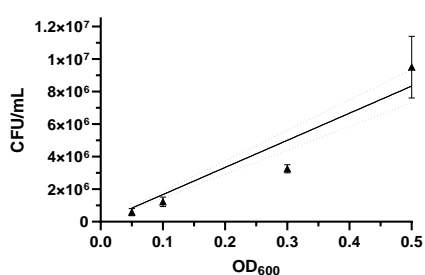
***E coli* NCTC 13919: OD versus CFU/mL calibration**



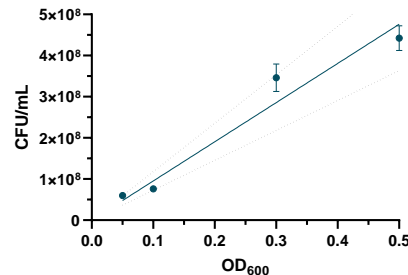
***P aeruginosa* ATCC 15442: OD versus CFU/ml calibration**



***C albicans* NCTC 10231: OD versus CFU/mL calibration**



***A baumannii* ATCC17978: OD versus CFU calibration**



***K. pneumoniae* NCIMB13281: OD versus CFU/mL calibration**

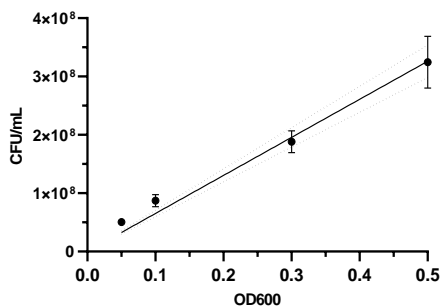


Figure 3.1: Optical density to CFU/mL calibration for each of the ESKAPE species used. Mean total viable count was obtained at each adjusted optical density with OD₆₀₀ by sampling each suspension and plating out, via spiral plating in triplicate, or Miles and Misra plating in sextuplicate. The line of regression for each organism was plotted in GraphPad Prism, taking the corresponding mean viable count ± SD for each optical density; n=3.

3.3 Determination of the NTP-induced Zone of Inhibition:

An important factor mediating the antimicrobial efficacy of NTP, in addition to the duration of treatment, is the proximity to target surfaces (Moreau, Orange and Feuilleley, 2008; Das, S, Gajula, VP, Mohapatra, S, Singh, Kar, 2022). Due to the limited diffusion distance of the majority of active species generated in the plasma effluent, the 'active zone' or physical distance over which the NTP may exert its effects according to plasma chemistry models, is limited depending on the species in question, and the physical state of the target material. For example, hydroxyl radicals may travel in air for a distance of tens of millimetres, but in aqueous solution, penetration depth may be reduced by several hundred-fold or more (Chen *et al.*, 2014). Therefore, a simple zone of inhibition (ZOI) procedure was used to obtain a measure of the area of antimicrobial activity produced by the NTP torch applicator used within the combined RF-MW system.

In order to assess the approximate size of the area targeted by the NTP jet from a fixed applicator-target distance, basic zone of inhibition (ZOI) studies were used to compare the relative dimensions of the active zone produced against each of the test species, and to ascertain any time-dependent increase in the size of this zone. Bacterial lawns were prepared on TSA plates (as described in Methods, Section 2.3), and once dried, were exposed to NTP treatments of 30 - 180s, using operating parameters of 10mm distance, 4 slm⁻¹ gas flow, 80W MW power, and 25% duty cycle. Following overnight incubation of treated plates at 37°C (aerobic conditions), ZOI measurements were taken.

In all species, there was a time-dependent increase in the plasma-induced zone of clearing, with a maximal effect noted in the majority of cases at the longest exposure time tested (180s) (Figures 3.2 and 3.3a) - d). The largest ZOI were measured in *E. coli* (14.05 ± 0.98mm), followed by *K. pneumoniae* (14.02 ± 1.94mm), *E. faecalis* (13.39 ± 0.85mm), and *S. aureus* (12.54 ± 1.03mm) (Figure 3.2). *A. baumannii* and *P. aeruginosa* only showed a mild increase in ZOI with prolongation of treatments to 180s (9.36mm ± 0.96mm, and 9.38mm ± 0.71mm, respectively), whilst in *C. albicans*, inhibitory zones measured the smallest of all tested species (maximal diameter of 9.11mm ± 1.77mm after 120s NTP exposure), and demonstrated no significant time-dependent enhancement of effect.

In several of the species investigated, inhibition of microbial growth within the cleared zones was incomplete (for example in *C. albicans* (Figure 3.4c) and d)), compared to *A. baumannii* (Figure 3.4a) and b)), and several breakthrough colonies were noted, either scattered chiefly around the perimeter, or at random across the entirety of the ZOI. However, this did not appear consistently from one replicate to another and did not exhibit obvious correlation with treatment duration. Argon control-treated microbial lawns showed no ZOI, indicating that the observed cleared zones

on NTP plates were attributable to the antimicrobial effect of plasma treatment rather than susceptibility to the drying effects (or other) of continuous gas flow exposure.

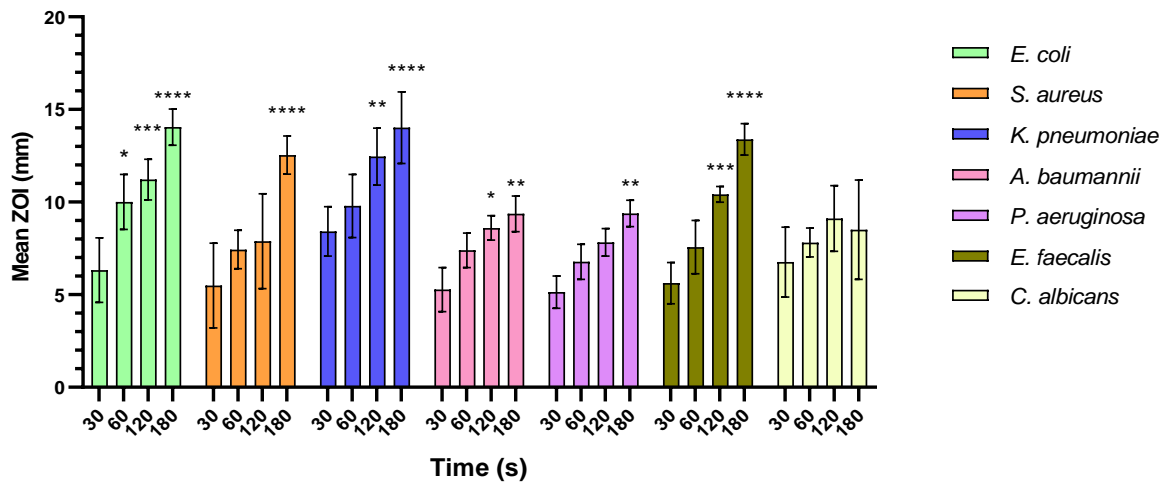


Figure 3.2: Determination of the diameter of ZOI induced by increasing duration of NTP treatment. Exposures performed at approximately 10mm torch-target distance, in triplicate; n=3. Significance was determined by 2-way ANOVA with Tukey's correction for multiple comparisons, comparing ZOI diameter at sequential treatment times with that seen at 30s. Thresholds for significance were determined as: * $p < 0.05$, ** $p < 0.01$, *** $p < 0.001$, **** $p < 0.0001$.

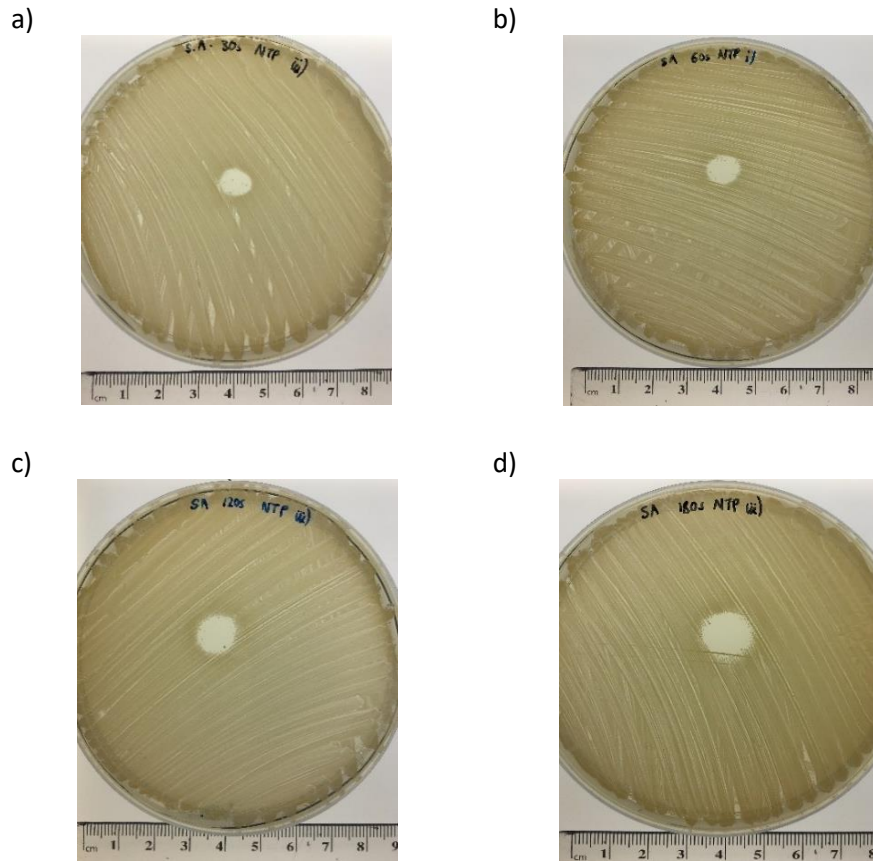


Figure 3.3: Illustration of ZOI's resulting from NTP treatments of *S. aureus* ATCC 6538 lawns following increasing exposure times. Plates are shown in ascending order of duration of treatment: 30s (a), 60s (b), 120s (c), and 180s (d).

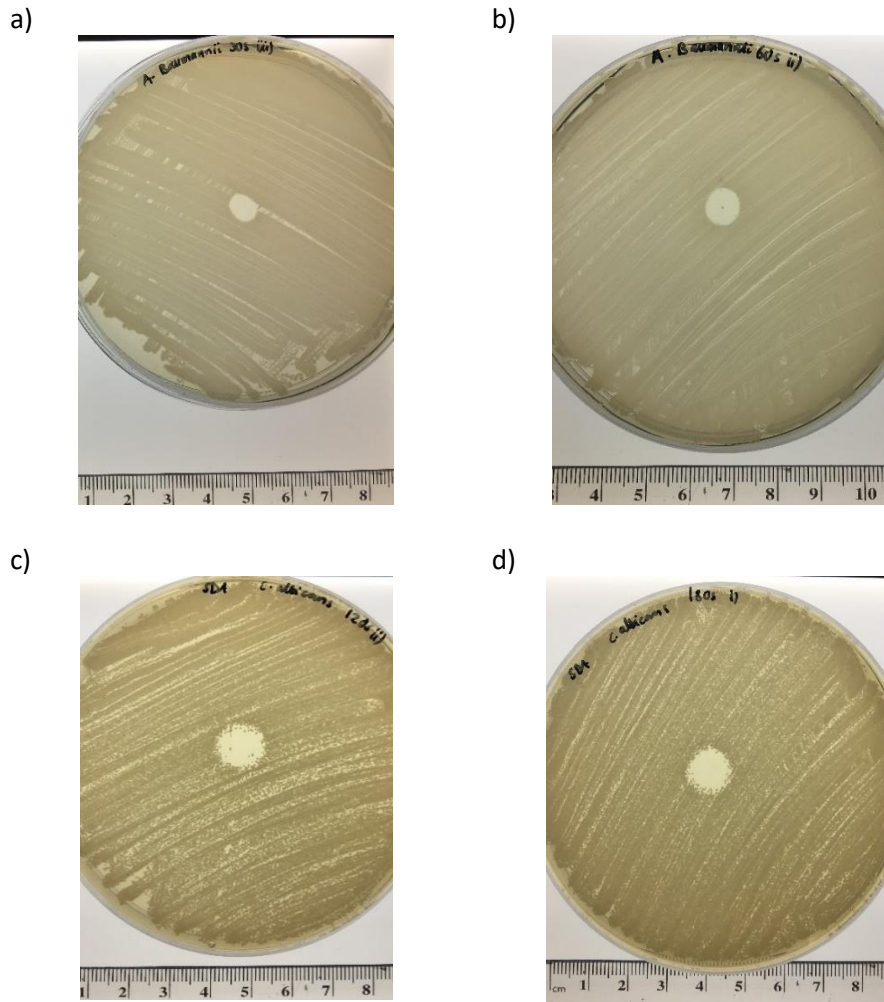


Figure 3.4: Illustrations of ZOIs resulting from NTP treatment of *A. baumannii* and *C. albicans* lawns on swab-inoculated agar plates, following increasing exposure times. The inhibition of growth was observed to be more complete in some species, such as *A. baumannii* – images a) (30s) and b) (60s) – than in others, e.g. *C. albicans* – images c) (120s) and d) (180s) – where breakthrough colonies were visible, and/or the ZOI was less sharply demarcated.

Measurement of the visible ZOI produced by NTP treatment using this approach provided a useful indication of the effective 'active zone' exerted upon the target surface at close (10mm) range, however it constitutes a fairly rudimentary measure as regards antimicrobial efficacy. The microbial suspension used for ZOI treatments on agar was adjusted to 0.2OD₆₂₀ (within the order of 6 – 9 Log₁₀ CFU/mL, dependent on species) however, no fixed volume was used to inoculate swab plates, as each swab was immersed in the test microbial suspension before application, using a similar method to that specified for antimicrobial susceptibility testing via disc diffusion (European Society of Clinical Microbiology and Infectious Diseases, 2024). This swab method was found to yield microbial lawns of greater density and uniformity than those obtained by spreading a fixed (100µL) volume over the agar surface.

The cleared zone seen in the exposed microbial lawn signifies inhibition of microbial adhesion and/or proliferation in the treated area directly within the path of the plasma effluent. However, prior to NTP treatments, the inoculum was applied and allowed to dry only for a short time, and therefore likely composed of only loosely adherent planktonic microbial cells, thus representing a significantly lower challenge than that occurring in actuality, in healthcare environments (Cahill *et al.*, 2014, 2017; Nkemngong *et al.*, 2020) and even moreso in chronic wound infections, where biofilms exhibit high levels of recalcitrance (Alves *et al.*, 2021). Higher densities of microbial loading may demonstrate stronger forces of adhesion, and greater tolerance to disinfection processes such as NTP treatment (Kamgang-Youbi *et al.*, 2008). Indeed, findings reported elsewhere show that heavier bacterial contamination is less effectively inactivated by plasma treatment *in vitro*, and that longer exposure to the active species generated by NTP correlates with larger ZOI (using indirect plasma treatment, i.e. via a plasma-activated solution (Joshi *et al.*, 2010).

3.4 Evaluation of antimicrobial efficacy using a quantitative non-porous surface test for bactericidal/ fungicidal activity:

The efficacy of non-thermal plasma (NTP) applied against planktonic microbial challenge was evaluated using a surface inoculation, treatment, and recovery protocol adapted from British Standards BS EN 13697:2015+A1:2019 'Quantitative non-porous surface test for the evaluation of bactericidal and/or fungicidal activity of chemical disinfectants used in food, industrial, domestic and institutional areas – Test without mechanical action (phase 2, step 2)'. Treatment of test surfaces composed of non-porous materials occurring commonly within the healthcare setting (grade 2b finish stainless steel 304, and silicone rubber), 'contaminated' by inoculation with a measured microbial load, enabled comparison of the reduction seen in viable bioburden achieved by NTP (relative to untreated controls) to that seen with alternative disinfectant products.

Quantification of the initial suspension used to make up the working suspension inoculated onto test coupons was standardised, using spectrophotometric measurement at the outset of each experiment. For all test species, an OD₆₀₀ of between 0.3 – 0.5 was equal to a viable count of 1.5 – 5 x 10⁸ CFU/mL, corresponding to the density specified in BS EN 13697 test procedures for preparation of the test working suspension. The exception was *Candida albicans*, which produced an equivalent viable count of only 5 x 10⁶ – 1 x 10⁷ CFU/mL within this OD₆₀₀ range (reflecting its larger cell size relative to the bacterial species used (Klis, de Koster, and Brul, 2014; Sutton, *et al.*, 2021), therefore an increased value of 0.7 OD₆₀₀ was chosen for this organism when preparing the working suspension at the test outset.

3.4.1 Optimisation of test methodology: the investigation of microbial viability on inoculated carrier surfaces

Initially, microbial loading of test surfaces was performed using a 50µL volume of the working suspension, as per the procedures described in BS EN 13697 methodology. The tolerance of test organisms to the drying step of this protocol was investigated, comparing viability at inoculation to residual viability of the dried inoculum, and also to a water-treated control, using 100µL sterile dH₂O for a contact time of 5 minutes, in place of an active biocidal solution. Substantial variation in the drying time, typically lasting between 80 – 110 minutes, was observed, and subsequently variation in the relative survival of the applied (dried but untreated) inoculum was also noted, particularly in Gram-negative test species (Figure 3.5, right).

P. aeruginosa viability demonstrated a 2.86 Log decrease, comparing the applied bioburden to that recovered from the carrier surface following drying (untreated) (p<0.0001), with water-treated samples showing a slightly greater Log reduction, of 3.52 Log (p<0.0001) (Figure 3.5, right). Water treatment therefore appeared to produce a slight but significant 0.65 Log reduction relative to untreated controls (p=0.0052) in *Pseudomonas*. In contrast, much smaller losses were seen in *S. aureus* viability, where there was only a 0.36 Log reduction during the drying process, relative to the initial applied microbial load (p=0.0027), and a 0.58 Log reduction with water treatment (p=0.0027) (Figure 3.5, left). The addition of water therefore resulted in a 0.22 Log further decrease, compared to dried untreated controls (p>0.05). These preliminary findings indicated a higher tolerance of *S. aureus* to the test protocol conditions, in agreement with findings reported elsewhere (Klarczyk *et al.*, 2023), and demonstrated its suitability for use as primary test organism in the evaluation of basic antimicrobial efficacy.

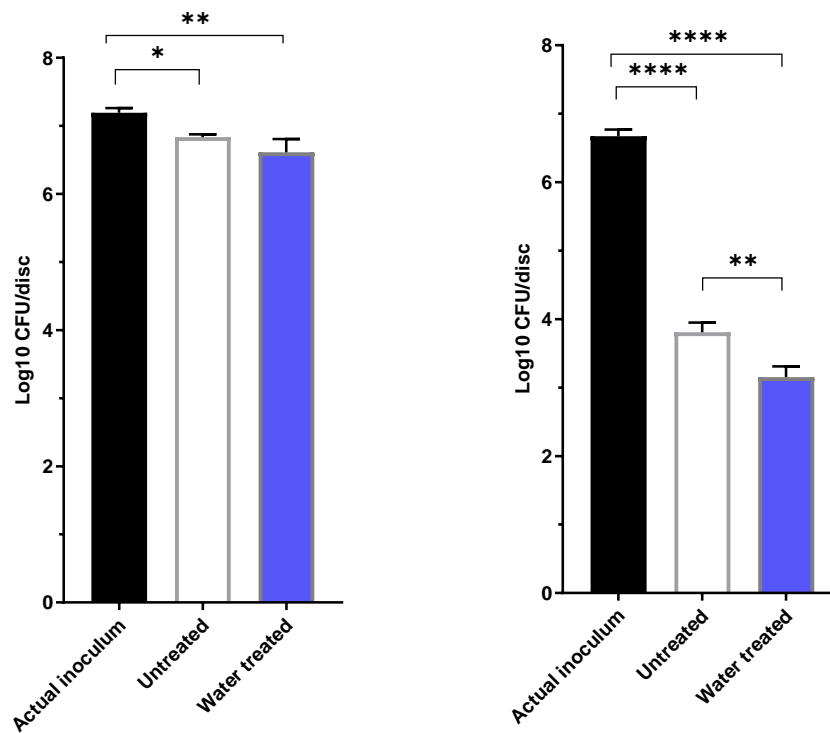


Figure 3.5: Viability of recovered 50µL inoculum after drying only (untreated), and after visible drying followed by sham treatment with H₂O (water treated), in comparison to the initial microbial load applied ('actual inoculum'), in *S. aureus* (left) and *P. aeruginosa* (right); n=3. Thresholds for significance were determined as: * p<0.05, ** p< 0.01, *** p<0.001, ****p<0.0001.

Although, as shown, microbial survival during the drying of the working suspension would be anticipated to decline to some degree, it was important to minimise this effect in order to achieve greater consistency in drying time and baseline microbial viability at the commencement of testing. Therefore, the inoculation volume and density of the working suspension were adjusted (Sections 2.4.2.1 and 2.4.2.2) using a 10µL volume of a 1:1 mixture of 0.5OD₆₀₀ microbial suspension: 0.6g/L BSA, which ensured drying times under laminar flow of ≤30 minutes, and associated mean viable loads of 5 - 6 Log₁₀ CFU/ coupon for all test species, excluding *C. albicans* NCTC 10231 (Figure 3.6). Poor tolerance of this organism to surface-drying has been noted elsewhere (Röhm-Rodowald *et al.*, 2014), therefore to compensate for this susceptibility, a 0.7OD₆₀₀ suspension was used for constitution of the working suspension, giving a 3.73 ± 0.12 Log₁₀ viable load after drying.

Despite this small modification of the protocol, subsequent comparison of the microbial load at inoculation to the total viable yield recovered from the coupon after surface-drying revealed a statistically significant reduction in the majority of species: *P. aeruginosa* (0.91 Log), *E. coli* ATCC 10536 (0.96 Log), carbapenem-resistant *E. coli* NCTC 13919 (0.76 Log), *C. albicans* (1.15 Log), *K. pneumoniae* (1.28 Log) (all p<0.0001), and *A. baumannii* (0.61 Log, p<0.001). The viability of Gram-positive organisms *S. aureus* (0.19 Log, p=0.49) and *E. faecium* (0.16 Log, p=0.89) appeared

relatively unaffected by drying, both showing a loss of <0.2 Log viable load over the drying period, which was not statistically significant. Of the other species tested, *A. baumannii* and carbapenem-resistant *E. coli* NCTC 13919 were also only slightly more impacted in comparison to the two Gram-positive organisms, demonstrating a reduction of <0.8 Log over the drying period, thus indicating only a mild susceptibility to evaporative effects. *K. pneumoniae* exhibited the greatest susceptibility to drying of all the bacterial species tested, whilst *P. pneumoniae*, despite showing moderate loss of viability, was selected as Gram negative test organism in subsequent applications of antimicrobial treatments due to its high frequency in clinical infection, and strong propensity for biofilm formation (Townsend *et al.*, 2016; Phan *et al.*, 2023).

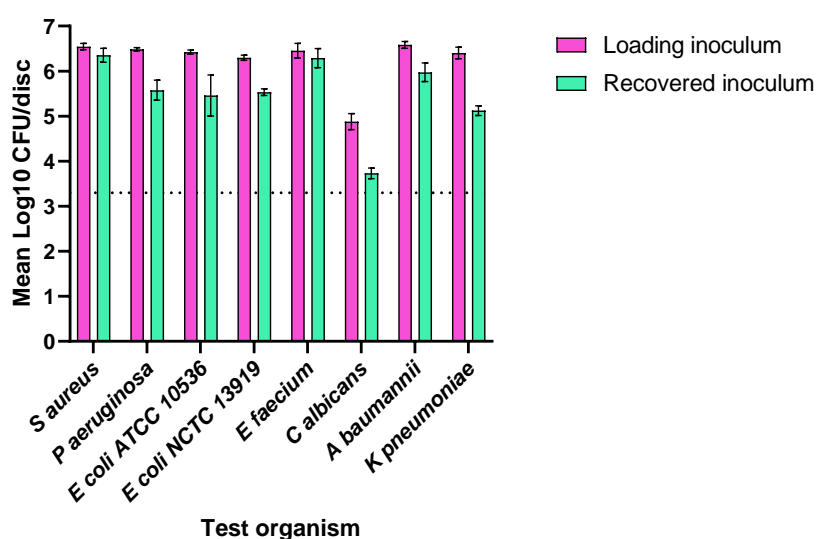


Figure 3.6: Comparison of the applied versus recovered viable load on stainless steel surfaces, following inoculation and drying, using a standardised microbial load (10µL of a 50% 0.5OD₆₀₀: 50% 0.6g/L BSA suspension, or for *C. albicans*, 50% 0.7OD₆₀₀: 50% 0.6g/L BSA suspension). *E. coli* NCTC 13919 (carbapenem-resistant) was included in addition to non-resistant strain ATCC 10536, to allow within-species comparison with a more clinically-relevant strain.

3.4.2 The effects of extended drying on surface-associated microbial viability

The stability of the viable microbial load upon test surfaces was investigated over an extended drying period, in order to ascertain at what point significant changes in the viability of (untreated) microbial inocula might occur over the time frame of testing on replicate coupons. To ensure valid interpretation of the effects of each of the different treatments investigated, the viability of the dried microbial suspension should remain stable over the period of testing. Any significant loss of viability, due for example to desiccation stress through evaporation, or osmotic stress through application of aqueous treatments to the dehydrated microbial load, and during recovery in neutralising medium, would confound the results of any treatments applied, since the variation in viability could be attributable to uncontrolled factors affecting microbial survival, in combination with the test treatments. Surface decontamination studies performed elsewhere have also

highlighted the significant negative impacts of procedural drying on inoculum viability, and additionally the effects of different inoculation methodologies (Cahill *et al.*, 2014; Katsigiannis, Bayliss and Walsh, 2021; Klarczyk *et al.*, 2023), therefore it was anticipated that survival of the applied microbial load would decline with prolongation of drying, particularly in Gram negative species, owing to the comparatively thinner peptidoglycan cell wall (typically measuring <10nm, versus Gram-positive cells walls, which normally are 20 – 80nm (Mai-Prochnow *et al.*, 2016)). Nevertheless, microbial response to, and tolerance of, desiccation is influenced by numerous metabolic, structural and genetic determinants, and is not invariably superior in Gram-positive species (Potts, 2001; Billi and Potts, 2002; Kramer, Schewebke, and Kampf, 2006; Katsigiannis, Bayliss and Walsh, 2021), and both Gram-positive and Gram-negative species were investigated with respect to extended drying-time.

Extended drying of the inoculated surface carriers was performed to determine the proportion of the applied microbial load surviving at sequential time points beyond the standard drying time of 20-30 minutes, and to discern whether time delay during the processing of coupons would significantly affect the viable yield. Since NTP treatments using the RF-MW system applicator could only be delivered to a single inoculated coupon at a time, it was important that microbial viability was consistent between replicates inoculated in parallel, and that no significant variation was introduced via inter-replicate delay. Therefore, inoculated surfaces were subjected to a prolonged drying period, beyond T_0 (i.e. the point at which the inoculum is 'visibly dry', and at which treatments should be applied according to the BS EN 13697 protocol).

The extended drying time-course showed a decline in viability in the primary test species, *S. aureus*, with a small initial reduction seen within 5 minutes (0.1 Log, $p=0.0408$), and a slight further reduction, although not significant, seen by 30 minutes additional drying time (0.54 Log, $p=0.42$). A similar trend was noted in *E. faecalis*, another Gram-positive organism, which appeared to undergo 0.2Log₁₀ loss of viability by 20 minutes extended drying, but this was not significant, and did not appear to decline further with prolongation to 30 minutes (Figure 3.7).

Of the Gram-negative species, *K. pneumoniae* appeared to be most strongly impacted by extended drying (Figure 3.7), showing a >1 Log reduction at 15 minutes (1.72 Log, $p=0.03$), and also at 30 minutes (1.01 Log, $p=0.003$), in agreement with results obtained previously, comparing initial microbial viability at to that at T_0 (after visible drying), which was most marked in *K. pneumoniae* of all the microbial species tested (Figure 6). *A. baumannii* showed a small but significant loss of viable load only within the first 5 minutes' extended drying, (0.22 Log, $p=0.002$), and relative stability thereafter, whilst *E. coli* viability remained consistent until the 30-minute timepoint, where a 0.38 Log reduction was seen ($p=0.02$). Recovery values for *P. aeruginosa* indicated sensitivity to prolongation of the drying period, however, the observed reduction in

viability did not attain significance at any of the tested timepoints (with a maximal 0.98 Log decrease occurring after 20 minutes, $p < 0.05$). The yeast *C. albicans* showed a reduction in viable recovered load after 15 minutes (0.88 Log, $p = 0.04$) and 20 minutes (0.51 Log, $p = 0.0006$) extended drying, in keeping with the low tolerance of this species to evaporative effects, reported elsewhere. Therefore, with the exceptions of *K. pneumoniae* and *C. albicans*, these findings provided satisfactory validation of the surface-testing protocol, ensuring that technical delays in the treatment and processing of replicate test coupons did not exceed 30 minutes.

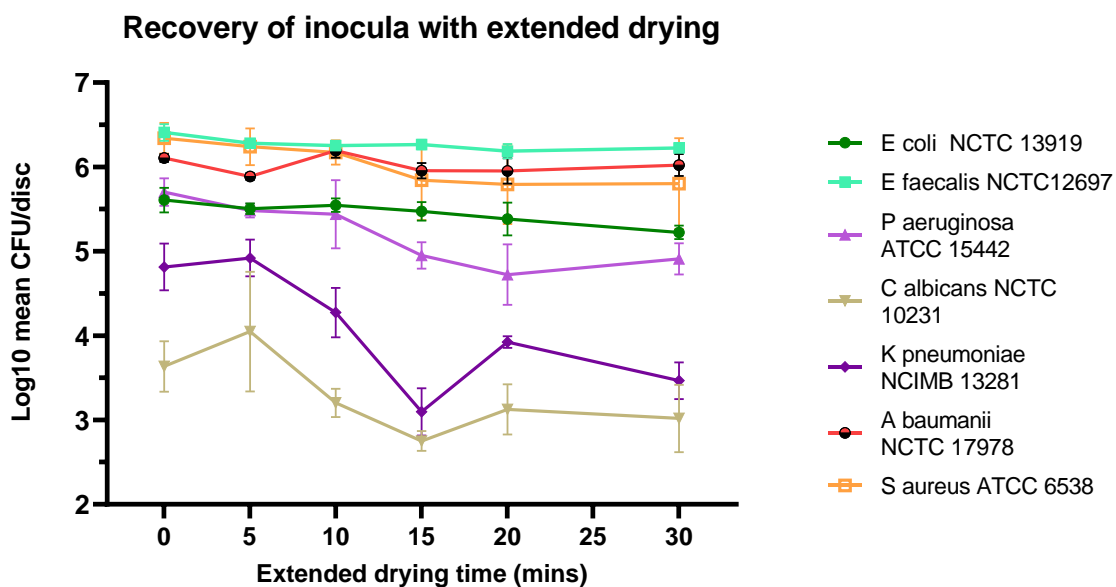


Figure 3.7: Time-course of extended drying of applied microbial inoculum on stainless steel, recovering the remaining viable load at time-points beyond 'visibly dry'. Stainless steel coupons were inoculated, allowed to visibly dry, and were subjected to extended drying for up to 30 minutes. $n=3$.

3.5 Direct NTP treatment of surface-associated planktonic microbial loads:

3.5.1 Preliminary test findings against a Gram-positive planktonic microorganism

Evaluation of the effect of direct NTP treatment on a Gram-positive microbial test species was undertaken by exposing surface-dried *S. aureus* planktonic inocula to the pulsed plasma jet, delivered via the torch-style NTP as described. A treatment time-course of exposures up to 180s was performed, using RF-MW generator parameters of 25% duty cycle, 4 slm⁻¹, and 10mm applicator-target distance. The system was initially operated with MW set to a power rating of 40W, however it was hypothesised that raising the MW power setting to 80W, could increase the antimicrobial potency of the emitted plasma, since power has been reported to be a key determinant of the antimicrobial effects induced by NTP (Gupta and Ayan, 2019; Hojnik *et al.*, 2019; Das, S, Gajula, VP, Mohapatra, S, Singh, Kar, 2022). Total energy delivered by plasma treatment for the specified times at both higher and lower power settings are shown in Table 3.1.

Duration (s)	25% Duty cycle at 80W (J)	25% Duty cycle at 40W (J)
30	0.6	0.3
60	1.2	0.6
90	1.8	0.9
120	2.4	1.2
180	3.6	1.8

Table 3.1: Energy delivered via the RF-NTP plasma system over a range of increasing exposure times, at 40W and 80W MW power settings, using 25% duty cycle (40ms ON: 160ms ON+OFF).

Time-matched treatments of *S. aureus* (SA) on stainless steel carriers showed a significant antimicrobial effect of both 40W MW- and 80W MW-generated NTP treatments, with similar Log reductions seen between the two groups at all exposure times (Figure 3.8). The maximal antimicrobial effect was achieved at 180s, with 3.19 Log reduction in the 80W treatment group, and 3.02 Log reduction in the 40W MW treated group (Figure 3.8). Argon control treatments produced a negligible effect on microbial viability, appearing consistent between timepoints, with a maximum Log reduction of 0.55 Log observed at 120s and 180s. Hereafter, the 80W MW setting was selected for all subsequent NTP treatments, since it was found to give a more consistent plasma jet overall. The 80W NTP treatments resulted in significant microbial inactivation of ≥ 2 Log when applied for 60s or more, showing a time-dependent trend in effect (Figures 3.8 and 3.9).

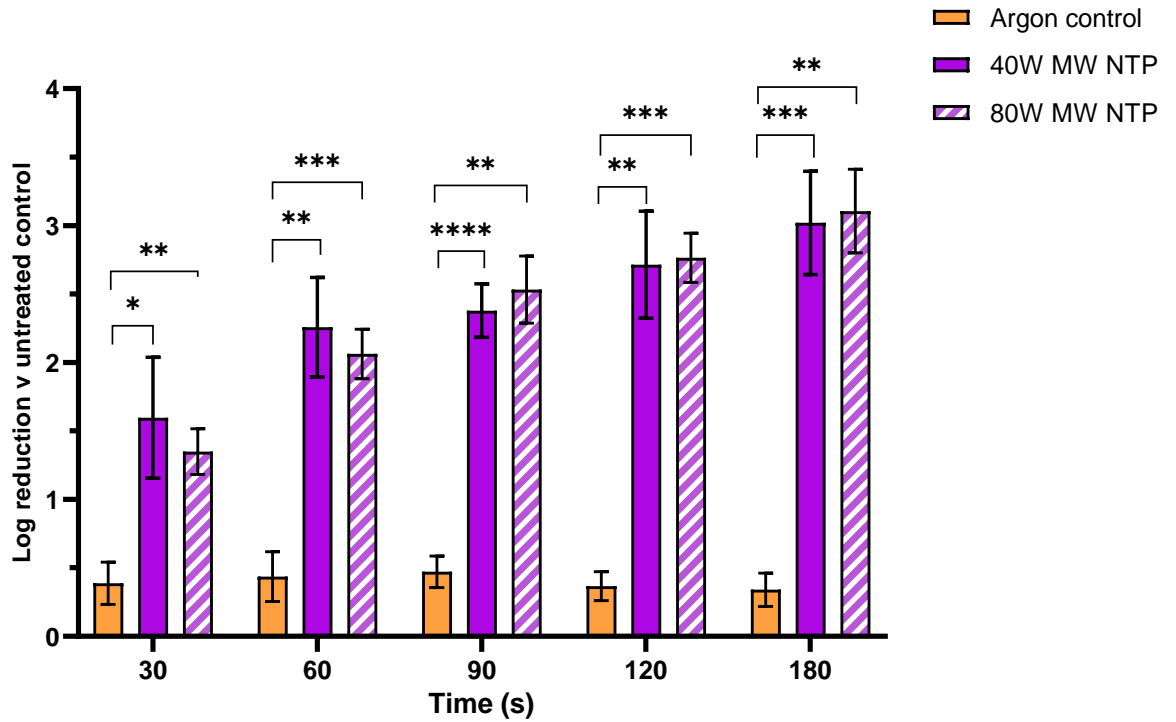


Figure 3.8: Log reduction in *S. aureus* recovered load from stainless steel coupons following treatment with RF-MW NTP generated at either 40W MW or 80W MW power, or an argon-only control, comparing the two treatment power settings against a single control group. Treatments were performed in triplicate; $n=3$. Thresholds for significance were determined as: * $p < 0.05$, ** $p < 0.01$, *** $p < 0.001$, **** $p < 0.0001$.

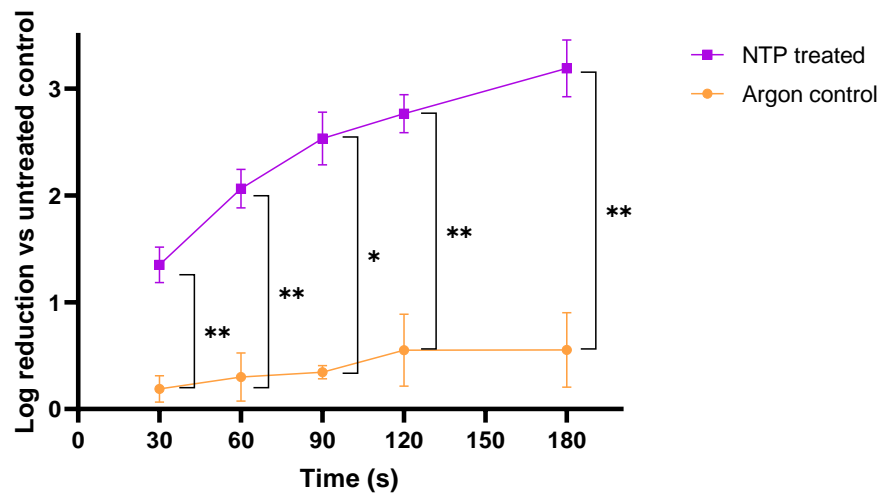


Figure 3.9: Log reduction in *S. aureus* viable recovered load from stainless steel surfaces following treatment with RF-MW NTP using 80W MW power, versus an argon-only control; test and control treatments performed in triplicate; $n=3$. Thresholds for significance were determined as: * $p < 0.05$, ** $p < 0.01$, *** $p < 0.001$, **** $p < 0.0001$.

3.5.2 Preliminary findings against a Gram-negative planktonic microorganism

It has been proposed that the effects of NTP upon Gram-negative and Gram-positive microbial species may differ, owing to physical distinctions in cell structure, i.e. the thicker peptidoglycan cell wall present in Gram-positive species, and the presence of an additional (inner) cell

membrane in Gram-negative bacteria (Lunov *et al.*, 2016; Mai-Prochnow *et al.*, 2016; Lee *et al.*, 2019; Poramapijitwat, *et al.*, 2020). Not only has the microbial response elicited by direct NTP been reported to show differential susceptibilities depending on the Gram-status (reflecting the differences in cell wall architecture and mechanical strength), but pre-treatment of surfaces or media with NTP has also been demonstrated to lead to altered viability, adhesion, proliferation and/ or biofilm-forming ability, with a greater effect seen against Gram-negative preference in some studies, but not universally (Lee *et al.*, 2019; Modic *et al.*, 2019; Nicol *et al.*, 2020). Therefore, to discern whether there was a similar antimicrobial effect against a Gram-negative test species to that seen against Gram-positive *S. aureus*, NTP treatments were applied to a strain of *P. aeruginosa* (NCIMB 10548/ ATCC15692) which has been implicated in wound, burn and urinary tract infections (NCIMB).

Stainless steel carriers inoculated with *P. aeruginosa* were subjected to direct NTP exposures, using the previously described method, for up to 180s (Figure 3.10). Log reductions were observed at all time-points within the NTP-treated group, revealing a significant inhibitory effect on microbial viability in comparison to the reduction seen with argon alone, at 30s (2.70 Log, $p=0.0006$), 90s (3.38 log, $p=0.0434$), and 120s (3.076 Log, $p=0.0017$). At the other time-points tested, antimicrobial effects were noted, with 3.22 Log reduction at 60s and 4.65 Log reduction at 180s. Argon treatment alone appeared to have a slight negative effect on microbial viability, with up to 0.585 Log reduction in recovered load seen at the 180s exposure time.

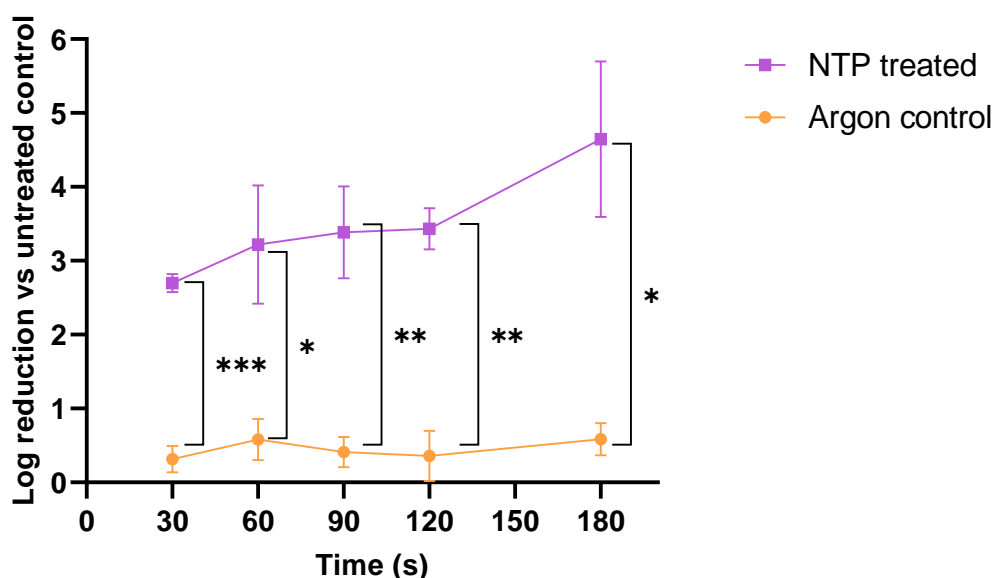


Figure 3.10. Treatment time-course of NTP against *P. aeruginosa* on stainless steel carriers, showing corresponding mean Log reduction per coupon. Treatments were performed in triplicate and results presented as mean Log reduction ($n=3$). Multiple paired t-tests were performed, one per time-point, to determine significance. Thresholds for significance were determined as: * $p<0.05$, ** $p<0.01$, *** $p<0.001$, **** $p<0.0001$.

Comparison with time-matched treatments on *S. aureus*-loaded surfaces revealed a slightly stronger antimicrobial effect of direct NTP applications against *P. aeruginosa*, with greater Log reductions noted at each time-point, with a 30s treatment on *P. aeruginosa* producing a similar Log reduction to that seen on *S. aureus* with 90 – 120s (achieving a reduction of 2.7 Log in the former, and between 2.06 Log - 2.5 Log reduction in the latter). The maximal effect of 4.65 Log reduction occurred at the longest exposure time studied, exceeding the corresponding reduction in *S. aureus* by 1.5 Log. It should be noted, however, that the viable load at T_0 (before subjecting to treatments) was 0.8 Log lower for *P. aeruginosa* than for *S. aureus* despite the application of equal initial inocula, potentially reflecting a lower tolerance to drying in the former, and possibly a greater susceptibility to the additional stress induced by NTP treatment.

3.6 Comparison of effects on an alternative test surface material

3.6.1 Direct NTP treatment of microbial loads applied to silicone carriers

To examine the antimicrobial efficacy of NTP when applied to test surfaces of a different material, silicone rubber coupons were inoculated with *S. aureus* and subjected to direct NTP, or time-matched argon control treatments. Silicone possesses several characteristics making it suitable for use in medical implants and devices, including low toxicity, good biocompatibility, mechanical strength, elasticity, heat stability, and chemical inertness. Silicone derivatives are therefore incorporated into a number of invasive medical products, such as pacemakers, pumps, prostheses, catheters and shunts (Teo *et al.*, 2016; Verma, 2016). Some silicone-based medical devices, such as urinary catheters, are however susceptible to microbial colonisation, albeit to a lesser degree than some other commonly-used polymers such as latex (Verma, 2016; Sabir *et al.*, 2017).

Other than the slightly larger surface area of the silicone coupons in comparison to that of the stainless-steel carriers used previously (approximately 126.68mm² and 78.54mm² respectively), test parameters (including the applied inoculum volume and drying time) remained constant.

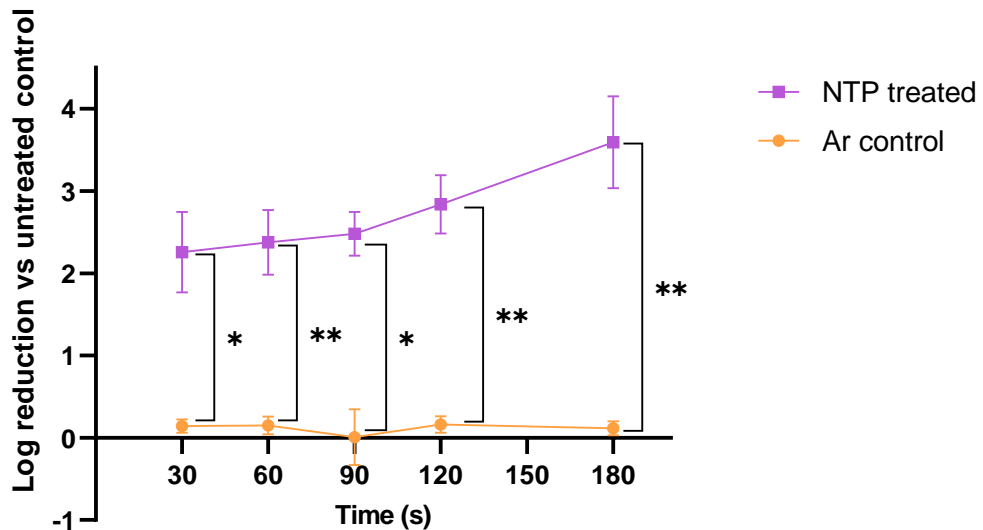


Figure 3.11: Treatment time-course of *S. aureus* on silicone rubber coupons, showing corresponding mean Log reductions per disc, with respect to untreated dried-only inoculum. Treatments were performed in triplicate, $n=3$. Multiple paired t -tests were performed, one per time-point, to test for significance. Thresholds for significance were determined as: * $p<0.05$, ** $p<0.01$, *** $p<0.001$, **** $p<0.0001$.

Log reduction in viable recovered load revealed a significant antimicrobial effect of NTP in comparison to argon-only controls. Results suggested a modest time-dependent enhancement, with a 30s treatment achieving 2.26 Log reduction in viable load, and 180s treatment achieving the maximal observed Log reduction in *S. aureus* (3.59 Log) (Figure 3.11). Time-matched argon control treatments showed negligible inhibitory effects, with ≤ 0.5 Log reduction seen at all tested timepoints. In comparison to the effect of NTP on stainless-steel associated inocula, the reductions seen on silicone were similar, achieving only a slightly greater maximal inhibitory effect (3.59 Log on silicone, 3.11 Log on steel), and a smaller enhancement with increased treatment time than was noted on stainless-steel. Initial viable load present at T_0 was similar between the two surface materials (6.46 Log on silicone, and 6.26 Log on stainless steel), indicating that the microbial challenge was consistent between experimental groups.

Testing upon silicone surfaces was not repeated for *P. aeruginosa*, since the demonstrated efficacy of NTP against this organism on inoculated steel was superior to that seen against *S. aureus*, and the effects of drying and treating *Pseudomonas* upon a more hydrophobic surface (such as silicone) were unlikely to show reduced efficacy, given the susceptibility of this organism to the drying process when applied to steel. Therefore, testing proceeded to evaluate the microbicidal efficacy of alternative biocides against *S. aureus* upon the primary test material, stainless-steel, to enable comparison with that of NTP.

3.7 Comparative antimicrobial efficacy of alternative antimicrobial products on surface-associated planktonic microbial viability

To provide a comparative measure of antimicrobial efficacy, biocompatible antiseptic compounds with known disinfecting activity were applied to microbially inoculated surfaces using the methods previously described, applying a 100µL volume of the test product for specified contact times, before neutralisation and recovery (following the method outlined in Section 2.4.4). The contact times used for these agents were modified as appropriate in cases where more rapid onset of action was known, notably povidone iodine (PVP-I), which was applied for a time-course of only 60s.

3.7.1 Efficacy of hydrogen peroxide against *S. aureus* on stainless steel

The antimicrobial effect of hydrogen peroxide (H₂O₂) was measured against *S. aureus*, applying treatments of 3% or 6% (v/v) aqueous H₂O₂ to inoculated stainless steel coupons over a 300s time-course. The selected concentrations corresponded to those traditionally utilised in wound antiseptics.

The higher of the two concentrations of H₂O₂ (6% v/v) appeared to induced antimicrobial effects at all time-points tested, consistently attaining a reduction of ≥1 Log CFU/coupon, with a trend for time-dependent enhancement of effect, although this did not attain significance in treatments of 30s – 180s, when compared to the effect of water controls. The greatest antimicrobial effects were achieved at 180s and 300s exposure times, producing Log reductions of 3.275 (p=0.064), and 4.925 (p=0.003) respectively (Figure 12), compared to water controls, where reductions of 0.47 Log, and 0.16 Log were seen. With 3% H₂O₂ treatments, the reduction in viable bioburden measured across all time-points was milder than the corresponding effects seen with 6% treatments, reaching a maximal 1.554 Log reduction at 180s (p>0.05), and a slightly lesser effect at 300s, where a reduction of 1.442 Log was noted only at (p>0.05).

Although both 3% and 6% treatments elicited apparent inhibitory effects on microbial viability at all time-points tested, the only statistically significant effect was at the maximal exposure time (300s), in treatments with 6% H₂O₂ (p<0.01, versus both 3% H₂O₂ and water control) (Figure 3.12). It was noted during colony enumeration that hydrogen peroxide-treated recovery suspensions from all time-points demonstrated delayed growth, for both 3% and 6%-treated samples, with colonies either failing to appear, or manifesting limited growth/ microcolonies only after the first overnight incubation. This response indicated the potent inhibitory effects exerted by hydrogen peroxide on both test organisms, since small colony variants (SCVs) are acknowledged to signify a microbial stress response, triggered as a result of environmental pressures such as antimicrobial treatment (Johns *et al.*, 2015).

In relation to the antimicrobial effect produced by direct NTP treatment of *S. aureus*, only the 6% H₂O₂ application produced comparable inhibitory activity, with a mean Log reduction of 3.28 after 180s contact time (compared to 3.19 Log reduction with NTP, time-matched exposure on steel). Within the H₂O₂ treatment group, only the 300s treatment at 6% demonstrated adequate antimicrobial efficacy to meet the 4 Log reduction criterion cited in the BS EN 13697 standards, with a 4.935 Log decrease in viable load observed at this contact time.

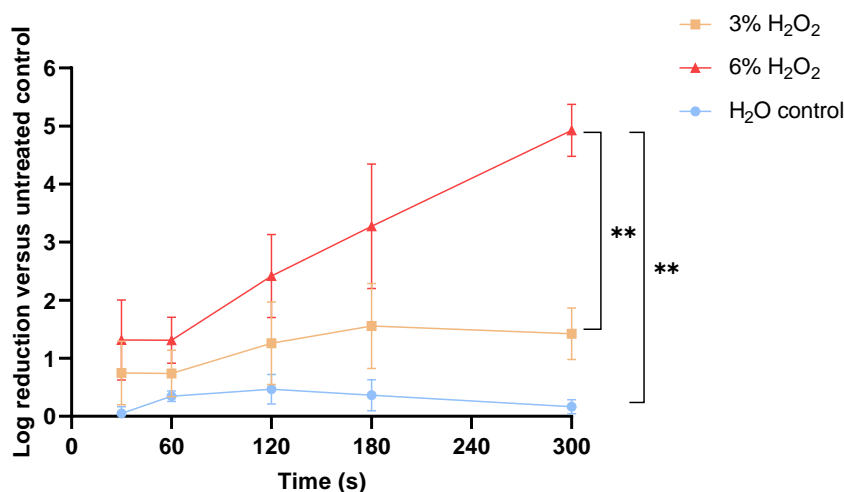


Figure 3.12: Treatment time-course of *S. aureus* treated with 3% or 6% H₂O₂ on stainless steel coupons, for contact times of 0-300s, showing corresponding Log reductions relative to the initial dried microbial load at T₀. Treatments were performed in triplicate; n=3. Significance was determined by two-way ANOVA with multiple comparisons. Thresholds for significance were determined as: * p<0.05, ** p<0.01, *** p<0.001, ****p<0.0001.

3.7.2 Efficacy of PVP-I against *S. aureus* on stainless steel

Polyvinylpyrrolidone iodine (PVP-I) was prepared in aqueous solution at concentrations of 5% and 10% (w/v), corresponding to those used in medicated (antiseptic) dressings, and in preparations used medically for the decontamination of wounds (Bigliardi *et al.*, 2017; Babalska, Korbecka-Paczkowska and Karpiński, 2021; Tan and Johari, 2021). Due to its rapid onset of action, a short treatment time-course was performed, measuring efficacy within a 60s contact period against the Gram-positive test organism *S. aureus*.

Applications of 5% and 10% PVP-I were highly efficacious at all time-points tested, eliciting significant Log reductions in viable load at contact times of as little as 20 seconds, and reducing recoverable bioburden to levels below the minimum level of detection (2 x 10¹ CFU/ coupon) at 30s (p<0.01) and 60s (p<0.0001) (Figure 3.13). At 20s exposure time, a near-complete elimination of microbial load appeared with both 5% and 10% PVP-I treatments, with mean Log reductions of 6.14 and 6.18 respectively, and only one biological replicate yielding viable recovered organisms for this contact period, occurring with 5% PVP-I. At longer contact times of 30 – 60s, total inactivation of viable bioburden was seen (within detection limits) at both test concentrations

($p < 0.0001$), equating to a 6.456 Log reduction. These results underlined the rapid and highly efficacious antimicrobial activity exerted by PVP-I, at both concentrations tested, attesting to its well-established use in clinical antiseptics (Woo, 2014; Bigliardi *et al.*, 2017; Swanson and Angel, 2017; Babalska, Korbecka-Paczowska and Karpiński, 2021)

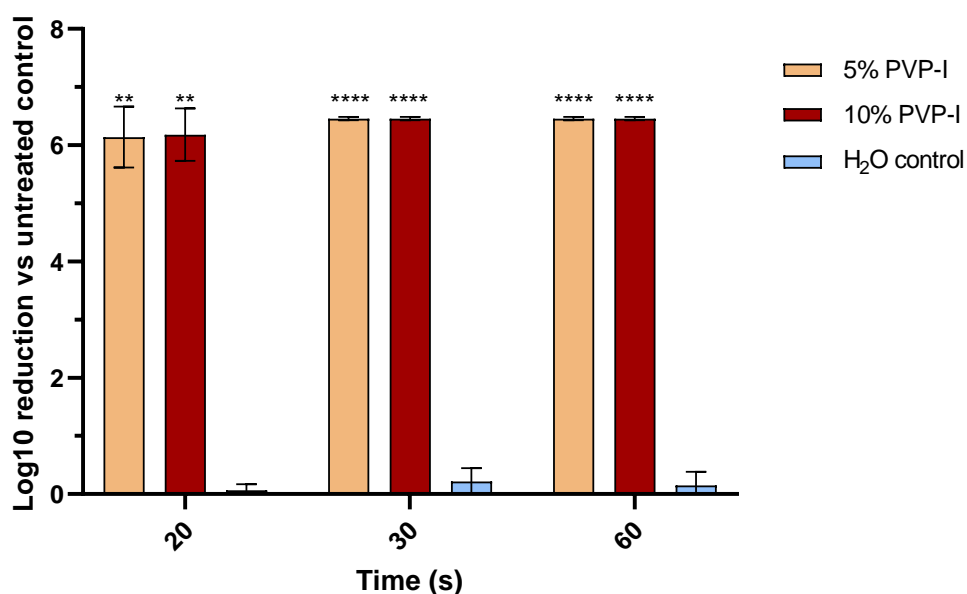


Figure 3.13: Treatment time-course of *S. aureus* treated with either 5% or 10% PVP-I on stainless steel surfaces, showing corresponding Log reductions relative to the initial dried microbial load at T_0 . Treatments were performed in triplicate, $n=3$. Significance was determined by 2-way ANOVA with Tukey's correction for multiple comparisons, comparing Log reduction achieved with PVP-I to that seen with H₂O controls. Thresholds for significance were determined as: * $p < 0.05$, ** $p < 0.01$, *** $p < 0.001$, **** $p < 0.0001$.

3.7.3 Efficacy of Electrochemically-activated saline solution (ECAS) against *S. aureus* on stainless steel

Electrochemical activation of aqueous solutions is a process being increasingly deployed for the sustainable generation of biocompatible disinfectants, whose efficacy is attributable principally to the production of hypochlorous acid (HOCl) within the output anolyte solution, and the associated high oxidising potential seen at acidic pH (Ignatov *et al.*, 2016; Yan, Daliri and Oh, 2021; Chen and Wang, 2022; García-Valdivia *et al.*, 2022). The system requirements are low, since only mains water and aqua-saline (brine) solution are necessary as input substances. The physicochemical profile of the anolyte and catholyte solutions can be modified by adjusting user-controllable generator parameters, to obtain differing free available chlorine (FAC) concentrations and ORP. Unless otherwise stated, ECAS was produced at a manufacturer's setting of 200ppm FAC, which was tested by colorimetric determination, and adjusted where necessary by dilution with dH₂O to obtain a stock solution of 200 ± 20 ppm FAC. The oxidation reduction potential (ORP) and pH of

200ppm ECAS were measured at each batch generation, and were within the ranges 1098.2 – 1131, and 5.01 – 6.35, respectively.

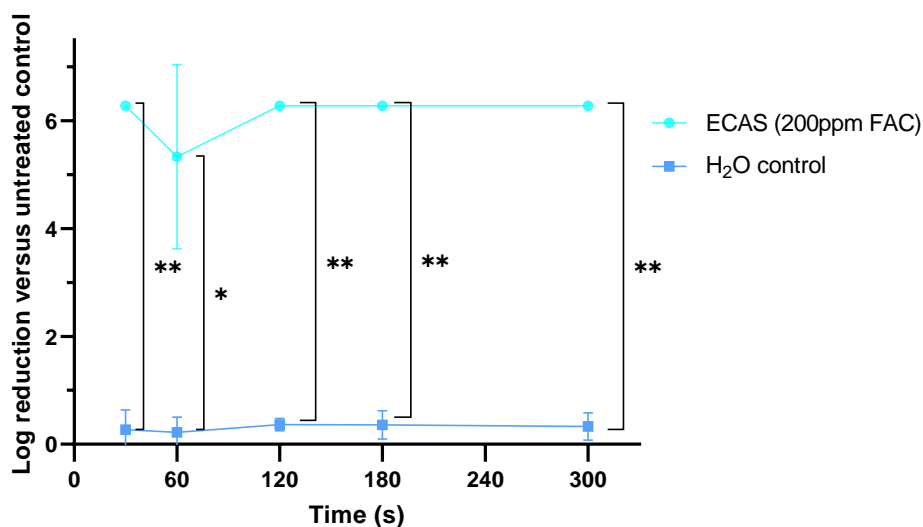


Figure 3.14. Treatment time-course with ECAS against *S. aureus* on stainless steel, showing corresponding Log reductions relative to the initial dried microbial load at T_0 . Treatments performed in triplicate, $n=3$. Significance was determined by multiple t-tests (one per time-point), with comparison to the Log change occurring in water controls. Thresholds for significance: * $p<0.05$, ** $p<0.01$, *** $p<0.001$, **** $p<0.0001$.

A 300s time-course was performed, to evaluate the onset and magnitude of the antimicrobial effect of ECAS when applied to *S. aureus*-inoculated stainless-steel surfaces. Treatments appeared to almost uniformly eradicate viable inoculum at all tested treatment times, with the exception of a single replicate at the 60s time-point, thus showing a significant antimicrobial effect against *S. aureus* under test conditions. At 30s, 120s, 180s and 300s contact times, ECAS reduced the viable recovered microbial load to sub-detectable levels (2×10^1 CFU/ coupon), equating to a mean Log reduction of 6.28, which was regarded as a complete-kill effect (Figure 3.14). Potential causes for the persistence of survivors in a single instance at the 60s time-point are various, but could include incomplete coverage of the inoculated coupon surface with the test product, contamination of the recovery suspension during recovery of coupons, or a genuine reduction in microbicidal potency. Due to the dependence of the antimicrobial activity of ECAS upon its metastable constituents generated by electrolytic activation, it is possible that failure to thoroughly mix the ECAS solution between replicates resulted in inhomogeneous distribution of critical reactive species at the time of application, resulting in incomplete microbicidal effects. Furthermore, the susceptibility of ECAS to ‘quenching’ or neutralising effects of organic compounds is well acknowledged (Thorn *et al.*, 2012; Ampiauw, Yaqub and Lee, 2021), therefore the presence of BSA in the working suspension may have inhibited the interaction of key species with the target inoculum.

As was found in surface tests performed with PVP-I (both 5% and 10% concentrations), ECAS demonstrated potent antimicrobial activity against *S. aureus* at the majority of contact times tested, reaching or exceeding the minimal 4 Log threshold of reduction necessary to meet non-porous surface disinfecting efficacy, as per BS EN 13697 standards. The rapidity of onset of action and completeness of efficacy were similar to those observed with PVP-I 5% and 10%, with the exception of the 60s anomaly noted in ECAS treatments, indicating that further testing would be advisable to ascertain whether contact times of >60s are indeed necessary to ensure 100% microbial kill with ECAS under these experimental conditions.

3.8 Efficacy of indirect NTP against planktonic microorganisms

3.8.1 Preliminary testing against *S. aureus* on stainless steel, using Plasma-Activated Solutions (PAS)

To discern whether antimicrobial effects could be achieved using indirect NTP exposure, plasma-activation of sterile deionised H₂O, distilled H₂O, or PBS was performed as detailed in Section 2.8.1, using a fixed activation time of 300s. Plasma-activated solutions (PAS) were then applied immediately to separate inoculated steel carriers to enable the determination of any antimicrobial activity present, potentially introduced via enrichment of the liquid volume with plasma-generated reactive species of sufficient stability and concentration to induce bactericidal effects.

Using a liquid volume of 6 – 7mL (some loss incurred through evaporation during the treatment process) and a 300s exposure period, each plasma-activated liquid was generated as described in Methods, Section 2.8.1. Sterile distilled and deionised water, and PBS were separately subjected to NTP activation, with gentle rotation of the microtiter treatment plate to facilitate mixing and even exposure during treatment. Immediately after activation, 100µL of each PAS was transferred to stainless steel test surfaces inoculated with *S. aureus* working suspension, prepared using the standardised protocol described previously (Section 2.4.2.1). After 300s contact time, carriers were processed by neutralisation, recovery and quantification of the remaining viable load. The Log reduction resulting from each treatment was calculated with reference to untreated dried controls (Figure 3.15).

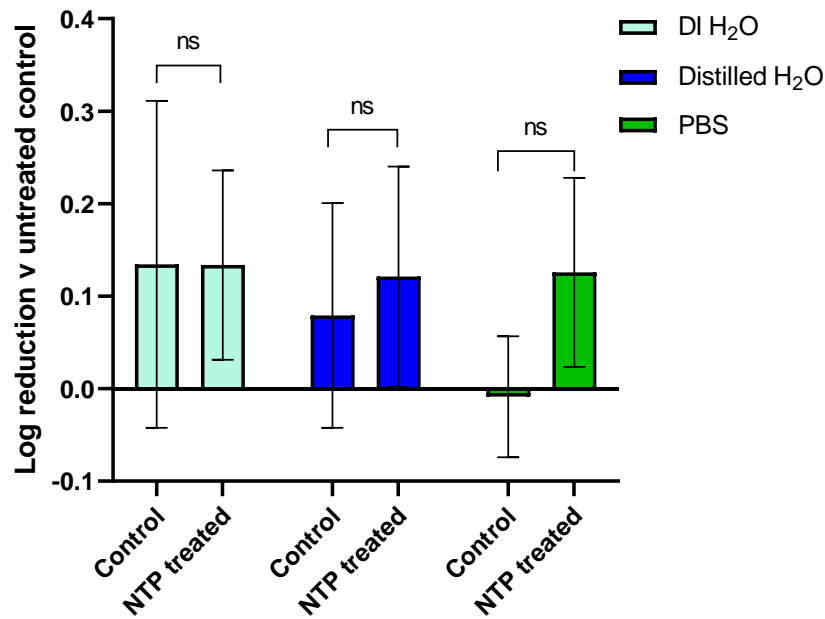


Figure 3.15: Log reduction in viable surface-associated *S. aureus* on stainless steel following treatment with plasma-activated solutions generated via RF-MW NTP exposure. Treatments were performed in triplicate; $n=3$. Significance was determined by 2-way ANOVA with Sidak's correction for multiple comparisons. Threshold for significance: $p<0.05$.

There was no significant inhibitory effect on inoculum viability observed following treatment with any of the applied PAS, with Log reductions <0.14 in each group ($p>0.05$) (Figure 3.15). A marginal mean Log reduction of 0.152 ($p < 0.05$) was seen with plasma-activated PBS (pPBS) in one biological replicate, compared to a 0.0535 Log increase (relative to dried untreated controls) in the matched PBS control, however this was a very subtle effect, and was not replicated with significance in subsequent repeats. Collated data showed a 0.126 Log reduction in the pPBS group, and a slight increase (0.009 Log) in untreated PBS controls ($p>0.05$). Deionised water was equally ineffective with and without plasma-activation, with a mean reduction of 0.134 Log observed with and without plasma-activation ($p>0.05$), whilst distilled water showed a similar negligible Log reduction of 0.121 with plasma-activation and 0.079 Log decrease in untreated matched controls ($p>0.05$). Thus, a 300s activation period failed to generate any significant antimicrobial activity within the exposed solutions, even when applied to inoculated surfaces very shortly after generation. Due to the short-lived and unstable nature of many of the reactive species generated in the plasma-liquid interface, combined with their short diffusion distances, it is unlikely that increased contact time would produce more decisive antimicrobial effects under the experimental conditions tested here. It is also possible that the presence of BSA, as an interfering substance, may have reduced any microbicidal activity present in the PAS to ineffectual levels.

3.9 Comparative effects of small-batch PAW generated by SBD-NTP treatment

3.9.1 Effects against surface-associated *S. aureus* on stainless steel:

The results obtained using RF-MW generated NTP were in contrast to findings with PAW generated using an alternative system configuration, using a surface barrier discharge (SBD) generation system. Using the SBD plasma jet, 15mL volumes of non-stirred sterile ultrapure deionised water were activated during a 300s exposure period (method detailed in Section 2.8.2), using input power of 25V, 25.5kHz, with 1.285A current. Aliquots of PAW were chilled before application to microbially inoculated surfaces using the previously described methodology (Section 2.4.2.1), testing exposure times of 30s, 60s and 300s.

Preliminary results, only, were obtained using this alternative generation system, with testing performed on day 0 (within 8 hours of PAW generation), and on day 2 (approximately 40h) post-generation, against *S. aureus* ATCC 6538 inoculated on stainless steel surfaces.

When applied on the same day as generated, SBD-PAW was seen to produce an approximate 1 Log reduction in viable load, relative to untreated controls, at the 30s (1.135 Log reduction) and 300s (1.376 Log reduction) treatment times, and a slightly smaller effect (0.913 Log reduction) with 60s treatment (Figure 3.16). Untreated water controls produced negligible effects upon viability at all time points, with a slightly more marked loss, relative to untreated controls, at the 300s exposure time (0.298 Log reduction) than was noted at 30s (0.04 Log decrease) and 60s (0.06 Log reduction).

Repeat testing at approximately 48 hours post-generation demonstrated markedly a decreased efficacy of PAW, with a small but significant antimicrobial effect seen only at the 300s treatment time, with 0.698 Log reduction, compared to the 0.218 Log reduction observed with water controls ($p < 0.05$). Shorter treatments yielded only modest reductions in viable recovered load, (equivalent to 0.308 Log at 30s; 0.593 Log at 60s) which were not significantly greater than those seen in matched controls ($p > 0.05$) (Figure 3.17). For any conclusions to be made about the possible antimicrobial effects of SBD-PAW, further testing would be required against the same test organisms and against a Gram-negative species to demonstrate spectrum of activity.

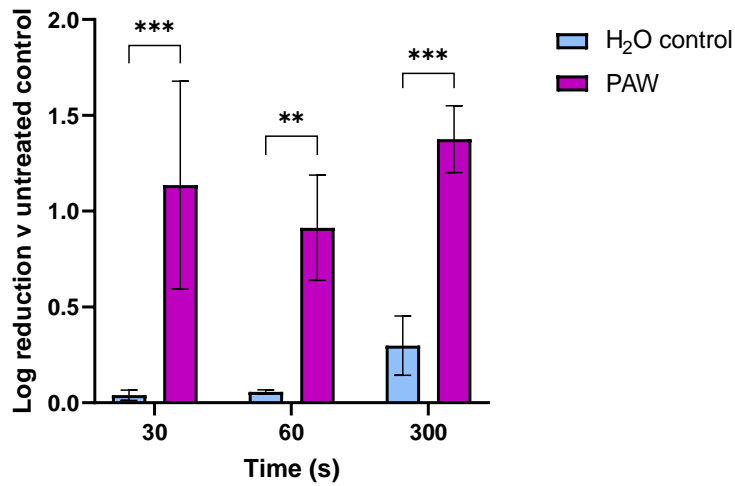


Figure 3.16: Treatment time-course of surface-associated *S. aureus* on stainless steel, treated with PAW generated in small batches by an alternative SDB-NTP system. PAW was tested on the day of generation (d0) in triplicate; n=1. Significance was determined by 2-way ANOVA, with Sidak's test for multiple comparisons. Thresholds for significance were determined as * $p < 0.05$, ** $p < 0.01$, *** $p < 0.001$, **** $p < 0.0001$.

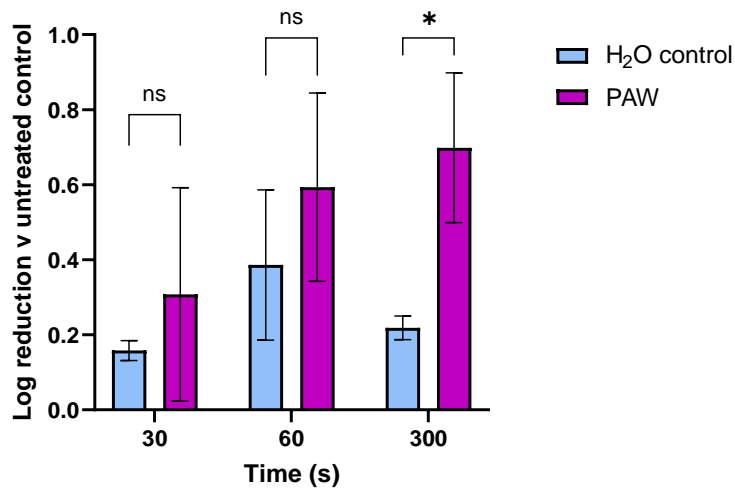


Figure 3.17: Treatment of surface-associated *S. aureus* on stainless steel with PAW generated in small batches by an alternative, SDB-NTP system, tested 2 days post-generation, in triplicate; n=1. Significance was determined by 2-way ANOVA, with Sidak's multiple comparisons test. Thresholds for significance were determined as: * $p < 0.05$, ** $p < 0.01$, *** $p < 0.001$, **** $p < 0.0001$.

3.9.2 Assessment of the antimicrobial efficacy of small-batch SDB-NTP-generated PAW in suspension

To determine its efficacy when applied in greater volumes, and when more homogeneously exposed to microbial challenge, suspension tests were carried out using small-batch SDB-PAW against both *S. aureus* ATCC 6538 and *P. aeruginosa* NCIMB 10548, for a fixed treatment period of 300s, using the method described in Section 2.5. The testing procedure followed a slightly modified version of the British Standards BS EN 1040 Suspension test for bactericidal or

disinfectant activity (BSI, 2005), and was validated under experimental conditions using the validation protocol outlined (Methods Section 2.5).

3.9.3 The effects of small-batch SBD PAW against *P. aeruginosa* in suspension

Owing to resource limitations and preliminary results for *S. aureus* being unquantifiable, the antimicrobial activity of PAW in suspension was only determined for *P. aeruginosa*. Total recovered viable load was compared against that obtained with non-activated water controls.

When applied 48 hours post-generation, SBD-PAW appeared to produce inhibitory effects against *P. aeruginosa* in suspension, with a Log reduction of 4.689 ± 0.701 relative to the expected load, in comparison to the 0.104 Log reduction seen in water controls ($p < 0.01$) (Figure 3.18). At the later testing time point (15 days post-generation), a smaller effect was observed with a 1.854 ± 0.698 Log reduction in PAW-treated *P. aeruginosa*, and a 0.004 Log difference in water controls (indicating a slight increase relative to expected yield) ($p > 0.05$).

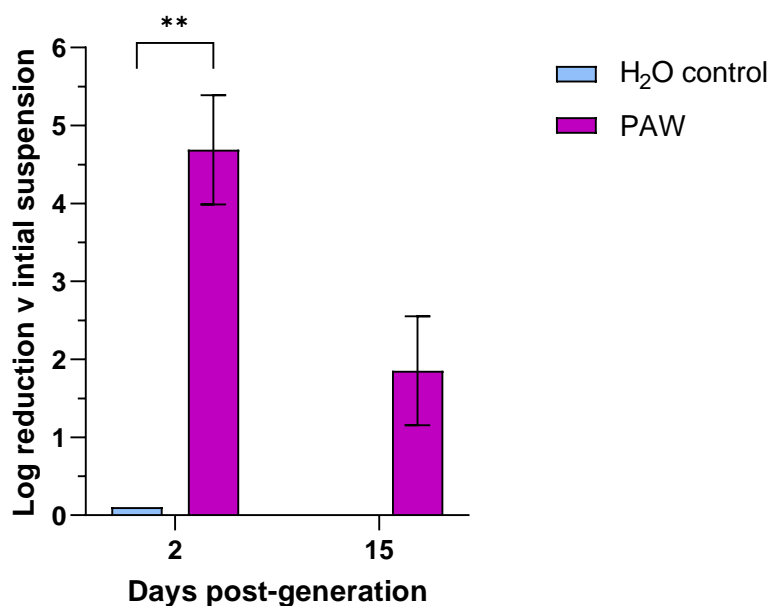


Figure 3.18: Log reduction in viable *P. aeruginosa* following suspension testing with PAW generated via small-batch SDB plasma system. Suspension treatments were carried out at 48h and 15 days after PAW generation, for a contact time of 300s, performed in triplicate; $n=1$. Significance was determined by 2-way ANOVA with Sidak's multiple comparisons test. Thresholds for significance were determined as: * $p < 0.05$, ** $p < 0.01$, *** $p < 0.001$, **** $p < 0.0001$.

Due to the low number of technical and experimental replicates, these findings must be interpreted with caution and lack statistical power, however they indicate a reduction in antimicrobial efficacy of SBD-PAW over time. It is possible that chemical instability in the SBD-PAW aliquots used in these assays might have led to changes in the reactive species profile over time, as has been reported in the literature (Traylor *et al.*, 2011; Liu *et al.*, 2018; Tsoukou, Bourke and Boehm, 2020). Storage at temperatures of $> -20^{\circ}\text{C}$ during transportation and even during the

experimental procedure itself (e.g. during equilibration to room temperature) may have contributed to a decline in key microbicidal species generated within SBD-PAW. Between testing time-points, PAW aliquots were frozen at -20°C, which again may have been insufficient to preserve levels of critical reactive species. To further characterise the antimicrobial activity of SBD-PAW, it would be important to repeat suspension testing upon *S. aureus*, to allow comparison between Gram-positive and Gram-negative organisms, and to examine the susceptibility of *S. aureus* in suspension as compared to dried surface-associated inoculum.

3.10 Antimicrobial suspension testing using PAW generated via large batch Surface Barrier Discharge (SBD)-NTP and falling-film flow

To determine whether the implied antimicrobial effects of PAW against *P. aeruginosa* seen in preliminary suspension tests could be replicated using SBD-PAW generated using a larger batch system, further experiments were undertaken, using PAW derived from an alternative up-scaled modified SBD-generated NTP treatment system. Large-batch SBD-PAW was produced using a cylindrical electrode and dynamic flow configuration (detailed in Section 2.8.3). Within this system, SBD-plasma was generated between a high voltage outer electrode supplied with 30V DC and an inner mesh-electrode, with a quartz dielectric barrier. A continuous flow of ultrapure deionised water, pumped upward from a sealed 1L beaker through a Perspex cylinder, was exposed to SBD plasma via ‘falling film’, i.e. a shallow stream flowing down the void between electrode and dielectric. This circulatory system enabled multiple-pass exposure of a larger ($\leq 1L$) volume of water, using a longer treatment period of at least 10 minutes, until the PAW reached a pH of between 3 and 3.5.

3.10.1 The effects of SBD-falling film PAW against *P. aeruginosa* and *S. aureus* in suspension

The efficacy of SDB-falling film-generated PAW was measured against both *P. aeruginosa* and *S. aureus* in suspension, to determine whether there was differential inhibition either Gram-negative or Gram-positive test species following PAW treatment. Suspension tests using large-batch SBD-PAW again were undertaken using a single fixed treatment period of 300s, treating with undiluted SDB-PAW which had been frozen in 50mL aliquots, then thawed 12-16h prior to testing, and brought to room temperature. On the day of testing, the pH of the SDB-PAW was measured to detect any change relative to that recorded immediately post-generation.

No inhibition of either *S. aureus* nor *P. aeruginosa* was seen with SDB-PAW, compared to recoveries obtained in water controls (Figure 3.19). This was despite the pH stability of PAW at the point of use, with measurements of 2.8 – 3.2, similar to the values seen on the day of SDB-PAW generation.

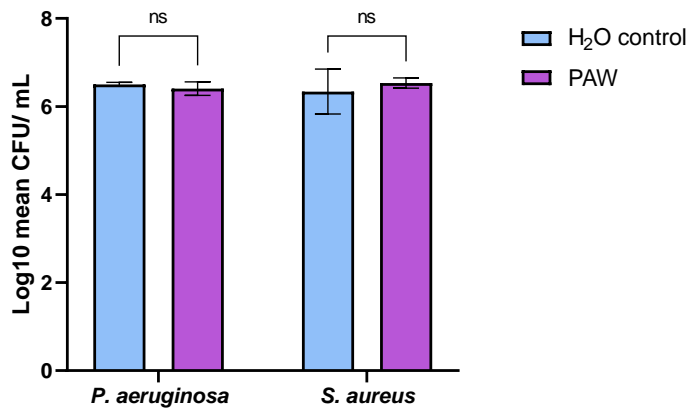


Figure 3.19. Log viable *P. aeruginosa* and *S. aureus* recovered following suspension testing with large-batch SDB-PAW, applied to test surfaces for a contact time of 300s, performed in triplicate; n=3. Significance was determined by paired t-test. Threshold for significance: $p < 0.05$.

Extension of contact time for up to 30 mins was attempted, to observe any emergence of effect of SDB-PAW, however, preliminary results again failed to show any antimicrobial activity in either test species at the selected exposure times ($p > 0.05$) (Figure 3.20). Additionally, the SDB-PAW aliquots used in this extended contact time test series had been stored at -20°C for 3 weeks prior to thawing and use, therefore it is possible that alterations had occurred in its chemical profile during this time and under these conditions, leading to changes in reactivity and biological effect, as has been alluded to previously (Shen *et al.*, 2016; Tsoukou, Bourke and Boehm, 2020). These findings must be regarded with caution, due to the lack of biological repeats, and therefore provided no more than an indication of presence or absence of microbicidal effect.

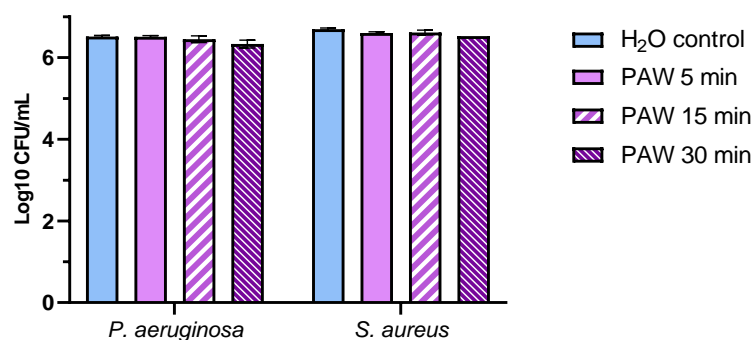


Figure 3.20. Log *P. aeruginosa* and *S. aureus* viable load recovered following extended exposure-time suspension testing with large-batch SDB-PAW. Treatments were applied for contact times of 300s – 30 minutes, and were performed in triplicate, n=1. Threshold for significance: $p < 0.05$

Although the SDB-PAW aliquots used in suspension testing were derived from a stock which had been subjected to consistent activation, storage and thawing procedures, and pH readings indicated no significant change had occurred during the interval between production and application, the highly complex chemistry inherent both during the plasma-activation process, and the post-generation reactions occurring in the immediate post-exposure period, and during

the freezing and thawing processes likely affected the physicochemical properties and hence antimicrobial activity of the SDB-PAW in these assays. Analyses of the evolution of PAW reactive species have demonstrated that storage conditions can strongly influence the stability of some of the predominant bioactive compounds generated within PAW (Traylor *et al.*, 2011; Shen *et al.*, 2016; Liu *et al.*, 2018), and that significant variability in relative concentrations of these species can occur between batches treated identically (Tsoukou, Bourke and Boehm, 2022). Therefore, in order to determine any significant changes in the PAW chemistry from the point of production to the point of use, it would be necessary to perform compositional analysis of each aliquot of PAW used in testing, for example quantification of H₂O₂ and total ROS, in addition to standard physicochemical measurements of pH, and ORP.

Since the SDB-PAW generation process was performed off-site with respect to the microbiological testing facilities, it was not possible to undertake antimicrobial efficacy testing with these plasma-activated products immediately, i.e. within <6h, during which time some of the more transient but highly potent reactive species generated may have, to some limited extents, persisted.

3.11 Antimicrobial suspension testing: dose-response of *S. aureus* and *P. aeruginosa* to ECAS

To provide a comparative measure of the inhibitory activity exerted by an alternative, highly-oxidising antimicrobial agent when introduced to a target organism in suspension, testing was performed using 200ppm ECAS, applied over a dilution range from 0.1% to 100% (v/v). *S. aureus* ATCC 6538 and *P. aeruginosa* NCIMB 10548 were again selected as Gram-positive and Gram-negative test organisms, respectively. Treatments were applied for a fixed duration of 300s, and were neutralised after this time, as described in Section 2.5. As per the test procedure, ECAS solutions were diluted to 80% of the prepared concentrations when introduced to the bacteria load, therefore the final concentrations in the test suspension were 0.08% (from 0.1%), 0.8% (from 1%), 8% (from 10%), 40% (from 50%) and 80% (from 100%). Povidone-iodine (5% w/v) was

included as a positive cytotoxic control, and sterile H₂O as a negative control. Results were reported as total viable load contained within the 10mL recovery suspension (Figure 3.21).

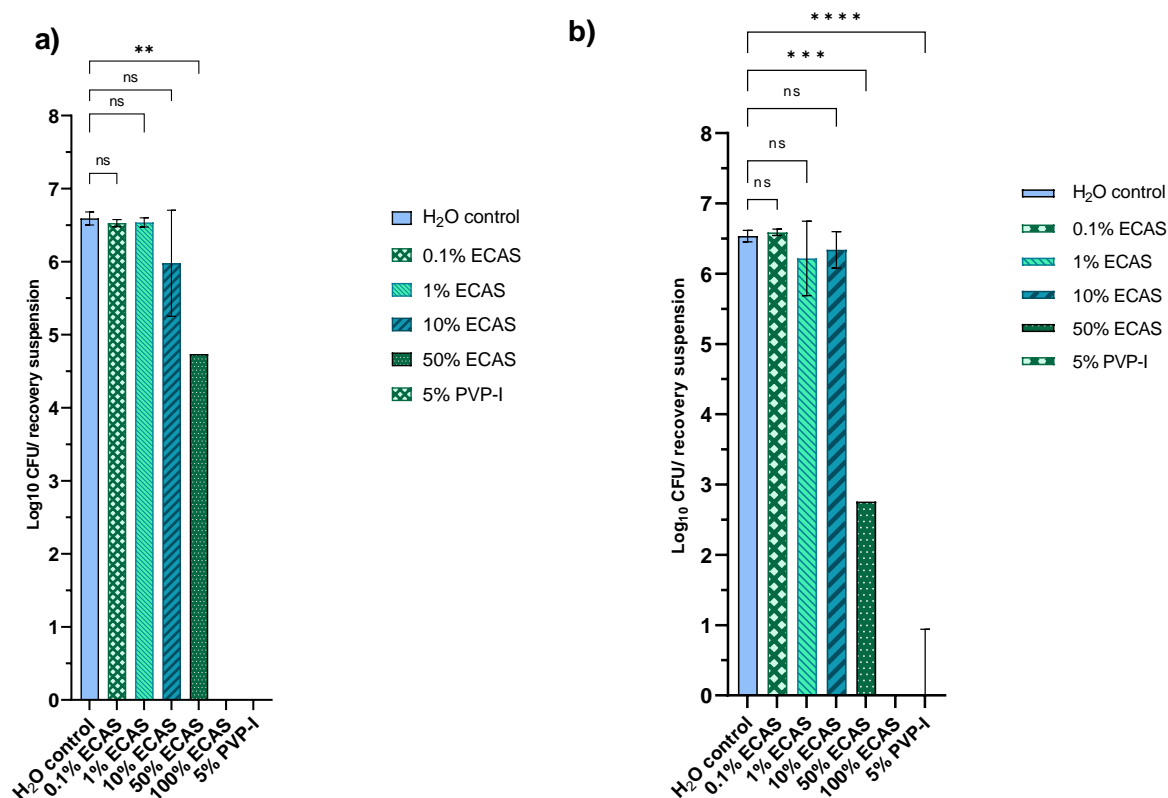


Figure 3.21. Antimicrobial suspension testing performed against *P. aeruginosa* (a) and *S. aureus* (b) using a fixed contact time of 300s, applying treatments with 0.1% - 100% ECAS (200ppm FAC) and 5% PVP-I as a positive control; treatments performed in triplicate, n=3. Analysis was performed using 2-way ANOVA with Dunnett's test for multiple comparisons. Thresholds for significance were determined as: * p<0.05, ** p<0.01, *** p<0.001, ****p<0.0001.

ECAS treatments in suspension showed an absence of significant antimicrobial effect at concentrations <50% (v/v), with recovered loads at 0.1%, 1% and 10% ECAS comparable to control. In *S. aureus*, treatment with 10% ECAS produced a 0.195 Log reduction in viable load as compared to water controls (p>0.05), and in *P. aeruginosa*, a corresponding reduction of 0.613 Log (p>0.05). In contrast, treatment with 50% ECAS (equating to 100ppm FAC) induced a reduction in *S. aureus* of 3.776 Log, with respect to water controls (p=0.0001), whilst in *P. aeruginosa*, a difference of 1.856 Log was seen (p<0.01). No viable organisms were recovered following 100% ECAS treatments in either organism, and similarly in PVP-I, equating to a Log reduction of >6.5 Log (p<0.0001, in both *S. aureus* and *P. aeruginosa*).

3.12 Discussion

The investigations undertaken here have demonstrated the significant effects of direct NTP against planktonic microbial loads when applied as a suspension combined with a low organic load, acting as an interfering substance (low concentration BSA), and subjected to pulsed NTP discharge for periods of 30s to 180s. The antimicrobial effect of direct NTP was seen to increase with extended exposure times in treatments on both *S. aureus* and *P. aeruginosa*, with a greater reduction across all time-points observed in the Gram-negative test species, although the inter-species difference was not statistically significant at each treatment time ($p < 0.05$ at 30s exposures only).

Zone of inhibition studies supported a correlation between exposure time and plasma-induced antimicrobial effects, with wider cleared zones seen following more prolonged treatments, with the exception of *C. albicans*, where the variance in measurement obtained may have obscured any such time-dependent trend. Further investigation into the NTP-induced response in a larger number of test organisms, including *Candida*, being the only fungal species included in this dataset, would provide a more detailed insight into the susceptibility of different microbial pathogens to direct NTP. Furthermore, some encroachment of growth into the inhibited zone was noted in several species, particularly *C. albicans*, within the 24-48h post-treatment incubation period, suggesting some recovery of proliferative potential following exposure, or that milder effects were induced in marginal areas of the plasma 'active zone', e.g. a temporary bacteriostatic effect rather than bactericidal. Subsequent to the ZOI testing phase, *S. aureus* ATCC 6538 and *P. aeruginosa* NCIMB 10548 were chosen as primary species of interest here, in view of their prevalence in clinically-associated biofilms, and chronic wound infections (Alves *et al.*, 2018; López *et al.*, 2019).

The comparative efficacies of alternative clinically-applicable antimicrobial agents, povidone-iodine (PVP-I), hydrogen peroxide (H_2O_2), and a hypochlorous acid-based solution generated by electrochemical activation (ECAS) were determined, testing against the same standard surface-associated planktonic microbial loads as used in NTP efficacy tests. Hydrogen peroxide appeared to exert antimicrobial activity in a dose- and exposure-time dependent manner, achieving strongest effects with 6% (v/v) treatment in 300s exposures, where almost 5 Log reduction in viable load was seen. The efficacy of 6% H_2O_2 over a 180s contact time was of a similar magnitude to that of direct NTP applied for the same duration. In contrast, PVP-I (at both 5% and 10% w/v concentrations) demonstrated a greater efficacy than both H_2O_2 and NTP, achieving near-complete eradication of viable load within a shorter treatment time-frame of up to 60s, exceeding 6 Log reduction in viable *S. aureus* bioburden. ECAS exhibited similar efficacy, again outperforming NTP at all time-points tested, reducing recoverable microbial loads to sub-detectable

levels, with the exception of a single replicate at 60s treatment. The reasons for this paradoxical result are undetermined, but could relate to technical error, such as failure to equilibrate the test suspension, or flawed application of the test product to inoculated surfaces.

Plasma-activated liquids generated using the RF-MW NTP system demonstrated no detectable antimicrobial efficacy, suggesting that this method of plasma treatment was unsuitable for efficient transfer of reactive species to the bulk liquids exposed to treatment, or that any such species entering the liquid medium rapidly deteriorated, potentially via secondary reactions with buffer constituents in the medium, or evolution of gaseous species from the treated solution. Plasma-activation of water using the small-batch SBD-NTP system did produce some encouraging results, however, producing significant effects on *P. aeruginosa* viability, in both non-porous surface testing, and suspension tests. The microbicidal activity of small-batch SBD PAW declined, however, following storage post-production, therefore it would seem that reactive species critical to the mode of action of PAW were lost in the interim between the point of plasma-activation and the application of treatments. This would be consistent with findings reported in the literature, illustrating the instability of several of the RONS generated by plasma-activation of liquids, and their dissipation, or accumulation over time, particularly when stored under inappropriate conditions.

The generation of PAW via a large-batch SBD-exposure process was carried out to investigate whether plasma-activation of a larger bulk volume of water could achieve effects consistent with that seen initially with small-batch SBD activation. PAW generated via this alternative SBD-treatment system did not produce any detectable antimicrobial effects against either Gram-positive or Gram-negative test organism when applied in suspension, failing to replicate the transient antimicrobial activity observed with the previous small-batch SBD product. However, there once again was a latent period between generation of the PAW and its use in testing, which may have prevented optimal antimicrobial effects from being captured at the point of use. Due to logistical factors and resource limitations, it was not possible to carry out more extensive experimental replicates to increase the interpretability and statistical power of the data obtained here. In future work, it would be imperative to optimise PAW handling, storage and transport procedures, to minimise any negative impacts upon product efficacy and stability, and thus validate further testing with SBD-PAW.

In contrast to PAW, ECAS exhibited strong antimicrobial activity in suspension tests, achieving complete kill effects in both test species at 100% concentration, and a near-4 Log reduction in *S. aureus* at the 50% concentration, and a near-2 Log reduction in *P. aeruginosa*. In all tests performed with ECAS, it was possible to conduct treatments almost immediately after generation of the activated ECAS solution, thereby maximising the possibility of exposing target microbial

loads to the metastable compounds generated within the solution. The physicochemical parameters of ECAS have also been demonstrated to be susceptible to changes in stability, depending on the environment in which it is storage (Ishihara *et al.*, 2017), therefore the ECAS produced for use in work presented here was generated as freshly as possible before commencing testing, with ORP, pH and FAC measurements taken to verify consistency of these parameters between batches.

3.12.1: Key conclusions:

Results obtained in the planktonic antimicrobial efficacy testing procedures performed here indicated significant microbicidal activity was achievable using the combined RF-MW system, on both Gram-positive and Gram-negative test organisms when applied to carrier surfaces. The application of aqueous antimicrobial products in quantitative surface disinfection tests demonstrated, in some instances, similar Log reductions to those produced by NTP treatments over similar exposure times, however the rapid and more complete microbicidal effect of PVP-I (both 5% and 10% w/v preparations) out-performed the maximal reduction in bioburden seen with plasma. Only treatment with ECAS 200ppm FAC demonstrated comparable time-kill efficacy to that observed with PVP-I.

Plasma-treatment of water was performed to investigate the efficacy of an alternative mode of delivery of plasma-generated reactive species, when produced directly in a liquid volume. The application of PAW as an effective aqueous antimicrobial solution has been reported extensively elsewhere, however attempts to reproduce similar results here were of very limited success. Using a small-batch SBD generation system, treating a small volume of liquid and introducing the resultant PAW to inoculated carrier surfaces yielded more successful results than the other generation methods employed, exerting a small but significant inhibitory effect of up to 1.3 Log against *S. aureus*, and when applied in suspension tests to *P. aeruginosa* in suspension (without organic contamination), a greater microbicidal effect was noted, with a Log reduction of approximately 4.7 Log. However, the marked decrease in antimicrobial efficacy observed after continued storage and repeat testing of small-batch DBD PAW inferred a loss of key reactive species, potentially due to unsuitable storage conditions, and inherent biochemical instability of such species or compounds in the activated solution. Similarly, use of a SBD plasma generator with falling-film flow system was investigated as an alternative approach, but the PAW obtained demonstrated no detectable antimicrobial activity against *S. aureus* or *P. aeruginosa* when applied in suspension tests and quantitative surface disinfection tests, even at extended contact times. These preliminary findings underlined the need to undertake further work, in order to optimise the methods utilised in PAW generation, handling and storage, and also highlighted the requirement for more robust product standardisation techniques to ensure consistency between batches, i.e. verifying not only physicochemical parameters such as ORP, pH and conductivity, but

also analysis of reactive species concentrations within the PAW produced, to determine the variance between solutions, and the changes occurring within a single batch over time.

Suspension testing of ECAS, investigating dose-response over a broad dilution range showed a significant antimicrobial effect at concentrations of $\geq 50\%$ v/v ECAS (equating to ≥ 100 ppm FAC), but negligible inhibition with concentrations below 10% v/v (< 20 ppm). Thus it can be recognised that despite exerting potent microbicidal activity on surface-associate microbial loads, the efficacy against both Gram-positive and Gram-negative microbial targets is strongly negated by dilution, when applied in suspension tests. The inclusion of an organic interfering substance was omitted in these procedures, to determine baseline antimicrobial efficacy without additional challenge, however in the *in vivo* setting, the presence of protein-rich fluids such as wound exudate would likely impact the antiseptic activity of applied treatments, limiting the maximum achievable concentration in situ.

These results as a whole reiterate the importance of conceiving antimicrobial testing protocols which take account of additional complicating factors occurring *in vivo*, by replicating the wound bed environment as far as is practicable, to increase the clinical relevance of results, and enable a more accurate indication of product performance in therapeutic applications, by extrapolation.

Chapter 4: The effects of NTP and alternative antimicrobials on bacterial biofilms

4.1 Background and introduction

Microbial biofilms represent the most recalcitrant and widespread phenotypic form adopted by microorganisms, occurring across an extremely diverse range of environmental niches, both biotic and abiotic, living as a complex consortium in which both cooperative and competitive interactions occur, and in which a broad array of phenotypic adaptations are expressed (Costerton, Geesey and Cheng, 1978; Donlan and Costerton, 2002; Stewart and Franklin, 2008; Flemming *et al.*, 2016). Biofilms demonstrate enhanced resistance to both chemical and physical interventions, and an ability to adhere to most surfaces and tissues, traits which allow them to rapidly colonise exposed areas, and, in living organisms, to proliferate to an extent which causes pathogenic infection (Bjarnsholt, 2013; Percival *et al.*, 2015; Percival, McCarty and Lipsky, 2015).

It is well established that biofilms are capable of withstanding concentrations of antimicrobials several-fold greater than the minimal inhibitory concentration (MIC) proven to be effective against their planktonic counterparts, reinforcing the magnitude of the challenge posed by these often complex microbial structures (Donlan and Costerton, 2002; Olsen, 2015; Omar *et al.*, 2017; Khatoon, *et al.*, 2018). To ensure effective inactivation of viable organisms from within biofilms, prevent regrowth, and minimise the risk of development of antimicrobial resistance, biocidal and antiseptic products must undergo rigorous testing to ensure adequate and consistent efficacy under appropriate conditions, which reflect the intended applications (Buckingham-Meyer, Goeres and Hamilton, 2007; Macià, Rojo-Molinero and Oliver, 2014; Krasowski *et al.*, 2021; Paleczny *et al.*, 2023; Paleczny, J, *et al.*, 2023). Antimicrobial agents purposed for decontamination and disinfection procedures against biofilms, whether formulated for application to abiotic materials, or to be used therapeutically *in vivo*, should therefore be subjected to performance-testing which confirms both their effectiveness in eliminating viable pathogenic organisms, and their safety and compatibility with the target surface or tissue, respectively (Buckingham-Meyer, Goeres and Hamilton, 2007; Bahamondez-Canas, Heersema and Smyth, 2019; Bayot and Bragg, 2022; Di Bonaventura and Pompilio, 2022).

To investigate the comparative efficacy of NTP treatment on microbial biofilms, two laboratory models were used to culture single species biofilms prior to the application of a range of treatments, including direct or indirect NTP (a novel antimicrobial technology), 10% PVP-I, 6% hydrogen peroxide, (representing the uppermost range of clinically-applied concentrations of these two standard antiseptic agents) (Eggers, 2019; Murphy and Friedman, 2019; Tan and Johari, 2021; NICE, 2024), or electrochemically-activated saline solution (ECAS) (a hypochlorous acid-based product, similar to commercially-available products known often as 'super-oxidising

solutions', or electrolysed water) (Johani *et al.*, 2018; Severing *et al.*, 2019; Dissemond, 2020; Yan, Daliri and Oh, 2021). Although biofilm-associated wound infections most frequently involve multiple pathogenic microbial species, the effects of treatments upon single species only were studied here, to assess antimicrobial efficacy in a simplified biofilm system in the absence of inter-species interactions.

Two dynamic *in vitro* systems were used for culture of single species biofilms, prior to testing, namely the Centers for Disease Control Biofilm Reactor (CBR) - a standard laboratory system used for a range of applications including the study of biofilm growth kinetics and the testing of inhibitory compounds or antibiofilm interventions, and the Continuous Perfusion Collagen Matrix – Drip Flow Reactor (DFR), an adaptation of the standard DFR (Goeres *et al.*, 2009), which was developed to facilitate biofilm culture under conditions simulating an infected wound-bed *in vivo* (Slade *et al.*, 2019; Slade, 2020), thereby offering a more advanced for the investigation of biofilm physiology in the wound micro-environment.

4.2 Surface-associated biofilms cultured within the CDC Biofilm Reactor (CBR)

The CBR enables a maximum of 24 replicate biofilms to be grown on coupons inserted into 8 polypropylene rods, housed within the reactor chamber and immersed in growth medium (see Methods, Section 2.6.1.1). Within the CBR, biofilms are generated under moderate shear force, owing to the continuous stirring action of a rotating central baffle, with the operation of the reactor divided into two phases, batch and continuous. The initial 24h batch phase represents a closed system in which the freshly inoculated growth medium is contained within the reactor chamber and stirred at a set rate, allowing initial microbial attachment and colonisation of the reactor coupons, and microbial proliferation to occur within the fixed volume of medium. Following the first 24h growth, continuous phase is initiated, in which the growth medium is continuously replenished, pumping fresh medium into the reactor and, after a 30-minute residence time, drained into a waste container, so as to limit the increase in microbial density within the reactor chamber, and also to prevent accumulation of microbial metabolites, secreted factors, and waste products, which would potentially influence the rate of biofilm growth.

4.2.1 Comparison of biofilm density formed on different coupon materials

Preliminary experimentation was undertaken to assess the relative density of *P. aeruginosa* (NCIMB 10548) biofilms grown on coupons composed of differing materials within the CBR after 48 hours. Resultant mean densities (Figure 4.1), demonstrated that similar levels of biofilm growth were obtained on the polymers polycarbonate (9.103 Log₁₀ CFU/coupon) and silicone (9.340 Log₁₀ CFU/coupon) coupons (p>0.05), and a slightly lower density was obtained on

stainless steel (8.397 Log₁₀ CFU/coverslip) ($p < 0.001$, compared to silicone; $p > 0.05$ in comparison to polycarbonate).

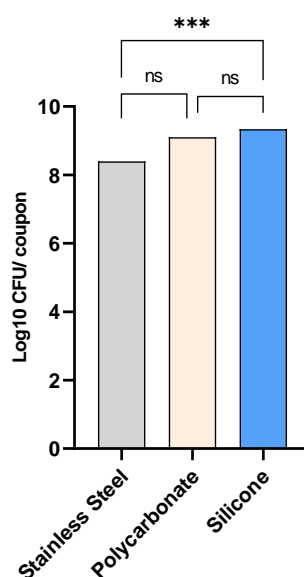


Figure 4.9: Total biofilm density of single species *P. aeruginosa* NCIMB 10548 biofilms grown within the CBR on three different surface materials for 48 hours (Polycarbonate and silicone coupons, $n = 9 \pm SD$; steel coupons, $n = 6 \pm SD$). Mean recovered load per coupon were compared by 2-way ANOVA with Tukey's test for multiple comparisons. Thresholds for significance: * $p < 0.05$, ** $p < 0.01$, *** $p < 0.001$, **** $p < 0.0001$.

Silicone and stainless steel were selected as the two substrate materials for biofilm culture in subsequent experiments, representing component materials used in the fabrication of an array of medical implants and/ or devices (Teo *et al.*, 2016; Zare *et al.*, 2021). Silicone is a synthetic polymer which can be specifically formulated according to the required function, with biomedical applications including flexible catheters, drains and shunts, fillers and in prosthetic implants, and in the coating and assembly of various implantable medical devices. Silicone is characterised by its high hydrophobicity and elasticity, gas permeability, thermal and mechanical stability, and its non-toxic, chemically inert nature (Zare *et al.*, 2021), making it an ideal biocompatible material. However, silicones also demonstrate susceptibility to microbial colonisation, which can lead to device failure, and device-associated infections (Gilmore *et al.*, 2018; Greenhalgh, Dempsey-Hibbert and Whitehead, 2019; Gupta and Ayan, 2019; Zare *et al.*, 2021). Microbial adhesion and biofilm formation on silicone has been demonstrated *in vitro* and is acknowledged as a cause of device-related infections in the healthcare setting (Verma, 2016; Sabir *et al.*, 2017; De-la-Pinta *et al.*, 2019; Zare *et al.*, 2021).

Stainless steel is one of the most widely used materials in the clinical environment, both for instrumentation, and prosthetic implants, particularly orthopaedic devices and surgical tools (Resnik *et al.*, 2020). Contamination of steel surfaces may present a source of cross-contamination and infection risk, upon even dry surfaces, when improperly sanitised or processed (Verran, J, Whitehead, 2005; Zhang *et al.*, 2011; Abreu *et al.*, 2013; Resnik *et al.*, 2020).

Microbial attachment to biomaterials, such as silicone and steel, is affected by the surface chemistry, hydrophobicity, charge and topography, meaning that modifications to such surface physicochemical characteristics can be manipulated to reduce the susceptibility to colonisation (Zhang *et al.*, 2011; Wu *et al.*, 2018; Zheng *et al.*, 2021). The functionalisation of stainless steel, silicone, and other biomaterial surfaces via a number of diverse technological processes, including anti-adhesion surface-coatings incorporating bioactive compounds and/or nano-engineered structures, and also plasma-mediated surface modification, offers a promising field of development for the generation of advanced materials for biomedical applications (Resnik *et al.*, 2020; Zheng *et al.*, 2021; Ma *et al.*, 2022). However, in addition to preventative technologies, effective treatments are necessary to inactivate biofilms *in situ*, and to eliminate biofouling caused by microbial biofilm formation upon multiple-use devices. The application of NTP upon pre-formed biofilms may represent an effective solution which can be applied at the point of need, without the introduction of harmful chemical agents, or toxic residues.

Therefore, silicone and steel coupons were selected for the testing of antimicrobial treatments on adherent biofilms cultured within the CBR, since these materials both constitute a common target for biological contamination and growth of biofilms in the healthcare setting. The anti-biofilm effects of direct and indirect NTP were investigated and the efficacy compared to that achieved with alternative aqueous antimicrobial agents.

4.3 Investigation of the effects of direct NTP on *Pseudomonas aeruginosa* and *Staphylococcus aureus* mono-species biofilms grown within the CBR

Direct NTP treatments were performed upon 48h mature CBR biofilms, treating each coupon bilaterally as previously described (Section 2.6.1.2). Initial attempts to remove the biofilm from one face of each coupons resulted in poor reproducibility (data not shown), therefore it was decided to apply NTP treatments to both sides, allowing evaluation of the effects against a larger and more consistent microbial biofilm population. To maintain aseptic technique, treatments were applied by stably fixing the CBR rods in a clamp-stand within a biological safety cabinet, treating one side of each of the three coupons for the designated time-period, then rotating the rod to treat the opposite face, rinsing with sterile PBS after the first treatment to minimise cross-contamination of the treatment from one side to another.

4.3.1 Comparative efficacy of direct NTP and 10% PVP-I

4.3.1.1 Effects on *P. aeruginosa* biofilms

P. aeruginosa NCIMB 10548 was grown within the CBR for 48 h according to the standard method, at which time test coupons were removed and subjected to test treatments with either 60s or 120s direct NTP, 30s povidone iodine (10% w/v), or left untreated (control). NTP treatment times corresponded to treatment time-frames reported from similar studies conducted on *in vitro*

biofilms elsewhere, as suitable for the determination of plasma-induced effects (Alkawareek *et al.*, 2012; Gupta and Ayan, 2019; Thana *et al.*, 2019) whilst the shorter PVP-I treatment time was selected due to its known rapid onset of action, as demonstrated in earlier planktonic testing times-courses. Treated biofilms were recovered dissociated from each coupon via vortexing and sonication, before sampling the resultant recovery suspension for the determination of surviving microbial load (as described in Section 2.6.1.2).

As demonstrated previously (see section 4.2.2), the *P. aeruginosa* biofilm density was higher on silicone compared to stainless steel coupons, with a mean viable recovery of 9.327 Log CFU/coupon, compared to 8.323 Log, respectively (Figure 4.2). Results indicated a time-dependent inhibitory effect of NTP, with mean Log reductions on silicone coupons of 0.652 CFU after 60s exposure, and 1.007 CFU after 120s treatments ($p>0.05$). An enhancement with increased treatment time was similarly seen on stainless steel surfaces, with 60s exposures achieving a 0.714 Log reduction, whilst 120s treatments produced a 1.385 Log reduction, a slight but significant increase in effect ($p<0.05$). Short exposure (30s) to PVP-I demonstrated superior efficacy to NTP treatments on both surface materials, achieving Log reductions of 2.259 on silicone coupons, and 3.032 on steel, thus exerting a greater microbicidal effect within a shorter time than that seen with plasma.

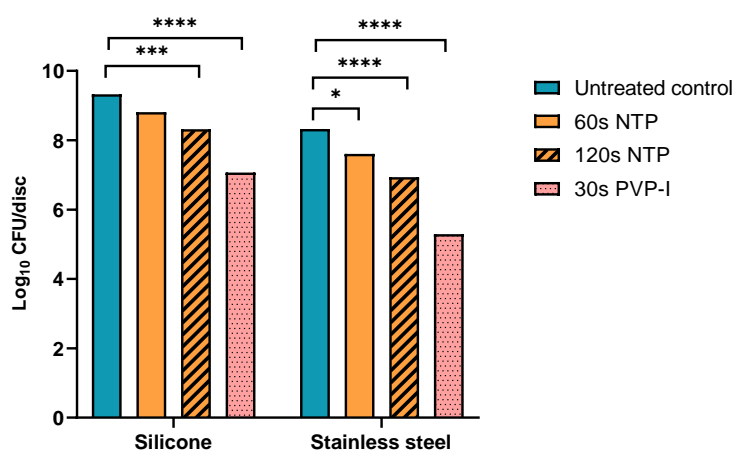


Figure 4.10: *P. aeruginosa* NCIMB 10548 biofilms were grown for 48h within the CBR, whereby coupons were subsequently removed and subjected to either a 60s or 120s NTP treatment or a 30s PVP-I treatment, each performed in triplicate ($n=3$). Mean Log CFU/coupon recovered following each treatment was compared between treatments by 2-way ANOVA with multiple comparisons. Thresholds for significance were determined as $*p<0.05$, $**p<0.01$, $***p<0.001$, $****p<0.0001$.

4.3.1.2 Effects on *S. aureus* biofilms

S. aureus ATCC 6538 biofilms were subjected to identical treatments as those applied to *P. aeruginosa*, attaining slightly lower final densities in the CBR under all conditions than those seen with *P. aeruginosa*. Untreated controls yielded mean biofilm densities of 6.552 Log on silicone controls, and 6.398 Log on stainless steel (Figure 4.3), and in contrast to *P. aeruginosa*, showed

similar colonisation/ growth on the two surface materials. Direct NTP treatments produced only a small anti-biofilm effect, with 60s exposure eliciting a slight reduction of 0.0723 Log on steel, and no reduction on silicone, whilst 120s treatments achieved mean reductions of 0.466 Log on steel and 0.381 Log on silicone, markedly smaller than the effects seen on *P. aeruginosa*. Povidone iodine 30s treatments gave the greatest inhibitory effect on both surface materials, with 1.893 Log decrease in viable bioburden on steel, and 2.473 Log reduction on silicone, therefore equalling the efficacy seen against *P. aeruginosa* on silicone, but not on steel.

The overall reduced density of *S. aureus* biofilms formed within the CBR, and the requirement to increase the nutrient concentration of the culture media tenfold relative to that used for *P. aeruginosa*, indicated a slightly lower capacity for biofilm formation under these experimental conditions than that evidenced by *Pseudomonas*, as has been observed by others (Stuermer *et al.*, 2021). Additionally, large variance in the PVP-I-induced effect on *S. aureus* on silicone was seen, suggesting possible variability in the biofilm tolerance of this treatment, heterogeneity in the biofilm formed on the test surface, or potentially unequal application of the treatment. This latter source of error may also have influenced the results obtained with NTP treatments, as the surface area within the direct target range of the NTP applicator may have allowed for a ‘margin effect’ on test coupons, whereby biofilm on the outer periphery was likely to have been subjected to reduced exposure to plasma constituents than the central zone directly beneath the NTP torch aperture.

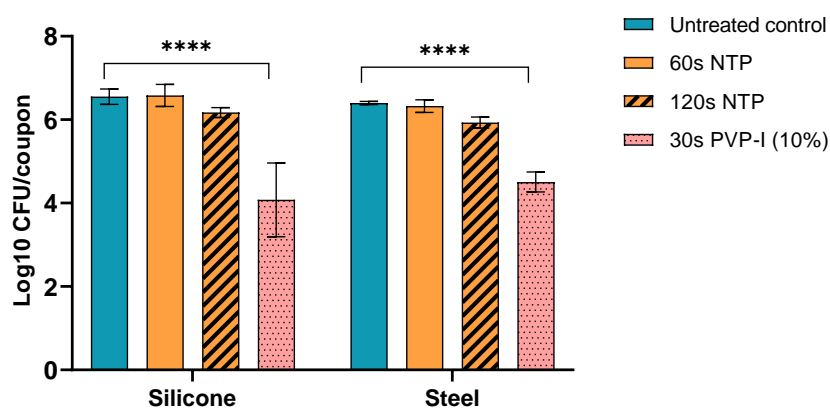


Figure 4.3. *S. aureus* ATCC 6538 biofilms were grown for 48h within the CBR, whereby coupons were subsequently removed and subjected to either a 60s or 120s NTP treatment or a 30s PVP-I treatment, each performed in triplicate ($n=3$). Mean Log recovered loads following treatments were compared by 2-way ANOVA with multiple comparisons. Thresholds for significance were determined as $*p<0.05$, $**p<0.01$, $***p<0.001$, $****p<0.0001$.

4.4 The comparative anti-biofilm activities of ECAS, hydrogen peroxide, and PAW

4.4.1 Effects on *P. aeruginosa* biofilms

To determine the effects of two relatively novel antimicrobials to that of a more established standard upon a single species biofilm, and to compare their relative efficacies to those seen in planktonic microbial testing, Electrochemically Activated Saline (ECAS, at 200 ± 20 ppm FAC), 6% hydrogen peroxide (v/v), and Plasma Activated Water (PAW, generated by large-batch SBD plasma activation of ultrapure dH₂O) were applied to *P. aeruginosa* (NCIMB 10548) biofilms grown for 48h within the CBR, treated bilaterally for 300s per side, and recovered as previously described (Section 2.6.1.2).

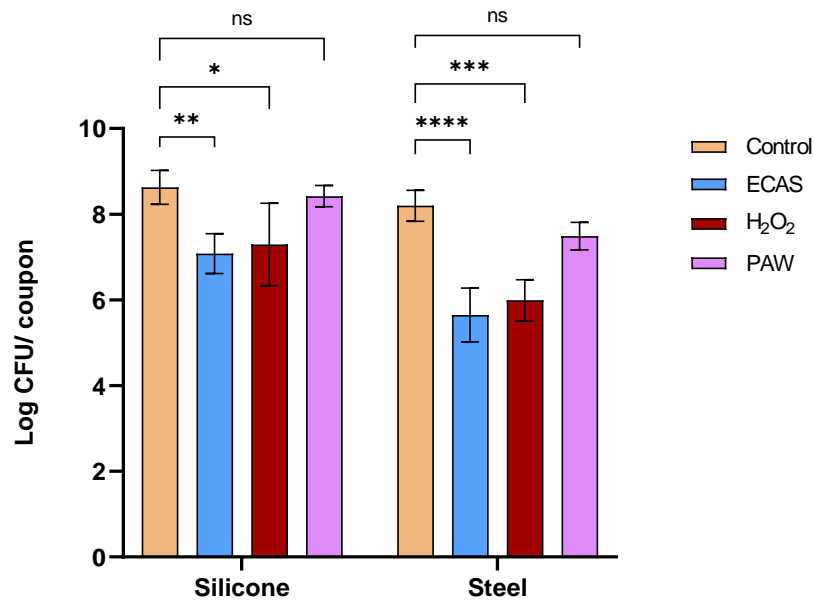


Figure 4.4: *P. aeruginosa* biofilms were grown to 48h within the CBR whereby coupons were removed and subjected to 300s treatment with either ECAS (200ppm FAC), 6% H₂O₂, or PAW (each performed in triplicate, n=3). The mean Log recovered loads following treatments were compared by 2-way ANOVA with Dunnett's multiple comparisons test. Thresholds for significance were determined as * $p < 0.05$, ** $p < 0.01$, *** $p < 0.001$, **** $p < 0.0001$.

Treatments produced similar trends in efficacy upon both test materials (Figure 4.4). Silicone-adherent biofilms showed the greatest reduction with ECAS treatments, demonstrating a 1.554 Log reduction relative to untreated controls, a significantly larger effect than that observed with PAW (a 0.214 Log decrease) ($p < 0.05$), but similar to that achieved with 6% (v/v) H₂O₂ (1.340 Log reduction) ($p > 0.05$). The greatest anti-biofilm effect on stainless steel also occurred with ECAS treatment, which attained a 2.594 Log reduction, markedly superior to the 0.706 Log reduction seen with PAW ($p < 0.01$), but similar to the inhibitory effect of H₂O₂, which produced a 2.248 Log decrease ($p > 0.05$). Therefore, ECAS and hydrogen peroxide, both potent oxidising agents, demonstrated similar antimicrobial efficacy against *P. aeruginosa*, achieving a greater effect on steel-associated rather than silicone-associated biofilms, whilst application of PAW exerted

negligible microbicidal effects on both test materials, failing to achieve as much as a 1 Log reduction .

Treatments with PAW and H₂O₂ both exhibited a stronger anti-biofilm effect on steel than silicone, potentially reflecting a stronger affinity of *P. aeruginosa* for silicone as a substrate for biofilm formation, as greater surface material hydrophobicity has been found to correlate with more profuse biofilm colonisation (De-la-Pinta *et al.*, 2019). Although the Log densities of biofilms formed upon untreated silicone and steel coupons were similar ($p>0.05$) (Figure 4.4), microbial interactions with the surface, may have contributed to the susceptibility of each respective biofilm to treatments, due to the effects of intrinsic surface properties of both the surface material and the adherent biofilm itself (Verma, 2016; De-la-Pinta *et al.*, 2019; Zheng *et al.*, 2021).

4.5 Investigation of the effects of traditional and novel antimicrobial agents against collagen matrix-associated biofilms

To enable the evaluation of the comparative effects of disinfectant and antiseptic compounds against biofilms in a milieu which more accurately simulates the topography of an infected wound, a modified Collagen Matrix - Drip Flow Reactor (DFR) model was used to grow single species biofilms over a 48h period. Minor adaptations were made to a previously described iteration of this model (Slade *et al.*, 2019), described in Section 2.7.1.

The DFR-collagen matrix system serves as a more advanced *in vitro* platform for the investigation of wound-associated biofilms, providing a more physiologically representative environment for biofilm growth. A hydrated, nutrient-rich substrate is incorporated via the use of a 3-dimensional semi-solid hydrogel substrate in which the microbial inoculum is allowed to embed and colonise throughout the model run-time. Combined with slow instillation of a simulated wound fluid (SWF), which replicates many of the components in serum/ physiological wound exudate, the model can be adapted to facilitate the introduction of different growth conditions or treatments to the separate channels of the reactor, in parallel, or to replicate biofilms at differing maturities, offering insight into interactions between growth kinetics and treatment efficacy.

4.5.1 Culture of *P. aeruginosa* biofilms within the DFR-collagen matrix model: steady-state densities obtained under control conditions

To quantify biofilm density obtained when operating the DFR-collagen matrix model under control conditions, and to ascertain consistency with previously published data (Slade *et al.*, 2019; Slade, 2020), *P. aeruginosa* biofilms were grown within the reactor, for 48 or 72h. The

comparative mature-state density of two strains were measured: the environmental strain *P. aeruginosa* ATCC 15442, and the clinically-associated strain *Pa* NCIMB 10548. Biofilms were supplied with a simulated wound fluid (SWF) input medium consisting of 50% FBS : 50% (8.5g/L NaCl, 1g/L peptone) solution, as used in the previously cited work.

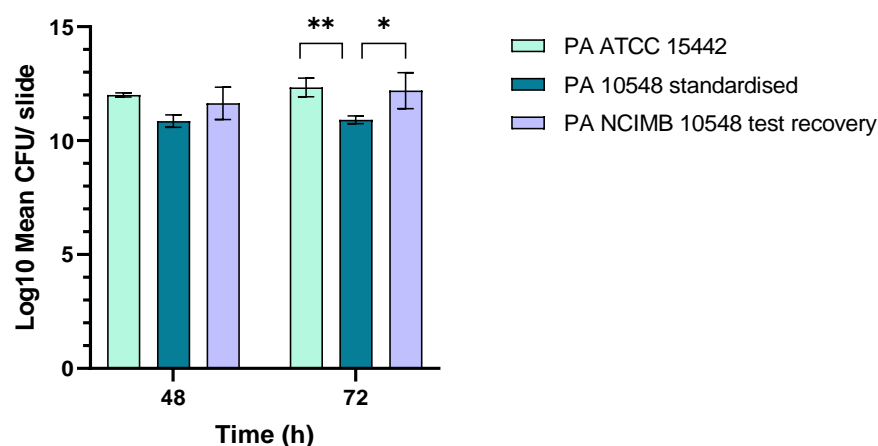


Figure 4.5. Mean biofilm density of *P. aeruginosa* biofilms cultured within the DFR – collagen matrix model, comparing growth at 48h and 72h in two strains, with reference to previously published ('standardised') data (Slade *et al.*, 2019) obtained using the clinically-associated strain, NCIMB 10548. Mean CFU/ slide per time-point was compared, for within-strain and inter-strain differences, using Mixed Effects analysis, with Sidak's test for multiple comparisons; n=3. Significance thresholds were determined as * $p < 0.01$, ** $p < 0.01$; *** $p < 0.001$, **** $p < 0.0001$.

Preliminary results yielded a mean biofilm density of 12.01 Log CFU/ slide at 48h growth, and 12.33 Log at 72h, for *Pa* ATCC 15442, whilst for *Pa* NCIMB 10548 the mean 24h density reached 11.64 Log, rising to 12.19 Log CFU at 72h (Figure 4.5). These values slightly exceeded those reported in the research performed by Slade *et al.*, in which mature steady-state biofilm densities of 10.857 Log at 24h, and 10.913 at 72h, were obtained with *P. aeruginosa* NCIMB 10548. Therefore, although the data obtained here indicated more abundant biofilm growth in both strains after 72h operation of the model, with a 1.28 Log higher density in NCIMB 10548 than the published data for this strain, and a 1.419 Log greater density in *Pa* ATCC 15442, measurements obtained at 48h were not significantly different and there was no significant continuation of growth over the 48h - 72h period within each comparative group ($p > 0.05$). This demonstrated that biofilms cultured using the laboratory model under standard conditions reached a steady-state plateau by 48h, and that mature biofilms of the two strains studied were also comparable in their final mature-state densities, despite exceeding the expected value as referenced in the literature. Following these initial biofilm growth studies, a modified SWF formulation containing a synthetic serum - as described by Oates and Mc Bain (2016) - was substituted for the previously used 50% FBS : 50% (8.5g/L NaCl, 1g/L peptone) SWF. This alternative SWF medium supported *Pa* NCIMB 10548 biofilm growth to similar densities at 48h maturity (≥ 10 Log CFU/ slide) as were seen with the original formula (data not shown), and was therefore used in all subsequent experiments.

4.5.2 Investigation of the antibiofilm effects of novel and traditional antimicrobial agents

To evaluate the efficacy of antimicrobial treatments when applied to *P. aeruginosa* NCIMB 10548 biofilms cultured within the DFR-collagen wound model, two approaches were employed. The first method entailed short-exposure treatments delivered to biofilms following their extraction from the model. This was performed by culturing replicate biofilms on coverslip coupons within the reactor, before removing them at 48h maturity, and subjecting each to short-exposure antimicrobial treatment before recovery and quantification of the remaining viable load, to determine treatment effect. The second approach entailed delivery of treatments to the wound-model biofilms *in situ*, during continuing operation of the DFR. In this method, 48h mature biofilms were cultured upon coverslip coupons, as before, and were treated via continuous drip-flow instillation through the input ports of the reactor channels, before recovery and quantification of viable biofilm.

The first approach aimed to elucidate the efficacy of directly-administered treatments upon 3D wound-like biofilms, in a static, single-immersion, short-exposure treatment protocol, in the absence of continuous SWF-feed input. The second approach attempted to simulate the dilution and quenching effects encountered when administering treatments in chronic wounds, where serum exudation may reduce the effective concentration of applied antiseptic treatments, and also interfere with the active components of such treatments, a constraint replicated experimentally by the continuous hydration and nutrient-supply provided to collagen-embedded biofilms with simulated wound fluid (SWF).

4.5.3 Initial adaptation of the DFR-collagen matrix model:

Preliminary data was obtained by incorporating 13mm glass coverslips as removable coupons (as outlined in Section 2.7.3). Results demonstrated a mean 48h biofilm yield from 13mm diameter coverslips of 9 - 10 Log CFU per coverslip (data not shown), however variation was clearly observable in the distribution of the biofilm down the length of the slide, upon visual examination, and therefore the positioning and number of coverslips placed on the slide were assumed likely to affect the uniformity of biofilm coverage upon replicate coverslips extracted from each slide. Biofilm growth appeared most dense and continuous in the central portion of the slide, therefore off-setting coverslips from centre was expected to result in asymmetry in the biofilm growth captured. Furthermore, the delicate consistency of the collagen matrix-biofilm complex on replicate coverslips also demanded careful handling, and complete excision of each coverslip biofilm sample was challenging, therefore technical limitations likely also contributed to the variability in density between untreated controls originating from a single slide, as well as between channels.

4.5.4 Application of antimicrobial treatments to collagen matrix-associated *P. aeruginosa* biofilms: short exposure, ex-model

Treatment of *P. aeruginosa* biofilms was first applied via single short-exposure immersion in aqueous biocides. This was performed in 12-well microtiter plates, treating individual biofilm-coated coverslips for a 5-minute period, using a 1mL volume of the selected agent. Two channels were reserved for full-slide biofilm recoveries, without extracting coverslip-adherent samples. This measure was included in order to provide confirmation of model repeatability (comparing the density of the untreated control biofilm, per slide, to previous results) and the absence/presence of effect of the applied treatment against a larger microbial target population, presenting a greater biomass (PAW-immersion).

Although the data obtained represents a single biological replicate, and therefore only allows for limited interpretation, it appeared to be in accordance with the results obtained in testing against CBR biofilms, using the same antimicrobial treatments. Untreated coverslip biofilms yielded a viable load equivalent to 9.40 Log CFU/coverslip, which was approximately 1.3 Log lower than that recovered from the full slide control biofilm (10.715 Log CFU), reflecting the reduced surface area of the coverslip in relation to that of the full slide (approximately 1:14) (Figure 4.6). The untreated full-slide yielded a lower biofilm density that was obtained in prior experimental replicates, but remained within the expected range as referenced previously in the literature, of 10 Log CFU/slide (Slade *et al.*, 2019)

Both ECAS (200ppm FAC) and 6% hydrogen peroxide appeared to produce a small inhibitory effect on viability, resulting in Log reductions per coverslip of 0.7 ($p < 0.01$) and 1.15 ($p < 0.001$), respectively, relative to control. Immersion in PAW failed to elicit any effect in coverslip biofilms, with a viable recovered load equivalent to 9.22 Log CFU/ coverslip, comparable to that of untreated controls (9.398 Log CFU) ($p > 0.05$). PAW immersion of the full slide biofilm was performed in one channel only, and data was therefore insufficient for robust statistical inference, however there was a small decrease in viable load of 0.53 Log/ slide compared to the untreated control ($p < 0.05$) - with recovered loads of 10.179 Log versus 10.715 Log, respectively – suggesting a marginal antimicrobial effect.

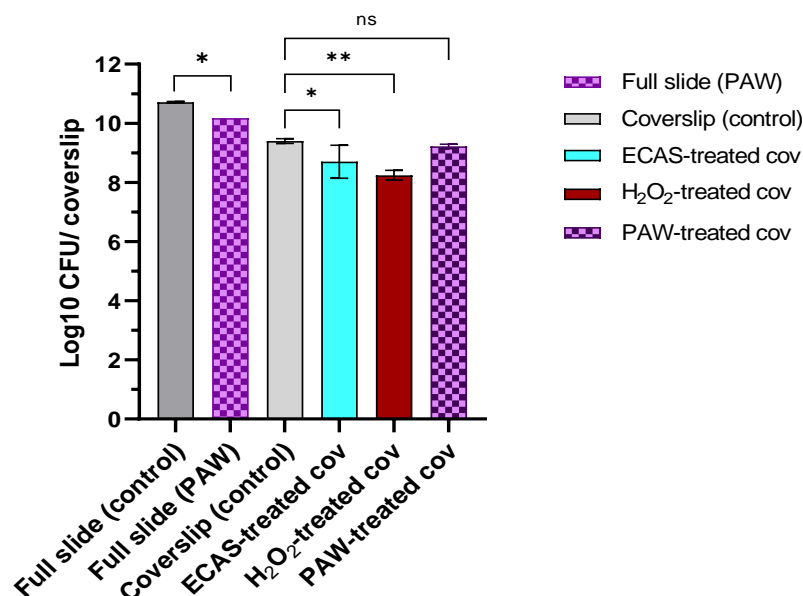


Figure 4.6: *P. aeruginosa* NCIMB viable load recovered from full slide biofilms and coverslip-adherent biofilms cultured to 48h within the DFR-collagen matrix model, subjected to single immersion treatments. Log CFU/coverslip was compared between treatments using one-way ANOVA with Dunnett's multiple comparison test. Log CFU/full slide were compared by unpaired t-test. Biofilms were sampled in triplicate; n=3 coverslip biofilms; n=2 full slide control; n=1 full-slide PAW treatment. Significance thresholds were determined as: * $p < 0.05$; ** $p < 0.001$, *** $p < 0.0001$, **** $p < 0.0001$.

The presence of organic components and inorganic ions within or upon the target has been reported to cause partial suppression of antimicrobial effect in a number of antimicrobial or disinfectant products, an observation which has been attributed to oxidative interactions between the reactive species of the product and native interfering substances within the target microenvironment, such as the abundance of serum in wounds *in vivo*, or the presence of organic soiling upon reusable medical devices (Maisetta *et al.*, 2008; Rutala and Weber, 2014; Esin *et al.*, 2022). In addition, products containing metastable active components, such as ECAS and PAW, may be rendered less effective following interaction with physiological contaminants such as serum, salts, and proteins present in the surroundings. One approach to overcoming this dampening effect in the context of the exuding wound could be the replenishment of the antimicrobial product on the target surface, i.e. applying the treatment as a continuous-flow irrigant (Esin *et al.*, 2022), to compensate for the quenching or neutralising effects of the interfering substances. To discern whether an improved microbicidal effect could be achieved using ECAS against *P. aeruginosa* biofilms, treatments were introduced within the DFR reactor using a continuous instillation approach rather than single immersion.

4.5.5 Application of antimicrobial treatments to collagen matrix-associated *P. aeruginosa* biofilms: periodic irrigation of biofilms within the DFR

A timed-irrigation procedure was used to treat biofilms within the DFR-collagen matrix model, with intervening re-feed periods, to assess the efficacy of repeated antimicrobial treatment, and

to discern whether any inhibitory effects upon biofilm viability were obscured or counteracted by replenishing SWF between antimicrobial treatments. ECAS was selected as treatment of interest, testing three different strengths in parallel, with FAC concentrations of 200ppm, 300ppm and 500ppm, prepared on the day of experimentation and connected aseptically to the inputs of the DFR. Treatments were applied to biofilms at 48h maturity, with three repeat exposure periods, as outlined in Section 2.7.3. Briefly, the SWF-feed was stopped, and the peristaltic pump rate increased to approximately 50mL/h, to clear SWF from the input tubing to the reactor, and prevent mixing with the treatment solutions. The channel inputs were then primed with either PBS (control) or ECAS (test) at the three different concentrations, and instillation of each treatment ensued for 30 minutes. Following treatment, the SWF feed to each channel was purged ECAS (or PBS), and SWF-feed was re-introduced, continuing for 1hr before switching again to ECAS or PBS-only infusion for another 30-minute period. The SWF-feed was again re-started for one hour, before a final 30-minute treatment period.

Viable recovered loads were compared within and between treatment groups. Comparison of replicate biofilms within treatment groups by one-way ANOVA showed significant variation, in both control biofilms and treatments ($p < 0.0001$, Control slide A; $p < 0.001$ Control slide B; $p < 0.001$ Control slide C; $p < 0.001$ 200ppm ECAS, slide D; $p < 0.001$, 300ppm ECAS slide E; $p > 0.05$, 500ppm ECAS slide F). (Figure 4.7a). This suggested heterogeneity in biofilm density over the slide surface, with recovered bioburden affected not solely by the treatment applied, but also according to the precise sampling site on the slide. Control channels which were irrigated with PBS during the 30-minute treatments windows, showed slight but significant disparities in viable loads obtained down the length of the slide, of up to 0.704 Log CFU/coverlip ($p < 0.0001$, Control slide A).

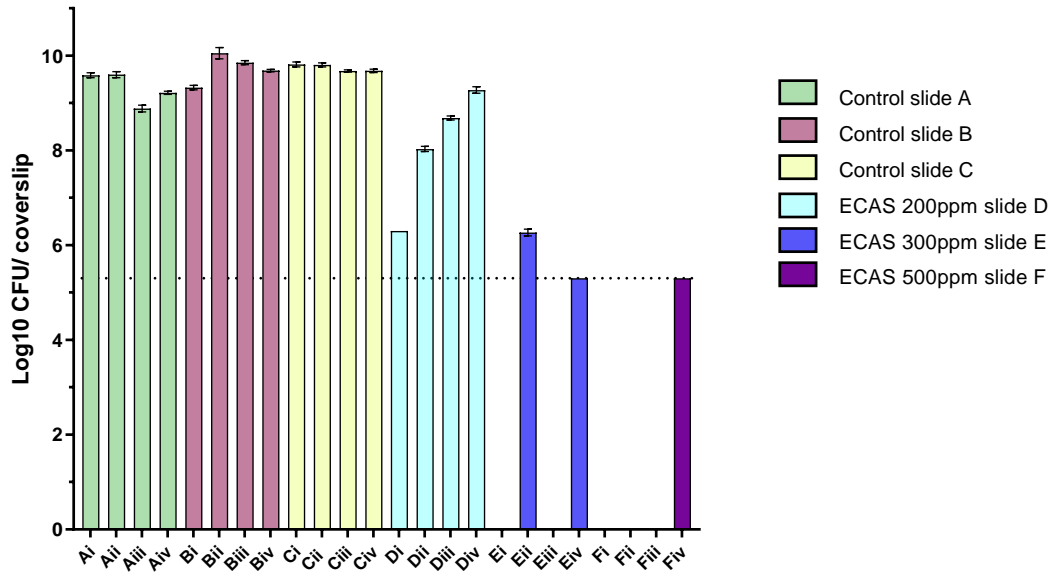
In ECAS-treated channels, there was also significant within-group variation, with up to 2.974 Log CFU disparity in 200ppm ECAS-treated recoveries ($p < 0.0001$), and the determination of surviving bioburden following higher concentration treatments (300ppm and 500ppm FAC) was limited by the dilution range chosen, and subsequent minimal limit of detection of 5.3 Log CFU/coverlip, which was insufficient for accurate measurement of the remaining viable microbial load in some replicates. Coverslip yields which were within enumerable range did indicate a possible dose-dependent effect (Figures 4.7a and 4.7b), but low replicate numbers prevented meaningful statistical interpretation. The recovered loads ($D_i - D_{iv}$) (Figure 4.7a) obtained from biofilms subjected to 200ppm treatments interestingly suggested a weakening of the antimicrobial effect down the length of the slide, with recoveries ranging from 6.301 Log (uppermost, i.e. proximal to SWF inflow port) to 9.275 Log (lowermost, i.e. proximal to waste drainage port) CFU/coverlip ($p < 0.0001$). This 'gradient' effect would support the proposed neutralising and or/ diluting effects of the components of both the biofilm EPS matrix, collagen hydrogel, and any remaining traces of

SWF as the ECAS solution drip-flows from top to bottom, resulting in a progressively diminished antimicrobial potency as the irrigated treatment flows down the collagen/biofilm matrix.

When collated data were viewed (Figure 4.7b), it was seen that mean recovery was significantly reduced in the 200ppm ($p<0.05$), 300ppm ($p<0.001$), and 500ppm ($p<0.01$) ECAS groups, as compared to control channels, with the largest reduction seen with 500ppm ECAS treatment, demonstrating a >4 Log CFU reduction. Comparing the different ECAS treatments, a significant further reduction was seen with the increase in concentration from 200ppm to 500ppm FAC, showing a 2.29 Log CFU difference ($p<0.01$), however there was no significance difference between 300ppm and 500ppm treated groups (0.48 Log CFU, $p<0.05$).

The preliminary findings of this testing regime appeared to indicate an inhibitory effect of ECAS on *P. aeruginosa* biofilms, and suggested a possible correlation between efficacy and hypochlorous acid (HOCl) concentration (reflected in the FAC level), although several procedural factors confounded interpretation of these results. Upon recovery of the treated biofilms, some evidence of degradation of the collagen matrix integrity was visible in channels irrigated with ECAS, which may have been attributable to biochemical interactions with the oxidant species present, but also potentially to the increased shear force imposed on biofilms by increasing the pump rate for the purposes of purging the channel tubing before and after treatments. This was a necessary step to ensure treatments passed throughout the full length of tubing and successfully reached the biofilm surface within the allotted time-period, however it may also have disturbed the structural integrity of the biofilms and collagen matrix with which they were associated, since the mechanical strength of collagen hydrogels is acknowledged to be weak, without the introduction of covalent cross-linking modifications (Sarrigiannidis *et al.*, 2021). Therefore, further optimisation of the instillation mode of delivery of aqueous treatments, and of the compatibility of differing strengths of ECAS with the DFR collagen hydrogel matrices when applied by this route, would be essential in further developing this methodology.

a) ***P. aeruginosa* biofilm recovery: 3 x ECAS instillation treatment**



b)

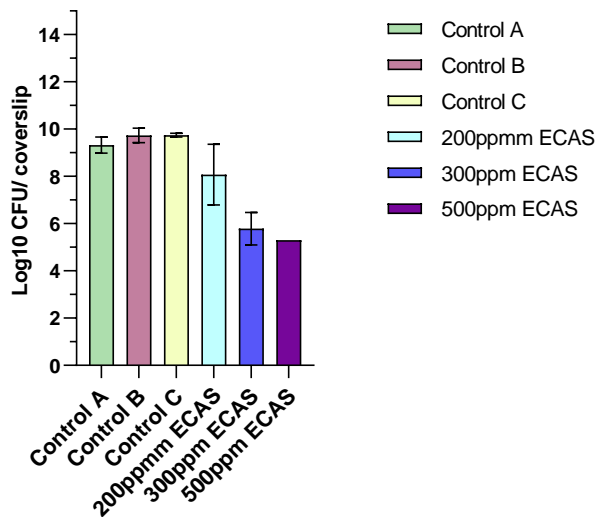


Figure 4.7: Viable load recovered from *P. aeruginosa* NCIMB 10548 biofilms adherent to 13mm diameter coverslips, cultured for 48h within the DFR-collagen matrix model, subjected to three repeat ECAS treatments via continuous instillation, with intervening re-feed periods of 1hr; n=4 per treatment group, sampled in triplicate. a) Recovered load per coverslip, shown; i-iv denote the descending order down the length of the slide; b) Mean recovered load per treatment group, shown. Comparisons by ordinary one-way ANOVA, with thresholds for significance: * p>0.05, ** p<0.01, ***p<0.001, **** p<0.0001. Significant differences stated within the text.

4.5.6 Investigation of the effects of single versus repeated exposures to antimicrobial irrigation of collagen matrix-associated *P. aeruginosa* biofilms:

In attempt to elucidate the comparative efficacy of applying successive ECAS treatments, by instillation onto biofilms within the DFR, and the extent to which re-introduction of SWF between treatments could counteract these effects, a modified procedure was employed. Continuous infusion treatments were performed for 30-minute periods, using a single concentration of ECAS

(300ppm), and comparing biofilm viability after one, two or three applications, with intervening SWF re-feed/ neutralisation periods of 1 hour. As before, time-matched PBS-controls were used to assess the potential for loss of biofilm through physical disturbance resulting from increased shear force at elevated drip-flow rates, as opposed to biochemical disruption by the reactive species present within ECAS. The re-introduction of SWF between treatments was intended to simulate the continued exudation of wound fluid onto the wound-bed, following antimicrobial irrigation, and to determine the capacity for the treated biofilm to recover from the preceding treatment. Repeat irrigation with ECAS was designed to show any 'dose-dependent' enhancement of antimicrobial effect achieved by periodic short-duration ECAS instillation, in comparison a single treatment, when combined with intervals of SWF 'exudation'.

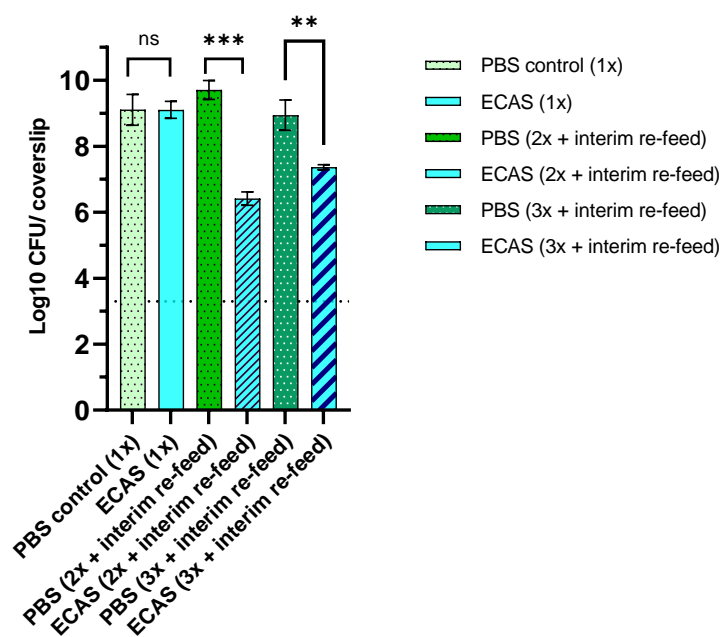


Figure 11: Viable load recovered from coverslip-adherent *P. aeruginosa* biofilms grown to 48h within the DFR-collagen matrix model, subjected to up to three repeat ECAS treatments via continuous instillation, with intervening re-feed periods of 1hr. Treatments were performed in quadruplicate, n=1. Significant differences were determined by two-tailed unpaired t-test (treatment versus control), and one-way ANOVA with multiple comparisons (single versus repeat treatment, within-group). Significance thresholds were determined as: *p<0.05, ** p<0.01, ***p<0.001, ****p<0.0001.

Following a single ECAS treatment (without SWF re-feed) a mean recovered load of 9.106 Log₁₀ CFU was seen, which was comparable to that seen in the matched PBS-control (9.103 Log₁₀ CFU, p>0.05) (Figure 4.8). After two treatments, with interim SWF re-feeding, a treatment effect appeared to emerge, with a 3.292 Log disparity seen between ECAS-treated biofilms (6.414 Log₁₀ CFU) and the PBS-matched control (9.706 Log₁₀ CFU) (p=0.0001). Biofilms exposed to three ECAS treatments, with intervening SWF re-feed periods, also appeared significantly reduced in comparison to their PBS-treated counterparts, but the treatment effect was smaller, with only a 1.577 Log₁₀ difference observed between ECAS-treated (7.367 Log₁₀ CFU) and PBS-treated biofilms (8.944 Log₁₀ CFU) (p<0.01).

Comparison of single versus repeated irrigation within treatment or control group was made, to determine the effects of successive instillations on biofilm viable load. No significant difference was discerned between PBS-controls treated for one, two or three 30-minute periods ($p < 0.05$) (Figure 4.8). Within the ECAS-treated group, however, a significant 2.689 Log_{10} difference was seen between once- and twice-treated biofilms ($p < 0.0001$). Paradoxically, biofilms subjected to three ECAS treatments exhibited a slight increase in viable load, as compared to those treated twice (7.367 Log_{10} versus 6.414 Log_{10} , respectively, $p < 0.01$), however thrice-treated biofilms were significantly reduced in comparison to those treated only once (1.736 Log reduction, $p < 0.0001$). Therefore it appeared that, overall, repeated ECAS treatments to some extent exerted a cumulative effect on biofilm viability, and that this was unlikely to be solely attributable to the increased shear stress incurred with elevated drip-flow rates during irrigated treatments.

4.5.6.1 Consideration of technical approach in repeated irrigation treatments in the DFR model

It was noted, once again, that there was considerable variance ($\leq 0.77 \text{Log}_{10}$ disparity) in the viable loads recovered from replicate coverslips originating from a single slide, which may be attributable to numerous factors. Heterogeneity in biofilm density down the length of the slide may have accounted for some of this variability, but it could also reflect a diminished antimicrobial effect of treatment as the ECAS solution passes down the biofilm, increasingly undergoing inactivation or dilution by encountering components of the biofilm matrix and residual SWF present on the slide surface, as previously postulated. Modification of the pump rate to increase the drip-flow introduction of treatments to biofilms *in situ* would likely need to be optimised, as would the number of repeat instalments of irrigated treatment, to better determine any effect of physical perturbation / shearing effect of elevated flow on the biofilm integrity, a limitation highlighted by Esin *et al* (2022).

In addition, the compatibility of applying ECAS, particularly at greater FAC strengths, to the collagen matrix must be verified, as deleterious interactions between the hypochlorous acid and hypochlorite species could potentially result in degradative effects upon the biofilm-supporting matrix, adding to the complexity of evaluating the microbicidal effect of ECAS on *P. aeruginosa* biofilms. During recovery of coverslip-associated biofilms from ECAS-treated channels, some loss of collagen hydrogel integrity was observed, however further investigation is required to ascertain the significance of this effect, and to determine whether it could be attributed higher concentrations of ECAS reactive species perturbing the polymerised collagen matrix.

4.6: Discussion:

The studies here performed on laboratory biofilm models demonstrated that, although capable of exerting small but significant inhibitory effects, the antimicrobial activity of direct NTP treatment on *in vitro* biofilms was of limited efficacy, and was markedly inferior in comparison to that of more established surface antiseptics treatments, such as PVP-I and hydrogen peroxide, when applied towards the upper end of their therapeutic range. The antimicrobial effects observed in treatments performed on surface-associated biofilms were emphatically reduced in comparison to those seen against planktonic targets of the same species (Chapter 3), underlining the greatly enhanced tolerance of biofilm-dwelling organisms to chemical and physical attack.

Using CBR single-species biofilms as the treatment target, modest reductions in *P. aeruginosa* viability were achieved using an NTP exposure time of 120s, however this was a comparatively prolonged duration, in return for a ≤ 1 Log reduction in viable load, when considered against the significantly greater effect observed with 10% povidone-iodine within only a quarter of the exposure time. Considering the very small diffusion distances typical of many of the plasma-generated species, and the transience/ instability of some of the more reactive constituents, it is likely that variability in the NTP profile contributed to the inconsistencies seen in microbial recoveries following treatment (Chen *et al.*, 2014; Szili *et al.*, 2018; Jabbariesgandani and Walsh, 2023).

Similarly, indirect NTP treatment using PAW as a vehicle for the delivery of PAW-generated reactive species proved significantly less efficacious than alternative aqueous antimicrobial solutions, H₂O₂ and ECAS, when applied for a fixed 300s contact time, although the latency between PAW generation, using large-batch SDB-plasma activation, and its application to biofilms was likely to have altered the physicochemical properties of the test solution, given the highly reactive nature of many of the key species produced in plasma-activated liquids (Lukes, Brisset and Locke, 2012; Lukes *et al.*, 2014; Liu *et al.*, 2018; Tsoukou, Bourke and Boehm, 2020; Sklias, Sousa and Girard, 2021).

Data obtained from testing performed on CBR biofilms, although providing a valuable comparison of antimicrobial activity amongst the candidate treatments, gives only an elementary indication of their likely efficacy when applied to biofilms existing in more complex environments, *in vivo*. The CBR model advantageously enables rapid generation of replicable biofilms under user-controlled growth conditions, and subsequently allows investigation of the effects of various parameters on biofilm growth, such as stir rate (shear force), temperature, nutrient composition of the input medium, and surface material. However, the relative simplicity of the system in comparison to the sites colonised by biofilms occurring in clinical settings must be recognised. Single species biofilms grown on a 2-dimensional surface, and treated in the absence of any interfering organic matter,

will provide much less formidable challenge to decontamination or disinfection practices than biofilms forming on medical instrumentation or equipment, in poorly-accessible niches, or in the microenvironment of a chronic wound or clinical infection.

The DFR-collagen matrix model in several respects offers a more informative means of assessing antimicrobial strategies in the context of clinically infected wounds, due to the incorporation of features more closely recreating the physiological environment of the wound-bed, in its design. The mature three-dimensional collagen-embedded biofilms grown using this model attained a higher density than those cultured upon the abiotic surfaces of CBR coupons, attributable in part to the larger surface area presented (1976mm³ per slide, compared to 1062mm² per bilateral CBR coupon surface), but also owing to the growth conditions which allow for the development of a more complex biofilm structure and topography through interactions with the underlying porous matrix, composed of a representative component of connective tissue, type I collagen (Slade *et al.*, 2019). The continuous drip-flow infusion of SWF supplied to collagen matrix biofilms in this *in vitro* model also serves to increase the degree of physiological authenticity, introducing only low-shear force, in contrast to the input medium used with the CBR model, which is introduced at higher flow-rate, stirred to create moderate-to-high shear force, and is comparatively low in nutrient concentration and complexity, therefore failing to accurately mimic several key aspects of the exuding wound. In view of these differences in operating parameters and fundamental design, each of the two biofilm models employed here may respectively provide an informative insight into the treatment response in biofilms forming on abiotic surfaces (using the CBR system) or in chronic wounds (the DFR-collagen matrix model).

Despite showing only low to moderate efficacy in testing within these two laboratory models, it is likely that the antimicrobial effects of direct NTP, and aqueous antiseptic treatments when applied *in vivo*, and against complex multi-species biofilms, would be significantly reduced in comparison, due the involvement of a myriad of additional, uncontrolled, host- and pathogen-related factors (Kirketerp-Møller *et al.*, 2008; Bjarnsholt, 2013; Malone *et al.*, 2017). Evidence of inter-species differences in susceptibility to plasma treatment of biofilms has been reported in *in vitro* studies performed elsewhere, which, along with interference introduced by the presence of inactivated cellular material, providing a protective 'shielding' effect, may lead to reduced efficiency of treatment when applied to target biofilms (Czapka, Maliszewska and Olesiak-Bańska, 2018). Incomplete removal of biofilm due to such factors *in vivo* could lead to the reformation and potentially dissemination of microbial biofilm, via persister cells which demonstrate the highest resistance to antimicrobial challenge, remaining viable in the face of severe biochemical and/or mechanical stress (Lebeaux, Ghigo and Beloin, 2014; Olsen, 2015; Flemming *et al.*, 2016; Omar *et al.*, 2017). Furthermore, in treating pathogenic biofilms via methods incorporating a degree of physical or chemical debridement, perturbation, or dissociation of any portion of the microbial

134

biomass, such as may occur with the application of antimicrobial treatments, some risk of dissemination of viable detached bioburden and re-seeding would need to be appropriately addressed, e.g. by concomitant antibiotic therapy (Fleming, D, Rumbaugh, 2018). Therefore, in order to achieve optimal anti-biofilm outcomes in therapeutic/ clinical interventions, it would likely be necessary to combine treatment modalities, including both pharmacological and physical approaches, and to devise optimised dosing regimens so as to reduce biofilm viability as far as possible and thereby maximise the efficacy of topically and systemically applied agents.

4.6.1: Key conclusions:

Investigations undertaken on single species biofilms, cultured using two laboratory models, the CBR and DFR-collagen matrix wound model, demonstrated the challenges encountered in attempting to reduce microbial colonisation of biofilm-contaminated surfaces and substrates, due to the elevated recalcitrance to treatments exhibited by biofilm communities, reflecting their more advanced structure and complex phenotypic profiles. In contrast to the significant inhibitory effects observed with antimicrobial treatments, including NTP, in planktonic microbial targets, modest reductions were seen only in response to povidone iodine, ECAS, and hydrogen peroxide, when applied via 'washing' or immersion of the surface-associated biofilms.

In treatments performed on CBR biofilms grown on steel or silicone coupons, PVP-I proved the most efficacious, achieving Log reductions of approximately 2 Log, or greater, against both *P. aeruginosa* and *S. aureus* within just 30s on either surface material, whilst NTP produced a maximal reduction of 1.39 Log, and 0.47 Log in each species, respectively, on steel. ECAS treatments (300s duration, 200ppm FAC) were slightly inferior in efficacy compared to those of PVP-I on *P. aeruginosa* CBR biofilms, but similar to H₂O₂ treatments, both appearing a little more effective on steel than silicone. Treatments using large batch SBD-PAW, as in planktonic efficacy testing, failed to induce significant microbial inactivation of *P. aeruginosa* when applied to CBR biofilms, on either silicone or steel.

Thus, it was seen that complete eradication of biofilms, even those cultured within a relatively simple *in vitro* model such as the CBR, and on non-porous substrate materials, was far from achievable using the treatment options and conditions explored here. In terms of quantitative effect, PVP-I was the most successful antimicrobial when used as a one-step treatment against these single species biofilms.

The DFR-collagen matrix model served to more closely simulate conditions present in a wound bed, enabling *P. aeruginosa* biofilm growth throughout a semi-solid, porous matrix, fed with medium containing several of the constituents present in physiological wound exudate. The

increased density and structural complexity of biofilms grown in this three-dimensional matrix model, as previously reported by Slade *et al.* (2019), provides a more appropriate *in vitro* system for the investigation of biofilm development, metabolism and susceptibility to treatments. Preliminary results obtained here from testing with single-application immersion treatments indicated that biofilms cultured within the collagen matrix model were more tolerant of antimicrobial challenge than their planktonic counterparts, or mono-species biofilms cultured on non-porous surfaces. A once-only treatment with ECAS or H₂O₂ achieved only a marginal effect on viability, with <1.0 Log reduction seen with ECAS (200ppm FAC), and approximately 1.2 Log reduction with hydrogen peroxide, suggesting that longer exposure times, or higher concentrations of these products may have been required to induce more marked results, although the dataset obtained here was small, confounding the interpretability of these findings.

Adopting an alternative mode of treatment delivery, using fixed-interval instillation of biofilms *in situ* within the DFR-collagen matrix wound model, attempts were made to investigate the efficacy of ECAS 'irrigation' of *P. aeruginosa* biofilms. One approach utilised a 'treat, feed, repeat' regimen, in which biofilms were subjected to treatment via drip-flow instillation of 220ppm, 300ppm or 500ppm ECAS, followed by re-feeding with SWF, then repeating the steps twice more, to determine the effects of re-introducing organic contamination between successive treatments, and whether biofilm viability was more markedly impacted at higher ECAS concentrations. Although greater FAC concentrations appeared to be associated with reduced viability in the recovered biofilm, suggesting a dose-dependent effect of repeated ECAS instillation treatments despite the intervening 're-feed' periods, it was not possible to draw firm conclusions due to low replicate numbers and the reduction of viable load to levels below the minimum level of detection. The higher flow rate at which ECAS (and PBS control) treatments were delivered, combined with the elevated chlorine-releasing potential and oxidising effects of stronger ECAS solutions, may have compromised the underlying collagen matrix integrity, in addition to exerting microbicidal effects on the attached biofilm purely via biochemical damage on the cellular/ EPS components. Therefore, the reductions seen in recoverable bioburden following repeated treatments cannot be attributed solely to interactions between ECAS and *Pseudomonas* biofilms, without further investigation of the effects of stronger ECAS solutions on the polymerised collagen matrix, in the absence of biofilm growth.

The second approach used to study the efficacy of ECAS instillation treatments on the wound-model biofilm was intended to demonstrate whether re-introduction of SWF to the biofilm after each ECAS 'irrigation' period had a mitigating effect on the overall microbicidal activity exerted. An intermediate ECAS concentration (300ppm) was used to treat 48h mature biofilms in ≤ 3 instillation periods of 30 minutes each, with an hour of re-feeding with SWF, increasing flow-rate during treatment periods, as before. Although a significant reduction in biofilm density was seen

in samples subjected to repeat instillations in comparison to PBS controls, the paucity of results obtained using this treatment protocol precludes robust statistical interpretation and formation of conclusions.

Further investigation using these techniques, and adaptation and optimisation of the DFR-collagen wound biofilm model would be imperative to provide more robust evidence elucidating the efficacy of antimicrobial instillation treatment of biofilms with intermittent re-introduction of simulated wound exudate. As previously mentioned, the development of specialised *in vitro* experimental models which accurately replicate aspects of the wound (micro)environment would potentially enhance the clinical translational value of research outputs gained from such testing platforms, due to their greater physiological authenticity, thereby biofilm phenotypes more representative of those occurring in chronic wound infections. The initial findings described here would therefore benefit from refinement to further develop the compatibility of the antimicrobial instillation strategy in this model, but also could be expanded upon by performing metabolic analyses, and imaging techniques such as SEM and CSLM, to enable more detailed assessment of biofilm viability, architecture, and integrity prior to, and following, treatments. The investigation of other wound-associated microbial pathogens, and progression of the model to incorporate mixed species biofilms, would also present fertile grounds for further research, reflecting the polymicrobial nature of chronic wound infections (Han *et al.*, 2011; Woods *et al.*, 2012; Chen *et al.*, 2021; Thaarup, *et al.*, 2022).

Chapter 5: Investigation of the eukaryotic response to NTP

The safety profile of antimicrobial agents intended for use in wound cleansing and antiseptics, and for decontamination of invasive/ implanted materials and devices, must be demonstrated via *in vitro* toxicity testing, before progressing to *in vivo* use in the clinic. It is imperative that any therapeutic cleansing or microbicidal product coming into contact with the skin, or any mucosal or epithelial surface, shows minimal cytotoxic effects. In products designed for applications in wound management, there should be no interference with the healing process, since any disruption in tissue repair risks prolonging chronicity, increasing morbidity and potentially mortality.

5.1 Selection of alternative antimicrobial products for comparison of cytotoxic effect

Povidone-iodine, or polyvinylpyrrolidone iodine (PVP-I), and hydrogen peroxide (H₂O₂) were selected as comparative antiseptic treatments in the investigation of NTP cytotoxicity, as they represent two agents which have traditionally been used in the cleansing and disinfection of skin, and superficial wounds.

5.1.1 Povidone-iodine:

PVP-I is a compound included in many antiseptic products used clinically, owing to its broad-spectrum, rapidly-acting antimicrobial efficacy (Woo, 2014; Eggers, 2019; Tan and Johari, 2021). This microbicidal activity has been attributed to a number of mechanisms, including strong oxidising interactions with certain functional groups of amino acids (thiol and amino groups) and fatty acids (carbon-carbon double bonds), resulting in structural damage and functional impairment of cellular components, inhibiting growth and viability, but the precise processes have yet to be fully elucidated (Lepelletier *et al.*, 2020; Maillard and Pascoe, 2024)

Similarly, the reported effects of PVP-I when applied to eukaryotic cells, and to *in vivo* mammalian models, are wide-ranging, with a lack of consensus regarding the impacts on wound-healing, cellular viability and membrane integrity. Povidone-iodine has been demonstrated *in vitro* to induce apoptotic or necrotic cell death, accompanied by a reduction in mitochondrial membrane potential, loss of cellular metabolic activity, impaired membrane integrity, and the elevated production of reactive oxygen intermediates, in both human- and rodent-derived cell lines (Kataoka *et al.*, 2006; Sun *et al.*, 2012; Sato *et al.*, 2014; Van Meurs *et al.*, 2014; Liu *et al.*, 2017; Steins *et al.*, 2023). Impaired cell proliferation and migratory activity has also been shown, in human and bovine epithelial cell models, and in human adipose-derived stem-cell – fibroblast 2D and 3D cultures, (Liu *et al.*, 2017; Ortega-Llamas *et al.*, 2022; Thongrueang *et al.*, 2022; Chelms-Burlacu, A, Tang, E, Pieptu, 2023), accompanied by upregulation of inflammatory cytokine expression in the latter, at concentrations approximately 100-fold lower than those used clinically. However, biocompatibility testing performed *in vitro* elsewhere has demonstrated PVP-I to be well-tolerated, showing absence

of an significant cytotoxicity in a murine fibroblast model, although the corresponding microbicidal effect was impeded by the presence of FBS in the treatment medium (Müller and Kramer, 2008).

Studies investigating the effects of PVP-I on wounds in animal models *in vivo* have revealed both enhanced healing, via promotion of re-epithelialisation and neovascularization, with concomitant upregulation of α -smooth muscle actin (SMA) and Transforming Growth Factor- β (TGF- β), noted in a rat acute wound model followed repeated PVP-I treatments (Wang *et al.*, 2017), and increased angiogenesis and fibroblast proliferation in a porcine partial-thickness dermal wound model, using 10% PVP-I impregnated wound dressings (Bennett *et al.*, 2001). The clinical evidence for PVP-I supports its use in therapeutic antisepsis principally on the basis of decreasing microbial bioburden, with some research citing additional benefits including improved rates of healing, and reductions in protease activity and localised inflammation (Fumal *et al.*, 2002; Eming *et al.*, 2006; Woo, 2014; Bigliardi *et al.*, 2017). Such findings therefore indicate limitations in the translatability of results obtained from *in vitro* models, with differences in treatment regimens, cell types, and growth conditions likely contributing to the lack of concordance observed, and poor correlation with the *in vivo* environment (Bigliardi *et al.*, 2017; Liu *et al.*, 2017).

5.1.2 Hydrogen peroxide:

Hydrogen peroxide (H₂O₂) is classed together with ozone and peracetic acid as a peroxygen, exerting its broad-spectrum antimicrobial effects via the potent oxidant activity of hydroxyl free radicals (OH[•]), which are released upon contact with the target organism, damaging lipids, proteins and nucleic acids, and perturbing ribosomal function (Mcdonnell and Russell, 1999; Linley *et al.*, 2012; Maillard and Pascoe, 2024). Hydrogen peroxide has been used at higher concentrations in the sterilisation and disinfection of surfaces and medical instrumentation, but at lower concentrations, typically 3% - 6% (v/v) it is commonly applied for topical disinfection of superficial wounds, and for antisepsis in surgical sites, in spinal operations and prosthetic joint surgery (Linley *et al.*, 2012; Romano *et al.*, 2022).

5.2 Cell line selection for *in vitro* cytotoxicity assay of antimicrobial treatments:

Two immortalised human cell lines were subjected to both direct and indirect NTP treatments in order to determine tolerance to, and any growth-promoting or inhibitory effects. The cell lines selected were of epithelial origin, H103 being derived from a malignant melanoma (ECACC 06092001), and A375 from an oral squamous cell carcinoma (ECACC 88113005), cultured under identical conditions (see Methods and Materials, Chapter 2). These epithelial cell lines were selected as an appropriate *in vitro* model for the investigation of tolerability and/ or cytotoxicity of treatments intended to be applied topically, such as to the surface of ulcerated tissue, or biofilm-infected wound involving the superficial epithelial layers.

5.2.1 Determination of cell growth rate under control conditions

The growth rate of each line was characterised by performing a 96h growth curve, measuring the increase in cell density with time, using Trypan Blue Dye Exclusion (TBDE) assay to quantify viable cells at sequential time-points. Briefly, H103 dermal cells or A375 fibroblasts were seeded in 24-well plates at an initial density of 2×10^4 /mL or 3.8×10^4 /mL respectively, in F12/HAMS DMEM supplemented with 10% FBS, 2mM L-Glutamine, and 0.5 μ g/mL sodium hydrocortisone succinate, which served as the standard growth medium for all mammalian cell culture experiments. Cells were incubated (at 37°C, humidified, and with 5% CO₂) over 96 hours, sampling wells at 12-hour intervals to determine the mean population doubling time (PDT) (Figure 5.1). Using simple linear regression of Log₂ cell number versus growth time, the PDTs were derived as 34.72 hours for H103, and 21.38 hours for A375.

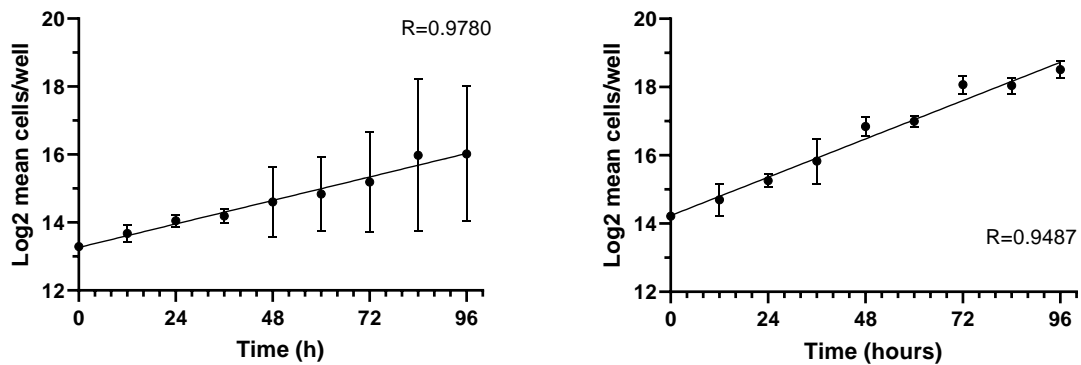


Figure 5.1: 96h growth curves of H103 (left panel) and A375 (right panel) epithelial cell lines, assessed by TBDE, to determine PD rate. Cells were cultured in triplicate wells to determine mean cell count per time-point \pm SD; n=3. Simple linear regression performed on GraphPad Prism.

5.3 Assessment of cytotoxic response to known antimicrobial compounds

5.3.1 Selection and optimisation of viability assay for accurate evaluation of treatment toxicity:

To provide a comparison to the eukaryotic response to NTP treatment, and to determine the reliability and repeatability of assay methodology, time-dose response studies were performed using the selected antimicrobial agents applied in surface disinfection testing, subjecting human epithelial cell lines to hydrogen peroxide (H₂O₂), ECAS, and PVP-I treatments. Preliminary testing was performed on H103 cells, treated with the antimicrobial agents H₂O₂ or ECAS, selecting doses found to elicit significant inhibitory effects against planktonic microbial challenge (Chapter 3, Investigation of the antimicrobial effects of non-thermal technologies on prokaryotes). However, the results obtained in the testing of NTP upon mammalian cell lines, under the experimental conditions used initially, suggested that modification of the testing parameters and assay method were necessary.

5.3.2 Preliminary studies of antiseptic treatment in short-term exposures

5.3.2.1 Assessment of ECAS treatment of H103 by TBDE

Initial treatments with 0.05 – 50 % (v/v) ECAS (200ppm FAC) were performed over a period of 24h or 48h, using Trypan Blue Dye Exclusion (TBDE) cell counting to quantify residual viable cell population, and to ascertain the validity and practicality of this method. Cells were seeded in 24-well microtitre plates and grown to approximately 70% confluence over 72h, and treated with up to 50% ECAS as described in Section 2.11.1, and total viable and non-viable counts obtained by TBDE. The percentage viability was calculated relative to the untreated control, which received DMEM:PBS (1:1) only, (PBS being the diluent in which ECAS treatments were prepared). Results yielded using this approach demonstrated substantial variability within replicate treatment groups, although concentration- and time-dependent cytotoxic effects were inferred (Figure 5.2).

Treatments applied for 24h demonstrated a negative effect on viability at ECAS concentrations >0.05% (Figure 5.2, left panel), with an approximate 22% loss of viability seen at 0.25% ECAS ($p>0.05$), and a near-continuous decline with progressively greater doses, reaching a residual viability of 20.6% with 25% ECAS ($p=0.01$), and almost complete lethality at 50% (0.104% residual viability, $p=0.002$). Results at the 2.5% dose appeared anomalous, with mean percentage viability of 92.55%, exceeding that observed at the preceding lower doses. This may have occurred through procedural errors, including inequal seeding and cell number prior to treatment, incomplete dissociation, recovery and enumeration of cells post-treatment, or inter-replicate delay in processing consecutive wells, although this anomaly may reflect genuine inconsistencies in cytotoxic effect within the lower concentration range.

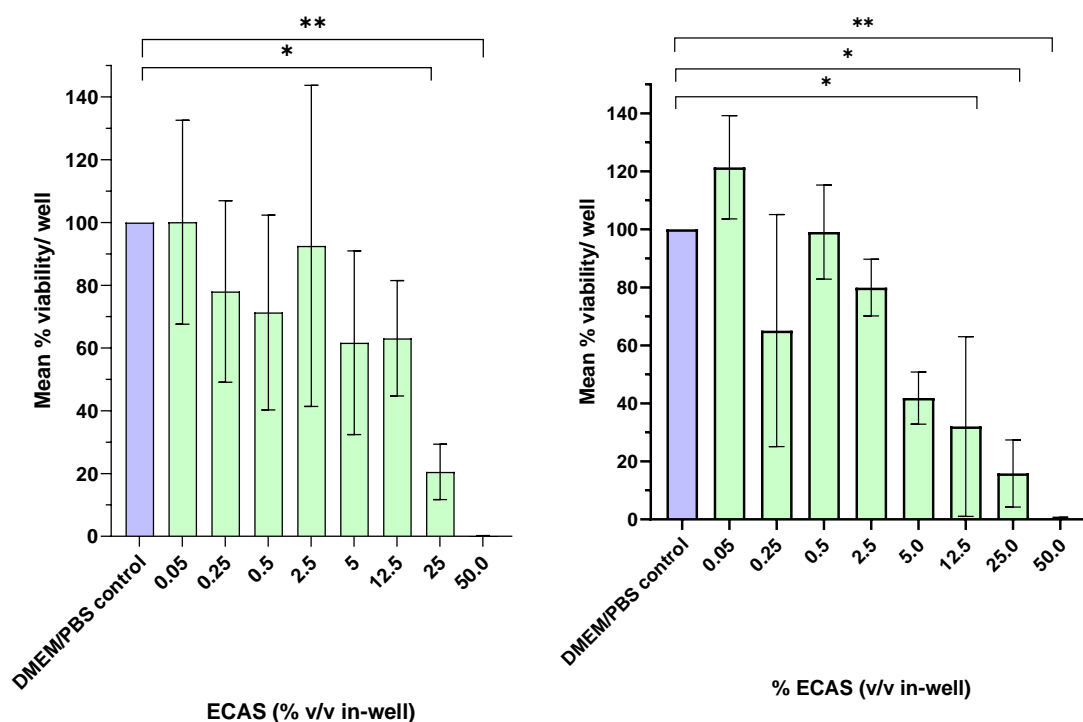


Figure 5.2: ECAS (200ppm) dose-response in H103 cells, over treatment periods of 24h (left) (n=3) and 48h (right) (n=2), determined by viable cell count using TBDE. Treatments were applied to 70% confluent cultures, 1:1 with complete culture medium in 24-well plates, to give the final 'in-well' concentrations shown. Viability was determined by dissociation and resuspension of cells for TBDE enumeration, expressing viability at % of untreated control viability (values represent mean \pm SD).

Despite the observed high degree of inter-replicate variance within the dataset, Log transformation was performed to obtain a non-linear regression curve (Log[% ECAS] versus % viability - variable slope (four parameters), least squares fit) using GraphPad Prism software, in attempt to calculate approximate EC_{50} of ECAS in the H103 cell line, for a 24h treatment period (Figure 5.3, left panel). The coefficient of determination reflected the large variation seen in cell viability in response to each ECAS dose ($r^2=0.5792$), and the IC_{50} given was 23.14%, equating to a FAC concentration of approximately 46.28ppm.

The assay was subsequently repeated, sampling after 48h contact time, to discern the comparative cytotoxicity of more prolonged ECAS treatments on the same cell line. Treatments over this extended contact time also indicated the absence of cytotoxicity at the lower range of ECAS concentrations tested, although there was again broad variance within treatment groups (Figure 5.2, right panel). Cell viability remained $\geq 65\%$ at concentrations of up to 2.5% ($p>0.05$), and appeared slightly enhanced with 0.05% ECAS treatment (the lowest tested dose) relative to PBS-controls ($p>0.05$). A more marked decline in viability from 79.9% to 41.8% was noted as treatment concentration increased from 2.5% to 5% ($p>0.05$), and the cytotoxic effect appeared to increase with further elevation of dose to the maximum applied concentration (50%) which, in agreement with 24h treatments, induced near-complete lethality, with $<1\%$ viable cells recovered ($p=0.004$).

Transformation of data to obtain the non-linear regression (variable slope (four parameters), least squares fit) was again applied, in attempt to obtain the IC₅₀ of 48h ECAS treatments (Figure 5.3, right). As for the 24h dose-response, the poor fit of the regression curve was indicative of the high variability in cell survival within each treatment group ($r^2= 0.782$), and the results were deemed unstable, making calculation of the IC₅₀ from this dataset unreliable.

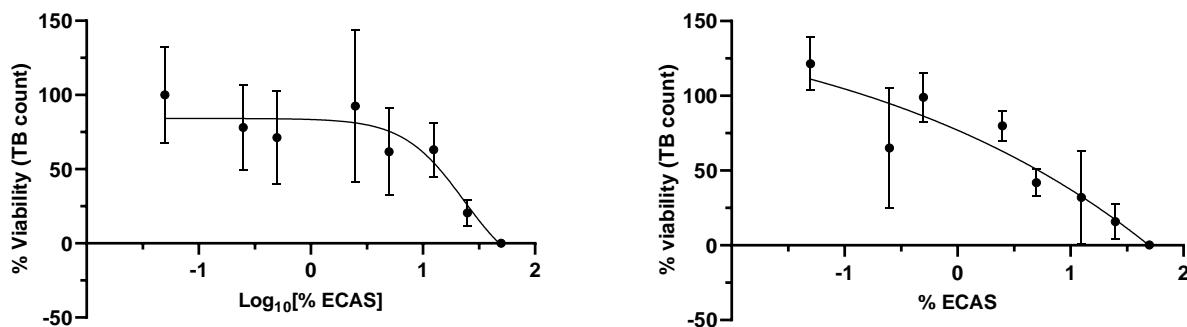


Figure 5.3: Non-linear regression of Log[inhibitor] versus response (variable slope, four parameters), obtained following 24h (left) and 48h (right) treatment of H103 with ECAS (200ppm), determining residual viability via TBDE count, results plotted using GraphPad Prism. Treatments were performed in triplicate; $n=3$ for 24h treatments, $n=2$ for 48h treatments.

5.3.2.2 Appraisal of cytotoxicity assessment methods

The disadvantages of TBDE quantitation of cells in the evaluation of cell viability or cytotoxic effects have been highlighted in the literature, with drawbacks such as time inefficiency, susceptibility to user-error and ambiguity of staining intensity when differentiating live and dead cells, and potential skewing of counts through errors in dilution and pipetting, amongst others (Riss, TL, Moravec, RA, Niles AL, Duellman, S, Benink H, Worzell, TJ, Minor, 2013; Piccinini *et al.*, 2017). This technique does not detect the specific cell injury processes leading ultimately to cell death, e.g. markers of genotoxicity or apoptosis, and it also is unable to detect fully lysed cells. In view of these factors, the dose ranges of treatments to be applied were reconsidered, and alternative methods of viability assessment to manual counting/ TBDE were pursued.

Determination of cytotoxicity was thereafter performed on each of the two cell lines, H103 and A375, via MTS-PMS and CellTiter Glo 2.0 assays, which are comparatively more streamlined methods, since they can be performed simultaneously for all replicate wells. In these assays, the quantification of viability is dependent on assay chemistry (based on the generation of a colorimetric or luminescent signal, respectively) rather than manual counting, and are thus less subject to user-error or imprecision. The MTS-PMS and CellTiter Glo assays were therefore utilised as single endpoint assays to evaluate the effects of NTP and comparator antimicrobial treatments on viability in the two experimental cell lines.

5.3.2.3 Assessment of hydrogen peroxide treatment of H103 by CTG2.0

A short-exposure time-course performed on the H103 cell line, using 0.3 – 10% (v/v) H₂O₂, indicated that treatments within this concentration range were highly cytotoxic over the timeframe investigated (Figure 5.4), with residual cell viability of <20% detected across all time-points, using CellTiter Glo 2.0 (CTG2.0) to determine cell viability.

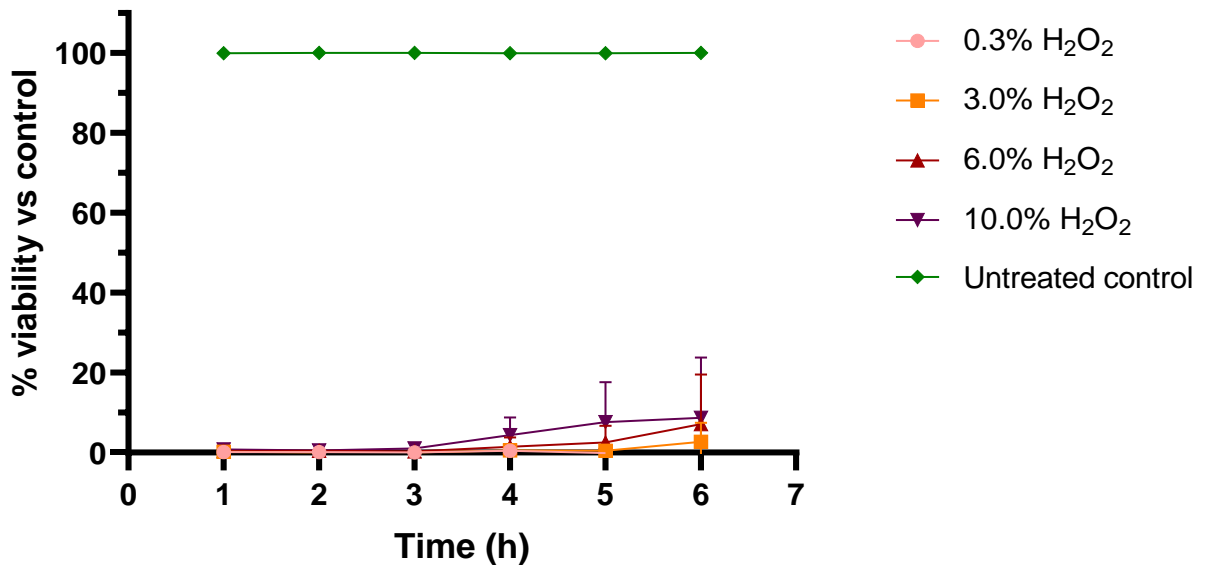


Figure 5.4: Hydrogen peroxide dose-response curve performed on H103, using Cell TiterGlo assay to evaluate viability relative to PBS-treated controls. Treatments were applied for intervals of ≤ 6 h (concentrations indicate final % H₂O₂ (v/v) when added 1:1 to culture medium), and were performed in triplicate, plotting mean % viability \pm SD; $n=3$.

5.4 Investigation of the effect of direct NTP on cellular viability

5.4.1 Comparative assessment of NTP-induced cytotoxicity via CellTiter Glo 2.0 and MTS-PMS assay

Initial studies were performed using NTP delivered directly to cell cultures, measuring cellular viability 24h post-treatment, to discern changes in viable cell number as an indicator of changes in proliferation rate, and overall population viability 24h post-exposure. Cells were seeded in standard culture medium in 24-well micro-titre plates at twice the standard seeding density and grown for 24 hours, to ensure a more uniform but sub-confluent monolayer across each well prior to treatment, to enable differences in post-treatment proliferation rate to be distinguished. In preliminary work, the culture medium was aspirated from each well immediately before treatments, leaving only a shallow film bathing the cells, however visible drying of this residual liquid was noted during treatment delivery, therefore a 200 μ L volume of PBS was subsequently used to maintain hydration in each well during NTP and argon treatments. Plasma was applied via the torch-style applicator, for 30s, 60s and 90s, with time-matched argon-only treatments performed as a control, to ascertain any effects of subjecting cell cultures to a continuous argon gas flow, since damage and loss of viability have

previously been reported, due to evaporation (Feibel *et al.*, 2023). Following treatment, the PBS was aspirated, and cells were re-fed with complete culture medium and returned to incubation for 24 hours before assaying viability, to allow for manifestation of plasma-induced effects, a time-frame selected in similar *in vitro* studies elsewhere using DBD-plasma and micro-plasma jet treatments (Biscop *et al.*, 2019; Lin *et al.*, 2019; Feibel *et al.*, 2023). Changes in cell viability were, as before, evaluated in comparison to the untreated control, to which no plasma or argon had been applied, firstly using Cell TiterGlo 2.0 luminescence assay (using cellular ATP content as a measure of viable cell population) and MTS-PMS assay (to quantify metabolically active cells) (see Methods -Sections 2.12.2 and 2.12.3).

5.4.1.1 Determination of post-treatment viability by CellTiter Glo 2.0

When treatment effect was assessed using CTG2.0, there appeared to be a trend for a decline in H103 cell viability with both NTP and argon-only treatments, in a time-dependent manner, although there was significant variance within each treatment group (Figure 5.5, left). The shortest treatment time of 30s resulted in an approximate 14% reduction in viability relative to the untreated control, in both NTP (86.7% residual viability) and argon-alone (86.6% residual viability) groups, showing no significant difference in effect ($p>0.05$) (Figure 5.5, left). When extended to 60s exposure, NTP further reduced the viable cell population to 70.6%, whilst argon treatment resulted in a slightly greater decrease, to 58.9% viability ($p>0.05$). After 90s treatments (the maximal direct exposure time tested), NTP induced a further decline to 58.3% viability, whereas argon-treated cells appeared more mildly affected, with residual viability of 69.5% versus control, however this difference was again non-significant ($p>0.05$).

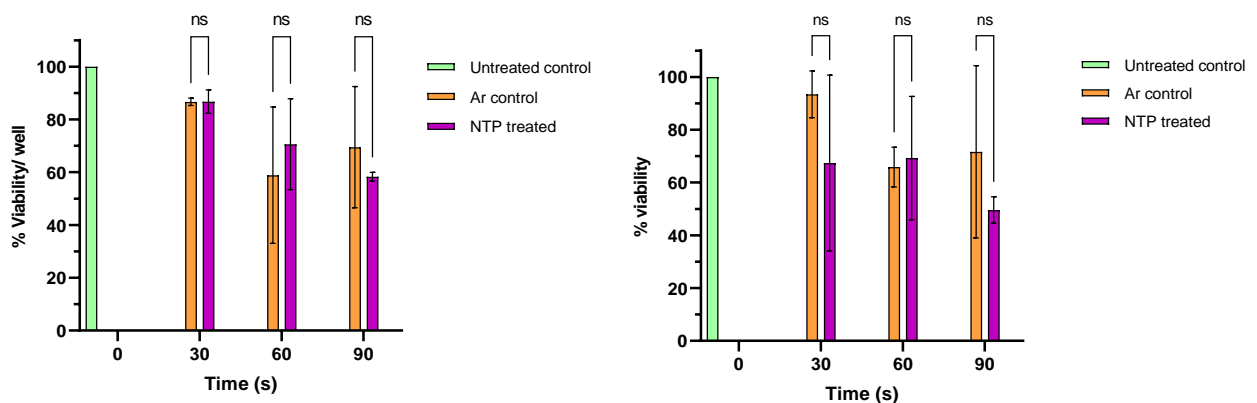


Figure 5.5. Treatment time-course of direct NTP application to H103 (left) and A375 (right) cells, assessed via CellTiter Glo 2.0 luminescent assay (left) at 24h post-treatment; treatments were performed in triplicate; $n=2$ for H103, $n=3$ for A375.

Similarly, the A375 cellular response to direct NTP treatments indicated a decline in viability with increasing exposure time, overall, when determined via CellTiter Glo (Figure 5.5, right), although wide variability was once again noted within treatment groups, and significance of plasma-induced

effects was not attained at any of the time-points tested. The minimum treatment time of 30s reduced viability levels to 67.4% that of untreated controls, whilst argon-only cells showed only minor effects, with 93.4% viability maintained. Increasing treatment duration to 60s appeared not to enhance the cytotoxic effect of NTP further, remaining 69.3% viable, however argon-treated controls at this time-point were reduced to a similar extent, with only 65.9% residual viability ($p>0.05$). Prolongation of treatment to 90s resulted in a reduction of viable population to 49.6% in the NTP group, whilst in argon-controls there was no further decrease, with viability measuring 71.6% relative to untreated controls, but no significant difference between the two groups.

These findings inferred a time-dependent attrition of the viable cell population in both H103 and A375 line, but did not demonstrate a significantly greater cytotoxic effect of NTP compared to that of argon alone, at any of the time-points tested. The need to dissociate and resuspend treated cells in 96-well micro-titre plates, prior to addition of the Cell TiterGlo reagent and subsequent measurement of luminescence, may have contributed at least in part to the broad variation seen in results obtained using this method of assessment, since an interim plate-handling step was required, thus negative impacts on cell viability, and incomplete recovery of cells from each well associated with this procedure cannot be excluded. Given the well-acknowledged sensitivity and accuracy of the CellTiter Glo assay in the determination of cell viability (Hannah *et al.*, 2001; Kleijn *et al.*, 2016; Ozlem, 2017), the observed inconsistencies in treatment effect were most likely attributable to technical inaccuracies, and/or incomplete recovery of cells during the process of detachment and transferral from 24-well to 96-well plates, although the results obtained may also indicate true variability in plasma-induced effects.

5.4.1.2 Alternative assessment of post-treatment viability by MTS-PMS

To ascertain whether an alternative viability assay could achieve a higher degree of precision and more streamlined process of quantification, the NTP time-course was repeated as before, and treated cells submitted for assessment via MTS-PMS assay. As previously mentioned, an advantage of this assay over CellTiter Glo is its compatibility with the 24-well plate format, allowing the MTS-PMS reagent to be added directly to cells *in situ*, within the same culture plate used for growth and treatment, meaning that cell dissociation and resuspension steps could be omitted. The assay serves as a proxy measure of viable cell population, since the colour change observed with the reduction of the MTS reagent in the presence of PMS is achieved by the mitochondrial enzymatic activity of living cells, generating a soluble formazan product which can be quantified colorimetrically (Riss, TL, Moravec, RA, Niles AL, Duellman, S, Benink H, Worzell, TJ, Minor, 2013; Ozlem, 2017). Results were obtained only for the H103 cell line using the MTS-PMS, but these served to confirm the suitability and reproducibility of this approach in evaluating plasma-induced cytotoxicity.

5.4.1.2.1 MTS-PMS assay calibration:

Calibration of the standardised cell suspensions against Abs₄₉₂ was performed at each assay, quantifying the formation of the coloured formazan product as a proxy measurement of metabolically-active cells (Figure 5.6), to confirm validity of the assay and consistency in the correlation between approximate cell number and product formation for each cell line. However, variation was noted between repeat assay standards, indicating that the accuracy of this method was reduced at the upper- and lower-most ranges of absorbance. Disparities in cell seeding density, and incubation time, may therefore introduce a source of error to the results obtained. Some of these factors have been highlighted elsewhere, including studies in which the MTS-PMS assay has been employed for measurement of cellular viability in the assessment of cytotoxic response (Malich, Markovic and Winder, 1997; Wang, Henning and Heber, 2010; Ozlem, 2017; Kamiloglu *et al.*, 2020).

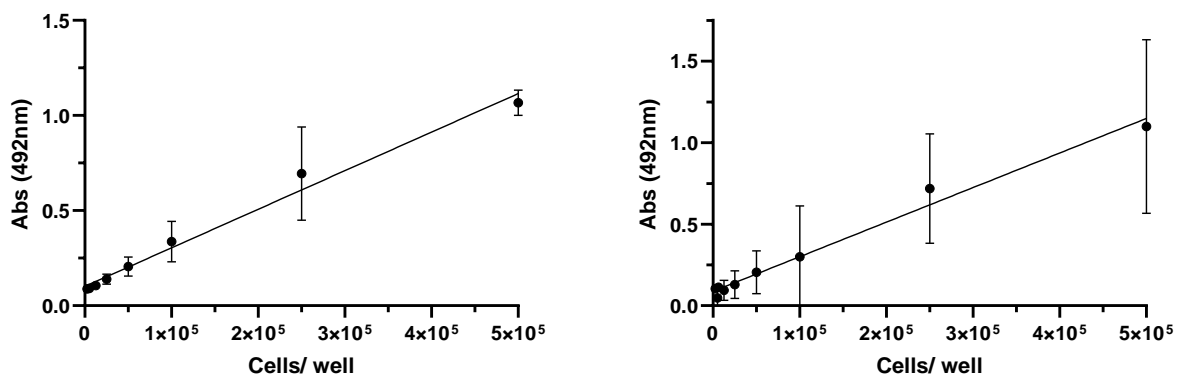


Figure 5.6: Calibration of cell density versus absorbance at 492nm using MTS-PMS metabolic activity assay, for quantification of viable cell population of H103 (left) and A375 (right). Standard cell suspensions were prepared by dilution from a concentrated starting suspension in phenol-red- and FBS-free medium, incubated with MTS-PMS reagent and the coloured product formed was measured by absorbance, in triplicate wells; $n=3$ for H103, $n=4$ for A375.

5.4.1.2.2 Determination of post-treatment viability by MTS-PMS

As before, viability was assessed at 24 hours after treatment, setting the untreated control group as a reference for 100% viability. At the point of assay, the post-treatment growth medium was aspirated from each well and replaced with serum- and phenol red- free medium, to prevent interference with the assay reagent and the sensitivity of colorimetric determination. MTS-PMS reagent was added for an incubation period of 50 minutes before reading the absorbance of the resultant coloured formazan product. Again, there was an implied time-dependent reduction in viable cell population in both NTP and argon-alone treatment groups, but interpretation of results was limited, as before, by the broad within-group variation in relative viability (Figure 5.7). The effect of 30s treatment appeared slightly greater in both NTP- and argon- treated cells, with only 66.1% and 73.3% residual viability, respectively ($p>0.05$). Increasing the exposure time to 60s resulted in a small further loss of viability, to 60.9% in the NTP group, and 64.7% in the argon-alone group ($p>0.05$). Prolongation of the treatment period to 90s led to a reduction to 53.2% residual viability in NTP-

treated cells, but negligible further change in the argon group, whose viability remained at 64.4%, demonstrating once again no significant difference in effect between plasma and argon-treated groups ($p>0.05$).

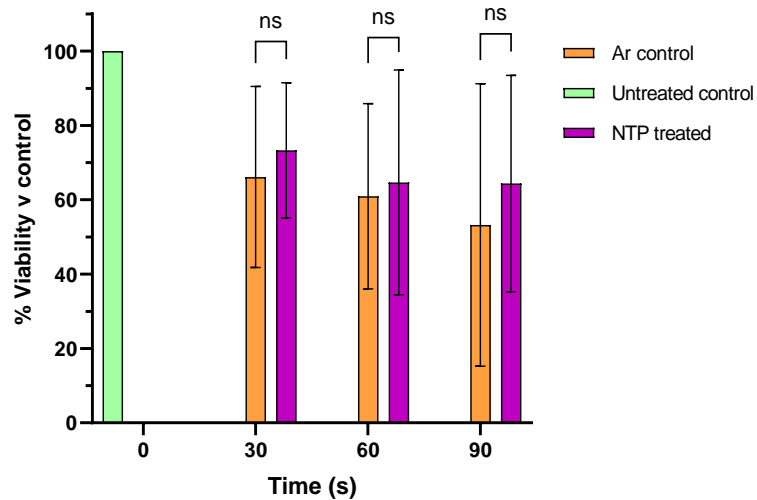


Figure 5.7: Treatment time-course of direct NTP application to H103 cells at 24h post-treatment, assessed via MTS-PMS colorimetric assay; treatments were performed in triplicate, and the effects on viability assessed by 2-way ANOVA $n=4$.

Due to the large inter-replicate variance seen, no firm interpretation can be made from these findings, with results obtained via both approaches suggesting considerable inconsistency in relative cell viability following identical treatments, but also indicating that potential sources of error during experimental procedures, such as unequal seeding, non-uniformity of exposure during treatments, inaccuracies in preparing reagents and/ or cell recovery suspensions, may have compromised the validity of these findings. The MTS-PMS assay was subject to a number of potential sources of error, including inconsistencies in preparation of the reagent (which was required to be freshly prepared on the day of the assay) and incubation time, inhomogeneous distribution of cells during suspension and subsequent dilutions, and limitations in the sensitivity of the assay to accurately determine cell number at the upper and lower extremes of the range of densities tested. Background absorbance (cell-free culture medium with MTS-PMS reagents) has been noted to be high for the MTS assay (particularly when compared to the more traditionally used MTT assay), which again may have contributed to the variability seen within the obtained results, and the limited sensitivity of the assay to detect differences in viable cell populations (Riss, TL, *et al.*, 2013).

5.5 Extended measurement of the effects of NTP on cell proliferation via live-cell imaging

In view of the single end-point results obtained via MTS-PMS and CTG 2.0, which provided only a snapshot of the impact of NTP treatment on cellular viability at an isolated time-point post-treatment, it was decided to monitor cells over a longer post-treatment period, to enable detection of any latent effects of NTP exposure upon cell proliferation. Although the MTS-PMS assay does not require sacrifice of the treated cell cultures, and therefore allows for continued incubation and the potential for assay repeats, its sensitivity to detect further changes in viable population as cell density surpasses a certain range was suspected to be a limiting factor (Figure 5.7). To enable an extended period of observation of the cellular response to treatment resulting from indirect mechanisms or secondary pathways, or recovery of relative viability after the initial inhibition seen at 24h, cells were submitted to the Incucyte® Live Cell Analysis System for continuous imaging and basic analysis of cell confluence.

A monitoring period of up to 72h was selected, as has been used for adherent cell line studies elsewhere (Maisch *et al.*, 2017; Smolková *et al.*, 2019), to identify the emergence of any latent inhibitory or stimulatory effects on cell proliferation at times beyond 24h post-treatment. A maximal monitoring period of 72h was selected since the density of control cell monolayers (where growth was highest) was anticipated to be a limiting factor, preventing any further accurate assessment of confluence, and impacting the continuation of proliferation and cellular viability due to depletion of nutrients in the growth media and accumulation of metabolic waste products, causing media acidification, as well as contact inhibition between cells. Therefore, imaging was recorded at 2-hourly intervals from 0h to 72h post-treatment, to discern divergence in the percentage viability and proliferation rates of NTP-treated cells and argon-treated controls.

Following previously described methods (Section 2.11.1), H103 and A375 cells were seeded in separate 24-well plates, at twice normal seeding density (1×10^4 and 2×10^4 , respectively) to promote a higher % confluence and greater homogeneity across the total well area at the time of treatment. Cells were incubated overnight for 24h to enable adherence and proliferation to sub-confluent levels of approximately 10-20% across all wells. The growth medium was then aspirated from each well, and was replaced with 200 μ L sterile PBS (to maintain hydration) before exposing each well to timed NTP or argon gas control treatment in turn, at a torch-to-target distance of approximately 10mm (from torch tip to the surface of the hydrate cell monolayer). Following treatments, the PBS was removed and replaced with 500 μ L complete DMEM per well, and culture plates were loaded into the Incucyte monitoring system for a 72h period, with results reported as mean percentage confluence for each treatment group. Analyses of between-group differences were undertaken using 2-way ANOVA with multiple comparisons, to discern differences relative to

untreated controls, and multiple paired t-tests to measure significance of NTP relative to argon-only treated cells.

5.5.1 Extended monitoring of H103: post-treatment growth response to NTP

Direct treatment of H103 cells with NTP appeared to exert growth-inhibiting effects following exposures of 30s, 60s and 90s duration, with percentage confluence markedly reduced in treated cell populations in comparison to time-matched argon-only controls (Figure 5.8). However, there was considerable variance in the 72-hour growth response evident in both control and NTP-treated groups. Cells subjected to the shortest NTP exposure (30s) initially showed only a slight reduction in viability, with only a 3.07% deficit compared to the argon control group, and 7.38% less than untreated controls, immediately post-treatment (both $p > 0.05$). Across subsequent time-points, the difference in proliferation between NTP- and argon-treated groups increased slightly, reaching 8.66% by 24h, and 26.44% by 48h, increasing only slightly to approximately 31% from 60h to the final 72h time-point. A negative effect on cell division was therefore indicated with both 30s NTP and argon treatments, markedly greater in the plasma group where final confluence of 53.24% was attained (versus 90.84% in untreated controls, and 84.04% in argon controls), but this not statistically significant at any time-point.

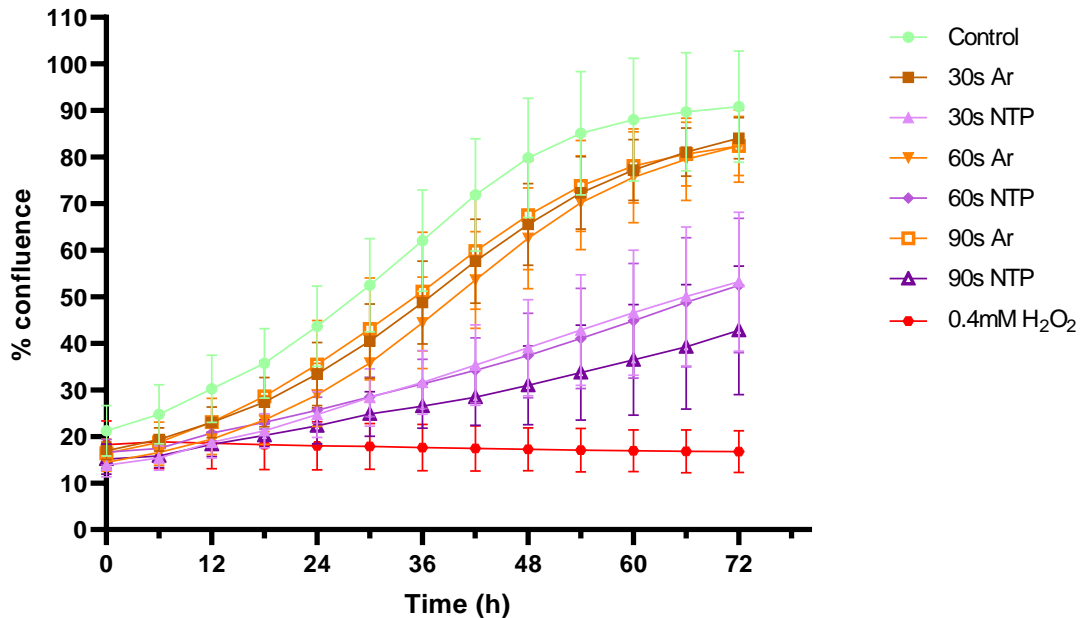


Figure 5.8: Post-treatment growth course of H103 cells from 0 -72h, following 0-90s direct NTP treatments, versus time-matched argon control. Percentage confluence was determined through Incucyte Live Cell analysis, performed in triplicate. Graphed values represent mean % confluence \pm SD; $n=3$. Two-way ANOVA with multiple comparisons was applied to determine significance relative to untreated controls, and multiple paired t-tests applied between NTP- and argon-control groups.

The 60s treatment groups showed a similar pattern, with confluence appearing similar at T=0, but NTP- and argon- treated populations were seen to diverge with increasing incubation time (Figure 150

5.8). Initial measurements showed marginally lower confluence in the 60s argon-only group, however this difference resolved over the following 24h, and by the 36h time-point, argon controls had reached a 13.15% superior confluence to that of the NTP-group, though not significant ($p>0.05$), and both groups appeared to show reduced growth in comparison to untreated controls (13.3% deficit in Ar-treated, and 30.44% deficit in NTP-treated, $p>0.05$). As time continued, the disparity in growth reached a difference of approximately 30%, which was maintained from approximately 54h to 72h post-treatment, with 60s NTP-treated cells reaching 52.41% final confluence, compared to 90.84% in untreated controls. Only at the 48h and 54h time-points was the difference between NTP-treated and untreated control groups significant, with a confluence shortfall of 42.44% ($p=0.044$) and 44.01% ($p=0.045$) respectively. Argon failed to induce a significant effect relative to the baseline control across the whole time-course ($p>0.05$), and it was noted that both NTP and argon-treated groups consistently achieved similar confluence to those subjected to 30s (matched) treatments within one biological replicate, indicating that extension of the treatment time had negligible effect. The 90s treatments NTP group demonstrated a small growth deficit early in the time-course (Figure 5.8), appearing 8.37% lower than argon controls and 11.9% below untreated controls by 18h (both $p>0.05$). The disparity between the NTP-treated cells and argon-controls continued to increase with time, reaching a 24.64% deficit compared to argon-treated wells by 36h, and 35.54% deficit compared to untreated controls. By 42h, 90s NTP-treated cells showed significantly reduced growth in relation to untreated controls, with a 43.44% difference in confluence seen ($p=0.04$). This disparity increased further up until 60h, where a maximal deficit of 51.62% was observed ($p=0.03$), and decreased marginally over the final 12h to 48.04%, at 72h ($p<0.05$).

In comparison, 90s argon treatment showed a lesser impact on cell proliferation, with initial confluence only 6.08% lower than that of untreated controls, rising gradually to a difference of 8.22% by 24h (both $p>0.05$) (Figure 5.8). At subsequent time-points, the 90s argon group maintained a slightly reduced confluence level relative to the untreated baseline, with the greatest difference in confluence reaching 12.29%, noted at 48h ($p>0.05$), thereafter falling slightly to $<10\%$, and attaining a final 82.38% confluence, compared to 90.84% in controls (8.46% disparity, $p>0.05$), and 42.81% in the time-matched NTP group (39.57% disparity, $p>0.05$). At none of the time-points recorded did 90s argon exposure show significant growth-limiting effects, indicating that the reduced proliferation seen with 90s NTP treatment was not attributable solely to the physical stress of being subjected to gas flow.

5.5.1.1. Interpretation of the NTP-response in H103 during extended cell-monitoring

These results suggested a correlation between NTP exposure time and reduction in proliferation, with the 90s-treated cells showing the greatest growth deficit in comparison to the time-matched argon controls (up to 41.65% difference ($p>0.05$) at 60h), and untreated controls (with a maximal

51.62% deficit, ($p < 0.05$) at 60h), an effect which was clearer at later time-points. Despite a sustained relative reduction in viability in NTP-treated populations, proliferative capacity was maintained to a degree, potentially reflecting incomplete exposure of the whole cell monolayer in each well to the reactive species in the NTP discharge, resulting in negligible impacts in marginal regions. NTP treatments of 30s and 60s NTP resulted in similarly reduced growth (final confluence deficits of 30.8% and 29.97% relative to control, respectively) indicating less extensive loss of viability, and/or retention of proliferative activity in some portions of the monolayer in these treated cell populations.

Examination of images taken across the breadth of argon- and NTP-treated wells did support the localised nature of the effects of these treatments, with sparser areas of cell adherence evident towards the centre of the well, in the area positioned directly below the NTP applicator aperture (Figure 5.9). Thus, physical detachment of cells from the culture plate surface may account at least in part to the reduced cell numbers observed following both NTP and gas-only treatments. The modification of cell adhesion molecule expression, as well as changes in migrational and clonogenic activities, have been reported in studies elsewhere investigating plasma-induced effects on epithelial cell models, reflecting the potential of NTP to affect cellular phenotype and transcriptional profile (Haertel *et al.*, 2011, 2014; Schmidt *et al.*, 2015, 2019; Dezest *et al.*, 2017). Therefore, further investigation of the cellular response at a molecular would be greatly advantageous in elucidating the effects of plasma exposure on cell behaviour and viability further.

Inequal initial seeding densities could account for some of the variation in cell confluence seen between experimental repeats, as it was impossible to fully dissociate cell aggregates at the initial seeding point prior to the application of treatments, and thus NTP or argon-only treatments would likely have been applied to a slightly variable absolute cell population. However, confluence levels at the initial (T=0h) time-point recorded in Incucyte analyses showed that standard deviation within the untreated control group did not exceed 5.4% in H103 and 15.1% in A375 cells (whereafter the variance in control group confluence decreased for this cell line), suggesting that this was not a significant source of error. Argon-treated cells exhibited a slightly reduced population at all time-points, however the rate of growth appeared similar to that of untreated controls, suggesting that the residual viable population post-treatment still possessed normal proliferative capacity, despite a net reduction in end-population size. Visual analysis of cell confluence was consistent with a localised effect of gas flow causing a loss of adherent viable population from the central zone of argon-treated wells, with marginal cells appearing to remain relatively unaffected (Figure 9). This observation is in agreement with *in vitro* studies performed elsewhere, in which direct NTP application to adherent epithelial cells has affected cell viability and re-growth (Wende *et al.*, 2010; Lou *et al.*, 2020).

A loss of viability due to the dehydrating effects of treatments here appears likely, since there was visible evaporation of liquid from the central target zone of treated wells, particularly after more

prolonged treatments, seen both macroscopically and under magnification. Hydrogen peroxide-treated cytotoxic positive controls demonstrated a complete absence of proliferation, with a slight reduction in percentage confluence seen across the entire time-course, indicating that long-term exposure to 0.4mM H₂O₂ (present within growth medium from 0-72h) was lethal to the initial seeded population, eliminating all viable cells. Hydrogen peroxide has been proposed as one of the principle mediators of NTP-elicited effects in both prokaryotic and eukaryotic cells (Bekeschus *et al.*, 2014; Haertel *et al.*, 2014; Ozlem, 2017; Smolková *et al.*, 2019), being a relatively stable oxidising species which forms at the interface between plasma effluent and carrier gas/ air/ liquid media present at the discharge zone, in this case overlaying the target cells. Although H₂O₂ quantification was not performed here on either the plasma effluent or intracellularly, use of a high concentration as a positive cytotoxic control was included as an indicator of the sensitivity of H103 and A375 cell lines to this ROS compound, and to confirm the accurate detection of resulting non-viable cells within the Incucyte.

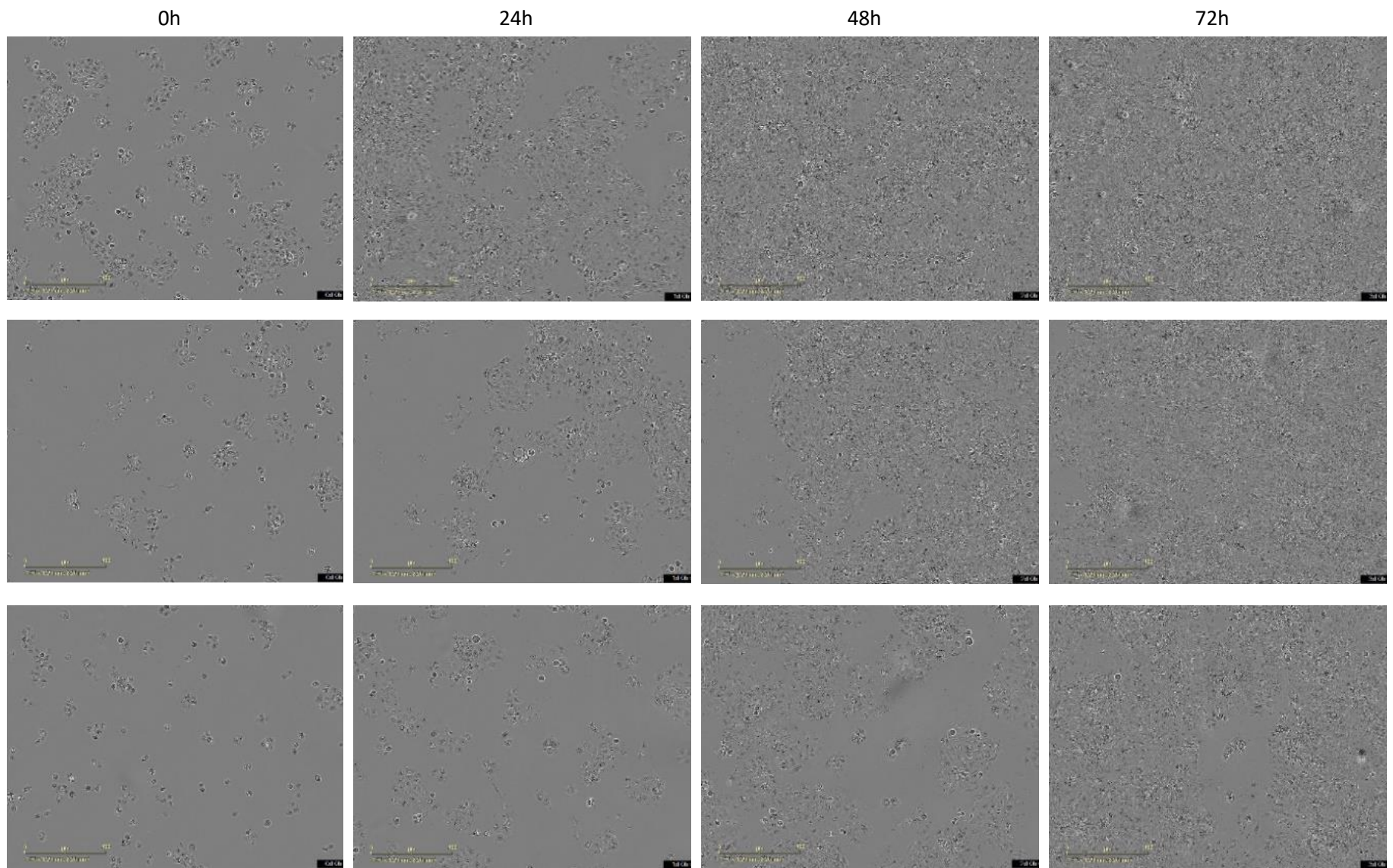


Figure 5.9: Image snapshots of H103 cells following no treatment (top), 30s argon control (middle), and 60s direct NTP (bottom), acquired at 10x magnification using Incucyte® Live Cell imaging analysis.

5.5.2 Extended monitoring of A375: post-treatment growth response to NTP

Direct NTP treated cells showed a clear divergence from their argon-treated control counterparts, with an inhibitory effect emerging after 18h in 30s, 60s and 90s NTP-treated populations (Figure 5.10). The 30s treatment groups showed distinct differences in growth, with an initial deficit in confluence seen in NTP-treated cells, showing an apparent 19.88% reduction in comparison to untreated controls ($p>0.05$), immediately after treatment. The relative depression of growth in the 30s NTP group became more marked with time, reaching a significant 40.84% deficit by 18h ($p=0.03$), and just exceeding 50% by 24h ($p=0.02$), rising to 69.09% ($p<0.0001$) by 48h, and decreasing only slightly over the final 24h, attaining a 72h confluence of 33.02% compared to 96.99% in controls (63.98% deficit, $p=0.05$). In argon-only controls, there was a small reduction in growth compared to the untreated control group, although to a much lower extent, appearing significant only at 30h (20.28% deficit, $p=0.04$) and 36h (18.79% deficit, $p=0.05$), a difference which modestly diminished over the latter 36h of recording, falling to a 10.14% disparity by 72h (86.86% versus 96.99%, $p>0.05$).

The 60s NTP-treated A375 group also demonstrated a significant reduction in proliferative activity, with a 19.88% lower confluence than untreated controls at the initial time-point ($p>0.05$) increasing to a 40.44% shortfall by 18h post-treatment ($p=0.03$) (Figure 5.10). Thereafter, the growth deficit continued to rise, reaching a maximum of 58% at 54h ($p=0.04$) which remained broadly unchanged until the final measurement at 72h (57.57% difference, $p>0.05$). In comparison to untreated controls, the reduced growth of 60s NTP-treated cells was more marked, with 44.04% difference emerging by 18h ($p=0.03$), and broadening to 63.8% by 36h ($p=0.0003$). As time progressed, this disparity gradually increased, reaching 70.53% at 48h ($p<0.0001$), and remaining consistently $\geq 66\%$ throughout the remainder of the time course. By the final 72h timepoint, NTP-treated cell population had plateaued at 30.74%, whereas untreated controls reached 96.99% confluence ($p=0.01$). Argon-only controls again exhibited reduced growth relative to untreated controls, however this difference did not exceed 20% and was not statistically significant at any time-point, with a final confluence of 88.31% attained, against 96.99% in the baseline control (8.68% deficit, $p>0.05$).

The longest treatment time of 90s NTP showed the greatest inhibitory effect on proliferation in A375, as was seen in H103 cells. At 18h, the growth deficit with respect to untreated controls was 43.43% ($p=0.02$), a difference which expanded with time, reaching 67.89% by 36h ($p=0.0002$), and 74.83% by 48h ($p=0.0002$), remaining largely consistent thereafter, with a 72h disparity of 72.73% compared to baseline ($p=0.01$) (Figure 10). In argon-only controls, there was a comparatively mild depression of growth, which did not exceed 25% difference relative to the untreated control group, measuring 19.35% at 24h, increasing slightly to a maximum of 23.16% by 42h, and settling to 21.32% by 72h, with statistical significance noted at none of the time-points ($p>0.05$). Cytotoxic

positive controls were subjected to 35% ethanol treatment, in order to induce rapid and uniform loss of viability and accurate detection of this lethality via Incucyte imaging, demonstrated a small but continuous decline relative to controls, throughout the duration of the analysis. From an initial confluence of 15.15%, there was a diminution to 12.12% by 24h, 11.44% by 48h, and a final measurement of 8.60% confluence at 72h, indicating complete failure of proliferation and likely detachment of the original seeded population, consistent with the lethal effects anticipated ($p \leq 0.05$ at all time-points $> 6h$).

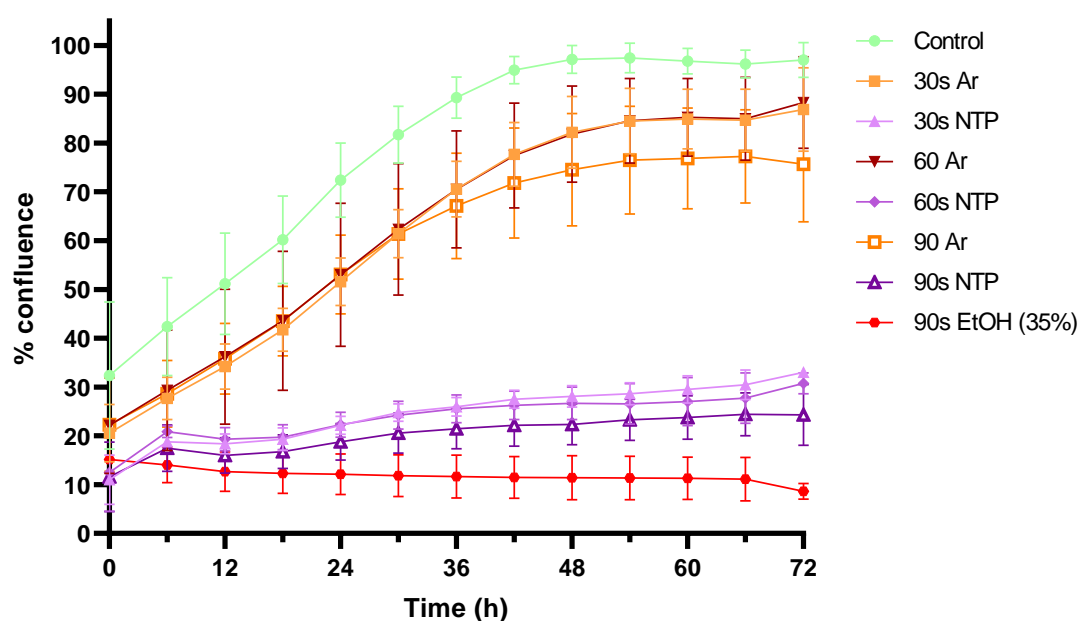


Figure 5.10: 72h post-treatment growth course of A375 cells following 0-90s direct NTP treatments, versus time-matched argon controls. Percentage confluence was determined through Incucyte® Live Cell analysis, performed in triplicate. Graphed values represent mean % confluence \pm SD; $n=3$. Two-way ANOVA with multiple comparisons was applied to determine significance relative to untreated controls, and multiple paired t -tests used to compare cultures treated in complete-medium versus serum-free.

5.5.2.1 Interpretation of the NTP-response in A375 during extended cell-monitoring

Therefore, NTP-treatment appeared to result in a significantly diminished proliferative cell population, an effect which remained throughout the duration of the 72h monitoring period. In comparison, argon-treated controls demonstrated a similar proliferative trend to that of untreated controls, but beginning at a lower initial density, indicating that NTP treatment had reduced the viable population immediately after treatment, but that surviving cells continued to proliferate, and did so at rates similar to the untreated control (Figure 5.10), reflecting similarity to the findings obtained in the H103 line.

Both the visual appearance of cells viewed under 10 x magnification microscope, and the images obtained during live cell analysis (Figure 5.11), were consistent with the application of both the argon-only gas flow and the NTP jet having localised effects, i.e. causing physical detriment to cells located directly beneath the NTP torch effluent, whilst leaving those located around the

perimeter relatively unaffected. This differential effect was apparent on microscopic examination of wells immediately after treatment, as a clearly demarcated circular area of devitalised cells, and was detected in more central fields of view on Incucyte® images (row 2, Figure 5.11), where a cleared region was perceptible. In argon controls, adjacent cells bordering this non-viable zone appeared to mobilise and proliferate into the cleared areas, whereas NTP-treated wells failed to recover to such an extent, and remained more sparsely populated (Figure 5.11, bottom row).

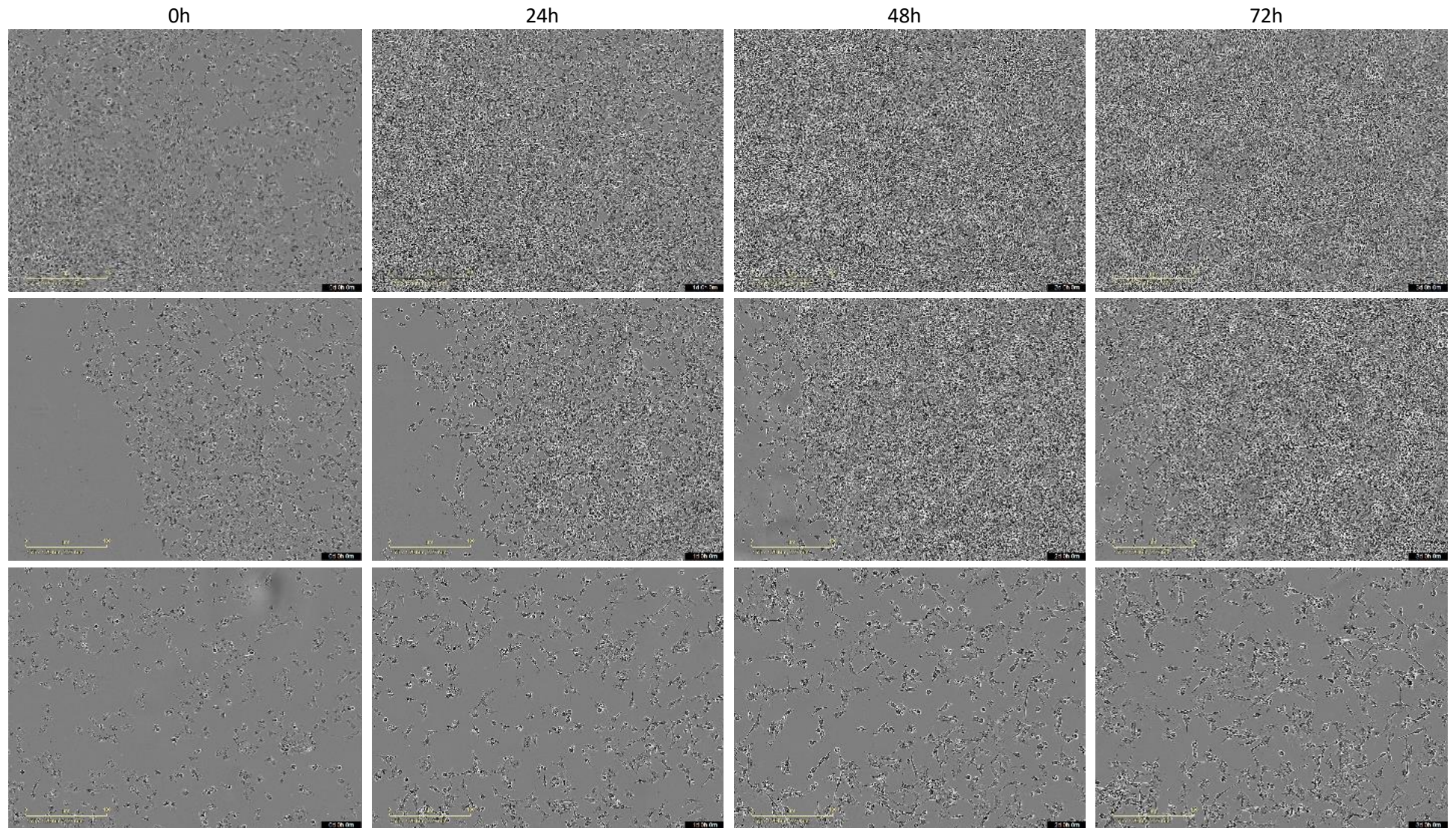


Figure 5.11: Image snapshots of A375 cells following no treatment (top), 30s argon control (middle), and 60s direct NTP (bottom), acquired at 10x magnification using Incucyte® Live Cell imaging analysis.

Although an inhibitory and time-dependent effect of direct NTP was seen on both cell lines, the reduction was more marked in A375 cells. This might relate in part to their more rapid growth rate, resulting in a greater divergence of treated from untreated cells as the latter underwent exponential growth from a larger initial viable population post-treatment. Studies performed elsewhere have investigated the effects of direct plasma treatment on the A375 cell line, using a floating electrode-dielectric barrier discharge system (FE-DBD), as well as plasma-treated PBS (using an NTP jet device and argon carrier gas), to determine the comparative susceptibility to treatments, relative to non-cancerous cell lines of the same cell type (Biscop *et al.*, 2019). Although the system configuration and treatment parameters differed from those used here, the authors did discern marked cytotoxicity followed both treatment modalities, with viability reduced to 30-40%.

5.6 Investigation of the cytotoxic response to topical antimicrobial agents

5.6.1 Dose-response studies of PVP-I and ECAS in H103 and A375 cells via CTG2.0 and MTS-PMS assay

PVP-I is used clinically in antiseptics of acute and chronic wounds, in pre-operative skin preparation, as well as peri-operative antiseptics, typically at concentrations between 7.5% – 10% in solution, and at lower concentration in other preparations such as antiseptic oral products (Woo, 2014; Eggers, 2019). Although clinically well-tolerated, caution as to its application in large open wounds is advised (NICE, 2024), and *in vitro* studies have demonstrated cytotoxicity at concentrations well below the clinical in-use range against primary human fibroblasts and keratinocytes, and also immortalised murine and human epithelial cell lines (Müller and Kramer, 2008; Sato *et al.*, 2014; García-Valdivia *et al.*, 2022; Ortega-Llamas *et al.*, 2022; Zhang *et al.*, 2023).

Assessment of the effects of PVP-I inclusion in 24h incubations with H103 and A375 cell lines was therefore performed over a similar concentration range as that demonstrated elsewhere to encompass cytotoxic thresholds in epithelial cells *in vitro*, using differing treatment regimens (Müller and Kramer, 2008; Sato *et al.*, 2014; Van Meurs *et al.*, 2014; Ortega-Llamas *et al.*, 2022; Zhang *et al.*, 2023). PVP-I was applied at concentrations between 0.002% and 2% (v/v) in PBS, prepared from a stock solution of 5% w/v in dH₂O, added in a 1:1 ratio with standard culture medium (therefore demi-diluting the initial dose). Treatments were applied to sub-confluent cell cultures 24h after seeding, incubated for a 24h treatment period, then sampled in triplicate for cell viability assay, using MTS-PMS and CellTiter Glo 2.0, as previously applied for cytotoxicity assessment. IC₅₀ was calculated for PVP-I and ECAS for each cell line by non-linear regression (Log[inhibitor] vs response – variable slope (four parameters)), and the results were summarised in tabular form (Table 5.1).

5.6.1.1. Determination of the IC₅₀ of PVP-I in H103 cells

For the H103 cell line, using CellTiter Glo 2.0 for the evaluation of end-point cell viability, the IC₅₀ of PVP-I was found to be 0.0733% (Figure 5.12, left panel). Cell viability remained close to control levels at the lower range of test concentrations, with PVP-I doses up to 0.01% showing no inhibitory effects, and a mild decline to $80.69 \pm 11.09\%$ viability with 0.05% PVP-I. Increases in applied dose to 0.075% PVP-I and above led to a sharp decline in the relative surviving cell population, with $56.47 \pm 23.63\%$ viability seen at 0.075%, and an approximate 10-fold sequential reduction with 1.0% PVP-I, with which treatment the cell viability only measured $5.99 \pm 8.11\%$. The maximal applied PVP-I concentration (1%) resulted in near-complete lethality, with $<1\%$ residual viability detected ($0.93 \pm 0.87\%$).

The MTS-PMS assay, using a slightly reduced number of dose concentrations (owing to the use of 24-well plate format, as opposed to the 96-well plates used with CTG2.0) but covering the same 0.001% - 1% (w/v) final concentration range, reported the IC₅₀ for PVP-I as 0.1056% (w/v) (Figure 5.12, right). The full dose-response curve derived using MTS-PMS demonstrated low toxicity at concentrations up to 0.01% PVP-I, with $\geq 95\%$ viability noted within this lower dose range, and only a slight reduction in cell viability to $87.51 \pm 10.11\%$ seen with an increase to 0.05% PVP-I. Further elevation of treatment concentration produced a progressive decline in cell viability, with $22.31 \pm 2.17\%$ of cells remaining viable following 0.5% PVP-I treatment, and a similar cytotoxic effect with 1.0% PVP-I, the maximum applied dose ($23.07 \pm 2.09\%$ viability).

Both assays demonstrated a marked degree of within-group variation as the treatment dose approached the IC₅₀, with greater variance noted at 0.075% PVP-I in the CTG2.0 assay, where viability was determined as $56.45\% \pm 23.63\%$, and at 0.1% PVP-I in the MS-PMS assay, where viability was measured as $62.77\% \pm 18.49\%$. Interestingly, results obtained using MTS-PMS suggested a markedly higher surviving portion of cells at the higher region of the concentration range, with up to approximately 78% loss of viability reported at 0.5% and 1% PVP-I treatments, doses which reduced residual viability by $\geq 98\%$ according to results obtained using CTG2.0 assay. A number of factors may have contributed to this lack of concordance, such as the slightly reduced number of doses selected across the test concentration range in MTS-PMS assays in comparison to CTG2.0 (a total of 7 concentrations (excluding medium-only control) tested in the former, and 10 in the latter), and also the sensitivity of the assay, as this assay has been noted elsewhere to under-estimate cytotoxic effect *in vitro* (Wang, Henning and Heber, 2010). Other contributing factors underlying this discordance may include the usage of differing plate formats (24-well as opposed to 96-well), inconsistencies in seeding density, and in constitution of the test reagent (MTS-PMS requires freshly prepared re-agent at each experimental repeat, whereas CTG2.0 utilised aliquots taken from a frozen stock), and also potential inaccuracies in dose

titration/ preparation, and application of treatments, e.g. pipetting technique, mixing/ homogenisation, and incubation time (manual in MTS-PMS, automated in CTG2.0).

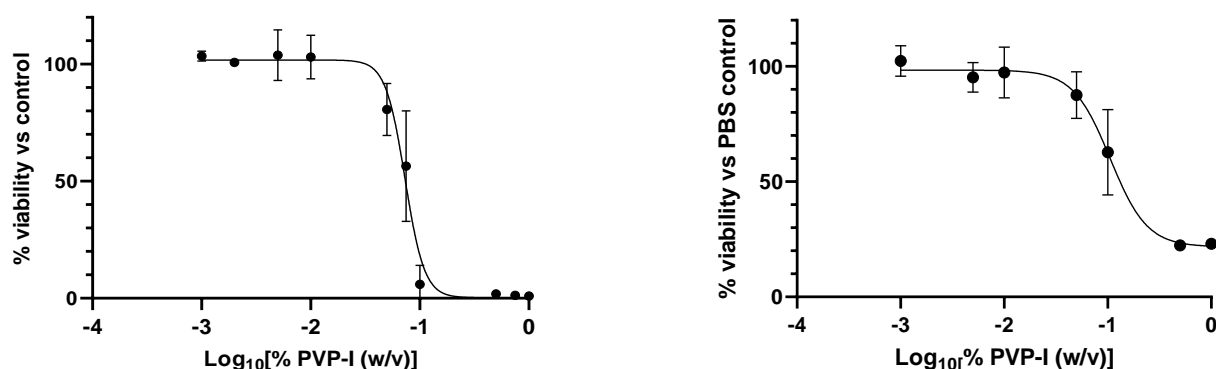


Figure 5.12: Dose-response curve for PVP-I treatment of H103 cells over a 24-h treatment period, assessed via CTG2.0 (left), and by MTS-PMS (right). Doses shown represent the final PVP-I concentration after adding in a 1:1 ratio to standard culture medium.

5.6.1.2 Determination of IC₅₀ of ECAS in H103 cells

The dose-response of ECAS was similarly investigated in the H103 line, providing a comparative measure of antiseptic-induced cytotoxicity to that elicited with PVP-I. Treatments were applied over a concentration range corresponding to those used in studies aiming characterise the *in vitro* cytotoxic profile of hypochlorous acid-based solutions, elsewhere (Severing *et al.*, 2019; Reis *et al.*, 2021). Treatments across a final concentration range of 0.1% - 50.0% (v/v) were prepared in PBS from a stock solution of 200-220ppm freely available chlorine (FAC), with corresponding final FAC concentrations of 0.2 – 110 ppm. Each dose was applied in triplicate to sub-confluent cell cultures, and incubated for a 24h exposure period, as performed in H103 cells. At the end of the treatment period, the final cell viabilities in each group were measured via MTS-PMS and CTG2.0, as before. The IC₅₀ was determined for each dataset, using mean values obtained from three independent experiments.

Using CTG2.0, the IC₅₀ was derived as 13.66% (v/v) ECAS (30.052ppm FAC) (Figure 5.13, left panel). Percentage viabilities displayed a larger degree of variance at doses close to the IC₅₀, particularly at the 10% and 15% doses, where percentage viabilities of $61.69 \pm 13.43\%$, and $32.034 \pm 23.10\%$ were observed. At concentrations $\leq 1\%$, minimal cytotoxicity was noted, with viability maintained at $\geq 94.4\%$. The maximum concentration applied, 50% ECAS (110ppm), reduced levels of cell viability to $0.431 \pm 0.72\%$, indicating negligible survival.

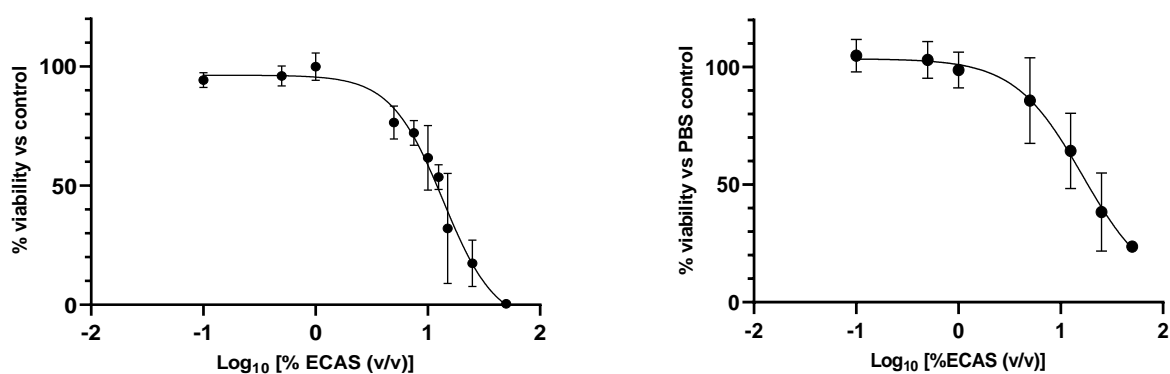


Figure 5.13: Dose-response curve for ECAS treatment of H103 cells over a 24h period, assessed via CTG2.0 assay (left), and MTS-PMS (right). Doses shown represent Log₁₀ of the final ECAS concentration, after adding in 1:1 ratio with standard cell culture medium.

The MTS-PMS assay indicated an IC₅₀ of 16.33% (v/v) ECAS (equivalent to 35.926ppm FAC) for the H103 line (Figure 5.13, right panel), although substantial variability in cytotoxic effect was observed at mid-range doses, between 5.0 – 25.0%, spanning the IC₅₀ region of the concentration range tested. At concentrations ≤1% ECAS, there was little to no effect with mean viabilities of ≥98%. Interestingly, the maximum tested dose of ECAS (50%) appeared markedly less cytotoxic using MTS-PMS when compared to results obtained with CTG2.0, with 23.77 ± 2.17% residual cell viability measured. The discrepancies seen between data outputs using each respective viability assay may be a product of the reduced number of doses tested in MTS-PMS assay versus CTG2.0, as previously mentioned, which may have affected the precision of the estimation of the true IC₅₀, but also the meta-stability of ECAS, being a complex product containing an array of active species generated via electrolysis of a weak saline solution, produced freshly for each experiment rather than from a standard single stock.

5.6.1.3 Determination of the IC₅₀ of PVP-I in A375 cells

The cytotoxicity of PVP-I was investigated for the A375 cell line, as previously described for H103, with PVP-I treatments between 0.001% and 1% (w/v) applied to cells for an exposure time of 24h before performing CellTiter Glo 2.0 or MTS-PMS assay. Using CTG2.0 assay, the IC₅₀ of PVP-I was determined as 0.0688% (Figure 5.14, left panel). As was seen in prior cytotoxicity testing on the H103 cell lines, there was substantial variance in viability levels resulting from treatments within the mid-range of tested concentrations, notably between 0.05% and 0.1% PVP-I, corresponding to the dose range spanning the IC₅₀ threshold. Little to no cytotoxic effect was observed with treatments up to 0.01%, with ≥98% viability maintained, however a sharp decline occurred at doses >0.05%, falling from 75.38 ± 16.39% with 0.05% PVP-I, to 49.98 ± 27.09% with 0.075% PVP-I. A strong cytotoxic response was seen with PVP-I treatments ≥0.5%, where residual viability

was reduced to 1-2% or less, indicating near-complete lethality (only $0.68 \pm 0.87\%$ cell surviving at the maximal 1% PVP-I dose).

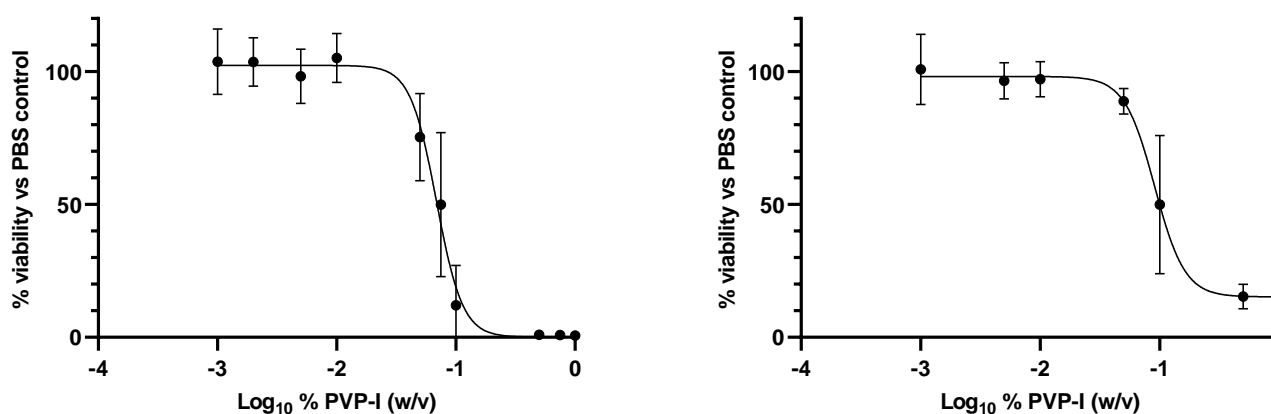


Figure 5.14: Dose response curve for PVP-I treatment of A375 cells over a 24h period, assessed via CTG2.0 (left) and by MTS-PMS assay (right). Doses shown represent Log₁₀ of the final PVP-I concentration, after adding in 1:1 ratio with standard cell culture medium

Data obtained using the MTS-PMS assay indicated the IC₅₀ for PVP-I as 0.09088% (Figure 5.14, right panel). At the lower range of test concentrations, from 0.001 – 0.01% PVP-I, cell viability remained close to 100%, however with a dose increase to 0.05% PVP-I and above, there was a marked reduction in viable cell population, notably at the 0.1% dose ($49.92 \pm 26.08\%$ viability), which most closely approximated the IC₅₀ using this assay. With treatments >0.1% PVP-I, relative viability fell to a minimum of approximately 15.4%, indicating incomplete toxicity (the maximal PVP-I treatment of 1% leaving a viable cell population of $15.37 \pm 4.44\%$, relative to untreated controls).

5.6.1.4 Determination of the IC₅₀ of ECAS in A375 cells:

Similarly, ECAS treatments were applied to A375 cell cultures for 24h contact time, to determine cytotoxic dose-response via CTG 2.0 and MTS-PMS assay, and to enable comparison with the response seen in H103. Results derived using CTG 2.0 showed an IC₅₀ of 6.386% (v/v) ECAS (95% CI upper limit 17.86%, lower limit indeterminable) in A375 cells, equivalent to 14.05ppm FAC (Figure 5.15, left). There was an absence of cytotoxic effect seen at the lowest applied ECAS doses, with viability equivalent to, or slightly greater than control levels with treatments up to 0.5%. Increasing the concentration beyond 1%, however, resulted in a steep decline in viable cell population, with only $45 \pm 15.9\%$ noted at 5% ECAS, diminishing to $40.52 \pm 4.05\%$ with 10% ECAS treatment, and $26.67 \pm 17.36\%$ viability with the 25% dose. The maximum applied dose (50% ECAS) appeared lethal, reducing residual cell viability to <1%.

In contrast, the MTS-PMS assay indicated an IC₅₀ of 11.63% (v/v) ECAS for the A375 cell line, equating to 22.586ppm FAC (Figure 5.15, right). Results obtained via this assay suggested cell

viability to be largely unaffected by ECAS at doses $\leq 1\%$, with a clear inhibitory effect first appearing at the 5% treatment, where relative viability measured $69.77\% \pm 13.4\%$. Further increases in ECAS concentration reduced the surviving cell population further, falling to $35.26 \pm 11.78\%$ viability noted with 25% ECAS, and further to $16.66 \pm 5.90\%$ at the maximum tested dose (50% ECAS). As was observed in the PVP-I dose-response obtained via MTS-PMS, the highest test concentration of ECAS did not absolutely reduce relative cell viability to 0%, despite this being the apparent response seen using CTG assay. This reiterates previous observation of differences in sensitivity between the two approaches, but also may reflect the different sources of error affecting each assay respectively, not least the differing plate-formats for cell culture, recovery and quantification (MTS-PMS being performed directly in the same microtiter plate in which cells were cultured and treated (24-wells) and CTG requiring dissociation of cells from the treatment plate, and resuspension in 96-well plates at the point of testing).

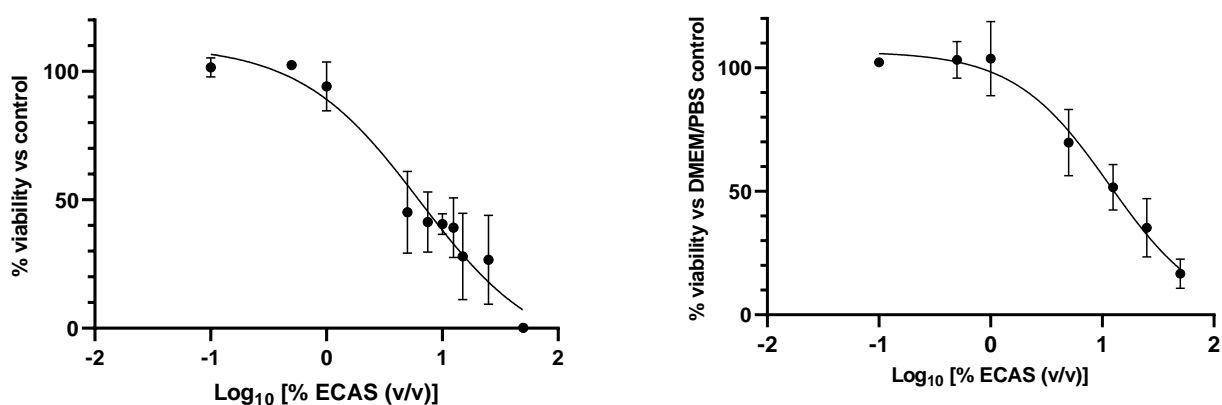


Figure 5.15: Dose response curve for ECAS treatment of A375 cells over 24h, assessed by CTG 2.0 assay (left) and MTS-PMS (right). Doses indicate Log_{10} of the final ECAS concentration, after adding in 1:1 ratio with standard cell culture medium.

	IC ₅₀ ECAS (% v/v) \pm 95% CI		IC ₅₀ PVP-I (%w/v) \pm 95% CI	
	CTG2.0	MTS-PMS	CTG2.0	MTS-PMS
H103	13.66 (10.78 – 24.43) [30.05ppm FAC]	16.33 (8.371 – n.d.) [35.93ppm FAC]	0.1056 (0.0657 - 0.0805)	0.0759 (0.0850 – 0.1662)
A375	6.386 (17.86 – n.d.) [14.05ppm FAC]	11.63 (5.432 – n.d.) [22.59ppm FAC]	0.0688 (0.0597 – 0.0779)	0.9088 (0.0750 - 0.1139)

Table 5.2: Summary of the IC₅₀ of ECAS and PVP-I in H103 and A375 cell lines, as determined by CellTiter Glo2.0 and MTS-PMS assay; values were derived from non-linear regression (Log_{10} [inhibitor] vs response – variable slope, four-parameter). IC₅₀ doses are quoted with 95% confidence intervals, following $n=3$ dose-response assays, performed in triplicate for each cell line.

5.6.2 Potential sources of error and variability in cytotoxic dose-response determination

The MTS-PMS assay provides an indirect measure of net cell viability, by colorimetric measurement of the formazan compound formed via the bio-reduction of MTS in the presence of PMS, thus indicating levels of NADPH-dehydrogenase enzymes present (Wang, Henning and Heber, 2010; Riss, TL, Moravec, RA, Niles AL, Duellman, S, Benink H, Worzell, TJ, Minor, 2013; Kamiloglu *et al.*, 2020). Overestimation of cell viability may therefore be possible if there is any latency between initiation of programmed or necrotic cell death and the decline in levels of active enzyme, for example dehydrogenase activity persisting transiently after cell lysis. Furthermore, interference with or skewing of absorbance readings may have occurred due to technical inaccuracies during the preparation of MTS-PMS reagent, or interactions between the treatment (ECAS) and the conversion of MTS to formazan.

An additional potential source of variability which may have added to the margin of error in the obtained results, was inconsistency in the initial cell number populating each well of the treatment plates. Although the calculated seeding density was standardised across all experiments, heterogeneity in actual seeding population density may well have occurred due to insufficient resuspension of cells following dissociation, and through the formation of aggregates, an inherent feature that is difficult to control when practising adherent cell culture (Reynolds *et al.*, 2018).

5.7 Cellular response to plasma-activated solutions (PAS)

Due to the apparent involvement of physical stressors during NTP treatments, including evaporative effects and physical perturbation of targeted cells, an alternative, indirect, mode of NTP delivery was adopted, whereby a fixed volume of either sterile PBS or serum-free cell culture medium was treated and then applied to cell cultures. Plasma treatment delivered via NTP jet operated with a carrier gas has been noted to negatively impact mammalian cell viability *in vitro*, attributed to necrotization of adherent cells as a result of the dehydrating effects of gas flow during plasma generation (Wende *et al.*, 2010). Indirect NTP-mediated effects have been reported numerously in the literature, particularly in the investigation of the antimicrobial applications of NTP and mechanisms of induced cell death in eukaryotic cells (Chen, Su and Liang, 2016; Dezest *et al.*, 2017; Park *et al.*, 2017; Griseti, Merbahi and Golzio, 2020; Tsoukou, Bourke and Boehm, 2022). Thus, indirect NTP treatment methods have been increasingly favoured for the investigation of the biological responses to NTP plasma in both prokaryotic and eukaryotic cultures *in vitro* (Wende *et al.*, 2010, 2016; Schmidt *et al.*, 2015).

In experiments investigating the effects of PAM here, to account for the possible quenching effects of FBS upon plasma-derived reactive species, cell treatments were performed with both

complete and serum-free media, in parallel. In these instances, 24-well cell culture plates comprised 12 wells of cells seeded in standard complete culture medium (HAMS/F12 DMEM, supplemented with 10% FBS, 2mM L-glutamine and 250µg sodium hydrocortisone succinate, containing phenol red), and 12-wells of cells seeded in serum- and phenol-red free HAMS/F12 DMEM.

An initial treatment time-course was carried out on H103 cells using MTS-PMS to measure any effects of pPBS and PAM on cell viability, when applied for exposures of 6 – 48h (Figure 5.16). PAM and pPBS were added to wells immediately after plasma exposure, at 24h post-seeding, and replaced with untreated medium at sequential 12-hourly intervals for the remainder of the 48h time-course. However, preliminary results revealed no significant changes in viable population, although a tendency towards increased viability was seen in treated groups. Since the detection of any indirect plasma induced effects may have been ‘diluted’ or obscured in shorter treatments, due to the replacement of treated media with untreated, and also affected by the sensitivity limits of MTS-PMS to distinguish differences in viable cell population, this approach was discontinued.

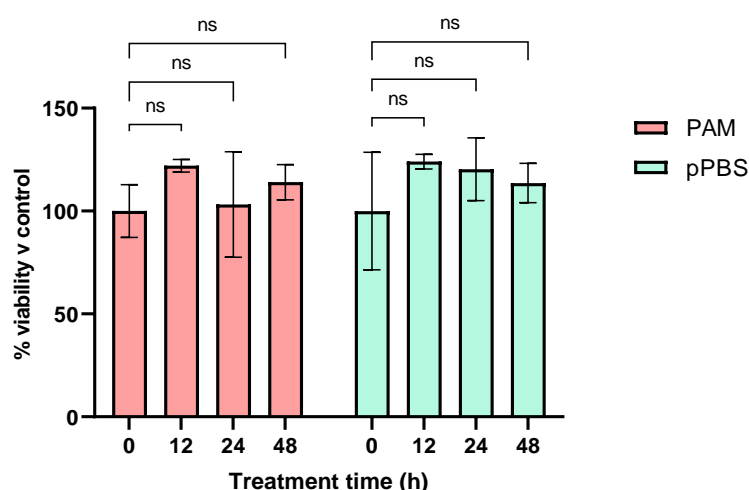


Figure 5.126. 48h treatment time-course of H103 treatments with either plasma-activated medium (PAM) or plasma-activated PBS (pPBS). Treatments were added to cells at T_0 and replaced at respective time-points with control (untreated) media during the remaining culture period, to 48h. Treatments were performed in triplicate, $n=1$.

5.7.1 Plasma-activated PBS:

Sterile PBS has been investigated as a medium by which NTP reactive species can be delivered to biological targets, including both microbial and mammalian cells, inducing cytotoxic effects (Sklias, Sousa and Girard, 2021; Tsoukou, Bourke and Boehm, 2022). To discern whether activation of PBS could elicit changes in the proliferative activity/ viability of mammalian cell cultures using the combined RF-MW NTP system described earlier, and whether a ‘dose’-dependent effect was seen, based on plasma activation time, plasma-treated PBS (pPBS) was applied to freshly seeded cell

cultures and remained in cell culture medium over the 72h monitoring period of live cell imaging analysis.

5.7.2 Extended monitoring of the H103 growth response to pPBS

Plasma treatment of PBS was performed directly before being added to cell cultures, in attempt to capture the effects of less stable species which may dissipate more rapidly, during the post-activation period. Plasma activation of PBS was performed as described in Chapter 2 (Methods Section 2.8.1). Each treatment plate comprised 12 wells of cells seeded in standard complete culture medium, and 12-wells of cells seeded in serum- and phenol-red free medium. This format was selected in order to assess any buffering effect of FBS on the NTP-activation effect, since complex organic components have been reported elsewhere to antagonise the bioactivity of reactive species within treated/ activated substrates (Kaushik *et al.*, 2015; Biscop *et al.*, 2019).

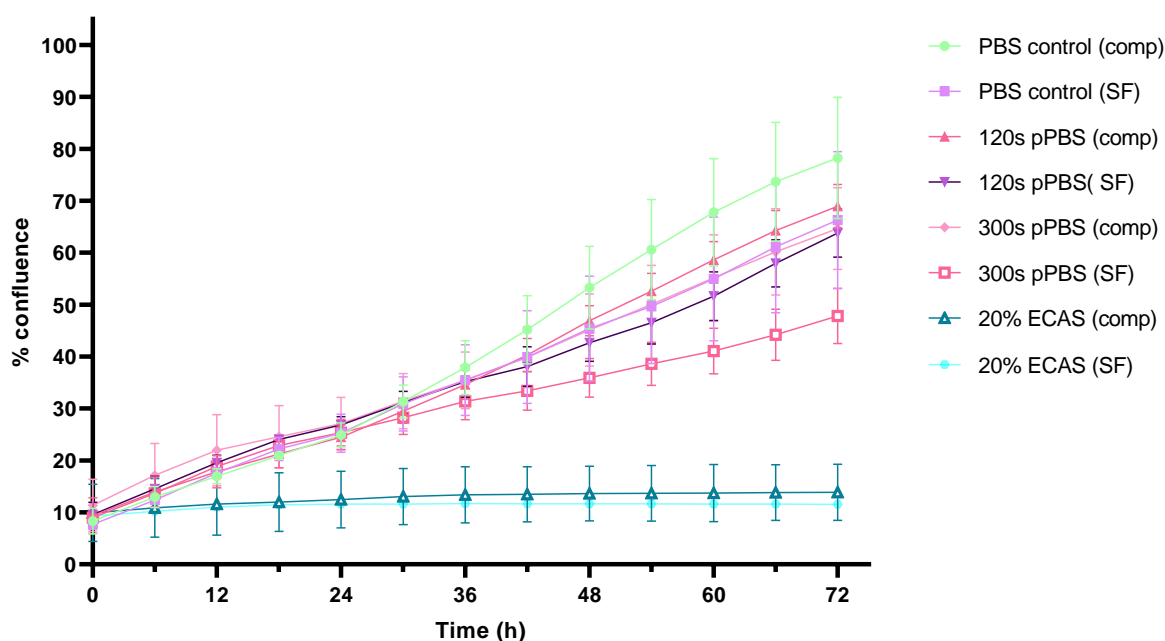


Figure 5.17: 72h growth course of H103 cells treated with 120s or 300s plasma-activated PBS (pPBS). Cell cultures were seeded in either complete (comp) or serum- and phenol red-free (SF) culture medium, to which pPBS or non-activated PBS (control) was added in an equal volume. Incucyte® Live Cell Analysis was used for quantification of mean % confluence, using 9 FOV per well, from treatments applied in triplicate. Percentage confluence between group was compared at 6-hourly intervals by 2-way ANOVA with multiple comparisons, using Dunnett's correction; n=3.

Prolonged exposure to pPBS over a 72h post-activation period appeared to have a negative impact on H103 cellular proliferation, although this effect was not found to be significant with either 120s or 300s-activated pPBS treatments, when comparing percentage confluence to that of control populations (Figure 5.17). A deficit in growth of up to 9.41% was seen in the 120s-activated pPBS group with complete medium, noted at the 66h time-point, whilst in the 300s pPBS group in complete medium, the effect was seen maximally at 72h, with a reduction in confluence of 13.60% relative to that of untreated controls ($p>0.05$). In the serum-free group, a similar growth response to pPBS was seen, although there appeared to be a slightly wider effect

margin between 300s-activated and 120s-activated pPBS treatments, with the former producing a confluence deficit of up to 18.52% relative to controls (at 72h), whilst the 120s-treated group demonstrated a maximal difference of 3.50% (noted at 60h). Results also indicated that serum-deprivation exerted a moderate inhibitory effect upon cell growth, in both controls and pPBS-treated groups, showing as a lag in growth in serum-free controls of up to 12.78% (at 60h growth) with respect to complete-medium controls, and up to 16.84% in pPBS-treated cells in SF- versus complete media (at 72h in the 300s-activated pPBS groups), although this difference failed to achieve statistical significance at any timepoint ($p>0.05$).

Overall, confluence measurements inferred that a longer plasma-activation time of PBS caused a slightly more marked impairment of cellular proliferation, with the endpoint confluence of 300s pPBS-treated wells reaching $64.65 \pm 7.85\%$ in complete medium ($p>0.05$), and $47.80 \pm 5.32\%$ in SF medium ($p>0.05$), in comparison to control wells whose final confluence levels attained $78.24 \pm 11.69\%$ (complete) and $66.32 \pm 13.19\%$ (SF). Significant growth limiting effects were noted only in ECAS-treated populations, at all timepoints from 30h (18.31% deficit, $p<0.05$) up to 72h (64.38% deficit, $p<0.01$) in complete medium. In serum-starved cells, a similar response was seen across the majority of timepoints from 6h (2.16% deficit, $p<0.5$) to 72h (54.78% deficit, $p<0.05$), although at 42h – 60h, the effect was not significant ($p>0.05$). It must be noted that the ECAS concentration selected for positive cytotoxic control treatments in H103 cells (20% v/v) was well above the IC_{50} dose range determined previously by CTG 2.0 and MTS-PMS assays (13.66% - 16.33%), thus it was unsurprising that percentage confluence in these groups failed to make more than negligible gains throughout the duration of the experiment, rising from $9.90 \pm 5.51\%$ to $13.87 \pm 5.40\%$ in complete medium, and from $9.30 \pm 0.17\%$ to $11.54 \pm 0.66\%$ in SF.

5.7.3 Extended monitoring of the H103 growth response to PAM

Plasma-activated medium (PAM) treatments produced similar findings to those observed with pPBS, suggesting a modest growth-limiting effect of PAM on cells in both complete and SF media, but once again failing to demonstrate a statistically significant difference to untreated controls (Figure 5.18), with the exception of the 300s PAM-treated cells in complete medium, whose endpoint confluence was reduced by 11.59% in comparison to control ($p=0.031$). Plasma activation time again appeared to enhance the inhibitory effect on cell proliferation, with 300s-activated media resulting in lower cell proliferation rates, with significantly lower confluence observed than in 120s-PAM treated cells by the 72h time-point (8.64% difference, $p<0.05$), and in serum-deprived cells, up to 22.23% difference between 300s- and 120s-pPBS treated groups at 72h, ($p>0.05$). Treatment with 120s PAM did not exert significant inhibition with respect to control in either serum-free or complete media groups at all timepoints ($p>0.05$).

Treatment with 20% ECAS induced a significant cytotoxic effect, as was seen before, with only minimal increases in treated cell confluence observed over the 72h monitoring period, in both complete medium (endpoint confluence $12.25 \pm 2.20\%$ versus $82.49 \pm 3.30\%$ in controls, $p < 0.0001$) and in SF (endpoint $9.29 \pm 0.58\%$ versus $65.40 \pm 15.11\%$ in SF controls, $p < 0.05$). These results support the hypothesis that the inclusion of serum in culture medium mitigates, to some extent, the potential biological effects of unstable reactive components present in the applied treatments, or alternatively serum depletion induces a more potent growth-limiting effect on cells than does the addition of plasma-activated solutions.

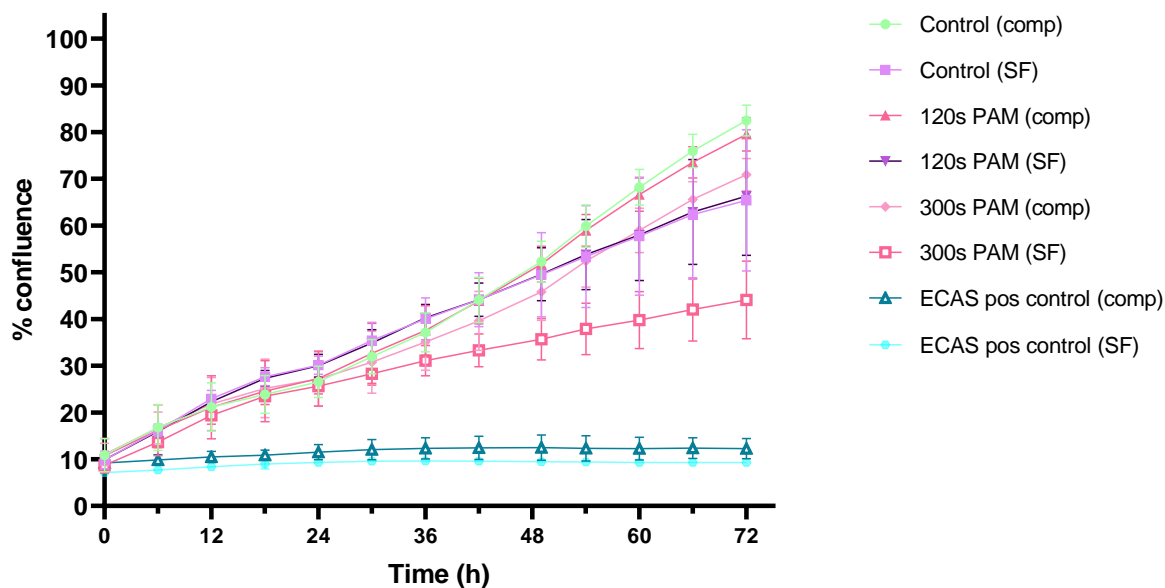


Figure 5.18: 72h growth course of H103 cells treated with 120s or 300s plasma-activated medium (PAM). Cell cultures were seeded in either complete (comp) or serum- and phenol red-free (SF) medium, to which PAM or non-activated SF medium (control) was added in 1:1 ratio. Mean % confluence was calculated from triplicate wells, each imaged using Incucyte® Live Cell Analysis using 9 FOV, analysed by 2-way ANOVA with Dunnett's correction for multiple comparisons, at 6-hourly intervals.

5.7.4 Extended monitoring of the A375 growth response to pPBS

A375 monolayers were treated with freshly activated pPBS, which had been exposed to NTP for 120s or 300s, in a 1:1 ratio with either complete (comp) or SF growth medium, as before. Over the subsequent 72h growth period, 6-hourly image analysis again suggested a slight inhibitory impact of pPBS upon cell growth, with 300s-pPBS treatments producing up to 10.10% difference in confluence relative to controls in complete media, and up to 13.32% deficit in SF-media (both $p > 0.05$), seen maximally at 72h, but not attaining significance (Figure 5.19). With 120s-pPBS, no effect was perceptible in the presence of serum, and only a weak inhibition seen in SF-media, with up to 4.17% deficit in confluence as compared to SF-controls ($p > 0.05$).

Exclusion of serum from the culture medium resulted in a pronounced reduction in cell growth rate universally (figure 5.19), with confluence in SF controls significantly inferior to that of complete-medium controls at 30h to 66h time-points, with a disparity of up to 46.65% ($p = 0.04$) at 169

66h, and respective endpoint measurements of $52.51 \pm 11.87\%$ (SF) versus $98.11 \pm 1.96\%$ (complete) confluence at 72h growth ($p > 0.05$). For the A375 cell lines, 10% ECAS (final concentration) was used as positive cytotoxic control, and elicited clear growth inhibiting effects in both complete and SF groups, with no net increase in cell confluence observed by the final timepoint, and a significant deficit in the 72h population of 85.39% versus control in complete medium, and 42.31% in SF (both $p < 0.0001$).

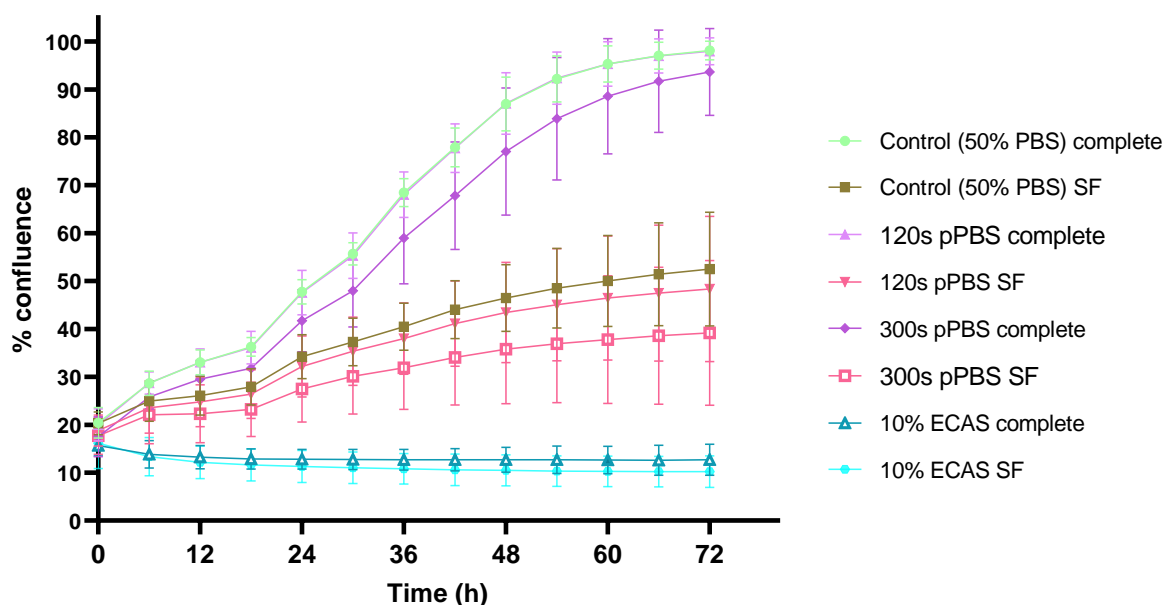


Figure 5.19: 72h growth course of A375 cells treated with 120s or 300s plasma-activated PBS (pPBS). Cell cultures were seeded in either complete (comp) or serum- and phenol red-free (SF) culture medium, to which pPBS or non-activated PBS (control) was added in an equal volume, treating in triplicate. Incucyte® Live Cell Analysis was used for quantification of mean % confluence, using 9 FOV per well, analysed by 2-way ANOVA with Dunnett's correction for multiple comparisons, at 6-hourly intervals; $n=3$.

5.7.5 Extended monitoring of the A375 growth response to PAM

Plasma activation of SF cell culture medium was performed as described, introducing 120s- or 300s-PAM to A375 cells freshly seeded in a 24-well microtitre plate, in a 1:1 ratio with either untreated complete (comp) or untreated SF medium. Analysis of cell confluence revealed a significant reduction with 300s PAM treatments in complete medium, evident within the 42h – 60h post-treatment period, showing a confluence shortfall of up to 13.64% versus complete-medium controls at 48h ($p < 0.05$), but not sustained with equal significance throughout the entire duration of monitoring, with a difference of 9.98% seen at 72 ($p > 0.05$) (Figure 5.20). Treatments with 120s-PAM elicited only modest reductions in proliferation, appearing as a deficit of up to 2.43% (seen at 42h, $p > 0.05$) in complete medium, and up to 7.43% difference in SF-medium (at 72h, $p < 0.05$).

Serum exclusion inhibited growth as was seen previously in pPBS controls, with a disparity of up to 36.10% confluence seen between complete- and SF- controls (noted at 54h growth, $p > 0.05$) (Figure 5.20). The inclusion of 10% ECAS in culture media exerted significant growth-limiting effects, producing a slow decline in confluence observed at all timepoints in complete medium from 6h (12.29% deficit versus control, $p < 0.05$) to the final 72h measurement, where confluence was 85.67% reduced compared to untreated control ($p < 0.0001$). In SF-medium, the cytotoxicity of ECAS was similarly apparent, resulting in a final 55.82% deficit in confluence relative to controls ($p < 0.0001$). The gradual loss of viable cells from the initial seeded population suggests that this concentration closely approximated the IC_{50} threshold for ECAS in A375, in agreement with the calculated IC_{50} values obtained from CTG 2.0 and MTS-PMS assays (6.39%, and 11.63%, respectively).

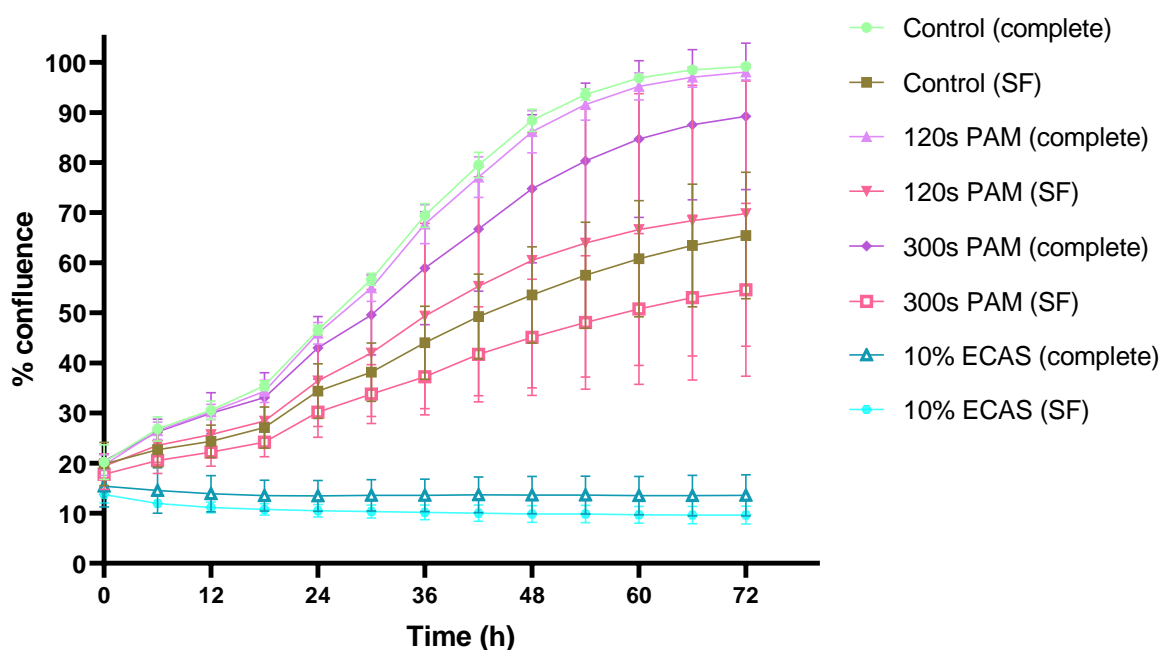


Figure 5.20: 72h growth course of A375 cells treated with 120s or 300s plasma-activated medium (PAM). Cell cultures were seeded in either complete (comp) or serum- and phenol red-free (SF) culture medium, to which pPBS or non-activated PBS (control) was added in an equal volume, to triplicate wells. Incucyte® Live Cell Analysis was used for quantification of mean % confluence, using 9 FOV per well. Analysis of measurements at 6-hourly intervals was performed by 2-way ANOVA with Dunnett's correction for multiple comparisons; $n=3$.

Since plasma treatment is known to induce acidification of aqueous solutions/media (Liu *et al.*, 2018; Simon *et al.*, 2022; Tsoukou, Bourke and Boehm, 2022), the pH of PBS and cell culture medium was measured post-exposure, to ascertain whether a reduction in pH was a potential contributing factor to the inhibitory effects observed on cell viability and proliferation. No acidification of pPBS or PAM was detected upon pH testing of remaining PAS, following cell treatments, with the pH of the former measuring 7.45/7.32, and the latter 7.94/8.07. Although the buffering capacity of PBS appreciably limits any alteration of pH, and the components of the

DMEM culture medium include a sodium bicarbonate buffer would likely have similar effects, the observed reduction in proliferation in both H103 and A375 with exposure to PAM and pPBS suggests inhibitory effects via alternative pathways, potentially by the generation of more stable reactive species generated during NTP treatment, or secondary species. Therefore, detailed species analysis of the plasma-treated solutions, and quantitative measurement of key RONS, including hydrogen peroxide, nitrite and nitrate, would provide critical elucidation of the mechanisms occurring to produce this growth-inhibitory effect.

5.8 Discussion

Through the investigations performed on both H103 and A375 cultures, it was demonstrated that the application of direct NTP was poorly tolerated and induced significant impairment of viability and proliferative capacity, in an exposure-time or plasma 'dose'-dependent manner. Reductions in population viability were discernible even after the shortest exposure time of 30s, in each of the two cell lines, and appeared enhanced by increasing treatment duration to 90s, although viability also decreased with exposure time in argon-controls. Use of single endpoint assays, CTG2.0 and MTS-PMS, indicated that the effects of time-matched NTP and argon-only treatments were similar, findings which may have been influenced by limitations in assay sensitivity, and also relating to the time-frame selected, which may have prevented the detection of delayed treatment-induced effects. Temporal onset and duration of effect has been noted to differ between cell lines subjected to NTP treatments in the research literature (Smolková *et al.*, 2019; Sklias, Sousa and Girard, 2021), which may be attributable in part to the differences in the persistence or stability of plasma-species and the initiation of secondary pathways in the cellular response, but also due to differences in the mode of delivery of NTP, and the assay regime selected.

Treatments in which direct NTP was applied to 24h-seeded cells showed considerable within-group variation in viability at 24 hours post-treatment. The seeding density remained consistent for each respective cell line between experimental repeats, however only 24 hours was allowed for adherence and growth prior to exposure to plasma, at which point cell confluence may not have been equal across all wells of the treatment plate, particularly in the H103 line, due to its slower population doubling time. Additionally, evaporative effects were noted during treatment with both argon and NTP, and were detectable under microscopic observation post-treatment, despite the introduction of 200 μ L PBS as a protective hydrating layer. This drying effect appeared most marked within the central portion of each well (the area directly below the NTP applicator effluent) and likely impacted cellular viability most heavily within this region, although perimeter effects may have occurred to a lesser degree. *In vitro* studies performed elsewhere have similarly

mitigated the evaporative effects of plasma gas flow on mammalian cell viability by the addition of a protective layer of growth medium or PBS during treatments (Kalghatgi *et al.*, 2011; Smolková *et al.*, 2019), however optimisation of this measure varies between sources, and is likely to depend on the specific plasma system configuration and treatment parameters applied. Therefore, any disparities in cell confluence pre-treatment could potentially have augmented the inter-replicate variability seen in post-treatment viability measurements. Inequalities in cell density stemming from seeding inhomogeneity are recognised as a source of error and uncertainty which can lead to skewing of results in *in vitro* assays, affecting growth, differentiation and signalling pathways (Reynolds *et al.*, 2018).

Argon-only treatments also appeared to exert negative effects on viability, but to a milder extent, and extended monitoring via live-cell imaging revealed that net proliferative capacity was sufficient to enable recovery and continued growth over a 72h post-treatment period. Macroscopic and microscopic observations of cells shortly after treatment supported the hypothesis that dehydration and/or physical detachment were in part accountable for this decrease in viable population, but image-analysis demonstrated the regrowth of cells into depopulated areas of treated well, suggesting that cytotoxic effects were not evoked.

Dose-response experiments with antimicrobial agents at concentrations used for therapeutic antiseptics, notably PVP-I and hydrogen peroxide, induced potent cytotoxic effects in both H103 and A375, necessitating modification of the test concentration range to prevent reduction of viability to levels below the limits of accurate detection via the assays used. Determination of the IC₅₀ of PVP-I, a traditional wound- and skin-cleansing antiseptic, and the hypochlorous acid-based product, ECAS, demonstrated similar 50% inhibitory concentrations for povidone-iodine, approximating 0.1% (w/v) for both cell lines, but a slightly greater sensitivity of A375 to ECAS, with a lower IC₅₀ for this product ascertained by both CTG2.0 and MTS-PMS assay (6.39% and 11.63%, respectively, compared to corresponding values of 13.66% and 16.33% in H103). Possibly the more rapid population doubling rate in A375 renders the cells more sensitive to ECAS and PVP-I treatments, both powerful oxidants, in comparison to the H103 line, which shows a PDT slightly over 1.5-fold that of A375.

The markedly reduced cytotoxic thresholds of cells subjected to antiseptic treatments *in vitro* has been demonstrated in studies elsewhere, with repeated or prolonged contact noted to enhance cytotoxicity (Ortega-Peña *et al.*, 2017; García-Valdivia *et al.*, 2022; Ortega-Llamas *et al.*, 2022; Steins *et al.*, 2023). In comparison to living tissue, two-dimensional epithelial monocultures represent a vastly simplified system, lacking the protective stratified structure, extracellular matrix, vascularization, and immune components of skin tissue *in vivo*, which integrates multiple cell types, cell-cell adhesions, and regulatory and signalling pathways (Boehnke *et al.*, 2007;

Lawton, 2019; Biggs *et al.*, 2020). Basic *in vitro* models are therefore more susceptible to the deleterious effects of physical and mechanical stressors, and exposure to toxic compounds, than living skin, itself the largest organ in the human body (Lawton, 2019; Sutterby *et al.*, 2022; Hofmann *et al.*, 2023). Due to these limitations, substantial research capacity has been invested into the development of more advanced laboratory skin models, to provide a more robust basis for the investigation of wound-repair processes and the effects of exogenous treatments (Boehnke *et al.*, 2007; Idrees *et al.*, 2021; Sutterby *et al.*, 2022; Hofmann *et al.*, 2023).

Recent renewed interest in the use of hypochlorous acid-based antiseptics has prompted further investigation and validation of its efficacy and safety as a component of wound-cleansing products (Armstrong *et al.*, 2015; Severing *et al.*, 2019; Dissemond, 2020), providing evidence of the biocompatibility of such solutions in cell cultures, and elucidating their cytotoxicity profiles *in vitro*. As the evidence-base underpinning the potential applications of hypochlorous acid solutions and electrochemical activation technologies increases, supported by high-quality research outputs, the uptake of such solutions into clinical trial and standardised use is also realised. Similar momentum is required in the investigation and development of NTP technologies and plasma-activation processes, in order to elucidate their potential therapeutic effects, and translation into healthcare applications.

5.9: Key conclusions:

The studies undertaken here demonstrate the cytotoxic thresholds of the two experimental cell lines, H103 and A375, when exposed to prolonged contact with traditional topical antiseptics (treatments of ≥ 24 h), and novel antimicrobial treatments, ECAS, direct NTP, and plasma-activated solutions (pPBS, PAW, and PAM). Cytotoxic effects were observed at antimicrobial concentrations several-fold lower than those used clinically, as may be anticipated in *in vitro* cell cultures in which many of the physical and physiological features of the *in vivo* wound bed are omitted. As has been previously highlighted, constructing a laboratory skin wound model which adequately replicates the complex, multi-layered structure of the skin *in vitro* presents substantial challenges, since it is impossible to incorporate the full complement of cell types, circulatory and immune system factors, and associated regulatory and signalling pathways, which co-ordinate tissue repair processes.

The two candidate cell lines used in the studies described were selected as representing epithelial cells of different anatomical origins, and thus enabling comparison of treatment response between two phenotypically distinct cellular populations. The application of topical antimicrobial products to cell monolayers of both H103 and A375 for a 24h period exhibited the poor biocompatibility of ECAS (dilutions from a maximal ≤ 100 ppm FAC stock), H₂O₂ and PVP-I within

concentration ranges demonstrating microbicidal efficacy against planktonic challenge, whilst direct treatments with NTP also produced a marked loss in viability at exposure times of ≤ 90 s. Use of the MTS-PMS assay and CTG 2.0 assay for a post-NTP treatment period of 24h did not reveal a clear trend in cell viability response, with high inter-replicate variability seen, possibly resulting from unequal exposure of cells to the 'active zone' of the NTP effluent.

Extended monitoring of NTP-treated cell populations for 72 hours post-exposure showed a clear deficit in viability with respect to untreated controls, an effect which was significant over a number of time-points, appearing to correlate with NTP exposure time, and persisting to the end of the monitoring period. This depression in viable population and growth rate was more pronounced in A375 cells (showing a confluence deficit of $\leq 74.8\%$ versus control, $p < 0.001$) than H103 ($\leq 51.6\%$ confluence deficit, $p < 0.05$), inferring a greater susceptibility to NTP-induced damage/ cell death. In contrast, exposure to argon alone did not produce significant impairment of population growth, resulting in smaller deficits in cell confluence as compared to controls, an effect which was slightly more marked in A375 than H103 (with reductions in confluence of 23.16% and 12.29%, respectively, $p > 0.05$), with signs of recovery evident towards the latter stages of the monitoring period.

To investigate the effects of indirect NTP treatment, thereby bypassing the physical trauma exerted upon cells during exposure to the pulsed NTP/gas flow during direct treatments, fixed volumes of PBS a cell culture medium were subjected to exposures of up to 300s using the RF-MW plasma generator, and were applied to cell cultures over an extended time period of 72 hours in complete or serum-free medium. A significant reduction in viable population ($\leq 11.59\%$ confluence deficit, $p < 0.05$) was noted in treatment of H103 with 300s-plasma activated medium (PAM), although this was seen in the serum-deprived group, where tolerance to PAM may have been impacted by the addition of a secondary stress factor. Treatments applied to A375 elicited a significant reduction in cell confluence with 300s PAM in complete medium, ($\leq 13.64\%$ deficit, $p < 0.05$), with a smaller effect of 120s PAM seen in SF medium (up to 7.4% confluence deficit, $p < 0.05$). Thus plasma-treated growth medium appeared to induce mild cytotoxic effects on cell viability and proliferation in both cell lines, an effect seen more clearly with medium subjected to the longer plasma-activation time.

ECAS was included as a positive cytotoxic control in extended monitoring studies (using 20% (v/v) ECAS against H103, equating to approximately 40ppm FAC, and 10% (v/v) against A375, or approximately 20ppm FAC), which produced an early and sustained cytotoxic effect in both cell lines, preventing any significant proliferative activity over the full duration of the study period. This finding was not unexpected, since the dose of ECAS applied to each cell line surpassed the IC_{50} derived for this product in dose-response testing.

The findings obtained therefore indicate low tolerability of the antimicrobial treatments investigated within concentration ranges which might be therapeutically applied for antiseptics in the cleansing of wounds during clinical management *in vivo*. Direct treatment with NTP also exerted negative effects on cell viability at 24h post-exposure, whilst indirect NTP treatment via plasma-activated PBS or cell-culture medium was seen to result in decreased levels of total population viability over the 72h post-treatment period. Differences in population doubling time between the two cell lines, and potentially disparities in metabolic activity, and anti-oxidant- or general stress-response pathways may have been contributory factors in the determination of sensitivity to direct and indirect NTP treatment in each cell line respectively. To more comprehensively elucidate NTP-mammalian cell interactions using *in vitro* approaches in future work, it would be beneficial to undertake a broader array of cell-based analyses, measuring biomarkers of oxidative stress and apoptosis induction, and also to determine the transcriptomic response to short exposures and more prolonged indirect treatments, as well as the capacity for recovery. These areas of investigation would be important to examine both in simple cell monocultures, and in more complex co-cultures, and three-dimensional cell culture systems.

Chapter 6: Summary of conclusions and final discussion

6.1 Alternative antimicrobial technologies: addressing the need for innovation

Even as the reporting of antimicrobial resistance improves, the spread of pathogenic AMR strains continues to pose a major threat to human and animal health, and together with the dangers of exhausting treatment options for the increasing incidence of healthcare-associated infections involving AMR, the urgency of this global health problem is becoming clearer (O'NEILL, 2016; Storr *et al.*, 2017; Tacconelli *et al.*, 2018; Tacconelli and Pezzani, 2019; Guest *et al.*, 2020; WHO, 2020). Along with the need for the advancement of diagnostic technologies, to enable more rapid and precise identification of infection-causing pathogens and thereby the selection of the most appropriate treatment choices, it is vital that novel antimicrobial interventions are sourced – for both prevention and intervention against established infection, where traditional antibiotics are becoming ineffective. Non-thermal energy technologies, such as cold atmospheric plasma or NTP, and electrochemical activation systems, represent fertile grounds for inter-disciplinary research and collaboration, and which could accelerate the development of novel antimicrobial solutions to meet current critical needs.

The research presented here aimed to investigate the antimicrobial effects of two non-thermal energy technology systems – non-thermal plasma (NTP) generation, and electrochemical activated saline (ECAS) generation – in the context of pathogenic microbial contamination, including bacterial biofilms, and to evaluate their antimicrobial efficacy and cytotoxicity, in comparison to currently-used standard solutions.

6.2 Relevance to the development of potential applications of NTP in healthcare

Over the past two decades, there has been resurgence of interest in the field of non-thermal plasma and its application in biomedicine and health, with particular emphasis on the areas of microbial inactivation, wound-healing, and cancer therapeutics (Fridman *et al.*, 2008; Metelmann, von Woedtke and Weltmann, 2018; Privat-Maldonado *et al.*, 2019; Choi, Uhm and Kaushik, 2021). Although the proposed mechanisms of action induced by NTP are diverse, and are intrinsically related to the particular configuration of each generating system, the principal determinants of the biological activity of NTP are the combined reactive oxygen and nitrogen species, excited gas species, energised electrons, free ions, and electromagnetic radiation, including UV and visible light (Dobrynin *et al.*, 2009; Chen *et al.*, 2014; Babaeva and Naidis, 2018; Metelmann, von Woedtke and Weltmann, 2018).

The direct application of NTP, as well as its exploitation via indirect methods, using plasma-activated liquids, is the focus of intensive research, in biomedical, engineering and physics

specialisms, as a means of stimulating or inhibiting particular biological pathways, developing advanced materials, or modifying chemical processes (Gupta and Ayan, 2019; Šimončicová *et al.*, 2019; Katsigiannis, Bayliss and Walsh, 2021). Although developments in applied NTP research have led to the successful engineering and production of marketable plasma devices for medical purposes, the use of such technologies remains relatively limited. To substantiate the evidence-base for NTP-based therapeutic applications, continued efforts must be made, with collaboration between scientific, engineering and clinical sectors, to provide robust research outputs and establish a road-map for the advancement of these technologies. The establishment of the 'Plasma Roadmap', a forum integrating knowledge and expertise, research developments and technological innovation in the field of low-temperature plasmas and their applications, has already provided a vital resource for the plasma specialist community, promoting a more unified platform for discourse and dissemination of research in this field, between all disciplines (Adamovich, *et al.*, 2022).

6.2.1 Outcomes of microbiological investigations into the effects of NTP

With regard to microbial decontamination and antisepsis, NTP has been demonstrated to induce rapid, broad-spectrum inhibitory effects against several clinically-relevant microbial species, in planktonic form and also within biofilms (Alkawareek *et al.*, 2014; Scholtz *et al.*, 2015; Czapka, Maliszewska and Olesiak-Bańska, 2018; Gupta and Ayan, 2019). In the studies undertaken here, the efficacy of direct plasma treatments using a prototype RF-MW NTP system, was evaluated, testing against microbial species frequently implicated in clinical infections and the contamination of medical equipment and environments.

Antimicrobial testing, using surface-associated planktonic targets, and microbial biofilms, revealed significant effects when NTP treatments were applied directly, although microbial inhibition was demonstrated to be dependent on plasma exposure-time, as has been observed in studies elsewhere (Joshi *et al.*, 2010; Alkawareek *et al.*, 2014). ZOI experiments indicated that the size of the inhibited area of microbial growth, reflecting the plasma 'active zone', increased as a function of the duration of treatment, within the parameters tested. Findings reported elsewhere have also ascertained a time-dependence of plasma ZOI on microbial lawns, cultured on solid and semi-solid agar, but determined that a maximum area of effect may be reached, which cannot be increased with further prolongation of treatment beyond a certain exposure time (Nicol *et al.*, 2020). The maximum exposure time used in testing against planktonic microbial challenge in the work presented here did demonstrate the most marked effect, in terms of growth inhibition in all but one of the species tested (data obtained from *C. albicans* cultures suggested a time-dependent enhancement of effect, but this was not statistically significant).

Some interspecies differences were noted, with *S. aureus* appearing more tolerant of NTP treatment than *P. aeruginosa* when in planktonic form, but biofilm testing allowed for more limited comparisons, due to the more abundant biofilm-formation and resilience in this form demonstrated by *P. aeruginosa*, which has been noted in studies elsewhere (Cheng *et al.*, 2019; Soares, Alexandre and Etienne, 2020; Rippon *et al.*, 2023). Nonetheless, some small inhibitory effects of NTP were noted in *P. aeruginosa* CBR biofilms. Despite some indirect plasma treatment, through the generation of plasma-activated water (PAW), failed to show a consistent microbicidal effect against either planktonic microorganisms or biofilms, although comparisons were limited due to differences in the processes used for PAW-production. The alternative (aqueous) antimicrobial solutions tested were shown to achieve superior antimicrobial efficacy, when applied at maximal test doses.

6.2.2 Outcomes of investigations into the effects of NTP on eukaryotic cells

The delivery of NTP treatments to two mammalian epithelial cell lines (H103 and A375) was also investigated, using both direct and indirect modes of application. Direct treatments induced a loss of viability in both cell lines, an effect which was not solely attributable to the dehydrating effect of the carrier gas flow (argon) used in generating the NTP, although some reduction in cell survival was also noted in gas-only controls. Indirect NTP treatments also appeared to cause moderate cytotoxic effects, when applied in the form of plasma-activated- PBS (pPBS) or cell culture medium (PAM) produced by RF-MW plasma-exposure, although this effect was not significant throughout the entire duration of cell-monitoring. However, both cell lines demonstrated a significant reduction in population viability in treatments with 300s-activated DMEM, when applied to cells seeded in complete culture medium, causing decreases in population growth of up to 11.59% (H103) and 13.64% (A375). However, the continued proliferation of cells following treatment application indicated some capacity to recover from the effects of indirect NTP, or a decline in cytotoxic effect with time, possibly due to diminishing concentrations of key reactive species through decomposition, or through the quenching effects of certain components present within the cell culture medium.

6.2.2.1 Direct versus indirect NTP treatment of mammalian epithelial cells

The effects of NTP, delivered both directly and indirectly, may have been somewhat mitigated by the presence of antioxidant components and buffer systems within the culture medium, such as pyruvate, as DMEM has been noted to possess greater antioxidant potential than RPMI, for example, therefore some of the reactive species generated within plasma-treated medium may have been quenched to some extent (Wende *et al.*, 2014, 2016). This process has been proposed as a possible explanation for the suspected loss of reactivity of more complex substrate solutions subjected to plasma treatment, and highlights the importance of optimising the treatment

medium and plasma delivery parameters in order to increase the activation potential of indirect plasma treatments (Sklias, Sousa and Girard, 2021).

Use of the SBD plasma generation system was advantageous in that it enabled large-volume NTP to be produced and simultaneously activation of greater volumes of liquid (15mL – 500mL, as opposed to the 6mL treated using the RF-MW system). Additionally, in place of a continuous supply of inert gas, which carries substantial costs and is a finite resource, humid air served as the transport medium between plasma effluent and target liquid volume, but also acted as a limiting factor in terms of the extent of diffusion of reactive species into the exposed water.

Previous research investigating the species generated using the SBD-falling film system deployed for producing large-batch PAW has demonstrated the evolution of RONS including nitrous oxide (N_2O) and ozone (O_3) in the plasma gaseous phase, which may be quenched by the presence of NO to form the highly soluble nitrogen dioxide (NO_2), and molecular oxygen (O_2) (Jabbariesgandani and Walsh, 2023). Within the aqueous phase, only the longer-lived species capable of diffusing across a greater distance were detectable, including nitrites (O_2^-) and nitrates (O_3^-), with the former likely to undergo oxidoreduction with ozone leading to the formation of more nitrate, although the relative proportions of both gaseous and aqueous phase plasma species may be significantly affected by operating parameters, including the applied voltage, treatment time, and mixing of ambient air within the reactor. Therefore, although the PAW generated by this system and used in antimicrobial and cell line treatments was produced using consistent conditions, the highly reactive properties of many of the oxidative species emitted and absorbed into the bulk liquid, and delay period between PAW generation and its application in experiments, likely contributed to a substantial change in physicochemical profile.

6.3 Relevance of this work to the field of electrochemical-activation technologies for application in healthcare

Despite long-standing knowledge of the processes involved in electrolytic- or electrochemical-activation of solutions, and their use for the production of biocidal solutions, technologies employing such processes for antimicrobial disinfection have only relatively recently become the focus of dedicated research and development (Lee, 2010; Thorn *et al.*, 2012; Reis *et al.*, 2021; Yan, Daliri and Oh, 2021). The electrolysis of low mineral saline solution, when current is applied to an immersed electrochemical cell immersed therein, initiates the generation of activated meta-stable chemical species, with distinct reactions occurring within the anodic and cathodic zones, resulting in the production of highly oxidising and highly reducing solutions, respectively. The antimicrobial potency of these solutions, dependent on their specific physicochemical profiles,

and the economical and efficient means of production, which demands only low input resources and generates biodegradable, nontoxic by-products, marks them out as an attractive alternative to many of the alternative biocidal products currently available, which are often limited by issues such as the generation of toxic residues, or harmful effects such as cytotoxicity, or irritant properties (Rahman, Ding and Oh, 2010; Ding *et al.*, 2016; Rasmussen, 2020; Chen and Wang, 2022). Furthermore, electrochemical activation of solutions for topical application as a cleansing agents for skin or wounds, has gained momentum, with a number of products now commercially available and used clinically (Severing *et al.*, 2019; Yan, Daliri and Oh, 2021; Esin *et al.*, 2022). The principal active compound, hypochlorous acid (HOCl), is an endogenously-occurring antimicrobial compound, produced by leukocytes during the oxidative burst response to injury and pathogen invasion (McKenna and Davies, 1988; Block and Rowan, 2020; Dissemond, 2020), therefore its mechanism of antimicrobial action is well-understood, and provides a rationale for its use in formulations for its use in clinical antiseptics (Sakarya *et al.*, 2014; Veasey and Muriana, 2016; Swanson and Angel, 2017; Dissemond, 2020).

In vitro evidence of cytotoxic effects has, however, raised concerns over the safety of electrochemically-activated solutions, particularly in the context of wound-care, where the interruption of cellular proliferation and migration would critically impair wound repair processes (Reis *et al.*, 2021). In addition, the efficacy of HOCl-based solutions in antimicrobial susceptibility testing has been variably reported, depending on the species investigated, concentration range applied, and experimental model used (e.g. as a planktonic culture, or within biofilms), amongst other parameters (Veasey and Muriana, 2016; Severing *et al.*, 2019; Rembe *et al.*, 2020; Wilsmann *et al.*, 2023). Differences in methodological approach and specific objectives have therefore contributed to a lack of broader consensus regarding the application of electrochemically-activated solutions, and their relatively infrequent use in the healthcare sector.

6.3.1 Outcomes of microbiological investigations into the effects of ECAS

Investigations were conducted here to ascertain the inhibitory effects of ECAS when applied to microbial targets, on contaminated abiotic surfaces, in suspension, and on single-species biofilms, with comparisons made to existing alternative topical antimicrobials. Results performed on planktonic microbial loads, both upon dried inoculated surfaces, and in suspension, showed a strong and almost absolute antimicrobial effect. Non-porous surface disinfection tests showed a reduction of surface-associated *S. aureus* to sub-detectable levels at contact times as short as 30s, demonstrating comparable antimicrobial efficacy to that of PVP-I (which was similarly effective at 5% and 10% concentrations), and a more efficient microbial reduction than that of hydrogen peroxide (3% or 6% strength). However, a low number of survivors were encountered during a longer treatment with ECAS, indicating that microbial inactivation was not uniformly exerted. Further investigation would be necessary to determine whether this was a reproducible finding.

Suspension tests demonstrated elimination of viable load using ECAS concentrations of $\geq 50\%$, i.e. a 40% (v/v) strength in the final test suspension (equating to 80-88ppm FAC) when applied for 300s exposure time. Therefore, ECAS was shown to be highly effective against both *S. aureus* and *P. aeruginosa* when applied to microbial loads in the form of suspension, without the addition of interfering substances.

6.3.2 Outcomes of investigations of the effects of alternative antimicrobial products in eukaryotic cells: results obtained with ECAS and PVP-I

ECAS treatments were also applied to two mammalian cell lines (as used in NTP testing), to measure the cytotoxic response and effects on cellular proliferation over longer contact periods, as a means to characterise the possible therapeutic range of concentrations and exposure times at which such antimicrobial products might be used. ECAS treatments for contact periods of 24h demonstrated significant toxic effects on both H103 and A375 cell lines, with an IC_{50} of 13.66% according to CTG2.0 assay, and 16.33% by MTS-PMS assay. In A375, there appeared to be slightly higher sensitivity to ECAS, with IC_{50} of 6.386% calculated via CTG2.0 and 11.63% using MTS-PMS assay.

PVP-I also showed significant cytotoxic effects within the concentration range tested, with close concordance on IC_{50} derived from CTG2.0 and MTS-PMS assay, with a reported 50% inhibitory dose in H103 of 0.1056% and 0.0759% from the two assays, respectively. The IC_{50} for PVP-I in A375 appeared similar, with 0.0688% as calculated from CTG2.0 assay, and 0.9088% from MTS-PMS. These results illustrate the cytotoxic sensitivity of both epithelial cell lines to treatment with clinically-relevant antimicrobials at concentrations which are, in the case of PVP-I, at least 10-fold lower than those applied for therapeutic antiseptics. The IC_{50} obtained for ECAS, although not as easily comparable to in-use concentrations (as hypochlorous acid solutions have yet to be widely standardised in clinical recommendations) are within a similar to those reported in *in vitro* cytotoxicity testing performed elsewhere on electrolytically-activated water (Reis *et al.*, 2021).

6.4 Challenges in the design and realisation of a physiologically representative *in vitro* wound-biofilm model

As has been acknowledged widely in the literature centred upon the study of biofilms, and antimicrobial technologies, the relative simplicity of laboratory biofilm models (even those of a more advanced configuration, as described above) and the absence of several physiological parameters, including signalling factors, immune response mediators and secreted components, places significant limitations on the clinical relevance and translatability of results obtained from such experimental models. The application of anti-biofilm treatments to a closed system *in vitro*

can be advantageous in terms of evaluating the effects on microbial viability via defined measures, and quantifying any inhibitory effects, however such systems are limited in their longevity (the capacity to maintain biofilms and administer repeated treatments over extended periods of time, reflecting recalcitrant biofilm infections *in vivo*, is restricted in most models), and often the diversity of microbial strains used (clinical isolates are often not selected, and even when such strains are used, substantial variability in susceptibility has been demonstrated, which could potentially skew/ confound results obtained). Therefore, notwithstanding the importance of accruing robust evidence of the effects and interactions of novel microbicidal agents upon laboratory-based biofilm platforms, the comparative efficacy of such interventions when applied in a vastly more complex system, such as the wound microenvironment in a living organism, will be subject to a myriad of complicating factors and likely show a reduced or dampened effect (Vyas, Xia and Mai-Prochnow, 2022).

Over the last few decades, the need for improved scientific and technological approaches for the investigation of microbial systems, in particular biofilm modelling, has led to a wealth of innovative devices and constructs, enabling more accurate simulation of biological milieus occurring in the environment, industry, and healthcare settings. Equally, in tissue-based research, the translation of toxicological findings obtained *in vitro* to the predicted effects with their clinical use, *in vivo*, is hindered by the greatly increased sensitivity of cultured mammalian cells to biocidal compounds when applied directly to simpler laboratory models, such as cell monolayers (Madorran *et al.*, 2020; García-Valdivia *et al.*, 2022; Ortega-Llamas *et al.*, 2022). Therefore, the determination of IC₅₀ values, though a valuable relative measure of cytotoxic response in model cell lines, provides only a preliminary indication of the possible effects of test substances in living tissue, e.g. human skin, where increased structural and functional complexity between the multiple cell types play integral regulatory and protective roles (Lawton, 2019). The need for more physiologically-appropriate laboratory skin and wound models, to aid the understanding of wound repair and infection processes, and to serve as a testing platform for therapeutic interventions has been recognised, and has stimulated research developments in this area (Ojeh and Navsaria, 2014; Kadam *et al.*, 2019).

Challenges abound in recreating a microbial-mammalian co-culture system as a surrogate model for clinical wound infection, since key physiological components of the wound environment are lacking, such as humoral factors – immune signalling factors, inflammatory mediators including neutrophil- and macrophage, and other blood-borne constituents - and also the continuous secretion of serous wound exudate, which supplies nutrients and hydration to the pathogens colonising the affected tissue, and also serves to dilute or neutralise, to some extent, any (topically) applied antimicrobial treatments (Cutting, 2003), as well as aiding dispersion of microbial cells from the primary infection site to another location. Therefore, caution must be

taken in interpreting the efficacy of any novel antiseptic or microbicidal substance observed in *in vitro* systems, since there is likely to be a substantially diminished effect in the far more complex *in vivo* setting. Furthermore, the cytotoxic index observed in simple mammalian cell culture systems can only provide a preliminary basis for the determination of toxicological effect in a living system, particularly in 2D mono-culture models grown upon an abiotic surface, which fails to replicate an *in vivo*-like milieu (Kadam *et al.*, 2019).

6.4.1 Co-culture models:

There are inherent challenges involved in designing and successfully operating an *in vitro* system incorporating both microbial and mammalian cell population simultaneously, although a number of co-culture models have been conceived. Introduction of single-species or multi-species microbial suspensions to mammalian cell line monolayers cultured in microtiter plates represents one approach, and has clearly shown the rapid decline in eukaryotic viability when challenged with microbial infection, resulting in a limited time-frame for meaningful experimentation (Çelebi-Saltik and Kart, 2021; Krasowski *et al.*, 2021). Indirect exposure of mammalian cells can be performed by incubation with biofilm-conditioned medium, obtained via the growth of microbial biofilms upon removable tissue-culture inserts, allowing soluble biofilm-secreted factors to be extracted and exposed to eukaryotic cell lines cultured separately (Çelebi-Saltik and Kart, 2021), although this format clearly provides limited simulation of a true co-culture, excluding the biofilm cellular component of a more holistic wound model.

Bacterial cellulose carriers (BCC) have been used to study the effects of microbicidal treatments on biofilms adhering to a 3D cellulose construct pre-populated with eukaryotic cells, frequently a fibroblast cell line, allowing evaluation of both biofilm and mammalian cell viability in a more complex arrangement than simple monolayer monoculture formats (Krasowski *et al.*, 2021; Paleczny *et al.*, 2023). Incorporation of both microbial and mammalian cell elements within a more complex, three-dimensional scaffold provides a more authentic wound-like environment in several respects than that of microtiter culture plates or tissue culture vessels, which offer very homogeneous growth conditions, and poorly mimic the structure of living tissue. Cellulose carrier-associated biofilm/ mammalian cell line co-cultures offer experimental utility for the investigation of biofilm attachment and proliferation upon a 'tissue-like' cellular/hydrogel substratum, and the effects of antimicrobial interventions to be evaluated. However, this configuration still represents a relatively simplified co-culture system, which may be limited in terms of experimental durability, considering the difficulties of maintaining cell line viability in the face of rapid expansion of the microbial component. The chief uses of BCC models therefore tend to be for investigating biofilm growth and their susceptibility to antimicrobial regimes, rather than the elucidation of mammalian cell responses and cytotoxicity thresholds.

Microfluidic devices offer a miniaturised flow system to be deployed, allowing investigation of the biofilm response to delivery of treatments via a dynamic (flow) system. The introduction of a low shear force, such as the steady flow of medium over the biofilm-colonised surface, more accurately recreates the *in vivo* growth environment of many clinically-occurring biofilms, such as those occurring in non-healing wounds, in device-associated infections, and in oral biofilm infections. Not only does this constant flow of media simulate the serous secretions occurring within a wound (Werthén *et al.*, 2010), which are simultaneously beneficial to the healing process and promote the proliferation of invading microbial species, but also influences microbial adhesion within the device, and prevents the accumulation of waste products, and may dilute concentration of any antimicrobial compounds introduced into the system.

It has been acknowledged in studies seeking to evaluate the anti-biofilm activity of antiseptics and antimicrobial cleansing products that results obtained using *in vitro* biofilm models frequently show significant variability, depending not only on the experimental design and culture parameters under which microbial biofilms are grown, and the duration of culture, but also upon the particular strains selected for testing. Since the more advanced biofilm systems generally better replicate the intrinsic *in vivo* conditions of a chronic wound, the discrepancies in reported biofilm eradication or reduction derived using more complex models, are perhaps to be expected (Vyas, Xia and Mai-Prochnow, 2022; Paleczny *et al.*, 2023).

6.5 Areas for investigation in future work:

As has been mentioned, a substantial array of different NTP-generation system configurations has been developed and used in the published works in the field of plasma science. Furthermore, operating parameters and treatment delivery regimes are equally varied, therefore, accurate characterisation and reporting of the generator utilised in each body of work is of great importance to advancing the development of algorithms for optimal use in relevant applications. In particular, it would be highly beneficial to perform species analysis of the component emitted in the NTP-effluent, and of the species generated within plasma-activated liquids, produced using the same system. This would also allow further comparison to be made between the species profiles of different generating systems, aiding optimisation of their design and appropriate application.

Additionally, it would be important to characterise the compatibility of plasma treatment with application upon different surfaces, to discern whether modifications to surface chemistry are induced, and to study any resultant effects on microbial adhesion and colonisation, another avenue of research which has not been touched upon in work carried out here (Modic *et al.*, 2019; Akdoğan and Şirin, 2021). Plasma pre-treatment of different surface materials could offer

the possibility of functionalising surfaces as a means to infection prevention and control in the healthcare environment.

Since the induction of oxidative stress is a fundamental cellular response common to both NTP and ECAS modes of action, it would be pertinent to investigate the transcriptional response to treatments with both direct and indirect plasma and ECAS, to decipher the changes in gene expression and proteomic fingerprint, as has been undertaken by several research groups in recent works (Ma *et al.*, 2014; Schmidt *et al.*, 2015, 2019; Privat-Maldonado *et al.*, 2019). Evaluation of the effects on markers of inflammatory activation, and on wound-healing repair pathways, would also be vital in the development of NTP and ECAS technologies for wound-care. In particular, it would be relevant to examine changes in response via the *in vitro* wound scratch assay (Lou *et al.*, 2020; Reis *et al.*, 2021), which unfortunately was not covered in the scope of this research.

It would also be of particular interest to compare oxidative responses and markers of apoptosis induction in malignant cancer cells to those of non-cancerous counterparts, since cancer-selective cytotoxic effects of NTP have been variously reported in the literature (Ma *et al.*, 2014; Kaushik *et al.*, 2015; Choi *et al.*, 2017; Han *et al.*, 2017; Mateu-Sanz *et al.*, 2021). This increased sensitivity to oxidative stress has been attributed to the saturation of tumour cells' anti-oxidant capacity, due to their elevated basal ROS production, although consensus has not been reached on the exact mechanisms by which cancer cell death is induced, or on the most effect means of plasma-treatment (Smolková *et al.*, 2019; Feil *et al.*, 2020; Sklias, Sousa and Girard, 2021). Exploring the relevance of NTP in cancer biology is already ongoing, but clearly this is a field of substantial magnitude and complexity, therefore the potential applications of NTP and/ or ECAS would likely be affected by a host of factors, such as cancer type, tumour phenotype, and genotype.

6.6 Translatability of *in vitro* research findings to clinical applications:

6.6.1 Considerations in evaluating the suitability of novel antimicrobial treatments

6.6.1.1 NTP technologies

As highlighted widely within the field of antimicrobial research and development, not only must microbicidal products intended for use in healthcare environments demonstrate efficacy against a range of relevant test microorganisms when tested under prescribed laboratory conditions, and the absence of any cytotoxic effects at concentrations to be used in the clinical setting, the mode and frequency of application must also be practicable, affordable and sustainable. Results obtained in work undertaken here indicate that significant reconfiguration or further development of the RF-MW NTP system would be necessary in order to achieve a design that

could achieve greater antimicrobial kill against planktonic microbial loads, but particularly against microbial biofilms, which represent a more intractable source of contamination and infection in working healthcare environments.

Certain aspects of the RF-MW NTP generator used in the work reported here would be disadvantageous in transitioning the technology in its current state to clinical use, necessitating reconsideration were this particular design to be developed further, for large-scale use. One such aspect which would be limiting in terms of cost-effectiveness and practicality, is the requirement for argon as a carrier gas, since this is an expensive resource, and in physical terms, the need to accommodate pressurised gas container in proximity to the NTP generator would hinder its portability and prevent its use in space-limited areas. Another fundamental issue is the very short-range of activity of the plasma effluent (as evidenced by zone of inhibition studies, and to an extent, cytotoxicity testing, where plasma effects appeared localised to a limited portion of the treated cell population). This limited zone of effect would require close proximity of the target surface or tissue to the NTP applicator, in order to ensure adequate exposure, and adequately capture the effects of the plasma effluent species.

6.6.1.2 Electrochemically-activated solutions

ECAS-based antimicrobial products could, in contrast, represent a more promising alternative, due to its more rapid and efficacious microbicidal activity, both on planktonic microbial deposits and biofilms, its low-cost generation system and low input requirements, and the comparative ease of use – being an aqueous product, allowing its application as an irrigant or wound-wash, or incorporated into dressings, hydrogels, ointments or other wound-care products which may be easily applied for the required contact time, at a quantifiable dose or concentration (Severing *et al.*, 2019; Alihosseini *et al.*, 2023). The antimicrobial activity of electrochemically-activated solutions is attributable to their physicochemical characteristics and the high levels of freely available chlorine (FAC), deriving from hypochlorous acid, and (to a lesser extent, at the acidic pH typical of ECAS anolyte) its dissociation to form hypochlorite and hydrogen ions (Severing *et al.*, 2019; Wilsmann *et al.*, 2023). The ability of HOCl to penetrate the cell wall via passive diffusion, and to interact with intracellular components, including nucleic acids and enzymes, causing oxidative damage and critical perturbation of transport and respiratory processes, accounts at least in part for the microbicidal effects of electrochemically-activated solutions (Wilsmann *et al.*, 2023).

Commercially available ECAS-based products are currently marketed as wound-cleansing and irrigating solutions, intended for use on moderately-infected wounds and as a preventative against the development of infection, where the bioburden is relatively light (Severing *et al.*, 2019), but the efficacy of such agents against chronic wound-associated biofilms has not been

widely established. In the investigations performed here, ECAS (applied as a 200-200ppm FAC solution) exhibited significant and rapidly-acting microbicidal efficacy against surface-dried planktonic loads, achieving Log reductions of ≥ 6 Log, however it showed much weaker inhibitory activity against mature *P. aeruginosa* CBR biofilms on silicone and steel substrates, producing reductions of <2 Log and <3 Log respectively, therefore leaving a substantial proportion of viable microbial load adhering upon treated surfaces. The inhibitory effects observed here with ECAS treatment against *Pseudomonas* CBR biofilms were, however, comparable to those achieved with 10% PVP-I and 6% hydrogen peroxide, two traditionally used antiseptic agents which have proven effective antimicrobial activity *in vivo*, but which have shown cytotoxic effects when applied to mammalian epithelial cell cultures *in vitro* (García-Valdivia *et al.*, 2022; Rueda-Fernández *et al.*, 2022) and chondrocyte, synoviocyte and tenocyte cultures, when applied separately and in combination (Romano *et al.*, 2022), demonstrating the potential to impair cell viability and proliferation. In addition, it would be important to determine the efficacy of ECAS against microbial challenge in the presence of an interfering substance, since the activity of numerous microbicidal agents can be significantly impaired by organic soiling, particularly proteinaceous deposits, and effect which has been illustrated experimentally elsewhere with ECAS (Veasey and Muriana, 2016), attributed to the reducing effect of organic contaminant substances on the reactive species of ECAS, before their microbicidal effects can be exerted upon the target pathogens.

Studies elsewhere have demonstrated low anti-biofilm efficacy of HOCl-based products against more complex, 3D biofilm models, such as bio-cellulose biofilm carriers, where negligible reductions in viable load have been achieved using products applied at FAC levels of 80 – 100ppm, (Severing *et al.*, 2019; Krasowski *et al.*, 2021) against single species biofilms, including those of clinical isolates of *P. aeruginosa*. Application of HOCl-based antiseptic (80ppm FAC) to mature 72h *P. aeruginosa* biofilms in a porcine skin explant model similarly showed poor efficacy (achieving 0.77 Log CFU/mL reduction) when used at clinically-relevant contact times (15 minutes), illustrating the enhanced resilience and recalcitrance of biofilms when grown in a more complex, physiologically-representative environment (Johani *et al.*, 2018). Thus, it is evident that more aggressive treatments, incorporating greater FAC concentrations and higher oxidizing potential, and/ or more prolonged treatment times are needed to produce significant inhibitory impact, even on *in vitro* biofilm models, indicating that clinical wound biofilms would require still more efficacious antiseptic applications, likely as part of a multi-modal approach, to maximise the reduction of bioburden by physical as well as pharmacological means.

6.7 Concluding remarks:

Through the investigations presented here, the performance of NTP treatments and ECAS in antimicrobial testing, and in the assessment of cytotoxicity in human cell lines, have been evaluated. Antimicrobials with a longer history of use have served as relevant comparators, in testing against planktonic microorganisms and microbial biofilms. Evidence of a more rapid inhibitory effect was seen against planktonic loads, using a representative for both Gram-positive and Gram-negative pathogenic bacteria. Efficacy tests performed on laboratory biofilm models clearly demonstrated the increased biocidal tolerance of these more complex microbial consortia, with the clinical antiseptic agent PVP-I surpassing the other comparator treatments included in this study, yet achieving a much-reduced effect in relation to that seen in applications against planktonic challenge. Three-dimensional wound biofilms, cultured under low shear flow and subjected to single-immersion treatments or repeated instillation of aqueous antimicrobial treatment, to simulate antiseptic wound irrigation, inferred a still greater degree of tolerance. Collagen matrix-associated *P. aeruginosa* biofilms subjected to ECAS treatments appeared to show a dose-dependent response to successive instillations, but also indicated some degree of neutralising effect - potentially a result of residual organic components interacting with key oxidising species within the ECAS, with the progression of flow over the biofilm.

Eukaryotic dose-response studies did not provide supportive evidence for the biocompatibility of antimicrobial treatments when applied within concentration ranges capable of establishing an antiseptic effect against microbial contamination, since cytotoxic thresholds were exceeded during the 24h contact period. Direct plasma treatments appeared to cause significant dose-dependent effects (dose being derived from exposure time) in both cell lines tested, whilst treatments with plasma-activated medium also induced significant reductions in population viability over a 72h treatment period, an effect which appeared to be compounded with serum-deprivation.

Further characterisation of the spectrum of activity, time-to-kill, and specific modes of action of the non-thermal energy technologies tested here would support advances in our understanding of the mechanisms by which their effects are exerted, in both prokaryotes and eukaryotic cells, and where their use in healthcare applications may be most relevant.

References

- Abreu, A. C. *et al.* (2013) 'Current and emergent strategies for disinfection of hospital environments', *Journal of Antimicrobial Chemotherapy*. doi: 10.1093/jac/dkt281.
- Adamovich, I, Agarwal, A, Ahedo, E, Alves, LL, Baalrud, S, Babaeva, N, Bogaerts, A, Bourdon, A, Bruggeman, PJ, Canal, C. (2022) 'The 2022 Plasma Roadmap: low temperature plasma science and technology', *Journal of Physics D: Applied Physics*, 55(37), p. 373001. doi: 10.1088/1361-6463/ac5e1c.
- Akdoğan, E. and Şirin, H. T. (2021) 'Plasma surface modification strategies for the preparation of antibacterial biomaterials: A review of the recent literature', *Materials Science and Engineering C*. doi: 10.1016/j.msec.2021.112474.
- Alamer, A. *et al.* (2022) 'Healthcare-Associated Infections (HAIs): Challenges and Measures Taken by the Radiology Department to Control Infection Transmission', *Vaccines*. doi: 10.3390/vaccines10122060.
- Alihosseini, C. *et al.* (2023) 'Do Commonly Used Antimicrobial Topicals Facilitate Venous Leg Ulcer Healing?', *Advances in Skin and Wound Care*. doi: 10.1097/01.ASW.0000926636.51805.d5.
- Alkawareek, M. Y. *et al.* (2012) 'Eradication of *Pseudomonas aeruginosa* Biofilms by Atmospheric Pressure Non-Thermal Plasma', *PLoS ONE*. doi: 10.1371/journal.pone.0044289.
- Alkawareek, M. Y. *et al.* (2014) 'Potential cellular targets and antibacterial efficacy of atmospheric pressure non-thermal plasma', *International Journal of Antimicrobial Agents*. doi: 10.1016/j.ijantimicag.2013.08.022.
- Allegranzi, B. *et al.* (2011) 'Burden of endemic health-care-associated infection in developing countries: Systematic review and meta-analysis', *The Lancet*. doi: 10.1016/S0140-6736(10)61458-4.
- Alves, P. J. *et al.* (2021) 'Update on the role of antiseptics in the management of chronic wounds with critical colonisation and/or biofilm', *International Wound Journal*. doi: 10.1111/iwj.13537.
- Alves, P. M. *et al.* (2018) 'Interaction between *Staphylococcus aureus* and *Pseudomonas aeruginosa* is beneficial for colonisation and pathogenicity in a mixed biofilm', *Pathogens and Disease*. doi: 10.1093/femspd/fty003.
- Ampiauw, R. E., Yaqub, M. and Lee, W. (2021) 'Electrolyzed water as a disinfectant: A systematic review of factors affecting the production and efficiency of hypochlorous acid', *Journal of Water Process Engineering*. doi: 10.1016/j.jwpe.2021.102228.
- Armstrong, D. G. *et al.* (2015) 'Expert Recommendations for the Use of Hypochlorous Solution: Science and Clinical Application.', *Ostomy Wound Management*.
- Assadian, O. *et al.* (2021) 'Practical recommendations for routine cleaning and disinfection procedures in healthcare institutions: a narrative review', *Journal of Hospital Infection*. doi: 10.1016/j.jhin.2021.03.010.
- Atiyeh, B. S., Dibo, S. A. and Hayek, S. N. (2009) 'Wound cleansing, topical antiseptics and wound healing', *International Wound Journal*. doi: 10.1111/j.1742-481X.2009.00639.x.
- Babaeva, N. Y. and Naidis, G. V. (2018) 'Modeling of Plasmas for Biomedicine', *Trends in Biotechnology*. doi: 10.1016/j.tibtech.2017.06.017.
- Babalska, Z. Ł., Korbecka-Paczkowska, M. and Karpiński, T. M. (2021) 'Wound antiseptics and european guidelines for antiseptic application in wound treatment', *Pharmaceuticals*. doi: 10.3390/ph14121253.
- Baeva, M. *et al.* (2012) 'Modeling of microwave-induced plasma in argon at atmospheric

- pressure', *Physical Review E - Statistical, Nonlinear, and Soft Matter Physics*. doi: 10.1103/PhysRevE.85.056404.
- Bahamondez-Canas, T. F., Heersema, L. A. and Smyth, H. D. C. (2019) 'Current status of in vitro models and assays for susceptibility testing for wound biofilm infections', *Biomedicines*, 7(2), pp. 1–31. doi: 10.3390/biomedicines7020034.
- Bayot, M. L. and Bragg, B. N. (2022) *Antimicrobial Susceptibility Testing, Stats Pearls Publishing, Treasure Island (FL)*. Available at: <https://www.ncbi.nlm.nih.gov/books/NBK539714/>.
- Bednar, N, Matovic, J, Stojanovic, G. (2013) 'Properties of surface dielectric barrier discharge plasma generator for fabrication of nanomaterials', *Journal of Electronics*, 71, pp. 1068–1075.
- Bekeschus, S. *et al.* (2014) 'Hydrogen peroxide: A central player in physical plasma-induced oxidative stress in human blood cells', *Free Radical Research*. doi: 10.3109/10715762.2014.892937.
- Bennett, L. L. *et al.* (2001) 'An in vivo comparison of topical agents on wound repair', *Plastic and Reconstructive Surgery*. doi: 10.1097/00006534-200109010-00011.
- Biggs, L. C. *et al.* (2020) 'Mechanical Forces in the Skin: Roles in Tissue Architecture, Stability, and Function', *Journal of Investigative Dermatology*. doi: 10.1016/j.jid.2019.06.137.
- Bigliardi, P, Langer, S, Cruz, JJ, Kim, SW, Nair, H, Srisawasdi, G. (2017) 'An Asian Perspective on Povidone Iodine in Wound Healing', *Dermatology*, 233. doi: 10.1159/000479150.
- Bigliardi, P. L. *et al.* (2017) 'Povidone iodine in wound healing: A review of current concepts and practices', *International Journal of Surgery*. doi: 10.1016/j.ijssu.2017.06.073.
- Billi, D. and Potts, M. (2002) 'Life and death of dried prokaryotes', *Research in Microbiology*. doi: 10.1016/S0923-2508(01)01279-7.
- BioSurface Technologies Corp (2016) 'CDC Biofilm Reactor (CBR) Operator' s Manual', (406), BioSurface Technologies Corporation
- Biscop, E. *et al.* (2019) 'Influence of cell type and culture medium on determining cancer selectivity of cold atmospheric plasma treatment', *Cancers*. doi: 10.3390/cancers11091287.
- Bjarnsholt, T. (2013) 'The role of bacterial biofilms in chronic infections', *APMIS*. doi: 10.1111/apm.12099.
- Blair, J. M. A. *et al.* (2015) 'Molecular mechanisms of antibiotic resistance', *Nature Reviews Microbiology*. doi: 10.1038/nrmicro3380.
- Block, M. S. and Rowan, B. G. (2020) 'Hypochlorous Acid: A Review', *Journal of Oral and Maxillofacial Surgery*. doi: 10.1016/j.joms.2020.06.029.
- Boehnke, K. *et al.* (2007) 'Effects of fibroblasts and microenvironment on epidermal regeneration and tissue function in long-term skin equivalents', *European Journal of Cell Biology*. doi: 10.1016/j.ejcb.2006.12.005.
- Boev, C. and Kiss, E. (2017) 'Hospital-Acquired Infections: Current Trends and Prevention', *Critical Care Nursing Clinics of North America*. doi: 10.1016/j.cnc.2016.09.012.
- Di Bonaventura, G. and Pompilio, A. (2022) 'In Vitro Antimicrobial Susceptibility Testing of Biofilm-Growing Bacteria: Current and Emerging Methods', in *Advances in Experimental Medicine and Biology*. doi: 10.1007/5584_2021_641.
- Boothby, IC, Cohen, JN, Rosenblum, M. (2020) 'Regulatory T cells in Skin Injury: At the Crossroads of Tolerance and Tissue Repair', *Science Immunology*, 5(47), p. eaaz9631. doi: 10.1126/sciimmunol.aaz9631.

- Boucher, H. W. *et al.* (2009) 'Bad bugs, no drugs: No ESKAPE! An update from the Infectious Diseases Society of America', *Clinical Infectious Diseases*. doi: 10.1086/595011.
- Bourke, P, Ziuzina, D, Han, L, Cullen, PJ, Gilmore, B. (2017) 'Microbiological interactions with cold plasma', *Journal of Applied Microbiology*, 123, pp. 308–324. doi: 10.1111/jam.13429.
- Brandenburg, R. (2017) 'Dielectric barrier discharges: progress in plasmas sources and on the understanding of regimes and single filaments', *Plasma Sources Science and Technology*, 26. doi: 10.1088/1361-6595/aa6426.
- Brown, A. (2018) 'When is wound cleansing necessary and what solution should be used?', *Nursing Times [online]*.
- Brown, J. L. *et al.* (2022) 'Assessing the inflammatory response to in vitro polymicrobial wound biofilms in a skin epidermis model', *npj Biofilms and Microbiomes*. doi: 10.1038/s41522-022-00286-z.
- Buckingham-Meyer, K., Goeres, D. M. and Hamilton, M. A. (2007) 'Comparative evaluation of biofilm disinfectant efficacy tests', *Journal of Microbiological Methods*. doi: 10.1016/j.mimet.2007.04.010.
- Busco, G. *et al.* (2020) 'The emerging potential of cold atmospheric plasma in skin biology', *Free Radical Biology and Medicine*. doi: 10.1016/j.freeradbiomed.2020.10.004.
- BSI (British Standards Institution) (2005) *BS EN 1040: 2005 Chemical disinfectants and antiseptics - Quantitative suspension test for the evaluation of basic bactericidal activity of chemical disinfectants and antiseptics (phase 1)*.
- BSI (British Standards Institution) (2020) 'BSI Standards Publication Chemical disinfectants and antiseptics – Quantitative non-porous surface test for the evaluation of bactericidal and / or fungicidal activity of chemical disinfectants used in food , industrial , domestic and without mechanical action (phase 2, step 2)'. Available at: <https://bsol.bsigroup.com/Bibliographic/BibliographicInfoData/00000000030407471>.
- BSI (British Standards Institution) (2023) *BS ISO 4768:2023 Measurement method of anti-biofilm activity on plastic and non-porous surfaces*. Available at: <https://bsol.bsigroup.com/Bibliographic/BibliographicInfoData/00000000030425861>.
- Cai, Z. (University of the West of England, Bristol, U. (2005) *Characterisation of electrochemically activated solutions for use in environmental remediation*.
- Cahill, O. J. *et al.* (2014) 'Cold air plasma to decontaminate inanimate surfaces of the hospital environment', *Applied and Environmental Microbiology*. doi: 10.1128/AEM.03480-13.
- Cahill, O. J. *et al.* (2017) 'Decontamination of hospital surfaces with multijet cold plasma: A method to enhance infection prevention and control?', *Infection Control and Hospital Epidemiology*. doi: 10.1017/ice.2017.168.
- Capriotti, K, Pelletier, J, Barone, S, Capriotti, J. (2018) 'Efficacy of dilute povidone-iodine against bacterial biofilms, fungal biofilms and fungal spores', *Clinical Research in Dermatology: Open Access*, 5, pp. 1–5. doi: 10.15226/2378-1726/5/1/00174.
- Çelebi-Saltik, B. and Kart, D. (2021) 'Dermal fibroblast cells interactions with single and triple bacterial-species biofilms', *Molecular Biology Reports*. doi: 10.1007/s11033-021-06391-0.
- Chelmus-Burlacu, A, Tang, E, Pieptu, D. (2023) 'Phenotypic Modulation of Adipose-Derived Stem Cells and Fibroblasts Treated with Povidone-Iodine and Chlorhexidine in Mono and Coculture Models', *Biomedicines*, 11(7), p. 1855. doi: 10.3390/biomedicines11071855.
- Chen, B. K. and Wang, C. K. (2022) 'Electrolyzed Water and Its Pharmacological Activities: A Mini-Review', *Molecules*. doi: 10.3390/molecules27041222.

- Chen, C. *et al.* (2014) 'A model of plasma-biofilm and plasma-tissue interactions at ambient pressure', in *Plasma Chemistry and Plasma Processing*. doi: 10.1007/s11090-014-9545-1.
- Chen, T.-P., Su, T.-L. and Liang, J. (2016) 'Plasma-Activated Solutions for Bacteria and Biofilm Inactivation', *Current Bioactive Compounds*, 13(1), pp. 59–65. doi: 10.2174/1573407212666160609082945.
- Chen, X. *et al.* (2021) 'A novel chronic wound biofilm model sustaining coexistence of *Pseudomonas aeruginosa* and *Staphylococcus aureus* suitable for testing of antibiofilm effect of antimicrobial solutions and wound dressings', *Wound Repair and Regeneration*. doi: 10.1111/wrr.12944.
- Cheng, Y. *et al.* (2019) 'Population dynamics and transcriptomic responses of *Pseudomonas aeruginosa* in a complex laboratory microbial community', *npj Biofilms and Microbiomes*. doi: 10.1038/s41522-018-0076-z.
- Choi, E. H., Uhm, H. S. and Kaushik, N. K. (2021) 'Plasma bioscience and its application to medicine', *AAPPS Bulletin*. doi: 10.1007/s43673-021-00012-5.
- Choi, J.-S. *et al.* (2017) 'Evaluation of non-thermal plasma-induced anticancer effects on human colon cancer cells', *Biomedical Optics Express*. doi: 10.1364/boe.8.002649.
- Costerton, J. W., Geesey, G. G. and Cheng, K. J. (1978) 'How bacteria stick.', *Scientific American*. doi: 10.1038/scientificamerican0178-86.
- Curieses Andres, CM, Perez de la Lastra, JM, Andres Juan, S, Plou, FJ, Perez-Lebena, E. (2022) 'The Role of Reactive Species on Innate Immunity', *Vaccines*, 10(10), p. 1735. doi: 10.3390/vaccines10101735.
- Curiesnes Andres, CM, Perez de la Lastra, JMP, Andres Juan, C, Plou, FJ, Perez-Lebena, E. (2022) 'Hypochlorous Acid Chemistry in Mammalian Cells - Influence on Infection and Role in Various Pathologies', *International Journal of Molecular Sciences*, 23(18), p. 10735. doi: 10.3390/ijms23180735.
- Cutting, K. F. (2003) 'Wound exudate: composition and functions', *British Journal of Community Nursing*. doi: 10.12968/bjcn.2003.8.sup3.11577.
- Czapka, T., Maliszewska, I. and Olesiak-Bańska, J. (2018) 'Influence of Atmospheric Pressure Non-thermal Plasma on Inactivation of Biofilm Cells', *Plasma Chemistry and Plasma Processing*. doi: 10.1007/s11090-018-9925-z.
- Cutting, K. F. (2003) 'Wound exudate: composition and functions', *British Journal of Community Nursing*. doi: 10.12968/bjcn.2003.8.sup3.11577.
- Das, S, Gajula, VP, Mohapatra, S, Singh, Kar, S. (2022) 'Role of cold atmospheric plasma in microbial inactivation and the factors affecting its efficacy', *Health Sciences Review*, 4(100037).
- De-la-Pinta, I. *et al.* (2019) 'Effect of biomaterials hydrophobicity and roughness on biofilm development', *Journal of Materials Science: Materials in Medicine*. doi: 10.1007/s10856-019-6281-3.
- Demidova-Rice, T. N., Hamblin, M. R. and Herman, I. M. (2012) 'Acute and impaired wound healing: Pathophysiology and current methods for drug delivery, part 1: Normal and chronic wounds: Biology, causes, and approaches to care', *Advances in Skin and Wound Care*. doi: 10.1097/01.ASW.0000416006.55218.d0.
- Demidova-Rice, TN, Hamblin, MR, Herman, I. (2012) 'Acute and Impaired Wound Healing: Pathophysiology and Current Methods for Drug Delivery, Part 2: Role of Growth Factors in Normal and Pathophysiological Wound Healing: Therapeutic Potential and Methods of Delivery', *Advances in Skin and Wound Care*, 25(8), pp. 349–370. doi:

10.1097/01.ASW.0000418541.3166.a3.

Dezest, M. *et al.* (2017) 'Mechanistic insights into the impact of Cold Atmospheric Pressure Plasma on human epithelial cell lines', *Scientific Reports*. doi: 10.1038/srep41163.

Dhekane, R., Mhade, S. and Kaushik, K. S. (2022) 'Adding a new dimension: Multi-level structure and organization of mixed-species *Pseudomonas aeruginosa* and *Staphylococcus aureus* biofilms in a 4-D wound microenvironment', *Biofilm*. doi: 10.1016/j.bioflm.2022.100087.

Ding, T. *et al.* (2016) 'Disinfection efficacy and mechanism of slightly acidic electrolyzed water on *Staphylococcus aureus* in pure culture', *Food Control*. doi: 10.1016/j.foodcont.2015.08.037.

Dissemond, J. (2020) 'Wound cleansing: Benefits of hypochlorous acid', *Journal of Wound Care*. doi: 10.12968/jowc.2020.29.Sup10a.S4.

Dobrynin, D. *et al.* (2009) 'Physical and biological mechanisms of direct plasma interaction with living tissue', *New Journal of Physics*. doi: 10.1088/1367-2630/11/11/115020.

Donlan, R. M. and Costerton, J. W. (2002) 'Biofilms: Survival mechanisms of clinically relevant microorganisms', *Clinical Microbiology Reviews*. doi: 10.1128/CMR.15.2.167-193.2002.

Dopcea, G. and Matei, F. (2018) 'REVIEW ON SOME CURRENT SKIN ANTISEPTICS.', *Scientific Bulletin Series F. Biotechnologies*.

Dowsett, C, Newton, H. (2005) 'Wound bed preparation: TIME in practice', *Wounds UK*, 1(3), pp. 58–70.

Eggers, M. (2019) 'Infectious Disease Management and Control with Povidone Iodine', *Infectious Diseases and Therapy*. doi: 10.1007/s40121-019-00260-x.

Eming, S. A. *et al.* (2006) 'A novel property of povidone-iodine: Inhibition of excessive protease levels in chronic non-healing wounds [7]', *Journal of Investigative Dermatology*. doi: 10.1038/sj.jid.5700474.

Eming, S. A., Martin, P. and Tomic-Canic, M. (2014) 'Wound repair and regeneration: Mechanisms, signaling, and translation', *Science Translational Medicine*. doi: 10.1126/scitranslmed.3009337.

Eriksson, E, Liu, PY, Schultz, GS, Martins-Green, M, Tanaka, R, Weir, D, Gould, LJ, Armstrong, DG, Gibbons, GW, Wolcott, R, Olutoye, OO, Kirsner, RS, Gurtner, G. (2022) 'Chronic wounds: Treatment consensus', *Wound Repair and Regeneration*, 30(2), pp. 156–171. doi: 10.1111/wr.12994.

Esin, S. *et al.* (2022) 'The antibacterial and antibiofilm activity of Granudacyn in vitro in a 3D collagen wound infection model', *Journal of Wound Care*. doi: 10.12968/jowc.2022.31.11.908.

European Committee for Standardization (2013) EN13624:2013 Chemical disinfectants Quantitative Suspension test for the Evaluation of Fungicidal Activity for Instruments used in the Medical Area: Test Methods and Requirements (Phase 2, Step 2).

European Committee for Standardization (2015) EN13727:2015 Chemical disinfectants Quantitative Suspension test for the Evaluation of Bactericidal Activity for Instruments used in the Medical Area: Test Methods and Requirements (Phase 2, Step 2).

European Society of Clinical Microbiology and Infectious Diseases (2024) *Antimicrobial susceptibility testing: EUCAST disk diffusion method v12.0*. Available at: https://www.eucast.org/fileadmin/src/media/PDFs/EUCAST_files/Disk_test_documents/2024_manuals/Manual_v_12.0_EUCAST_Disk_Test_2024.pdf.

Feibel, D. *et al.* (2023) 'Gas Flow-Dependent Modification of Plasma Chemistry in μ APP Jet-Generated Cold Atmospheric Plasma and Its Impact on Human Skin Fibroblasts', *Biomedicines*. doi: 10.3390/biomedicines11051242.

- Feil, L. *et al.* (2020) 'Cancer-selective treatment of cancerous and non-cancerous human cervical cell models by a non-thermally operated electrosurgical argon plasma device', *Cancers*. doi: 10.3390/cancers12041037.
- Fleming, D, Rumbaugh, K. (2018) 'The Consequences of Biofilm Dispersal on the Host', *Scientific Reports*, 8, p. 10738. doi: 10.1038/s41598-018-29121-2.
- Flemming, H. C. *et al.* (2016) 'Biofilms: An emergent form of bacterial life', *Nature Reviews Microbiology*. doi: 10.1038/nrmicro.2016.94.
- Foster, S. (2023) *Stevens-Johnson Syndrome Treatment & Management, Medscape, Drugs and Diseases*. Available at: <https://emedicine.medscape.com/article/1197450-treatment#d11>.
- Founou, R. C., Founou, L. L. and Essack, S. Y. (2017) 'Clinical and economic impact of antibiotic resistance in developing countries: A systematic review and meta-analysis', *PLoS ONE*. doi: 10.1371/journal.pone.0189621.
- Fridman, G. *et al.* (2008) 'Applied plasma medicine', *Plasma Processes and Polymers*. doi: 10.1002/ppap.200700154.
- Fumal, I. *et al.* (2002) 'The beneficial toxicity paradox of antimicrobials in leg ulcer healing impaired by a polymicrobial flora: A proof-of-concept study', in *Dermatology*. doi: 10.1159/000057729.
- Gajic, I. *et al.* (2022) 'Antimicrobial Susceptibility Testing: A Comprehensive Review of Currently Used Methods', *Antibiotics*. doi: 10.3390/antibiotics11040427.
- García-Valdivia, M. *et al.* (2022) 'Cytotoxicity, Epidermal Barrier Function and Cytokine Evaluation after Antiseptic Treatment in Bioengineered Autologous Skin Substitute', *Biomedicines*. doi: 10.3390/biomedicines10061453.
- Gilliver, S. (2009) 'PHMB: a well-tolerated antiseptic with no reported toxic effects', *Journal of wound care*.
- Gilmore, B. F. *et al.* (2018) 'Cold Plasmas for Biofilm Control: Opportunities and Challenges', *Trends in Biotechnology*. doi: 10.1016/j.tibtech.2018.03.007.
- Goeres, D. M. *et al.* (2009) 'A method for growing a biofilm under low shear at the air-liquid interface using the drip flow biofilm reactor', *Nature Protocols*. doi: 10.1038/nprot.2009.59.
- Gold, M. H. *et al.* (2020) 'Topical stabilized hypochlorous acid: The future gold standard for wound care and scar management in dermatologic and plastic surgery procedures', *Journal of Cosmetic Dermatology*. doi: 10.1111/jocd.13280.
- Goswami, AG, Basu, S, Banerjee, T, Shukla, V. (2023) 'Biofilm and wound healing: from bench to bedside', *European Journal of Medical Research*, 28, p. 157. doi: 10.1186/s40001-023-01121-7.
- Grassi, L. *et al.* (2019) 'The antimicrobial peptide lin-SB056-1 and its dendrimeric derivative prevent pseudomonas aeruginosa biofilm formation in physiologically relevant models of chronic infections', *Frontiers in Microbiology*. doi: 10.3389/fmicb.2019.00198.
- Gray, D. *et al.* (2010) 'PHMB and its potential contribution to wound management', *Wounds UK*.
- Green, J. *et al.* (2014) 'The impact of chronic venous leg ulcers: A systematic review', *Journal of Wound Care*. doi: 10.12968/jowc.2014.23.12.601.
- Greenhalgh, R., Dempsey-Hibbert, N. C. and Whitehead, K. A. (2019) 'Antimicrobial strategies to reduce polymer biomaterial infections and their economic implications and considerations', *International Biodeterioration and Biodegradation*. doi: 10.1016/j.ibiod.2018.10.005.
- Grassi, L. *et al.* (2019) 'The antimicrobial peptide lin-SB056-1 and its dendrimeric derivative prevent pseudomonas aeruginosabiofilm formation in physiologically relevant models of chronic

- infections', *Frontiers in Microbiology*. doi: 10.3389/fmicb.2019.00198.
- Gray, D. *et al.* (2010) 'PHMB and its potential contribution to wound management', *Wounds UK*.
- Green, J. *et al.* (2014) 'The impact of chronic venous leg ulcers: A systematic review', *Journal of Wound Care*. doi: 10.12968/jowc.2014.23.12.601.
- Greenhalgh, R., Dempsey-Hibbert, N. C. and Whitehead, K. A. (2019) 'Antimicrobial strategies to reduce polymer biomaterial infections and their economic implications and considerations', *International Biodeterioration and Biodegradation*. doi: 10.1016/j.ibiod.2018.10.005.
- Griseti, E., Merbahi, N. and Golzio, M. (2020) 'Anti-cancer potential of two plasma-activated liquids: Implication of long-lived reactive oxygen and nitrogen species', *Cancers*. doi: 10.3390/cancers12030721.
- Grzybowski, A., Kanclerz, P. and Myers, W. G. (2018) 'The use of povidone-iodine in ophthalmology', *Current Opinion in Ophthalmology*. doi: 10.1097/ICU.0000000000000437.
- Guest, J. F. *et al.* (2020) 'Modelling the annual NHS costs and outcomes attributable to healthcare-associated infections in England', *BMJ Open*. doi: 10.1136/bmjopen-2019-033367.
- Guest, J. F., Fuller, G. W. and Vowden, P. (2020) 'Cohort study evaluating the burden of wounds to the UK's National Health Service in 2017/2018: Update from 2012/2013', *BMJ Open*. doi: 10.1136/bmjopen-2020-045253.
- Gupta, T. T. and Ayan, H. (2019) 'Application of non-thermal plasma on biofilm: A review', *Applied Sciences (Switzerland)*. MDPI AG. doi: 10.3390/app9173548.
- Haertel, B. *et al.* (2011) 'Non-thermal atmospheric-pressure plasma can influence cell adhesion molecules on HaCaT-keratinocytes', *Experimental Dermatology*. doi: 10.1111/j.1600-0625.2010.01159.x.
- Haertel, B. *et al.* (2014) 'Non-thermal atmospheric-pressure plasma possible application in wound healing', *Biomolecules and Therapeutics*. doi: 10.4062/biomolther.2014.105.
- Han, A. *et al.* (2011) 'The importance of a multifaceted approach to characterizing the microbial flora of chronic wounds', *Wound Repair and Regeneration*. doi: 10.1111/j.1524-475X.2011.00720.x.
- Handorf, O. *et al.* (2018) 'Nonthermal plasma jet treatment negatively affects the viability and structure of *Candida albicans* SC5314 biofilms', *Applied and Environmental Microbiology*, 84(21), pp. 1–15. doi: 10.1128/AEM.01163-18.
- Hannah, R. *et al.* (2001) 'CELLTITER-GLO™ LUMINESCENT CELL VIABILITY ASSAY: A SENSITIVE AND RAPID METHOD FOR DETERMINING CELL VIABILITY', *Cell Notes*.
- Harries, RL, Bosquanet, DC, Harding, K. (2016) 'Wound bed preparation: TIME for an update', *International Wound Journal*, 13(Supp. 3), pp. 8–14. doi: 10.1111/iwj.12662.
- Hoekstra, M. J., Westgate, S. J. and Mueller, S. (2017) 'Povidone-iodine ointment demonstrates in vitro efficacy against biofilm formation', *International Wound Journal*. doi: 10.1111/iwj.12578.
- Hofman, AG, Deinsberger, J, Oszwald, D, Weber, B. (2024) 'The Histopathology of Leg Ulcers', *Dermatopathology*, 11(1), pp. 62–78. doi: 10.3390/dermatopathology11010007.
- Hofmann, E. *et al.* (2023) 'Human In Vitro Skin Models for Wound Healing and Wound Healing Disorders', *Biomedicines*. doi: 10.3390/biomedicines11041056.
- Højby, N, Bjarnsholt, T, Moser, C, Bassi, GL, Coenye, T, Donelli, G, Hall-Stoodley, L, Hola, V, Imbert, C, Kirketerp-Møller, K, Lebeaux, D, Oliver, A, Ullman, AJ, Williams, C. (2015) 'ESCMID guideline for the diagnosis and treatment of biofilm infections 2014', *Clinical Microbiology and Infection*, 21(Suppl. 1), pp. S1-25. doi: 10.1016/j.cmi.2014.10.024.

- Hojnik, N. *et al.* (2019) 'Effective Fungal Spore Inactivation with an Environmentally Friendly Approach Based on Atmospheric Pressure Air Plasma', *Environmental Science and Technology*. doi: 10.1021/acs.est.8b05386.
- Holmes, A. H. *et al.* (2016) 'Understanding the mechanisms and drivers of antimicrobial resistance', *The Lancet*. doi: 10.1016/S0140-6736(15)00473-0.
- Idrees, A. *et al.* (2021) 'Fundamental in vitro 3D human skin equivalent tool development for assessing biological safety and biocompatibility – towards alternative for animal experiments', *4open*. doi: 10.1051/fopen/2021001.
- Ignatov, I. *et al.* (2016) 'Studying electrochemically activated NaCl solutions of anolyte and catholyte by methods of non-Equilibrium energy spectrum (NES) and differential non-equilibrium energy spectrum (DNES)', *Journal of Medicine, Physiology and Biophysics*.
- International Standards Organization (ISO) (2019) ISO 20776-1 (2019) Susceptibility testing of infectious agents and evaluation of performance of antimicrobial susceptibility test devices - Part 1: Broth micro-dilution reference method for testing the in vitro activity of antimicrobial agents against rapidly growing aerobic bacteria involved in infectious diseases.
- International Standards Organization (ISO) (2021) ISO 20776-2 (2021) Clinical laboratory testing and in vitro diagnostic test systems - Susceptibility testing of infectious agents and evaluation of performance of antimicrobial susceptibility test devices - Part 2: Evaluation of performance of antimicrobial susceptibility test devices against reference broth microdilution
- Ishihara, M. *et al.* (2017) 'Stability of weakly acidic hypochlorous acid solution with microbicidal activity', *Biocontrol Science*. doi: 10.4265/bio.22.223.
- Jabbariesgandani, A. and Walsh, J. L. (2023) 'Factors affecting decolourization efficiency of indigo carmine in a coaxial surface plasma falling film reactor', *Journal of Water Process Engineering*. doi: 10.1016/j.jwpe.2023.103632.
- James, GA, Swogger, Wolcott, R, De Lancey Pulcini, E, Secor, P, Sestrich, J, Costerton, JW, Stewart, P. (2008) 'Biofilms in chronic wounds', *Wound Repair and Regeneration*, 16(1), pp. 37–44. doi: 10.1111/j.1524-475X.2007.00321.x.
- Järbrink, K. *et al.* (2016) 'Prevalence and incidence of chronic wounds and related complications: A protocol for a systematic review', *Systematic Reviews*. doi: 10.1186/s13643-016-0329-y.
- Johani, K. *et al.* (2018) 'Evaluation of short exposure times of antimicrobial wound solutions against microbial biofilms: From in vitro to in vivo', *Journal of Antimicrobial Chemotherapy*. doi: 10.1093/jac/dkx391.
- Johns, B. E. *et al.* (2015) 'Phenotypic and Genotypic Characteristics of Small Colony Variants and Their Role in Chronic Infection', *Microbiology Insights*. doi: 10.4137/mbi.s25800.
- Jones, I. A. and Joshi, L. T. (2021) 'Biocide use in the antimicrobial era: A review', *Molecules*. doi: 10.3390/molecules26082276.
- Joshi, S. G. *et al.* (2010) 'Control of methicillin-resistant Staphylococcus aureus in planktonic form and biofilms: A biocidal efficacy study of nonthermal dielectric-barrier discharge plasma', *American Journal of Infection Control*. doi: 10.1016/j.ajic.2009.11.002.
- Junker, J. P. E., Caterson, E. J. and Eriksson, E. (2013) 'The microenvironment of wound healing', *Journal of Craniofacial Surgery*. doi: 10.1097/SCS.0b013e31827104fb.
- Kadam, S. *et al.* (2019) 'Bioengineered Platforms for Chronic Wound Infection Studies: How Can We Make Them More Human-Relevant?', *Frontiers in Bioengineering and Biotechnology*. doi: 10.3389/fbioe.2019.00418.
- Kalghatgi, S. *et al.* (2011) 'Effects of non-thermal plasma on mammalian cells', *PLoS ONE*, 6(1), pp. 198

1–11. doi: 10.1371/journal.pone.0016270.

Kamgang-Youbi, G. *et al.* (2008) 'Impact on disinfection efficiency of cell load and of planktonic/adherent/ detached state: Case of *Hafnia alvei* inactivation by Plasma Activated Water', *Applied Microbiology and Biotechnology*. doi: 10.1007/s00253-008-1641-9.

Kamiloglu, S. *et al.* (2020) 'Guidelines for cell viability assays', *Food Frontiers*. doi: 10.1002/fft2.44.

Karaman, DS, Manner, S, Fallarero, A, Rosenholm, J. (2016) 'Current Approaches for Exploration of Nanoparticles as Antibacterial Agents', in *Antibacterial Agents*. IntechOpen, pp. 61–86. doi: <http://dx.doi.org/10.5772/57353>.

Kataoka, M. *et al.* (2006) 'Toxic effects of povidone-iodine on synovial cell and articular cartilage', *Clinical Rheumatology*. doi: 10.1007/s10067-005-0133-x.

Katsigiannis, A. S., Bayliss, D. L. and Walsh, J. L. (2021) 'Cold plasma decontamination of stainless steel food processing surfaces assessed using an industrial disinfection protocol', *Food Control*, 121(August 2020), p. 107543. doi: 10.1016/j.foodcont.2020.107543.

Kaushik, N. *et al.* (2015) 'Responses of solid tumor cells in DMEM to reactive oxygen species generated by non-thermal plasma and chemically induced ROS systems', *Scientific Reports*. doi: 10.1038/srep08587.

Kaushik, N. K. *et al.* (2018) 'Biological and medical applications of plasma-activated media, water and solutions', *Biological Chemistry*. doi: 10.1515/hsz-2018-0226.

Kawakita, T. and Landy, H. J. (2017) 'Surgical site infections after cesarean delivery: epidemiology, prevention and treatment', *Maternal Health, Neonatology and Perinatology*. doi: 10.1186/s40748-017-0051-3.

Kettle, AJ, Winterbourn, C. (1997) 'Myeloperoxidase: a key regulator of neutrophil oxidant production', *Redox Reports*, 3, pp. 1–15. doi: 10.1080/13510002.1997.11747085.

Khalid, M., Petroianu, G. and Adem, A. (2022) 'Advanced Glycation End Products and Diabetes Mellitus: Mechanisms and Perspectives', *Biomolecules*. doi: 10.3390/biom12040542.

Khatoun, Z, McTiernan CD, Suuronen EJ, Mah TF, A. E. (2018) 'Bacterial biofilm formation on implantable devices and approaches to its treatment and prevention', *Heliyon*, 4(12), p. e01067. doi: 10.1016/j.heliyon.2018.e01067.

Khosravi, S, Jafari, A, Zamani, H, Nilkar, M. (2022) 'Synergistic antimicrobial effects of atmospheric pressure non-thermal argon plasma and ciprofloxacin antibiotic against multi-drug resistant *P. aeruginosa* biofilm', *Journal of Applied Physics*, 131(21), p. 213301. doi: 10.1063/5.0091001.

Kim, JH, Ahamed, A, Chen, K, Lebig, EG, Petros, B, Saeed, A, Martins-Green, M. (2022) 'Chapter 21 - Skin microbiota and its role in health and disease with an emphasis on wound healing and chronic wound development', in *Microbiome, Immunity, Digestive Health and Nutrition*, pp. 297–311. doi: 10.1016/B978-0-12-822238-6.00027-3.

King, B. and Barrett, S. (2016) 'PHMB made easy', *Wounds UK*, 12(4), pp. 1–4. Available at: <https://www.wounds-uk.com/resources/details/phmb-made-easy>.

Kirketerp-Møller, K. *et al.* (2008) 'Distribution, organization, and ecology of bacteria in chronic wounds', *Journal of Clinical Microbiology*. doi: 10.1128/JCM.00501-08.

Klarczyk, B. R. *et al.* (2023) 'Evaluation of temperature, drying time and other determinants for the recovery of Gram-negative bacterial pathogens in disinfectant efficacy testing', *Journal of Hospital Infection*, 141, pp. 17–24. doi: 10.1016/j.jhin.2023.08.006.

Kleijn, A. *et al.* (2016) 'A Systematic Comparison Identifies an ATP-Based Viability Assay as Most Suitable Read-Out for Drug Screening in Glioma Stem-Like Cells', *Stem Cells International*. doi:

10.1155/2016/5623235.

Klis, FM, de Koster, CG, Brul, S. (2014) 'Cell wall-related biomarkers and bioestimates of *Saccharomyces cerevisiae* and *Candida albicans*', *Eukaryotic Cell*, 13, pp. 2–9. doi: 10.1128/EC.00250-13.

Knoedler, S, Knoedler, L, Kauke-Navaroo, M, Rinkevich, Y, Hundeshagen, G, Harhaus, L, Kneser, U, Pomahac, G, Orgill, DP, Panayi, A. (2023) 'Regulatory T cells in skin regeneration and wound healing', *Military Medical Research*, 20, p. 49. doi: 10.1186/s40779-023-00484-6.

Kramer, A, Schwebke, I, Kampf, G. (2006) 'How long do nosocomial pathogens persist on inanimate surfaces? A systematic review', *BMC Infectious Diseases*, 6, p. 130.

Krasowski, G. *et al.* (2021) 'In vitro evaluation of polihexanide, octenidine and NaClO/HClO-based antiseptics against biofilm formed by wound pathogens', *Membranes*. doi: 10.3390/membranes11010062.

Lawton, S. (2019) 'Skin 1: the structure and functions of the skin', *Nursing Times [online]*, 115(12), pp. 30–33.

Leeper, D. J. and Durani, P. (2008) 'Topical antimicrobial therapy of chronic wounds healing by secondary intention using iodine products', in *International Wound Journal*. doi: 10.1111/j.1742-481X.2007.00406.x.

Lebeaux, D., Ghigo, J.-M. and Beloin, C. (2014) 'Biofilm-Related Infections: Bridging the Gap between Clinical Management and Fundamental Aspects of Recalcitrance toward Antibiotics', *Microbiology and Molecular Biology Reviews*. doi: 10.1128/mubr.00013-14.

Ledwoch, K. *et al.* (2019) 'Artificial dry surface biofilm models for testing the efficacy of cleaning and disinfection', *Letters in Applied Microbiology*. doi: 10.1111/lam.13143.

Lee, EY, Knox, C, Phillips, E. (2023) 'Worldwide Prevalence of Antibiotic-Associated Stevens-Johnson Syndrome and Toxic Epidermal Necrolysis', *JAMA Dermatology*, 159(4), pp. 384–392. doi: 10.1001/jamadermatol.2022.6378.

Lee, M. J. *et al.* (2019) 'The antibacterial effect of non-thermal atmospheric pressure plasma treatment of titanium surfaces according to the bacterial wall structure', *Scientific Reports*. doi: 10.1038/s41598-019-39414-9.

Lee, S. W. (2010) *Biological Decontamination using Electrochemically Activated Solutions*. University of the West of England.

Lepelletier, D. *et al.* (2020) 'Povidone iodine: Properties, mechanisms of action, and role in infection control and staphylococcus aureus decolonization', *Antimicrobial Agents and Chemotherapy*. doi: 10.1128/AAC.00682-20.

Li, M, Hou, Q, Zhong, L, Zhao, Y, Fu, X. (2021) 'Macrophage Related Chronic Inflammation in Non-Healing Wounds', *Frontiers in Immunology*, 12, p. 681710. doi: 10.3389/fimmu.2021.681710.

Lin, A. *et al.* (2019) 'Non-Thermal Plasma as a Unique Delivery System of Short-Lived Reactive Oxygen and Nitrogen Species for Immunogenic Cell Death in Melanoma Cells', *Advanced Science*. doi: 10.1002/advs.201802062.

Lindholm, C. and Searle, R. (2016) 'Wound management for the 21st century: combining effectiveness and efficiency', *International Wound Journal*. doi: 10.1111/iwj.12623.

Linley, E. *et al.* (2012) 'Use of hydrogen peroxide as a biocide: New consideration of its mechanisms of biocidal action', *Journal of Antimicrobial Chemotherapy*. doi: 10.1093/jac/dks129.

Lipp, C. *et al.* (2010) 'Testing wound dressings using an in vitro wound model', *Journal of Wound Care*. doi: 10.12968/jowc.2010.19.6.48468.

- Lisse, TS, King, BL, Rieger, S. (2016) 'Comparative transcriptomic profiling of hydrogen peroxide signalling network in zebrafish and human keratinocytes: Implications toward conservation, migration and wound healing', *Scientific Reports*, 6, p. 20328. doi: 10.1038/srep20328.
- Liu, J. X. *et al.* (2017) 'Povidone-iodine Solutions Inhibit Cell Migration and Survival of Osteoblasts, Fibroblasts, and Myoblasts', *Spine*. doi: 10.1097/BRS.0000000000002224.
- Liu, Z. C. *et al.* (2018) 'Post-discharge evolution of reactive species in the water activated by a surface air plasma: A modeling study', *Journal of Physics D: Applied Physics*. doi: 10.1088/1361-6463/aab635.
- Lloyd, G. *et al.* (2010) 'Gas plasma: Medical uses and developments in wound care', *Plasma Processes and Polymers*. doi: 10.1002/ppap.200900097.
- Loo, A. E. K. and Halliwell, B. (2012) 'Effects of hydrogen peroxide in a keratinocyte-fibroblast co-culture model of wound healing', *Biochemical and Biophysical Research Communications*. doi: 10.1016/j.bbrc.2012.05.100.
- López, M. *et al.* (2019) 'A review on non-thermal atmospheric plasma for food preservation: Mode of action, determinants of effectiveness, and applications', *Frontiers in Microbiology*. doi: 10.3389/fmicb.2019.00622.
- Lou, B. S. *et al.* (2020) 'Helium/Argon-Generated Cold Atmospheric Plasma Facilitates Cutaneous Wound Healing', *Frontiers in Bioengineering and Biotechnology*. doi: 10.3389/fbioe.2020.00683.
- Lukes, P. *et al.* (2014) 'Aqueous-phase chemistry and bactericidal effects from an air discharge plasma in contact with water: Evidence for the formation of peroxyxynitrite through a pseudo-second-order post-discharge reaction of H₂O₂ and HNO₂', *Plasma Sources Science and Technology*. doi: 10.1088/0963-0252/23/1/015019.
- Lukes, P., Brisset, J. L. and Locke, B. R. (2012) 'Biological Effects of Electrical Discharge Plasma in Water and in Gas-Liquid Environments', in *Plasma Chemistry and Catalysis in Gases and Liquids*. doi: 10.1002/9783527649525.ch8.
- Lunov, O. *et al.* (2016) 'The interplay between biological and physical scenarios of bacterial death induced by non-thermal plasma', *Biomaterials*. doi: 10.1016/j.biomaterials.2015.12.027.
- Van Meurs, S. J. *et al.* (2014) 'Selection of an optimal antiseptic solution for intraoperative irrigation: An in vitro study', *Journal of Bone and Joint Surgery*. doi: 10.2106/JBJS.M.00313.
- Müller, G. and Kramer, A. (2008) 'Biocompatibility index of antiseptic agents by parallel assessment of antimicrobial activity and cellular cytotoxicity', *Journal of Antimicrobial Chemotherapy*. doi: 10.1093/jac/dkn125.
- Ma, C. *et al.* (2022) 'Plasma for biomedical decontamination: from plasma-engineered to plasma-active antimicrobial surfaces', *Current Opinion in Chemical Engineering*. doi: 10.1016/j.coche.2021.100764.
- Ma, Y. *et al.* (2014) 'Non-thermal atmospheric pressure plasma preferentially induces apoptosis in p53-mutated cancer cells by activating ROS stress-response pathways', *PLoS ONE*. doi: 10.1371/journal.pone.0091947.
- Macià, M. D., Rojo-Molinero, E. and Oliver, A. (2014) 'Antimicrobial susceptibility testing in biofilm-growing bacteria', *Clinical Microbiology and Infection*. doi: 10.1111/1469-0691.12651.
- Madorran, E. *et al.* (2020) 'In vitro toxicity model: Upgrades to bridge the gap between preclinical and clinical research', *Bosnian Journal of Basic Medical Sciences*. doi: 10.17305/bjbms.2019.4378.
- Mai-Prochnow, A. *et al.* (2014) 'Atmospheric pressure plasmas: Infection control and bacterial responses', *International Journal of Antimicrobial Agents*. doi: 10.1016/j.ijantimicag.2014.01.025.

Mai-Prochnow, A. *et al.* (2016) 'Gram positive and Gram negative bacteria differ in their sensitivity to cold plasma', *Scientific Reports*. doi: 10.1038/srep38610.

Maillard, J.-Y. (2005) 'Antimicrobial biocides in the healthcare environment: efficacy, usage, policies, and perceived problems.', *Therapeutics and clinical risk management*.1(4): 307-20

Maillard, J.-Y., Kampf, G. and Cooper, R. (2021) 'Antimicrobial stewardship of antiseptics that are pertinent to wounds: the need for a united approach', *JAC-Antimicrobial Resistance*. doi: 10.1093/jacamr/dlab027.

Maillard, J. Y. (2005) 'Biocides: Health care applications', *Pharmaceutical Journal*.

Maillard, J.-Y. and Pascoe, M. (2024) 'Disinfectants and antiseptics: mechanisms of action and resistance', *Nature Reviews Microbiology*, 22(1), pp. 4–17. doi: 10.1038/s41579-023-00958-3.

Maisch, T. *et al.* (2017) 'Investigation of toxicity and mutagenicity of cold atmospheric argon plasma', *Environmental and Molecular Mutagenesis*. doi: 10.1002/em.22086.

Maisetta, G. *et al.* (2008) 'Evaluation of the inhibitory effects of human serum components on bactericidal activity of human beta defensin 3', *Peptides*. doi: 10.1016/j.peptides.2007.10.013.

Malich, G., Markovic, B. and Winder, C. (1997) 'The sensitivity and specificity of the MTS tetrazolium assay for detecting the in vitro cytotoxicity of 20 chemicals using human cell lines', *Toxicology*. doi: 10.1016/S0300-483X(97)00151-0.

Malone, M. *et al.* (2017) 'The prevalence of biofilms in chronic wounds: A systematic review and meta-analysis of published data', *Journal of Wound Care*. doi: 10.12968/jowc.2017.26.1.20.

Manoukian, S. *et al.* (2021) 'Bed-days and costs associated with the inpatient burden of healthcare-associated infection in the UK', *Journal of Hospital Infection*. doi: 10.1016/j.jhin.2020.12.027.

Masia, M. D. and Dettori, M. (2022) 'Antimicrobial Resistance, Healthcare-Associated Infections, and Environmental Microbial Contamination', *Healthcare (Switzerland)*. doi: 10.3390/healthcare10020242.

Mateu-Sanz, M. *et al.* (2021) 'Cold atmospheric plasma: A new strategy based primarily on oxidative stress for osteosarcoma therapy', *Journal of Clinical Medicine*. doi: 10.3390/jcm10040893.

Mcdonnell, G. and Russell, A. D. (1999) 'Antiseptics and disinfectants: Activity, action, and resistance', *Clinical Microbiology Reviews*. doi: 10.1128/cmr.12.1.147.

Van Meurs, S. J. *et al.* (2014) 'Selection of an optimal antiseptic solution for intraoperative irrigation: An in vitro study', *Journal of Bone and Joint Surgery*. doi: 10.2106/JBJS.M.00313.

McKenna, S. M. and Davies, K. J. A. (1988) 'The inhibition of bacterial growth by hypochlorous acid. Possible role in the bactericidal activity of phagocytes', *Biochemical Journal*. doi: 10.1042/bj2540685.

Meade, E., Slattery, M. A. and Garvey, M. (2021) 'Biocidal resistance in clinically relevant microbial species: A major public health risk', *Pathogens*. doi: 10.3390/pathogens10050598.

Medicines and Healthcare Products Regulatory Agency (MHRA), UK Government (2020) *MHRA: A guide to what is a medicinal product*. Available at: https://assets.publishing.service.gov.uk/government/uploads/system/uploads/attachment_data/file/872742/GN8_FINAL_10_03_2020__combined_.pdf.

Metcalf, D., Bowler, P. and Parsons, D. (2016) 'Wound Biofilm and Therapeutic Strategies', in *Microbial Biofilms - Importance and Applications*. doi: 10.5772/63238.

Metelmann, H. R., von Woedtke, T. and Weltmann, K. D. (2018) *Comprehensive clinical plasma* 202

medicine: Cold physical plasma for medical application, *Comprehensive Clinical Plasma Medicine: Cold Physical Plasma for Medical Application*. doi: 10.1007/978-3-319-67627-2.

Mishra, R. *et al.* (2020) 'Natural Anti-biofilm Agents: Strategies to Control Biofilm-Forming Pathogens', *Frontiers in Microbiology*. doi: 10.3389/fmicb.2020.566325.

Misic, A. M., Gardner, S. E. and Grice, E. A. (2014) 'The Wound Microbiome: Modern Approaches to Examining the Role of Microorganisms in Impaired Chronic Wound Healing', *Advances in Wound Care*. doi: 10.1089/wound.2012.0397.

Modic, M. *et al.* (2019) 'Targeted plasma functionalization of titanium inhibits polymicrobial biofilm recolonization and stimulates cell function', *Applied Surface Science*. doi: 10.1016/j.apsusc.2019.05.153.

Mohapatra, S. S., Dwibedy, S. K. and Padhy, I. (2021) 'Polymyxins, the last-resort antibiotics: Mode of action, resistance emergence, and potential solutions', *Journal of Biosciences*. doi: 10.1007/s12038-021-00209-8.

Moreau, M., Orange, N. and Feuilleley, M. G. J. (2008) 'Non-thermal plasma technologies: New tools for bio-decontamination', *Biotechnology Advances*. doi: 10.1016/j.biotechadv.2008.08.001.

Mulani, M. S. *et al.* (2019) 'Emerging strategies to combat ESKAPE pathogens in the era of antimicrobial resistance: A review', *Frontiers in Microbiology*. doi: 10.3389/fmicb.2019.00539.

Müller, G. and Kramer, A. (2008) 'Biocompatibility index of antiseptic agents by parallel assessment of antimicrobial activity and cellular cytotoxicity', *Journal of Antimicrobial Chemotherapy*. doi: 10.1093/jac/dkn125.

Muller, M. (2018) 'Bacterial silver resistance gained by cooperative interspecies redox behaviour', *Antimicrobial Agents and Chemotherapy*, 62(8), pp. e00672–e00618.

Murphy, E. C. and Friedman, A. J. (2019) 'Hydrogen peroxide and cutaneous biology: Translational applications, benefits, and risks', *Journal of the American Academy of Dermatology*. doi: 10.1016/j.jaad.2019.05.030.

Myers, J. A., Curtis, B. S. and Curtis, W. R. (2013) 'Improving accuracy of cell and chromophore concentration measurements using optical density', *BMC Biophysics*. doi: 10.1186/2046-1682-6-4.

NCIMB (no date) NCIMB 10548. Available at: <https://store.ncimb.com/page/Strains record name display/89620>.

NHS National Services Scotland, ARHAI (Antimicrobial Resistance and Healthcare Associated Infection) (2021) *Standard Infection Control Precautions and Transmission Based Precautions Literature Review: Management of Care Equipment*. Available at: <https://www.nipcm.hps.scot.nhs.uk/media/1672/2021-02-sicp-tbp-lr-equipment-v1.pdf>.

Naylor, N. R. *et al.* (2018) 'Estimating the burden of antimicrobial resistance: a systematic literature review', *Antimicrobial Resistance and Infection Control*. doi: 10.1186/s13756-018-0336-y.

NCIMB (no date) NCIMB 10548. Available at: <https://store.ncimb.com/page/Strains record name display/89620>.

NHS England, UK Government (2022) *National infection prevention and control manual (NIPCM) for England*. Available at: <https://www.england.nhs.uk/national-infection-prevention-and-control-manual-nipcm-for-england/>.

NICE (2011) *Healthcare-associated infections: prevention and control [PH36]*. Available at: <https://www.nice.org.uk/guidance/ph36/resources/healthcareassociated-infections-prevention-and-control-pdf-1996300832965>.

- NICE (2014) *Infection Prevention and Control Quality Standard [QS61]*. Available at: <https://www.nice.org.uk/guidance/qs61/resources/infection-prevention-and-control-pdf-2098782603205>.
- NICE (2024) *Hydrogen Peroxide, British National Formulary*. Available at: <https://bnf.nice.org.uk/drugs/hydrogen-peroxide/#medicinal-forms>.
- NICE (2024) *Povidone-iodine, British National Formulary*. Available at: <https://bnf.nice.org.uk/drugs/povidone-iodine/>.
- NICE Guideline [CG139] (2012) 'Healthcare-associated infections: prevention and control in primary and community care | Guidance and guidelines', *Clinical guideline [CG139]*.
- Nicol, M. K. J. *et al.* (2020) 'Antibacterial effects of low-temperature plasma generated by atmospheric-pressure plasma jet are mediated by reactive oxygen species', *Scientific Reports*. doi: 10.1038/s41598-020-59652-6.
- Nkemngong, C. A. *et al.* (2020) 'A rapid model for developing dry surface biofilms of *Staphylococcus aureus* and *Pseudomonas aeruginosa* for in vitro disinfectant efficacy testing', *Antimicrobial Resistance and Infection Control*, 9(1), pp. 1–9. doi: 10.1186/s13756-020-00792-9.
- Noor, A, Zubair, M, A. (2015) 'Diabetic foot ulcer - A review on pathophysiology, classification and microbial etiology', *Diabetes & Metabolic Syndrome*, 9(3), pp. 192–9. doi: 10.1016/j.dsx.2015.04.007.
- Oates, A, McBain, A. (2016) 'Growth of MRSA and *Pseudomonas aeruginosa* in a fine-celled foam model containing sessile commensal skin bacteria', *Biofouling*, 32(1), pp. 25–33. doi: 10.1080/08927014.2015.117607.
- O'Neill, J. (2016) *Antimicrobial Resistance : Tackling a crisis for the health and wealth of nations, Review on Antimicrobial Resistance*.
- O'NEILL, J. (2016) 'THE REVIEW ON ANTIMICROBIAL RESISTANCE', *Archives of Pharmacy Practice*. doi: 10.4103/2045-080x.186181.
- Oaks, R. (Ohio U. H. C. of O. M. and Cindass, R. (Brooke A. M. C. (2021) *Silver Sulfadiazine, Treasure Island (FL): StatPearls Publishing*. Available at: <https://www.ncbi.nlm.nih.gov/books/NBK556054/>.
- Oates, A, Lindsay, S, Mistry, H, Ortega, F, McBain, A. (2018) 'Modelling antiseptics using defined populations of facultative and anaerobic wound pathogens grown in a basally perfused biofilm model', *Biofouling*, 34(5), pp. 507–518. doi: 10.1080/08927014.2018.1466115.
- Oates, A, McBain, A. (2016) 'Growth of MRSA and *Pseudomonas aeruginosa* in a fine-celled foam model containing sessile commensal skin bacteria', *Biofouling*, 32(1), pp. 25–33. doi: 10.1080/08927014.2015.117607.
- Ofstead, C. L. *et al.* (2015) 'Persistent contamination on colonoscopes and gastroscopes detected by biologic cultures and rapid indicators despite reprocessing performed in accordance with guidelines', *American Journal of Infection Control*. doi: 10.1016/j.ajic.2015.03.003.
- Ojeh, N. O. and Navsaria, H. A. (2014) 'An in vitro skin model to study the effect of mesenchymal stem cells in wound healing and epidermal regeneration', *Journal of Biomedical Materials Research - Part A*. doi: 10.1002/jbm.a.34950.
- Olsen, I. (2015) 'Biofilm-specific antibiotic tolerance and resistance', *European Journal of Clinical Microbiology and Infectious Diseases*. doi: 10.1007/s10096-015-2323-z.
- Olsson, M. *et al.* (2019) 'The humanistic and economic burden of chronic wounds: A systematic review', *Wound Repair and Regeneration*. doi: 10.1111/wrr.12683.
- Omar, A. *et al.* (2017) 'Microbial biofilms and chronic wounds', *Microorganisms*. doi:

10.3390/microorganisms5010009.

Ortega-Llamas, L. *et al.* (2022) 'Cytotoxicity and Wound Closure Evaluation in Skin Cell Lines after Treatment with Common Antiseptics for Clinical Use', *Cells*. doi: 10.3390/cells11091395.

Ortega-Peña, S. *et al.* (2017) 'In vitro microbicidal, anti-biofilm and cytotoxic effects of different commercial antiseptics', *International Wound Journal*. doi: 10.1111/iwj.12625.

Ozlem, S. A. (2017) 'In Vitro Cytotoxicity and Cell Viability Assays: Principles, Advantages, and Disadvantages', *Genotoxicity - A predictable Risk to Our Actual World*.

Paleczny, J. *et al.* (2021) 'The high impact of staphylococcus aureus biofilm culture medium on in vitro outcomes of antimicrobial activity of wound antiseptics and antibiotic', *Pathogens*. doi: 10.3390/pathogens10111385.

Paleczny, J, Brozyna, M, Dudek, B, Woyton, A, Chodaczek, G, Szajnik, M, Junka, A. (2023) 'Culture Shock: An Investigation into the Tolerance of Pathogenic Biofilms to Antiseptics in Environments Resembling the Chronic Wound Milieu', *International Journal of Molecular Sciences*, 24(24), p. 17242. doi: 10.3390/ijms242417242.

Paleczny, J. *et al.* (2023) 'Comparison of antibiofilm activity of low-concentrated hypochlorites vs polyhexanide-containing antiseptic', *Frontiers in Cellular and Infection Microbiology*. doi: 10.3389/fcimb.2023.1119188.

Park, J. Y. *et al.* (2017) 'Plasma-Functionalized Solution: A Potent Antimicrobial Agent for Biomedical Applications from Antibacterial Therapeutics to Biomaterial Surface Engineering', *ACS Applied Materials and Interfaces*. doi: 10.1021/acsami.7b14276.

Park, W. H. (2013) 'The effects of exogenous H₂O₂ on cell death, reactive oxygen species and glutathione levels in calf pulmonary artery and human umbilical vein endothelial cells', *International Journal of Molecular Medicine*. doi: 10.3892/ijmm.2012.1215.

Percival, S. L., McCarty, S. M. and Lipsky, B. (2015) 'Biofilms and Wounds: An Overview of the Evidence', *Advances in Wound Care*. doi: 10.1089/wound.2014.0557.

Percival, S. L., Suleman, L., *et al.* (2015) 'Healthcare-Associated infections, medical devices and biofilms: Risk, tolerance and control', *Journal of Medical Microbiology*. doi: 10.1099/jmm.0.000032.

Percival, S. L., Vuotto, C., *et al.* (2015) 'Biofilms and wounds: An identification algorithm and potential treatment options', *Advances in Wound Care*. doi: 10.1089/wound.2014.0574.

Percival, S. L. *et al.* (2015) 'Healthcare-Associated infections, medical devices and biofilms: Risk, tolerance and control', *Journal of Medical Microbiology*. doi: 10.1099/jmm.0.000032.

Pereira, BMP, Wang, X, Tagkopoulos, I. (2021) 'Biocide-Induced Emergence of Antibiotic Resistance in Escherichia coli', *Frontiers in Microbiology*, 12, p. 640923. doi: 10.3389/fmicb.2021.640923.

Phan, S. *et al.* (2023) 'Relative Abundance and Detection of Pseudomonas aeruginosa from Chronic Wound Infections Globally', *Microorganisms*. doi: 10.3390/microorganisms11051210.

Piccinini, F. *et al.* (2017) 'Cell Counting and Viability Assessment of 2D and 3D Cell Cultures: Expected Reliability of the Trypan Blue Assay', *Biological Procedures Online*. doi: 10.1186/s12575-017-0056-3.

Plattfaud, I, Besser, M, Severing, A-L, Sturmer, EK, Oplander, C. (2021) 'Plasma medicine and wound management: Evaluation of the antibacterial efficacy of a medically certified cold atmospheric argon plasma jet', *International Journal of Antimicrobial Agents*, 57, p. 106319. doi: 10.1016/j.ijantimicag.2021.106319.

Poramapijitwat, P, Thana, P, Boonyawan, D, Janpong, K, Kuensaen, C, Charerntantanakul, Wu, LD, Sarapirom, S. (2020) 'Effect of dielectric barrier discharge plasma jet on bactericidal and human dermal fibroblast adult cells: In vitro contaminated wound healing model', *Surface & Coatings Technology*, 402, p. 126482. Available at: <https://doi.org/10.1016/j.surfcoat.2020.126482>.

Posnett, J. *et al.* (2009) 'The resource impact of wounds on health-care providers in Europe.', *Journal of wound care*. doi: 10.12968/jowc.2009.18.4.41607.

Potts, M. (2001) 'Desiccation tolerance: A simple process?', *Trends in Microbiology*. doi: 10.1016/S0966-842X(01)02231-4.

Powell, K., Pujji, O. J. S. and Jeffery, S. (2021) 'Wound healing: What is the NICE guidance from the UK?', *Journal of Wound Care*. doi: 10.12968/jowc.2021.30.3.172.

Presterl, E, Suchomel, M, Eder, M, Reichmann, S, Lassnigg, A, Graninger, W, Rotter, M. (2007) 'Effects of alcohols, povidone-iodine and hydrogen peroxide on biofilms of *Staphylococcus epidermidis*', *Journal of Antimicrobial Chemotherapy*, 60, pp. 417–420. doi: 10.1093/jac/dkm221.

Price, B. L. *et al.* (2016) 'Development of a novel collagen wound model to simulate the activity and distribution of antimicrobials in soft tissue during diabetic foot infection', *Antimicrobial Agents and Chemotherapy*. doi: 10.1128/AAC.01064-16.

Privat-Maldonado, A. *et al.* (2019) 'ROS from Physical Plasmas: Redox Chemistry for Biomedical Therapy', *Oxidative Medicine and Cellular Longevity*. doi: 10.1155/2019/9062098.

Public Health England (2012) *Healthcare associated infections (HAI): point prevalence survey, England: A point prevalence survey on level of healthcare-associated infections (HAI) and levels of antimicrobial use in hospitals in England in 2016*. Available at: <https://www.gov.uk/government/publications/healthcare-associated-infections-hcai-point-prevalence-survey-england#full-publication-update-history>.

Rahman, S. M. E., Ding, T. and Oh, D. H. (2010) 'Effectiveness of low concentration electrolyzed water to inactivate foodborne pathogens under different environmental conditions', *International Journal of Food Microbiology*. doi: 10.1016/j.ijfoodmicro.2010.03.020.

Rai, S. *et al.* (2021) 'Hydrogen Peroxide: Its Use in an Extensive Acute Wound to Promote Wound Granulation and Infection Control – Is it Better Than Normal Saline?', *International Journal of Lower Extremity Wounds*. doi: 10.1177/15347346211032555.

Rasmussen, E. (2020) 'Hypochlorous Acid (HOCl) for disinfection, antiseptis, and wound care in Core Categories', *Application for Inclusion in the 2021 WHO Essential Medicines List - Briotech, Inc.*

Raziyeva, K, Kim, Y, Zharkinbekov, Z, Kassymbek, K, Jimi, S, Saparov, A. (2021) 'Immunology of Acute and Chronic Wound Healing', *Biomolecules*, 11(5), p. 700. doi: 10.3390/biom11050700.

Reis, R. *et al.* (2021) 'Toxicity, mutagenicity and stability assessment of simply produced electrolyzed water as a wound healing agent in vitro', *Human and Experimental Toxicology*. doi: 10.1177/0960327120952151.

Rembe, J. D. *et al.* (2020) 'Antimicrobial Hypochlorous Wound Irrigation Solutions Demonstrate Lower Anti-biofilm Efficacy Against Bacterial Biofilm in a Complex in-vitro Human Plasma Biofilm Model (hpBIOM) Than Common Wound Antimicrobials', *Frontiers in Microbiology*. doi: 10.3389/fmicb.2020.564513.

Resnik, M. *et al.* (2020) 'Strategies for improving antimicrobial properties of stainless steel', *Materials*. doi: 10.3390/ma13132944.

Reynolds, P. M. *et al.* (2018) 'Controlling fluid flow to improve cell seeding uniformity', *PLoS ONE*. doi: 10.1371/journal.pone.0207211.

Ríos-Castillo, A. G., González-Rivas, F. and Rodríguez-Jerez, J. J. (2017) 'Bactericidal Efficacy of

- Hydrogen Peroxide-Based Disinfectants Against Gram-Positive and Gram-Negative Bacteria on Stainless Steel Surfaces', *Journal of Food Science*. doi: 10.1111/1750-3841.13790.
- Rippon, M. et al. (2023) 'Effectiveness of a polyhexamethylene biguanide-containing wound cleansing solution using experimental biofilm models', *Journal of Wound Care*. doi: 10.12968/jowc.2023.32.6.359.
- Riss, TL, Moravec, RA, Niles AL, Duellman, S, Benink H, Worzell, TJ, Minor, L. (2013) 'Cell Viability Assays', in *Assay Guidance Manual [Internet]*. Eli Lilly & Company and the National Center for Advancing Translational Sciences. Available at: <https://www.ncbi.nlm.nih.gov/books/NBK144065/>.
- Rippon, M. et al. (2023) 'Effectiveness of a polyhexamethylene biguanide-containing wound cleansing solution using experimental biofilm models', *Journal of Wound Care*. doi: 10.12968/jowc.2023.32.6.359.
- Robinson, G. M. et al. (2010) 'Evaluation of the efficacy of electrochemically activated solutions against nosocomial pathogens and bacterial endospores', *Letters in Applied Microbiology*. doi: 10.1111/j.1472-765X.2009.02790.x.
- Röhm-Rodowald, E. et al. (2014) 'Effect of different drying conditions for the viability of *Candida albicans* present on carriers.', *Roczniki Państwowego Zakładu Higieny*.
- Romano, V. et al. (2022) 'Cell Toxicity Study of Antiseptic Solutions Containing Povidone–Iodine and Hydrogen Peroxide', *Diagnostics*. doi: 10.3390/diagnostics12082021.
- Rueda-Fernández, M. et al. (2022) 'Effect of the most common wound antiseptics on human skin fibroblasts', *Clinical and Experimental Dermatology*. doi: 10.1111/ced.15235.
- Russell, AD, Day, M. (1993) 'Antibacterial activity of chlorhexidine', *Journal of Hospital Infection*, 25(4), pp. 229–238. doi: 10.1016/0195-6701(93)90109-d.
- Rutala, W. A. and Weber, D. J. (2014) 'Disinfection, Sterilization, and Control of Hospital Waste', in *Mandell, Douglas, and Bennett's Principles and Practice of Infectious Diseases*. doi: 10.1016/B978-1-4557-4801-3.00301-5.
- Sabir, N. et al. (2017) 'Bacterial biofilm-based catheter-associated urinary tract infections: Causative pathogens and antibiotic resistance', *American Journal of Infection Control*. doi: 10.1016/j.ajic.2017.05.009.
- Sahiner, A, Halat, E, Algin Yapar, E. (2019) 'Comparison of bactericidal and fungicidal efficacy of antiseptic formulations according to EN 13727 and EN 13624 stanards', *Turkish Journal of Medical Sciences*, 49, pp. 1564–1567. doi: 10.3906/sag-1906-53.
- Sakarya, S. et al. (2014) 'Hypochlorous acid: An ideal wound care agent with powerful microbicidal, antibiofilm, and wound healing potency', *Wounds*.
- Santajit, S. and Indrawattana, N. (2016) 'Mechanisms of Antimicrobial Resistance in ESKAPE Pathogens', *BioMed Research International*. doi: 10.1155/2016/2475067.
- Sarrigiannidis, S. O. et al. (2021) 'A tough act to follow: collagen hydrogel modifications to improve mechanical and growth factor loading capabilities', *Materials Today Bio*. doi: 10.1016/j.mtbio.2021.100098.
- Sato, S. et al. (2014) 'Povidone-iodine-induced cell death in cultured human epithelial HeLa cells and rat oral mucosal tissue', *Drug and Chemical Toxicology*. doi: 10.3109/01480545.2013.846364.
- Sattar, S. A. (2004) 'Current issues in testing, selection and use of microbicides in infection control: a critical review', *Australian Infection Control*. doi: 10.1071/hi04084.
- Sauer, K, Camper, AK, Ehrlich, GD, Costerton, JW, Davies, D. (2002) '*Pseudomonas aeruginosa*

displays multiple phenotypes during development as a biofilm', *J. Bacteriology*, 184(4), pp. 1140–1154.

Sauer, K, Stoodley, P, Doeres DH, Hall-Stoodley, L, Burmolle, M, Stewart, PS, Bjarnsholt, T. (2022) 'The biofilm life-cycle - expanding the conceptual model of biofilm formation', *Nature Reviews Microbiology*, 20(10), pp. 608–620. doi: 10.1038/s41579-022-00767-0.

Scalise, A. *et al.* (2015) 'Microenvironment and microbiology of skin wounds: The role of bacterial biofilms and related factors', *Seminars in Vascular Surgery*. doi: 10.1053/j.semvascsurg.2016.01.003.

Schilrreff, P, Alexiev, U. (2022) 'Chronic Inflammation in Non-Healing Skin Wounds and Promising Natural Bioactive Compounds Treatment', *International Journal of Molecular Sciences*, 23(9), p. 4298. doi: 10.3390/ijms23094928.

Schmidt, A. *et al.* (2015) 'Cell migration and adhesion of a human melanoma cell line is decreased by cold plasma treatment', *Clinical Plasma Medicine*. doi: 10.1016/j.cpme.2015.05.003.

Schmidt, A. *et al.* (2019) 'Nrf2 signaling and inflammation are key events in physical plasma-spurred wound healing', *Theranostics*. doi: 10.7150/thno.29754.

Scholtz, V. *et al.* (2015) 'Nonthermal plasma - A tool for decontamination and disinfection', *Biotechnology Advances*, 33(6), pp. 1108–1119. doi: 10.1016/j.biotechadv.2015.01.002.

Schroeder, M., Brooks, B. D. and Brooks, A. E. (2017) 'The complex relationship between virulence and antibiotic resistance', *Genes*. doi: 10.3390/genes8010039.

Schultz, G. *et al.* (2017) 'Consensus guidelines for the identification and treatment of biofilms in chronic nonhealing wounds', *Wound Repair and Regeneration*. doi: 10.1111/wrr.12590.

Scottish Government (2023) *Scottish Healthcare Associated Infection (HCAI) Strategy 2023 - 2025*. Available at: <https://www.gov.scot/binaries/content/documents/govscot/publications/strategy-plan/2023/06/scottish-healthcare-associated-infection-hcai-strategy-2023-2025/documents/scottish-healthcare-associated-infection-hcai-strategy-2023-2025.pdf>

Sen, C. K. *et al.* (2009) 'Human skin wounds: A major and snowballing threat to public health and the economy: PERSPECTIVE ARTICLE', *Wound Repair and Regeneration*, pp. 763–771. doi: 10.1111/j.1524-475X.2009.00543.x.

Sen, C. K. (2019) 'Human Wounds and Its Burden: An Updated Compendium of Estimates', *Advances in Wound Care*. doi: 10.1089/wound.2019.0946.

Sethi, KD, Felgate, H, Diaz, M, Faust, K, Kiy, C, Clarke, P, Härtel, C, Rupp, J, Webber, M. (2021) 'Chlorhexidine gluconate usage is associated with antiseptic tolerance in staphylococci from the neonatal intensive care unit', *JAC-Antimicrobial Resistance*, 3(4). doi: 10.1093/jacamr/dlab173.

Severing, A. L. *et al.* (2019) 'Safety and efficacy profiles of different commercial sodium hypochlorite/hypochlorous acid solutions (NaClO/HClO): Antimicrobial efficacy, cytotoxic impact and physicochemical parameters in vitro', *Journal of Antimicrobial Chemotherapy*. doi: 10.1093/jac/dky432.

Shen, J. *et al.* (2016) 'Bactericidal Effects against *S. aureus* and Physicochemical Properties of Plasma Activated Water stored at different temperatures', *Scientific Reports*. doi: 10.1038/srep28505.

Shrestha, P. *et al.* (2018) 'Enumerating the economic cost of antimicrobial resistance per antibiotic consumed to inform the evaluation of interventions affecting their use', *Antimicrobial Resistance and Infection Control*. doi: 10.1186/s13756-018-0384-3.

Siddiqui, A. R. and Bernstein, J. M. (2010) 'Chronic wound infection: Facts and controversies', *Clinics in Dermatology*. doi: 10.1016/j.clindermatol.2010.03.009.

- Sifri, Z, Chokshu, A, Cennimo, D, Horng, H. (2019) 'Global Contributors to Antibiotic Resistance', *Journal of Global Infectious Diseases*, 11(1), pp. 36–42. doi: 10.4103/jgid_110_18.
- Simon, S. *et al.* (2022) 'Influence of Potable Water Origin on the Physicochemical and Antimicrobial Properties of Plasma Activated Water', *Plasma Chemistry and Plasma Processing*. doi: 10.1007/s11090-021-10221-3.
- Šimončicová, J. *et al.* (2019) 'Technical applications of plasma treatments: current state and perspectives', *Applied Microbiology and Biotechnology*. doi: 10.1007/s00253-019-09877-x.
- Sklias, K., Sousa, J. S. and Girard, P. M. (2021) 'Role of short- and long-lived reactive species on the selectivity and anti-cancer action of plasma treatment in vitro', *Cancers*. doi: 10.3390/cancers13040615.
- Slade, E. A. *et al.* (2019) 'An in vitro collagen perfusion wound biofilm model; with applications for antimicrobial studies and microbial metabolomics', *BMC Microbiology*. doi: 10.1186/s12866-019-1682-5.
- Slade, E. A. (2020) *An in vitro investigation of microbial volatile analysis for diagnosis of wound infection*. University of the West of England.
- Smolková, B. *et al.* (2019) 'Non-thermal plasma, as a new physicochemical source, to induce redox imbalance and subsequent cell death in liver cancer cell lines', *Cellular Physiology and Biochemistry*. doi: 10.33594/000000009.
- Stacey, M. (2011) 'Chronic Venous Insufficiency and Leg Ulceration: Principles and Vascular Biology', in *Mechanisms of Vascular Disease: A Reference Book for Vascular Specialists*. Available at: <https://www.ncbi.nlm.nih.gov/books/NBK534282/>.
- Soares, A., Alexandre, K. and Etienne, M. (2020) 'Tolerance and Persistence of *Pseudomonas aeruginosa* in Biofilms Exposed to Antibiotics: Molecular Mechanisms, Antibiotic Strategies and Therapeutic Perspectives', *Frontiers in Microbiology*. doi: 10.3389/fmicb.2020.02057.
- Steins, A. *et al.* (2023) 'Cell death and barrier disruption by clinically used iodine concentrations', *Life Science Alliance*. doi: 10.26508/lsa.202201875.
- Stewart, P. S. and Franklin, M. J. (2008) 'Physiological heterogeneity in biofilms', *Nature Reviews Microbiology*. doi: 10.1038/nrmicro1838.
- Storr, J. *et al.* (2017) 'Core components for effective infection prevention and control programmes: New WHO evidence-based recommendations', *Antimicrobial Resistance and Infection Control*. doi: 10.1186/s13756-016-0149-9.
- Stuermer, E. K. *et al.* (2021) 'Comparative analysis of biofilm models to determine the efficacy of antimicrobials', *International Journal of Hygiene and Environmental Health*. doi: 10.1016/j.ijheh.2021.113744.
- Sun, P. *et al.* (2012) 'Diluted povidone-iodine inhibits tumor growth through apoptosis-induction and suppression of SOD activity', *Oncology Reports*. doi: 10.3892/or.2011.1537.
- Sutterby, E. *et al.* (2022) 'Evaluation of in vitro human skin models for studying effects of external stressors and stimuli and developing treatment modalities', *VIEW*. doi: 10.1002/VIW.20210012.
- Soares, A., Alexandre, K. and Etienne, M. (2020) 'Tolerance and Persistence of *Pseudomonas aeruginosa* in Biofilms Exposed to Antibiotics: Molecular Mechanisms, Antibiotic Strategies and Therapeutic Perspectives', *Frontiers in Microbiology*. doi: 10.3389/fmicb.2020.02057.
- Stewart, P. S. and Franklin, M. J. (2008) 'Physiological heterogeneity in biofilms', *Nature Reviews Microbiology*. doi: 10.1038/nrmicro1838.
- Storr, J. *et al.* (2017) 'Core components for effective infection prevention and control

programmes: New WHO evidence-based recommendations', *Antimicrobial Resistance and Infection Control*. doi: 10.1186/s13756-016-0149-9.

Stuermer, E. K. *et al.* (2021) 'Comparative analysis of biofilm models to determine the efficacy of antimicrobials', *International Journal of Hygiene and Environmental Health*. doi: 10.1016/j.ijheh.2021.113744.

Suleyman, G, Alangaden, G, Bardossy, A. (2018) 'The Role of Environmental Contamination in the Transmission of Nosocomial Pathogens and Healthcare-Associated Infections', *Current Infectious Disease Reports*, 20(12). doi: 10.1007/s11908-018-0620-2.

Sutterby, E. *et al.* (2022) 'Evaluation of in vitro human skin models for studying effects of external stressors and stimuli and developing treatment modalities', *VIEW*. doi: 10.1002/VIW.20210012.

Sutton, JAF, Carnell, OT, Lafagne, L, Gray, J, Biboy, J, Gibson, JF, Pollitt, EJG, Tazoll, SC, Hajdamowicz, NH, Salamanga, B, Pidwill, GR, Condliffe, AM, Renshaw, SA, Vollmer, W, Foster, S. (2021) 'Staphylococcus aureus cell wall structure and dynamics during host-pathogen interaction', *PLoS Pathogens*, 17(3), p. e1009468. doi: 10.1371/journal.ppat.1009468.

Swanson, T. *et al.* (2016) 'IWII wound infection in clinical practice consensus document 2016 update', *Wound Practice & Research: Journal of the Australian Wound Management Association*.

Swanson, T. and Angel, D. (2017) 'Wound Infection in Clinical Practice Update', *Australian nursing & midwifery journal*, 24(8), p. 33.

Szili, E. J. *et al.* (2018) 'Tracking the Penetration of Plasma Reactive Species in Tissue Models', *Trends in Biotechnology*. doi: 10.1016/j.tibtech.2017.07.012.

Tacconelli, E. *et al.* (2018) 'Surveillance for control of antimicrobial resistance', *The Lancet Infectious Diseases*. doi: 10.1016/S1473-3099(17)30485-1.

Tacconelli, E. and Pezzani, M. D. (2019) 'Public health burden of antimicrobial resistance in Europe', *The Lancet Infectious Diseases*. doi: 10.1016/S1473-3099(18)30648-0.

Tan, E. L. and Johari, N. H. (2021) 'Comparative in vitro evaluation of the antimicrobial activities of povidone-iodine and other commercially available antiseptics against clinically relevant pathogens.', *GMS hygiene and infection control*. doi: 10.3205/dgkh000376.

Tang, KWK, Miller BC, Moore, J. (2023) 'Antimicrobial Resistance (AMR)', *British Journal of Biomedical Science*, 80, p. 11387. doi: 10.3389/bjbs.2023.11387.

Teo, A. J. T. *et al.* (2016) 'Polymeric Biomaterials for Medical Implants and Devices', *ACS Biomaterials Science and Engineering*. doi: 10.1021/acsbiomaterials.5b00429.

Thaarup, IC, Iversen, AKS, Lichtenberg, M, Bjarnsholt, T, Jakobsen, T. (2022) 'Biofilm Survival Strategies in Chronic Wounds', *Microorganisms*, 10(4), p. 775. doi: 10.3390/microorganisms10040775.

Thana, P. *et al.* (2019) 'A compact pulse-modulation cold air plasma jet for the inactivation of chronic wound bacteria: development and characterization', *Heliyon*. doi: 10.1016/j.heliyon.2019.e02455.

Thongrueang, N. *et al.* (2022) 'An in vitro comparison of antimicrobial efficacy and cytotoxicity between povidone iodine and chlorhexidine for treating clinical endometritis in dairy cows', *PLoS ONE*. doi: 10.1371/journal.pone.0271274.

Thorn, R. M. S. *et al.* (2012) 'Electrochemically activated solutions: Evidence for antimicrobial efficacy and applications in healthcare environments', *European Journal of Clinical Microbiology and Infectious Diseases*. doi: 10.1007/s10096-011-1369-9.

Tomczyk, S. *et al.* (2022) 'The first WHO global survey on infection prevention and control in

- health-care facilities', *The Lancet Infectious Diseases*. doi: 10.1016/S1473-3099(21)00809-4.
- Townsend, E. M. *et al.* (2016) 'Development and characterisation of a novel three-dimensional inter-kingdom wound biofilm model', *Biofouling*. doi: 10.1080/08927014.2016.1252337.
- Traylor, M. J. *et al.* (2011) 'Long-term antibacterial efficacy of air plasma-activated water', *Journal of Physics D: Applied Physics*. doi: 10.1088/0022-3727/44/47/472001.
- Tsoukou, E., Bourke, P. and Boehm, D. (2020) 'Temperature stability and effectiveness of plasma-activated liquids over an 18 months period', *Water (Switzerland)*. doi: 10.3390/w12113021.
- Tsoukou, E., Bourke, P. and Boehm, D. (2022) 'Efficacy of plasma activated saline in a co-culture infection control model', *Scientific Reports*. doi: 10.1038/s41598-022-20165-z.
- UK Government (2022) Regulation (EU) No 528/2012 of the European Parliament and of the Council of 22 May 2012 concerning the making available on the market and use of biocidal products (Text with EEA relevance), Regulations originating from the EU 2012 No.258. Available at: <https://www.hse.gov.uk/biocides/introduction.htm>.
- UK Health and Safety Executive (HSE) (no date, visited 2024) Biocides: introduction to regulation, supply and use, Biocides: Introduction. Available at: <https://www.hse.gov.uk/biocides/introduction.htm>.
- Veasey, S. and Muriana, P. M. (2016) 'Evaluation of electrolytically-generated hypochlorous acid ("electrolyzed water") for sanitation of meat and meat-contact surfaces', *Foods*. doi: 10.3390/foods5020042.
- Ventola, C. L. (2015) 'The Antibiotics Resistance Crisis Part: Part 1: Causes and Threats', *Pharmacy and therapeutics*.
- Verma, A. (2016) 'Differences in Bacterial Colonization and Biofilm Formation Property of Uropathogens between the Two most Commonly used Indwelling Urinary Catheters', *JOURNAL OF CLINICAL AND DIAGNOSTIC RESEARCH*. doi: 10.7860/jcdr/2016/20486.7939.
- Verran, J, Whitehead, K. (2005) 'Factors affecting microbial adhesion to stainless steel and other materials used in medical devices', *International Journal of Artificial Organs*, 28(11), pp. 1138–1145. doi: 10.1177/039139880502801111.
- Vickery, K. *et al.* (2012) 'Presence of biofilm containing viable multiresistant organisms despite terminal cleaning on clinical surfaces in an intensive care unit', *Journal of Hospital Infection*. doi: 10.1016/j.jhin.2011.07.007.
- Van Der Vliet, A. and Janssen-Heininger, Y. M. W. (2014) 'Hydrogen peroxide as a damage signal in tissue injury and inflammation: Murderer, mediator, or messenger?', *Journal of Cellular Biochemistry*. doi: 10.1002/jcb.24683.
- Vyas, H. K. N., Xia, B. and Mai-Prochnow, A. (2022) 'Clinically relevant in vitro biofilm models: A need to mimic and recapitulate the host environment', *Biofilm*. doi: 10.1016/j.biofilm.2022.100069.
- Wang, L. *et al.* (2017) 'Transforming growth factor β plays an important role in enhancing wound healing by topical application of Povidone-iodine', *Scientific Reports*. doi: 10.1038/s41598-017-01116-5.
- Wang, P., Henning, S. M. and Heber, D. (2010) 'Limitations of MTT and MTS-based assays for measurement of antiproliferative activity of green tea polyphenols', *PLoS ONE*. doi: 10.1371/journal.pone.0010202.
- Weir, D, Swanson, T. (2019) 'Ten top tips: Wound cleansing', *Wounds International*, 10(4), pp. 8–11.

- Weltmann, K. D. *et al.* (2009) 'Atmospheric pressure plasma jet for medical therapy: Plasma parameters and risk estimation', *Contributions to Plasma Physics*. doi: 10.1002/ctpp.200910067.
- Wende, K. *et al.* (2010) 'Distinctive activity of a nonthermal atmospheric-pressure plasma jet on eukaryotic and prokaryotic cells in a cocultivation approach of keratinocytes and microorganisms', *IEEE Transactions on Plasma Science*. doi: 10.1109/TPS.2010.2052835.
- Wende, K. *et al.* (2014) 'Redox-based assay for assessment of biological impact of plasma treatment', *Plasma Processes and Polymers*. doi: 10.1002/ppap.201300172.
- Wende, K. *et al.* (2016) 'Risk assessment of a cold argon plasma jet in respect to its mutagenicity', *Mutation Research - Genetic Toxicology and Environmental Mutagenesis*. doi: 10.1016/j.mrgentox.2016.02.003.
- Werthén, M. *et al.* (2010) 'An in vitro model of bacterial infections in wounds and other soft tissues', *APMIS*. doi: 10.1111/j.1600-0463.2009.02580.x.
- White, R. and Cutting, K. (2008) 'Critical colonisation of chronic wounds: Microbial mechanisms', *Wounds UK*.
- WHO (World Health Organisation) (2011) *Report on the burden of endemic health care-associated infection worldwide: Clean care is safer care*, World Health Organization.
- WHO (2016) *Guidelines on core components of infection prevention and control programmes at the national and acute health care facility level*, World Health Organization.
- WHO (2020) 'Global Antimicrobial Resistance and Use Surveillance System (GLASS) Report, Early Implementation 2020', WHO.
- WHO (2021) 'Global Antimicrobial Resistance Surveillance System (GLASS)', *Global Antimicrobial Resistance Surveillance System (GLASS)*.
- WHO (2024) *Bacterial Priority Pathogens List 2024*. Geneva. Available at: <https://iris.who.int/bitstream/handle/10665/376776/9789240093461-eng.pdf?sequence=1>.
- WHO (World Health Organization) Expert Committee (2021) *WHO Essential Medicines List: Recommendation - Hypochlorous Acid, Essential Medicines List Recommendations*. Available at: <https://list.essentialmeds.org/recommendations/1300>.
- Wilkinson, H. N. and Hardman, M. J. (2023) 'Wound healing: Cellular mechanisms and pathological outcomes', in *Advances in Surgical and Medical Specialties*. doi: 10.1098/rsob.200223.
- Wilsmann, D. E. *et al.* (2023) 'Antibiofilm activity of electrochemically activated water (ECAW) in the control of Salmonella Heidelberg biofilms on industrial surfaces', *Brazilian Journal of Microbiology*. doi: 10.1007/s42770-023-01005-2.
- Wittmann, C, Chockley, P, Singh, SK, Pase, L, Lieschke, GJ, Grabher, C. (2012) 'Hydrogen Peroxide in Inflammation: Messenger, Guide, and Assassin', *Advances in Haematology*, p. 541471. doi: 10.1155/2012/541471.
- Von Woedtke, T. *et al.* (2019) 'Plasma medicine: A field of applied redox biology', *In Vivo*, 33(4), pp. 1011–1026. doi: 10.21873/invivo.11570.
- Wolcott, R, Fletcher, J. (2014) 'The role of wound cleansing in the management of wounds', *Wounds International*, 1(1), pp. 25–31. Available at: <https://woundsinternational.com/wp-content/uploads/sites/8/2023/02/randall.pdf>.
- Woo, K. Y. (2014) 'Management of non-healable or maintenance wounds with topical povidone iodine', *International Wound Journal*. doi: 10.1111/iwj.12017.
- Woods, J. *et al.* (2012) 'Development and application of a polymicrobial, in vitro, wound biofilm

- model', *Journal of Applied Microbiology*. doi: 10.1111/j.1365-2672.2012.05264.x.
- Wound Healing and Management Node Group (WHMNG) (2016) 'Evidence Summary: Wound Management - Chlorhexidine', *Wound Practice and Research - Wounds Australia Journal*, 25(1), pp. 49–51.
- Wu, S. *et al.* (2018) 'Role of the Surface Nanoscale Roughness of Stainless Steel on Bacterial Adhesion and Microcolony Formation', *ACS Omega*. doi: 10.1021/acsomega.8b00769.
- Yan, P., Daliri, E. B. M. and Oh, D. H. (2021) 'New clinical applications of electrolyzed water: A review', *Microorganisms*. doi: 10.3390/microorganisms9010136.
- Zare, M. *et al.* (2021) 'Silicone-based biomaterials for biomedical applications: Antimicrobial strategies and 3D printing technologies', *Journal of Applied Polymer Science*. doi: 10.1002/app.50969.
- Zhang, M. *et al.* (2023) 'Analysis of povidone iodine, chlorhexidine acetate and polyhexamethylene biguanide as wound disinfectants: in vitro cytotoxicity and antibacterial activity', *BMJ Nutrition, Prevention and Health*. doi: 10.1136/bmjnph-2022-000431.
- Zhang, X. *et al.* (2011) 'Surface microstructures and antimicrobial properties of copper plasma alloyed stainless steel', *Applied Surface Science*. doi: 10.1016/j.apsusc.2011.09.091.
- Zheng, S. *et al.* (2021) 'Implication of Surface Properties, Bacterial Motility, and Hydrodynamic Conditions on Bacterial Surface Sensing and Their Initial Adhesion', *Frontiers in Bioengineering and Biotechnology*. doi: 10.3389/fbioe.2021.643722.
- Zhu, G. *et al.* (2017) 'Hydrogen Peroxide: A Potential Wound Therapeutic Target?', *Medical Principles and Practice*. doi: 10.1159/000475501.

